DISSERTATION

Titel der Dissertation

Cell biological characterization of stomatin-like protein-1 (SLP-1) and stomatin

angestrebter akademischer Grad

Doktor der Naturwissenschaften (Dr. rer.nat.)

Verfasser:	Mag. Mario Mairhofer
Matrikel-Nummer:	9306817
Dissertationsgebiet (lt. Studienblatt):	A 091 490 Molekulare Biologie
Betreuer:	Univ.-Prof. Dr. Rainer Prohaska

Wien, am 08. April 2008

PhD thesis   *Mario Mairhofer*

PhD thesis   *Mario Mairhofer*

PhD thesis   *Mario Mairhofer*

1 SUMMARY

The human stomatin protein family consists of 5 members, the prototype stomatin protein, stomatin-like protein 1 (SLP-1), SLP-2, SLP-3, and the kidney-specific podocin protein, whose precise functions have remained largely unknown up to now. This lack of knowledge may be explained by the hydrophobic nature and the tight membrane association of these proteins, which still pose a challenge for the biochemist and molecular cell biologist. Nevertheless, genetic data from *C. elegans* stomatin-like proteins UNC-1, UNC-24, and MEC-2 as well as knock-out experiments in mice (stomatin, SLP-2, SLP-3) and analysis of genetic data in human steroid-resistant nephrotic syndrome (podocin) indicate an important, but perhaps redundant function for these proteins in most tissues.

In this work, the major focus was put on human SLP-1 protein, the least characterized family member. Due to the lack of an antibody against SLP-1, I prepared SLP-1 constructs fused to different tags (GFP, myc-epitope, HA-epitope) and exogenously expressed and characterized the tagged proteins with biochemical and molecular cell biological methods. Similar to stomatin, the tagged SLP-1 protein was localized to perinuclear vesicles, however, in contrast to stomatin it was not found on the plasma membrane by immunofluorescence and immunoelectron microscopy. Subcellular fractionation and biochemical analysis confirmed the endosomal localization. Comparison of the localization of SLP-1 with different organelle marker proteins by immunofluorescence studies revealed that these peri-nuclear vesicles are late endosomes/lysosomes. The degree of co-localization between SLP-1 and different late endosomal/lysosomal markers was variable and indicated a broad distribution of the protein over different late endosomal sub-compartments. Several truncation mutants and point mutants of the SLP-1 protein were constructed and led to the identification of a tyrosine-based N-terminal late endosomal/lysosomal targeting signal in the first 10 amino acids of the protein. In chimeric constructs, where the N-terminus of stomatin was replaced by the N-terminus of SLP-1, this motif was found to be sufficient to direct the fusion protein to late endosomes/lysosomes and abolish the plasma membrane localization of stomatin. C-terminal deletions of SLP-1 also compromise the correct subcellular localization of this protein, as exemplified by one construct, which was found to be mis-targeted to cytoplasmic aggregates and tubular structures. This truncation was also analyzed by electron microscopy and the cytoplasmic aggregates were found to be small lipid bodies or droplets. Most likely, the over-expression of the SLP-1 truncation mutant was the cause for the appearance of these characteristic structures.

Our hypothesis that the human SLP-1 and stomatin proteins could form a complex like their *C. elegans* counterparts UNC-24 and UNC-1 was tested in this thesis and the interaction between endogenous stomatin and exogenously expressed, tagged SLP-1 was verified by co-

immunoprecipitation analyses. These two proteins also showed co-localization in immunofluorescence experiments, and most importantly, over-expression of SLP-1 caused a re-distribution of endogenous stomatin from the plasma membrane to late endosomes. These data strongly support the notion that hetero-oligomeric complexes between stomatin and SLP-1 are formed, whose functional properties might differ from the known stomatin homo-oligomers. Biochemical and cell biological evidence indicates that SLP-1 forms an oligomeric structure. Like the prototype stomatin protein, SLP-1 is enriched in detergent-resistant membranes (DRMs), similar to lipid rafts, although it is not present at the plasma membrane. A major difference between stomatin and SLP-1 was found in respect to the targeting to lipid bodies/droplets. Wild-type SLP-1 was never detected on these neutral lipid storage organelles, whereas stomatin and a C-terminal truncation mutant of SLP-1 were readily detected there and showed the characteristic ring-shaped appearance.

Based on the unique domain structure of SLP-1, containing a stomatin and a sterol carrier protein-2 (SCP-2) domain, and its enrichment in lipid rafts, we supposed that the protein could function in cholesterol/lipid transport. I used filipin staining to analyze the subcellular distribution of cholesterol in cells exogenously expressing SLP-1 and found no obvious differences to control cells. But when I blocked the transport of cholesterol from the late endosomal compartment to the plasma membrane with a synthetic aminosteroid, I encountered big differences between cells expressing SLP-1 and control cells. Over-expression of SLP-1 caused the formation of enlarged, cholesterol-filled perinuclear structures. This means that the distribution of cholesterol in the late endosomal compartment can be modified by the expression of SLP-1. A truncation mutant in which the SCP-2 domain of SLP-1 was deleted did not show this effect, indicating that this domain is necessary to modify cholesterol distribution. Finally, live cell imaging of SLP-1-GFP revealed the dynamics of SLP-1 on perinuclear vesicles and led to the finding that the protein is inhomogeneously distributed on the surface of big endosomal structures and that smaller, rapidly diffusing vesicles are also positive for SLP-1-GFP. These small vesicles either transiently attach to the bigger structures or fuse and pinch off these structures as discrete entities. The precise nature of these transport intermediates remains to be clarified.

In a second part of my work, I tried to expand our knowledge about the prototype family member, the stomatin protein. I established a fluorescence recovery after photobleaching (FRAP) assay and demonstrated that deletion of the outermost C-terminus of stomatin modifies the diffusion properties of this protein. The mobile fraction and the diffusion speed both increase when the outermost C-terminus, which is essential for oligomerization and lipid raft association, is deleted.

To identify potential interaction partners and functional mechanisms where stomatin could play a role, I performed 2D PAGE analyses of platelet DRM fractions and identified the proteins and post-translational modifications (PTMs) of stomatin by mass spectrometry (at the Mass Spectrometry Unit). In resting platelets, the protein was detected in 3 separate spots, one close to the theoretical isoelectric point and two spots shifted towards the acidic end, which may correspond to one and two additional negative charges, respectively. The mass

spectrometric analyses for PTMs revealed a potential novel phosphorylation site (serine-231) and a cryptic, yet unknown modification, which was detected on three consecutive stomatin peptides. The significance of these modifications remains to be determined. Finally, another strategy was taking advantage of the increasing number of reported mutations in the *C. elegans* stomatin homologues MEC-2 and UNC-1. I identified conserved residues, whose mutations cause a phenotype in the worm, and constructed the respective point mutations in the human stomatin protein. The analyses of the mutants are only at the beginning but indicate that this strategy will lead to new insights in the mechanisms which direct the subcellular targeting and transport of this protein.

1 ZUSAMMENFASSUNG

Die humane Stomatin-Proteinfamilie besteht aus 5 Mitgliedern, dem Prototypen Stomatin, Stomatin-like protein 1 (SLP-1), SLP-2, SLP-3 und das Nieren-spezifische Podocin-Protein, deren genaue Funktion noch weitgehend unbekannt ist. Das geringe Wissen über diese Proteinfamilie kann durch die hydrophobe Natur und die enge Assoziierung dieser Proteine mit Membranen erklärt werden, da diese Faktoren noch immer eine große Herausforderung für Biochemiker und Zellbiologen darstellen. Genetische Daten aus dem Modellorganismus *C. elegans*, knock-out Experimente in Mäusen und genetische Daten von Patienten mit Steriod-Resistant Nephrotic Syndrome lassen auf eine wichtige, aber wahrscheinlich redundante Funktion für diese Proteine schließen.

Der Schwerpunkt dieser Arbeit liegt auf dem humanen SLP-1 Protein, dem am wenigsten charakterisierten Familienmitglied. Da kein Antikörper gegen das humane SLP-1 Protein erhältlich war, habe ich das SLP-1-Protein mit unterschiedlichen Tags verknüpft (GFP, myc-Epitop und HA-Epitop) und exogen exprimiert und die Fusionsproteine mit biochemischen und zellbiologischen Methoden charakterisiert.

In Analogie zu Stomatin wurde das getaggte SLP-1-Protein auf perinucleären Vesikeln detektiert, zeigte aber im Gegensatz zu Stomatin keine Plasmamembran-Lokalisation in der Immunfluoreszenz- und Immunoelektronen-Mikroskopie. Subzelluläre Fraktionierung und biochemische Analyse bestätigten die endosomale Lokalisation. Durch Vergleich der Lokalisation von SLP-1 mit unterschiedlichen Organellenmarkern in Immunfluoreszenz-Versuchen konnte gezeigt werden, dass es sich bei den perinucleären, SLP-1-positiven Vesikeln um Late Endosomes (LEs) handelt. Die Co-Lokalisation mit unterschiedlichen Markern für dieses Kompartiment war variabel und wies auf eine breite Verteilung von SLP-1 über die diversen LE-Subkompartments hin. Die Konstruktion von verschiedenen Verkürzungs- und Punkt-Mutanten des SLP-1-Proteins führte zur Identifizierung eines Tyrosin-basierenden N-terminalen Sortiersignals in den ersten 10 Aminosäuren des Proteins. In chimären Konstrukten, in denen der N-terminus des Stomatin-Proteins durch den N-Terminus von SLP-1 ersetzt wurde, war dieses Motiv hinreichend, um das Fusionsprotein zu LEs/Lysosomen zu dirigieren und die Plasma-Membran-Lokalisation von stomatin zu unterbinden. C-Terminale Deletionsmutanten von SLP-1 zeigen auch Auswirkungen auf die korrekte subzelluläre Lokalisierung, wie am Beispiel eines Konstruktes klar wurde, welches zu cytoplasmatischen Aggregaten und tubulären Strukturen fehlgeleitet wird. Diese C-terminale Verkürzung wurde in Elektronenmikroskopie-Experimenten untersucht, und es konnte gezeigt werden, dass die zytoplasmatischen Aggregate kleine Lipid Bodies (alternativer Name Lipid Droplets) darstellen. Wahrscheinlich führte die Über-Expression der SLP-1-Verkürzungsmutante zur Ausbildung dieser charakteristischen Strukturen.

Unsere Hypothese, dass die menschlichen SLP-1- und stomatin-Proteine einen Komplex

bilden könnten wie ihre *C. elegans* Gegenstücke UNC-24 und UNC-1, wurde in dieser Arbeit verifiziert. Komplexbildung zwischen endogenem Stomatin und exogen exprimiertem, getaggtem SLP-1 konnte in Immunpräzipitations-Experimenten gezeigt werden. Beide Proteine ko-lokalisierten in Immunfluoreszenz-Experimenten auf Late Endosomes, und interessanterweise veränderte sich die Lokalisation von endogenem Stomatin bei Überexpression von SLP-1, wobei eine klare Verschiebung von der Plasmamembran zu Late Endosomes festzustellen war. Diese Daten verweisen darauf, dass hetero-oligomere Komplexe zwischen Stomatin und SLP-1 gebildet werden, und dass sich die Eigenschaften dieser hetero-oligomeren Komplexe von den bekannten homo-oligomeren Stomatin-Komplexen stark unterscheiden könnten. Biochemische und zellbiologische Ergebnisse unterstützen eine oligomere Struktur von SLP-1. Wie Stomatin ist auch SLP-1 in sogenannten Detergent-Resistant Membranes (DRMs) oder Lipid Rafts angereichert, obwohl es nicht an der Plasmamembran zu finden ist. Einer der Hauptunterschiede zwischen SLP-1 und Stomatin wurde in Bezug auf die Assoziierung mit Lipid bodies/droplets festgestellt. Wild-Typ SLP-1 wurde nie auf der Oberfläche dieser Lipid-Speicherorganellen detektiert, wohingegen sowohl Stomatin als auch eine C-terminale Verkürzung von SLP-1 auf Lipid bodies detektiert wurden und die charakteristische, ringförmige Färbung zeigten.

Basierend auf der einzigartigen Domänenstruktur von SLP-1, welches eine Kombination von einer Stomatin–Domäne und einer Sterol Carrier Protein-2 (SCP-2)-Domäne beinhaltet, und auf der Anreicherung in lipid rafts, kamen wir zu der Annahme, dass eine Funktion des Proteins im Cholesterin/Lipid-Transport möglich ist. Ich verwendete den Farbstoff Filipin, um die subzelluläre Verteilung von Cholesterin in Zellen, die SLP-1 überexprimieren, zu untersuchen. Dabei fand ich keine augenfälligen Unterschiede zu Kontroll-Zellen. Aber als ich den Cholesterin-Transport von den Late Endosomes zur Plasma-Membran mit einem synthetischen Aminosteroid inhibierte, fand ich große Unterschiede zwischen Kontrollzellen und SLP-1-exprimierenden Zellen. Überexpression von SLP-1 führte zur Bildung von stark vergrößerten, Cholesterin-gefüllten perinukleären Strukturen. Dieses Ergebnis zeigt, dass die Cholesterin-Verteilung im Late-endosomalen Kompartment durch die Expression von SLP-1 verändert werden kann. Eine Verkürzungsmutante, bei der die SCP-2-Domäne entfernt wurde, zeigte diesen Effekt nicht, wodurch gezeigt wird, dass diese Domäne für die Modifizierung der Cholesterin-Verteilung notwendig ist.

Live-Cell-Imaging gab schließlich Aufschlüsse über die Dynamik des SLP-1-Proteins auf den perinukleären Vesikeln und zeigte, dass das SLP-1-Protein meist sehr inhomogen auf der Oberfläche von größeren Vesikeln verteilt ist und dass es einen zweiten Pool von kleineren, sehr schnell diffundierenden Vesikeln gibt. Diese kleinen Vesikel können entweder kurzfristig mit größeren Strukturen interagieren, oder sie fusionieren und schnüren sich dann wieder als diskrete Einheiten von den größeren Vesikeln ab. Worum es sich bei diesen kleinen, schnellen Strukturen genau handelt, muss erst geklärt werden.

In einem zweiten Teil meiner Arbeit versuchte ich unser Wissen über das stomatin-Protein selbst zu erweitern. Ich konnte einen Fluorescence Recovery After Photobleaching (FRAP)-Assay etablieren und zeigen, dass die Deletion des äußersten C-Terminus von Stomatin die

Diffusionseigenschaften des Proteins in der Plasmamembran beeinflusst. Sowohl die mobile Fraktion als auch die Diffusionsgeschwindigkeit erhöhen sich, sobald der C-Terminus, der auch für die Oligomerisierung und die Lipid-Raft-Assoziierung notwendig ist, deletiert ist.

Um potentielle Interaktionspartner und funktionelle Mechanismen, bei denen Stomatin eine Rolle spielen könnte, auszumachen, führte ich 2D-PAGE-Analysen von Thrombozyten-DRM-Fraktionen durch und ließ die Proteine und post-translationelle Modifikationen (PTMs) von Stomatin durch Massenspektrometrie identifizieren (Mass Spectrometry Unit, VBC). In unaktivierten Thrombozyten wurden 3 Spots für Stomatin gefunden, einer nahe am theoretischen iso-elektrischen Punkt, und zwei zur sauren Seite verschobene Spots, die eine bzw. zwei zusätzliche negative Ladungen darstellen könnten. Die massenspektroskopische Analyse auf PTMs ergab eine potentielle neue Phosphorylierungsstelle für Stomatin (Serin-231) und eine kryptische, bis jetzt unbekannte Modifikation, die auf drei aufeinanderfolgenden Stomatin-Peptiden gefunden wurde. Die Natur und Bedeutung dieser Modifikation muss erst genauer untersucht werden.

Schließlich habe ich in einem letzten Ansatz versucht, das zunehmende Wissen über Mutationen in den Stomatin-verwandten Proteinen MEC-2 und UNC-1 in *C. elegans* für die Untersuchung des humanen Proteins auszunutzen. Ich habe zuerst konservierte Aminosäuren in der Sequenz identifiziert, bei denen Mutationen einen Phänotyp im Wurm verursachen. Dann habe ich die entsprechenden Punktmutationen im humanen Stomatin-Protein konstruiert. Die Analyse dieser Punktmutationen steht erst am Anfang, aber erste Ergebnisse lassen vermuten, dass diese Strategie zu neuen Einsichten in die Transport- und Targeting-Mechanismen des Proteins führen werden.

2   INTRODUCTION

2.1 The stomatin protein family

The human stomatin protein family currently comprises 5 members: stomatin (Hiebl-Dirschmied et al., 1991b; Stewart et al., 1992), stomatin-like protein (SLP)-1 (alternative names hUNC-24, STOML-1, STORP) (Gilles et al., 2000; Seidel and Prohaska, 1998), SLP-2 (Wang and Morrow, 2000), SLP-3 (Goldstein et al., 2003; Kobayakawa et al., 2002) (alternative name SRO) and podocin (Boute et al., 2000). These 5 proteins all share a stomatin-homology region and are part of the much larger SPFH (stomatin-prohibitin-flotillin-HflK/C) superfamily (Tavernarakis et al., 1999). Of this superfamily, prohibitins and flotillins are also present in humans. The core SPFH domain is of very ancient origin, as it is already found in several archaebacteria and bacteria. Members of the SPFH family are found throughout the prokaryotic and eukaryotic kingdom, in E. coli, yeasts, fungi, plants and all animals from *C. elegans* to mammals. The numerous members of the SPFH protein family are thought to descend from a common ancestor, which must have evolved before the separation of archaebacteria and eubacteria. In the course of evolution of higher eukaryotes, the family has branched and the clearly distinct stomatin, flotillin and prohibitin families have developed. Another hypothesis, which was published recently (Rivera-Milla et al., 2006), suggests convergent evolution of different family members from different precursors instead of divergent evolution. As the main branches of the family are all of very ancient origin, it is very difficult to make a decision based on phylogenetic data of current organisms. Nevertheless, the ancient origin supports a basic function for SPFH family members. I will mainly focus on the stomatin family members here, a short summary of the status of research on prohibitins, flotillins and HflK/C proteins is given in chapter 2.3.

Figure 1 shows a neighbour joining tree of the human members of the stomatin protein family. SLP-2 has diverged most early and probably represents the most ancient member of the family. It is missing the characteristic, unusually long hydrophobic stretch of amino acids found before the SPFH domain in all 4 other members. SLP-1 represents a combination of the SPFH domain with a C-terminal SCP-2 domain. Orthologues of SLP-1 and SLP-2 are already detected in *C. elegans*. In the course of evolution of higher organisms, the prohibitin and SLP-3 proteins have evolved. They both share high sequence homology with stomatin over its whole length. Podocin is already found in fish and contains an elongated N-terminus which probably is responsible for its special function in the nephrotic system. SLP-3 is only 3 amino acids longer than human stomatin, and shares 68% identity and 84% similarity with stomatin. It is probably the result of a gene duplication event in mammals, and its expression is

restricted to olfactory neurons in mice. The current knowledge on the five stomatin family members is summarized in the following section.

Figure 1: Neighbour joining tree of the human stomatin family
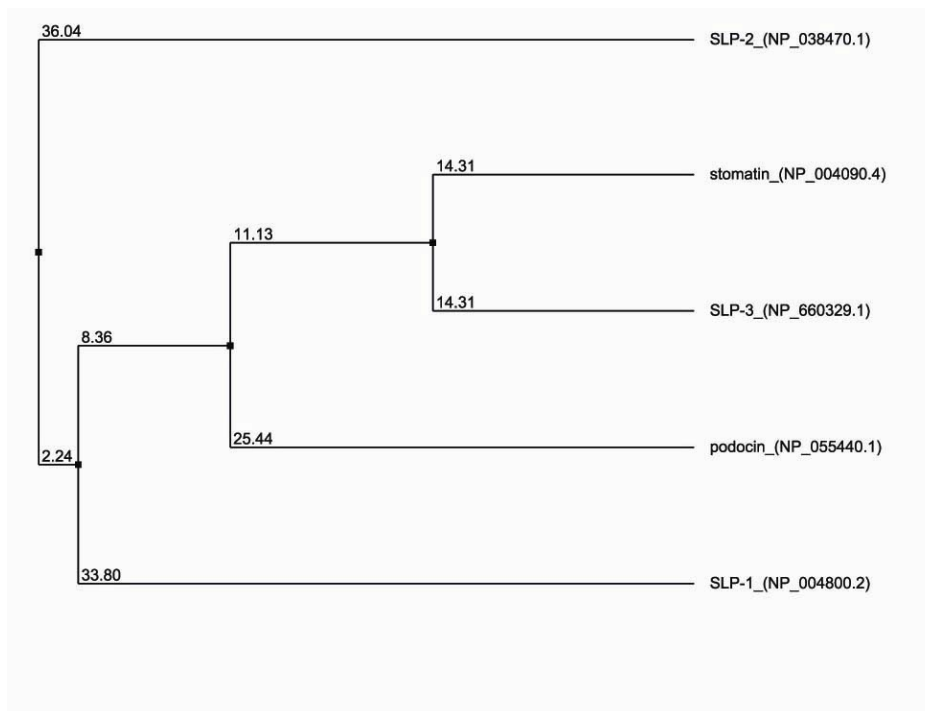
Figure 1: Neighbour joining tree of the human stomatin family proteins. The tree is based on an alignment computed with the ClustalW programme (http://www.ebi.ac.uk/clustalw/). The Entrez accession numbers for the protein sequences are given in brackets.

2.1.1 Stomatin

Human stomatin was described as a major integral membrane protein of human erythrocytes (band 7.2b)(Hiebl-Dirschmied et al., 1991a). It was found to be missing in mouth-shaped = stomatocytic erythrocytes of patients suffering from a rare, hereditary anemic condition named "overhydrated hereditary stomatocytosis" (OHSt)(Wang et al., 1991). These stomatocytes show an increased membrane permeability for monovalent cations (Na+, K+) and therefore increased osmotic fragility, giving rise to a decreased lifetime of the erythrocytes. The band 7.2b protein was renamed to stomatin, as its lack was considered to cause the disease(Stewart et al., 1992). Analysis of the stomatin gene in patients revealed that no mutations are present in the gene or in the promoter region, raising the first doubts on the causative role of stomatin OHSt(Fricke et al., 2003). Later, it was shown that erythrocyte precursors of OHSt patients contain normal amounts of stomatin and that the protein is lost from the precursors during a terminal maturation step(Fricke et al., 2005). Additionally, stomatin knock-out mice were viable without any obvious phenotype and, especially, with normal erythrocytes(Zhu et al., 1999). Therefore, a defect in stomatin is not the cause for OHSt, but the increased cation permeability could be linked to the absence of stomatin from

the erythrocyte membrane. Stomatin contains an unusually long, hydrophobic sequence close to its N-terminus, which is an atypical membrane domain, as it probably is integrated into the membrane in the form of a hydrophobic hairpin, with both N- and C-terminus in the cytoplasm. This was deduced from findings that Serine-9 can be phosphorylated in intact erythrocytes in response to cAMP(Salzer et al., 1993), and from protease protection studies in intact erythrocytes. This peculiar organisation of the integral membrane domain is shared with the caveolin protein family. The stomatin promoter shows the typical features of a house-keeping gene, like the absence of a TATA-box and binding sites for general transcription factors (SP1, AP1, AP2, CP1/2, NFκB, CREB). Two imperfect sequences for erythroid factors (EKLF and GATA-1) were also found(Unfried et al., 1995). The mRNA is detected in almost all tissues and cell types, consistent with a basic function of the stomatin protein(Unfried et al., 1995). Stomatin was shown to be palmitoylated on two cysteine residues, on cysteine-29 and, to a lesser extent, on cysteine 86(Snyers et al., 1999b). The protein forms high-order-oligomers in UAC cells(Snyers et al., 1998), erythrocytes(Salzer and Prohaska, 2001) and platelets(Mairhofer, 2001), with an oligomer size of approximately 300 kDa. One of the most important features of stomatin is its association with detergent-resistant, cholesterol- and sphingolipid-rich membrane domains, also termed lipid rafts(Mairhofer et al., 2002; Salzer and Prohaska, 2001; Snyers et al., 1999a). The protein was shown to be localized to the plasma membrane and to late endosomes in UAC cells (ratio 1:1 PM:LEs in UAC cells) and several other cell types. Plasma membrane stomatin colocalizes with filamentous actin even when the cells are treated with actin-filament-disrupting drugs like cytochalasin D(Snyers et al., 1997). Upon polarization of MDCK cells(Snyers et al., 1999a) or HepG2 cells (M. Mairhofer, unpublished observations), stomatin translocates to the apical surface. Lipid rafts are thought to play an essential role in apical protein sorting, therefore it is not surprising that stomatin is sorted to the apical PM. Recently, Ellen Umlauf from our group could show that stomatin is also associated with cytoplasmic lipid droplets (alternative designation lipid bodies)(Umlauf et al., 2004). This finding supports the proposed hairpin structure for the hydrophobic domain, because proteins with membrane-spanning transmembrane domains are excluded from the lipid monolayer limiting the droplets(Brown, 2001). In another publication, a region in the C-terminus of stomatin was identified, which is essential for lipid raft association and oligomerization of the protein. Point mutations in single amino acids were shown to differentially affect either oligomerization or lipid raft association(Umlauf et al., 2006), with the conclusion that oligomerization is not required for lipid raft association. The recent discovery that stomatin interacts with acid-sensing ion channels (ASICs) and modifies the gating properties of some ASICs(Price et al., 2004) is very interesting, because it fits very well to data from *C. elegans*, where stomatin orthologues were shown to interact with members of the degenerin channel family(Sedensky et al., 2004; Zhang et al., 2004a), and it could also explain the defect in cation permeability observed in OHSt patients. The mechanism for regulation of channel activity by stomatin is not clear yet. A model deduced from prokaryotes, where stomatin-related proteins form an operon with membrane-linked proteases(Green et al., 2004), suggests that the C-terminus of stomatin

directly interacts with the channel pore, inhibiting transport activity. Proteolytic cleavage of the stomatin C-terminus causes detachment of stomatin from the pore, thereby increasing ion transport. This so-called ball-and-chain model(Stewart, 1997) is highly speculative and not really backed up by experimental data. A direct interaction between ion channels and stomatin is supported by co-immunoprecipitation experiments in different systems(Price et al., 2004; Zhang et al., 2004a). Nevertheless, one must be aware that co-IPs of membrane proteins are prone to false positives due to incomplete solubilization of cellular membranes. Immunoprecipitations of lipid raft proteins are even more critical due to the inherent detergent-resistence of the raft domains. Therefore, it could also be true that stomatin and ion channels are both localized to lipid rafts, and that the regulation of ion channel activity happens by influencing the local properties of the membrane(Huber et al., 2006). The spider venom VSTX1, for example, was shown to have a dramatic influence on ion channel activity, but it does not affect channel activity by direct binding, but rather by changing the properties of the surrounding plasma membrane(Lee and MacKinnon, 2004). Two stomatin orthologues from *C. elegans* were shown to influence sensitivity to volatile anesthetics, which probably also affect membrane properties instead of direct binding to ion channels(Morgan et al., 1990; Rajaram et al., 1998). As outlined above, the function of the stomatin protein probably lies in the regulation of ion channels, but many details are still missing. Based on its enrichment in lipid rafts and its close linkage to the cytoskeleton, stomatin might play an important role as a membrane organizer, influencing the local properties of the inner leaflet of the plasma membrane. Unpublished data from E. Umlauf, which show that a photoreactive, radiolabeled cholesterol is bound by the core SPFH domain of stomatin, also support this role. Another string of evidence indicates that stomatin interacts with the glucose transporter GLUT-1 and negatively affects glucose transport (Zhang et al., 2001; Zhang et al., 1999). GLUT-1 is at least partially lipid raft-associated in erythrocytes and in nucleated cells. Conditions which induce an increased demand for glucose cause an increase of the non-raft associated fraction of GLUT-1, suggesting a mechanism where the activity of GLUT-1 is determined by association/dissociation of membrane microdomains(Rubin and Ismail-Beigi, 2003; Rubin and Ismail-Beigi, 2004). It remains to be determined if stomatin directly influences GLUT-1 activity or if it rather acts by influencing its distribution between rafts and non-raft domains. It is also interesting that, although human erythrocytes strongly express GLUT-1, this protein is not expressed in mouse erythrocytes. If stomatin function in human erythrocytes was coupled to the GLUT-1 protein, this would explain why the erythrocytes of the stomatin knock-out mouse did not show the expected stomatocytic phenotype.

2.1.2   Stomatin-like protein-1(SLP-1)

SLP-1 was identified as the human homologue of *C. elegans* UNC-24 protein, which gives rise to an uncoordinated phenotype when the gene is mutated. The unc-24 gene could be mapped and sequenced, revealing the protein sequence of UNC-24. The protein contains a unique combination of an SPFH-domain followed by a SCP-2 domain (Barnes et al., 1996).

This combination is also found in the human SLP-1 protein. On multiple tissue northern blots, a strong expression of SLP-1 was observed in the brain, along with a considerable expression in skeletal muscle and heart, with only low levels of expression in other tissues (Seidel and Prohaska, 1998; Wang and Morrow, 2000). SLP-1 was therefore considered to be the brain-specific stomatin, because stomatin was long considered to be absent from the brain. This view had to be corrected, because several groups have shown that stomatin is present in nerve cells of humans and rodents(Fricke et al., 2000; Mannsfeldt et al., 1999). Stomatin and SLP-1 are now considered to be co-expressed in the brain, and in the light of findings from *C. elegans*, they could function in a hetero-oligomeric complex there. A second group also cloned the SLP-1 gene (they named it STORP) and mapped it to chromosome 15q22(Gilles et al., 2000). They deduced a slightly different protein sequence to Seidel et al, which was confirmed to be correct after the completion of the human genome. Like Seidel et al., they performed multiple tissue northern blotting and found SLP-1 to be ubiquitously expressed, although their data were clearly of lower quality than the data of Seidel et. al..

Figure 2: Multiple sequence alignment of mammalian SLP-1 proteins and UNC-24

Figure 2: Multiple sequence alignment of four mammalian SLP-1 proteins and C. elegansUNC-24. The alignment shows that the mammalian SLP-1 protein sequences are extremely well conserved, whereas there are big differences to UNC-24.

The number of isolated EST clones isolated from brain and microarray data support a preferential expression of SLP-1 in the nervous system, but low-level expression of SLP-1 in other tissues could be of interest in the light of a proposed regulatory function of SLP-1 on stomatin. Gilles et al. also analysed different tumor cell lines and again detected the SLP-1 mRNA in all analysed cell lines. If SLP-1 were expressed in these established tumor cell lines, the endogenous protein could be studied in one of these cell culture systems. In their characterization of the human SLP-2 protein, Wang et al. also analysed the tissue distribution of SLP-1 by northern blotting and also found strong expression in the brain and substantial expression in heart and skeletal muscle(Wang and Morrow, 2000). Verification of SLP-1 protein levels in different tissues and cell lines will eventually clarify the discrepancies between these studies.

2.1.3 SLP-2

SLP-2 was cloned and characterized in detail some years ago(Wang and Morrow, 2000). The protein does not contain a continuous hydrophobic domain close to its N-terminus, as do all other members of the stomatin protein family. The amino acid sequence shows the least homology to human stomatin, indicating the biggest evolutionary difference. The mRNA was shown to have a broad tissue distribution and the protein was detected in a wide range of cell lines, similar to stomatin. It was also detected in mature red blood cells, giving rise to a double band in western blots. Interestingly, the higher moleclular weight (MW) band was found to be largely detergent insoluble, whereas the lower MW band was largely soluble. This behaviour suggests that a post-translational modification, perhaps palmitoylation, is required for SLP-2 to partition into DRMs or lipid rafts. In support of a broad tissue distribution and lipid raft association of SLP-2, the protein was identified in several proteomic studies of lipid rafts (Sprenger et al., 2004). Recent reports revealed that SLP-2 expression is upregulated in esophageal squamous cell carcinoma (ESCC) and in other cancer types(Zhang et al., 2006). An ESCC cell line transfected with antisense SLP-2 showed decreased cell growth, proliferation, tumorigenecity, and cell adhesion(Zhang et al., 2006). This finding raises the possibility that SLP-2 upregulation is associated with the transformation of normal cells into tumor cells. During the writing of this thesis, Hajek et al. reported that SLP-2 is localized to mitochondria and forms a complex with mitofusin-2(Hajek et al., 2006). The authors deduced that SLP-2 is associated with the inner mitochondrial membrane and faces the intermembrane space. This mitochondrial localization is very interesting in respect to reports that SLP-2 expression is up-regulated in several carcinomas. Several important questions concerning SLP-2 are still unresolved, the subcellular localization of the protein, for example, seems to be different in different cell types, and possible interactions with other stomatin family members have not been examined. Recently, two conference abstracts were published, which both report that the mouse knock-out of SLP-2 is embryonically lethal, which indicates an important function for SLP-2.

2.1.4 SLP-3

SLP-3 was discovered shortly after the completion of the human genome sequence. It is the "youngest" stomatin family protein and has probably evolved by a gene duplication of the stomatin gene in mammals. It shares 68% identity and 84% similarity with stomatin in the homologous region, and the genomic organization is very similar. The biggest differences are found in exon 1, so this exon could have evolved independently and become fused to exons 2-6 of a common progenitor. The mouse gene and protein were analysed in more detail and the transcript as well as the protein were found to be restricted to the olfactory epithelium, whereas vomeronasal neurons were negative for mSLP-3 staining(Kobayakawa et al., 2002). The promoter of the mouse and human gene contains a consensus site for the olfactory-specific transcription factor Olf-1. The protein was shown to be membrane-associated and enriched in a cilia membrane fraction of the olfactory epithelium. Mouse SLP-3 was detected in lipid rafts and was found to co-immunoprecipitate with caveolin-1 and adenylyl cyclase type III (ACIII), and cAMP-production was enhanced after incubation of cilia with an anti-SLP-3 antibody(Kobayakawa et al., 2002). These results indicate that SLP-3 could be involved in generating olfactory signals in a complex with caveolin and ACIII.

Recently, a paper describing the knockout of SLP-3 in mice was published. In their work, Wetzel et al. showed that the SLP-3 knockout mice have distinct defects in mechanosensation. The animals are viable and fertile, and they also respond to touch, but they show no response to certain mechanical stimuli, and certain types of mechanosensory neurons in the skin of the mice are defective (Wetzel et al., 2007).

2.1.5 Podocin

Podocin was discovered in an effort to identify a causative gene for autosomal recessive steroid resistant nephritic syndrome(Boute et al., 2000). The gene, named NPHS2, was mapped to 1q25-31. Positional cloning revealed that the NPHS2 gene encodes a novel stomatin family protein, which was almost exclusively expressed in the podocytes of fetal and mature kidney glomeruli. The protein was named podocin, and numerous mutations in the gene, which cause defects in glomerular filtration, have been described. Interestingly, most disease-causing mutations were found in the central region homologous to stomatin(Caridi et al., 2005).

Not surprisingly, podocin was found to be enriched in lipid rafts(Schwarz et al., 2001). The protein was shown to interact with nephrin (the protein product of the NPHS1 gene) and with CD2AP(Schwarz et al., 2001). Nephrin was identified as the protein product of the gene mutated in the finnish type of hereditary nephrotic syndrome, the most severe disorder(Kestila et al., 1998). Knockout-mice lacking CD2AP develop a nephrotic syndrome resembling NPHS mutations(Shih et al., 1999). All three proteins were shown to form a high-MW complex in lipid rafts, and lipid rafts were implicated in nephrin phosphorylation(Huber et al.,

2003). The clinical manifestations of mutations in the NPHS2 gene have drawn attention to the podocin protein. A great number of publications describing new cases and mutations have been published recently. To date, about 20 different NPHS2 mutations have been described in familial or sporadic cases of steroid-resistant nephrotic syndrome (Caridi et al., 2005). Some of the findings presented above, especially the complex between nephrin, podocin and CD2AP, have been challenged recently (Fan et al., 2006). Nevertheless, the essential role of podocin for the integrity of the glomerular slit diaphragm is undisputed, and future research will help improve treatment and diagnosis of hereditary nephrotic syndromes. In support of an interaction between podocin and nephrin, Nishibori et al. described podocin mutants, which interfere with wild-type nephrin trafficking(Nishibori et al., 2004). A recent paper also provided insights into the mode of plasma membrane targeting of podocin (Roselli et al., 2004). The protein was shown to be targeted to the PM through the classical exocytic pathway, and several mutated podocin variants were shown to be mislocalized (either to the ER or to late endosomes). Other mutations did not abolish PM targeting. Mutations causing mistargeting to the ER showed a more early onset of the nephrotic syndrome compared to mutations targeted to the PM. Another report stated that a podocin mutant retained in the ER (R138Q) could be refolded and correctly targeted to the PM through the addition of chemical chaperones(Ohashi et al., 2003). These compounds might lead to the development of novel therapeutic strategies for patients with podocin mutations. In a very interesting article dealing with the cholesterol binding properties of podocin and MEC-2, Huber et al. demonstrated that podocin binds cholesterol in its SPFH domain and that cholesterol binding is essential for regulation of a TRP family ion channel in kidney cells (Huber et al., 2006). For our group, which is interested in the function of stomatin, mutations in amino acids conserved between stomatin and podocin might provide insights into the function of the core stomatin region.

2.2 Stomatins in *C. elegans*: Mecs and Uncs and several more!

Several stomatin family members have been identified in genetic screens of the model organism *C. elegans*. The genetic data underline the importance of stomatin family members in *C. elegans* and had a big impact on the proposed function of human stomatin.

Shortly after the genomic sequence of *C. elegans* was finished, it was recognized that the worm genome contains 10 different stomatin family members. Compared to the human genome, which contains only 5 stomatin family members, this is striking, because for the most protein families, the number of members has increased during the course of evolution from a simple worm to homo sapiens. Three stomatin family proteins, MEC-2, UNC-1 and UNC-24, have been characterized in detail. All three were identified in genetic screens and mutations in the genes were found to cause distinct phenotypes. Evidence was collected that these proteins have important functions in the nervous system of the worm, influencing normal locomotion, mechanosensation and sensitivity to volatile anesthetics. These data have

led to the proposal that human stomatin might have a similar function and that the common mechanism could be the interaction of stomatin family members with ion channels. A detailed overview of the data for each protein is presented in the following section.

2.2.1   The MEC-2 protein and mechanosensation in *C. elegans*

Mechanotransduction, the conversion of mechanical stimuli into an electrical signal, is an essential feature of all higher organisms. Hearing, touch sense and sense of acceleration are only a subset of features which rely on specialized mechanosensory cells, which generate electrical currents and transduce these signals to the CNS(Gillespie and Walker, 2001). Touch receptors in mammals are very difficult to study, because they are deeply embedded in the skin and only constitute a small fraction of total skin cells. The nematode *C. elegans*, which is composed of a constant number of cells and can be subjected to genetic screening methods after induced mutagenesis, was chosen by Martin Chalfie to study mechanotransduction (Chalfie and Au, 1989; Way and Chalfie, 1988). The worm contains only 6 touch receptor neurons (see figure 2A), which are characterized by typical 15-protofilament microtubules instead of 12-protofilament structures found in other cells. Chalfie and colleagues developed an assay to detect a changed response towards gentle or harsh touch and identified hundreds of so-called **mec**hanosensory mutants(Chalfie and Au, 1989; Chalfie and Sulston, 1981). Thirteen genes are needed for touch cell function (mec-2, mec-4 through mec-10, mec-12, mec-14, mec-15 and mec-18)(Gillespie and Walker, 2001). These genes are most likely directly involved in mechanosensation, because they do not cause general nerve cell degeneration. Several of these components fit well to the proposed model of an ion channel, which is linked to the extracellular matrix and to the microtubule cytoskeleton (figure 2C). The *C. elegans* MEC-2 protein, which shows high sequence similarity with stomatin in its central region (see alignment Figure 4), plays a central role in this model because it is proposed to link the ion channel composed of MEC-4 and MEC-10 to the microtubule cytoskeleton. Generation of force through touch displaces the extracellular matrix and thereby generates a mechanical force on the ion channel, which opens if the force is bigger than a threshold value. Expression of MEC-2 was shown to be restricted to the 6 touch receptor neurons(Huang et al., 1995). The MEC-2 protein contains an elongated N- and C-terminus compared to stomatin, the C-terminus containing a SH3 domain(Huang et al., 1995). Both extra portions of MEC-2 are not found in any proteins of mammals. In experiments where a permanently active channel (MEC-4D/MEC-10D) was expressed in Xenopus oocytes together with MEC-2, the activity of the mutant channels was increased by a factor of 40(Goodman et al., 2002). Deletion of either the elongated C-terminus or the N-terminus or both termini abolished this increase, indicating that both termini are involved in the regulation of channel activity(Goodman et al., 2002).

Figure 3: *C. elegans* mechanotransduction
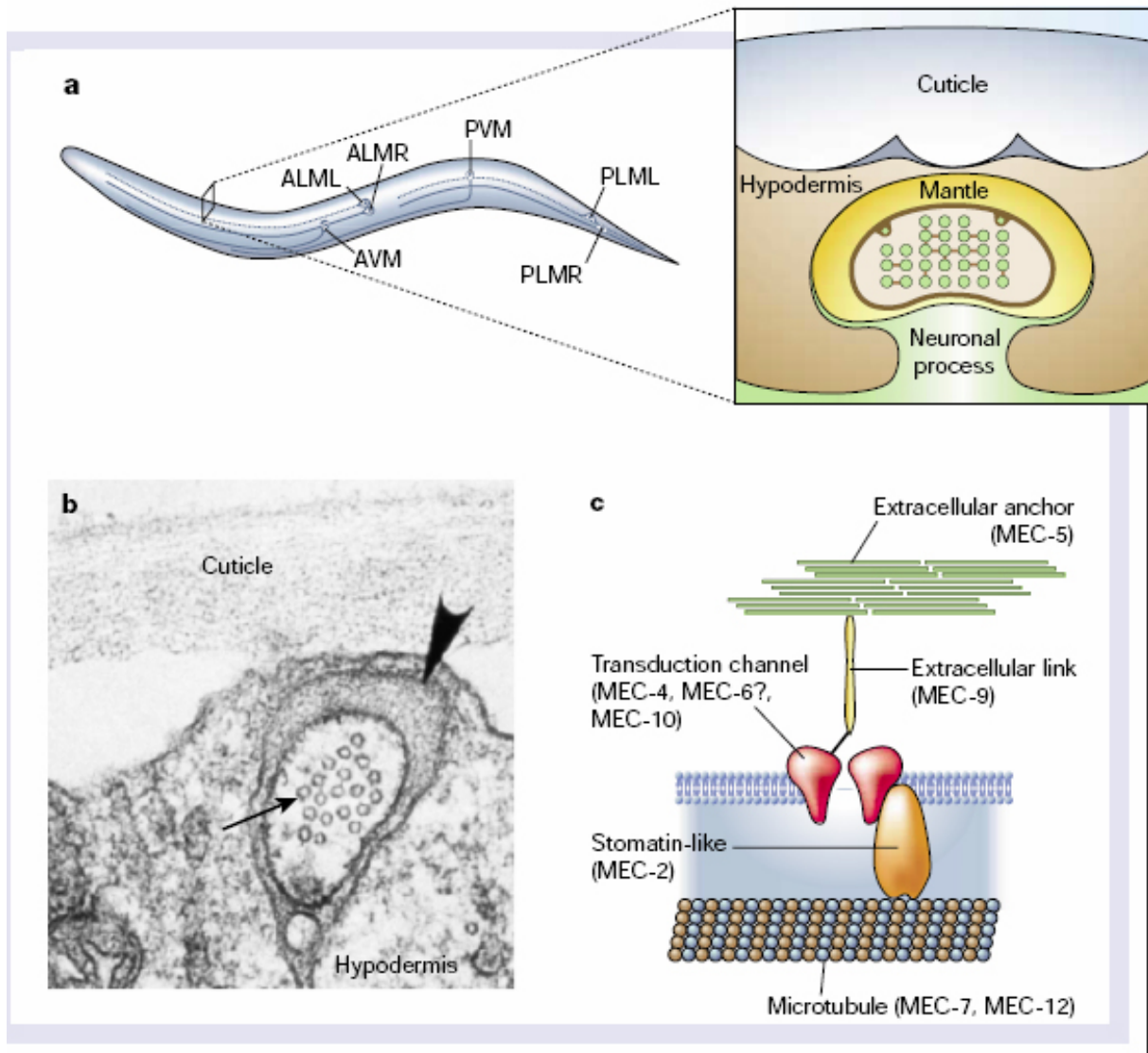
Figure 3: C. elegans touch-receptor structure and transduction model. Reprinted from (Gillespie and Walker, 2001). (A) View of C. elegans showing positions of mechanoreceptors. AVM, anterior ventral microtubule cell; ALML/R, anterior lateral microtubule cell left/right; PVM, posterior ventral microtubule cell; PLML/R, posterior lateral microtubule cell left/right. (B) Electron micrograph of a touch receptor neuron process. Mechanotransduction may ensue with a net deflection of the microtubule array relative to the mantle, a deflection detected by the transduction channel. Arrow, 15-protofilament microtubules; arrowhead, mantle. (C) Proposed molecular model for touch receptor. Hypothetical locations of mec proteins are indicated.

Nevertheless, these truncation mutants retained the ability to evoke small, but detectable, amiloride-sensitive currents. The central stomatin-homologous region of MEC-2 showed a strong dominant-negative effect when coexpressed with full-length MEC-2, indicating an oligomeric structure of MEC-2(Goodman et al., 2002). Interestingly, also stomatin could induce small, amiloride-sensitive currents when coexpressed with the mutant channel and also acted dominant-negative on full-length MEC-2(Goodman et al., 2002). This result suggests the formation of hetero-oligomers between MEC-2 and human stomatin. The interaction between MEC-2 and both the MEC-4 and MEC-10 channel subunits could be confirmed by

coimmunoprecipitation experiments in Xenopus extracts(Goodman et al., 2002).

In genetic screens for touch-insensitive mutants, 54 alleles of mec-2 were identified. More than half of these are missense mutations mapped to conserved positions in the central stomatin-like domain(Zhang et al., 2004a) (Figure 4). The data summarized above support a function for stomatin in the regulation of ion channels. Based on the findings that stomatin is palmitoylated and enriched in lipid rafts, Goodman et. al. summarize their results in this way,"We propose that the highly conserved, stomatin-like domain of MEC-2 provides an essential structural scaffold for interaction with DEG/ENaC proteins, with the lipids surrounding the channel or both."(Goodman et al., 2002) Recently, another stomatin family protein from *C. elegans*, UNC-24 was shown to be also expressed in touch receptor neurons(Zhang et al., 2004a). Unc-24 mutants are touch sensitive, but they strongly enhanced the touch-insensitive phenotypes of some mec animals(Zhang et al., 2004a). Also, UNC-24 protein could not replace MEC-2 in Xenopus patch-clamp experiments, but it was co-immunoprecipitated with MEC-2 as well as MEC-4(Zhang et al., 2004a). Further work will be necessary to clarify the influence of stomatin proteins on ion channels, but as Price et al.(Price et al., 2004) and Huber et al.(Huber et al., 2006) have described recently, this mechanism is also of high interest in humans.

For our work, the described MEC-2 mutants (P134S = *u274* allele; C140/174A = palmitoylation-deficient) deficient in cholesterol-binding could provide important insights also in the function of the human stomatin(Huber et al., 2006). As a consequence of these findings, a function of PHB-domain proteins in maintainance/formation of cholesterol-rich micro-environments and thereby regulating the function of ion channels is now accepted by most of the researchers in the field.

2.2.2   Uncoordinated worms: UNC-1 and UNC-24

Both the unc-1 and unc-24 mutants were identified in early genetic screens for genes essential for normal locomotion of the worm (Brenner, 1974). Wild-type worms show a sinusoid locomotion. After chemical or radiation-induced mutagenesis, worms with defects in locomotion could easily be separated from normal worms. Unc-1 and unc-24 alleles both showed defects in locomotion(Brenner, 1974). The genes could be cloned more than two decades later and revealed that both genes code for proteins which are homologous to human stomatin (Barnes et al., 1996; Rajaram et al., 1998).

UNC-1:

UNC-1 has approximately the same length as human stomatin and shows 52% identity to the human protein. Dominant and recessive alleles of unc-1 could be isolated in genetic screens(Park and Horvitz, 1986). These alleles showed complex genetic interactions, which led to the suggestion that the protein product of unc-1 should exist in an oligomeric form(Park and Horvitz, 1986).

Figure 4: Alignment of MEC-2 and human stomatin

Figure 4: Multiple sequence alignment of MEC-2 and human stomatin. Point mutations in conserved amino acids are marked by red boxes, whereas point mutations in non-conserved amino acids are marked by green boxes. The yellow boxes represent point mutations, where the mutated amino acid in the corresponding mec-allele is the same as in the stomatin sequence.

After the cloning of the unc-1 gene, the molecular defects in several different unc-1 alleles were identified(Rajaram et al., 1998). Some of these defects are missense mutations of amino acids conserved between UNC-1 and stomatin, which are very interesting for the investigation of the human protein function (see alignment Figure 47). The unc-1 gene was already found to be involved in regulating the sensitivity of *C. elegans* to volatile anesthetics(Morgan et al., 1990). Volatile anesthetics (VAs) are indispensable tools for medicine since they had been

introduced more than 150 years ago, yet their mode of action is very incompletely understood. *C. elegans* was chosen as a model system to identify target sites for the action of volatile anesthetics, because its nervous system is very simple compared to mammals. Recessive loss-of-function-mutations in unc-1 made the animals hypersensitive to diethylether, whereas the sensitivity to other VAs like halothane, enflurane and isoflurane remained unchanged(Morgan et al., 1990). Importantly, such mutations in unc-1 also suppressed the hypersensitivity of unc-79-animals to halothane and instead made the animals hypersensitive to diethylether(Morgan et al., 1990). Dominant unc-1 mutations increased sensitivity to all volatile anesthetics, but did not suppress unc79 hypersensitivity to halothane(Rajaram et al., 1998). Different alleles of unc-1 often had different effects on the sensitivity to volatile anesthetics. Reporter constructs with GFP under the control of the unc-1 promoter as well as expression of UNC-1-GFP fusions and immunostaining of the UNC-1 protein showed that unc-1 is broadly expressed in the nervous system of the worm(Rajaram et al., 1999). The unc-8 gene, which encodes a member of the degenerin family of sodium channels, shows a similar pattern of expression and mutant unc-8 alleles affect locomotion and anesthetic sensitivity similar to unc-1. Several unc-8 mutants could suppress the phenotypes of unc-1 alleles, but the opposite behaviour, suppression of unc-8 phenotypes by certain unc-1 alleles, was also observed. A complex of UNC-1, UNC-8 and UNC-79 was suggested, which should be a direct target for volatile anesthetics(Rajaram et al., 1999). Recently, UNC-1 was shown to be essential for lipid raft targeting of UNC-8 and could be coimmunoprecipitated with an anti-UNC-8 antibody(Sedensky et al., 2004). These results strongly support the proposed complex of UNC-1 and UNC-8.

UNC-24:

The first unc-24 alleles had also been described by S. Brenner in 1974. Unc-24 mutants especially have difficulties moving forward, whereas their backward motion is more pronounced (but also not wild-type)(Brenner, 1974). Unc-24 therefore was classified as a candidate B-circuit-specific gene (the B circuit of motor neurons is thought to govern forward locomotion). Worms carrying both unc-4 and unc-24 mutations cannot move at all and were used to screen for revertants of the unc-4 phenotypes (Miller et al., 1993). The function of the unc-24 gene was recognized to be closely related to the unc-1 gene. Null-alleles of both genes cause a similar locomotory defect, and mutations in both genes can suppress the hypersensitivity of animals with mutations in unc-79 to halothane (Sedensky et al., 2001). Additionally, an extragenic suppressor acting on both genes was described (Riddle and Brenner, 1978). The unc-24 gene was found to code for a protein sequence, which contained an SPFH domain and a SCP-2 domain in its C-terminus(Barnes et al., 1996). The long hydrophobic domain was also shared with stomatin, and a similar structure with both N- and C-termini cytoplasmic and a hydrophobic hairpin anchoring the protein to the PM was suggested. Based on this unique domain structure, a function of UNC-24 in lipid transfer between closely apposed membranes was proposed. Later, Sedensky et al. described a genetic

interaction between unc-24 and unc-1 and showed that the localization of UNC-1 is changed in unc-24 null animals(Sedensky et al., 2001). The protein is targeted to the PM of neurons in wild-type animals, whereas it accumulates in the perinuclear region of these neurons in unc-24 null animals, and the amounts of UNC-1 were strongly reduced. Further, unc-24 was found to be fully epistatic to unc-1 in respect to locomotion defects as well as to anesthetic sensitivity(Sedensky et al., 2001). The authors concluded that UNC-24 probably affects the expression or the stability of the UNC-1 protein, and propose that hetero-oligomers constisting of UNC-1 and UNC-24 might explain this behaviour. Later, they showed that, whereas unc-1 interferes with lipid raft targeting of UNC-8, UNC-24 does not interfere with lipid raft targeting of UNC-1 as initially expected(Sedensky et al., 2004).

A novel extragenic genetic suppressor of unc-1 and unc-24: ssu-1 (suppressor of stomatin uncoordination)

Recently, a gene was identified which suppresses the phenotype of unc-1 and unc-24 mutations(Carroll et al., 2006). The gene was cloned and was found to be a cytosolic ethanol sulfotransferase. Ssu-1 is the only such sulfotransferase in *C. elegans*. Reporter constructs revealed that its expression in the nervous system is not as broad as unc-1 expression, but that it is restricted to two ASJ neurons(Carroll et al., 2006). The mutation in ssu-1, which is responsible for suppression of the phenotype of unc-1, was identified as a deletion removing a big part of the C-terminus of the protein(Carroll et al., 2006). Based on its expression in ASJ neurons, which function in endocrine signalling, it was proposed that ssu-1 modifies signalling molecules, most probably sterols(Carroll et al., 2006). These signalling molecules must have some effect on the UNC-1 and UNC-24 proteins or on the ion channels putatively regulated by these proteins. If unc-1 negatively regulates the unc-8 degenerin channel, an unc-1 null mutation should cause increased channel activity, which leads to an unc phenotype. Ssu-1 activity is somehow necessary for the manifestation of this phenotype, because ssu-1(0) and unc-1(0) animals show normal locomotion. Mec-2 mutations were not suppressed by ssu-1, therefore ssu-1 is not a general suppressor of all stomatin family members(Carroll et al., 2006). The mechanism which is responsible for the suppression of the unc mutations is still unclear. Carroll et al. suggest that SSU-1 could be responsible for the sulfation of steroids, which are functioning as a second messenger and must be transported to the neurons where they could regulate UNC-1 and associated ion channels. Interestingly, neurosteroids have been shown to modulate the activity of GABA (A) receptors in the human brain (Majewska, 1992). In addition, the cholesterol content of the plasma membrane was found to influence the modulation of GABA (A) activity (Sooksawate and Simmonds, 2001). A mechanism where UNC-1 and sulfo-sterol signals generated by SSU-1 cooperatively regulate ion channel activity in *C. elegans* neurons can be envisaged. A central question for the future is whether similar mechanisms operate in human cells.

2.2.3   Even more stomatins in *C. elegans*

In addition to the three genes discussed above, sequencing of its genome revealed that *C. elegans* contains 6 more genes with protein products similar to stomatin. These genes are not well characterized, and some of them might be pseudogenes. STO-1, STO-2 and STO-5 have an extended N-terminus compared to human stomatin. Interestingly, they all have a characteristic long, hydrophobic domain close to their N-terminus. The amino acid sequence in this hydrophobic domain is not well conserved, but conservation is generally very high in the core stomatin domain after the hydrophobic region. Examination of a multiple sequence alignment of all stomatin family proteins in *C. elegans* except UNC-24 illustrates the high conservation, which leads us to the conclusion that the tertiary structure of this central region is probably well conserved. UNC-1, MEC-2 and STO-1 to STO-6 are closely related to human stomatin and not to SLP-1/UNC-24 or SLP-2. A SLP-2 orthologue is also present (named stomatin-like-1=STL-1 to increase confusion). STL-1 shows 60% identity and 80% similarity to human SLP-2. No functional data are available for this gene/protein. It is an interesting question why *C. elegans* contains 8 closely related stomatins, whereas mammals (to our knowledge) only contain 3 closely related stomatin family members (stomatin, SLP-3 and podocin). At the moment, answers to this question are purely speculative. One possibility is that some functions of the stomatin proteins in *C. elegans* might have been transferred to the flotillin protein family, which is not represented in the *C. elegans* genome. The sto-1 and sto-2 genes were recently identified as candidate genes for a specific expression in ciliated neurons of *C. elegans* by two independent methods (serial analysis of gene expression (SAGE) and a bioinformatics screen for binding sites of a cilia-specific transcription factor)(Blacque et al., 2005). This is the first evidence that these genes could have a specialized function. Reporter constructs under the control of the sto-6 promoter were recently found to be broadly expressed in the nervous system of *C. elegans* (Zhang et al., 2004b). The same study also revealed that UNC-24 is probably widely expressed in the nervous system of the worm. No experimental data are available for sto-3. All 6 sto genes are found on the X chromosome, and are probably the result of gene duplications. Most of the predicted genes are supported by cDNA-sequences, and they are also present in different worms like *C. briggsae* and *C. remanei*. Therefore, it is possible that every different stomatin fulfils a specialized function, but as we can not be sure if the sto-1 to sto-6 genes are functional and expressed, future work could also show that the number of expressed stomatin family members is even lower than in mammals.

In addition to these "core" stomatin family members, the *C. elegans* genome also contains 2 prohibitin genes.

2.3 The distantly related prohibitin, flotillin and HflK/C protein families

2.3.1 The prohibitin protein family: A mitochondrial story at the PM?

Two genes encoding prohibitin family proteins are present in mammals: *PHB1* and *PHB2*. The two proteins share a highly conserved mid-region, whereas the N- and C-termini are less conserved(Coates et al., 1997). Prohibitin homologues have been described in mammals, *C. elegans*, plants and yeast. These family members are highly conserved, suggesting an important function for the proteins. Additionally, homologues to both proteins were also found in the Cyanobacterium *Synechocytis*(Coates et al., 1997), highlighting the ancient origin. Prohibitin-1 has been described as an intracellular protein, which blocks DNA synthesis. It has been cloned in an effort to identify anti-proliferative genes, and micro-injection of the in-vitro synthesized mRNA into fibroblasts and HeLa cells resulted in strongly reduced DNA synthesis(Nuell et al., 1991). Several years later, a refined analysis showed that the growth-suppressive activity of the prohibitin mRNA is localized to the 3' UTR and that microinjection of the protein-coding sequence alone had no effect(Jupe et al., 1996). Prohibitin could be localized to mitochondria(Coates et al., 1997; Ikonen et al., 1995) and the *S. cerevisiae* homologues of prohibitin-1 and -2 were found to regulate replicative lifespan of the yeast(Coates et al., 1997). Deletions of either the *PHB1* or *PHB2* or both genes resulted in decreased survival of the cells after a number of cell divisions compared to control cells(Coates et al., 1997). The effects of the deletions were additive, suggesting that *PHB1* and *PHB2* may be involved in the same processes(Coates et al., 1997). Defective mitochondrial segregation was observed in *PHB* mutants and was suggested as an explanation for the shortened replicative life span(Piper et al., 2002).

Interestingly, prohibitin-1 and prohibitin-2 were also described to non-covalently associate with the IgM antigen receptor on B lymphocytes(Terashima et al., 1994) (prohibitin-2 was consequently named as BAP37, this designation is still common) and were found to be enriched in B cell lipid rafts(Mielenz et al., 2005). These studies suggest that the prohibitins can associate with the plasma membrane in lymphocytes. Similar to other SPFH family members, the prohibitins were shown to form high-order hetero-oligomers, but in the inner mitochondrial membrane(Nijtmans et al., 2000). Nijtmans et al. suggested a function as membrane-bound chaperones for the yeast Phb1/2 complex based on observations that it stabilizes mitochondrial translation products and is up-regulated when the balanced expression of COX-subunits is disrupted(Nijtmans et al., 2000). Tatsuta et al. also analysed the yeast prohibitins and confirmed the hetero-oligomeric complex in the inner mitochondrial membrane. They identified an unconventional, non-cleavable N-terminal presequence, which is essential for mitochondrial targeting of the yeast Phb1 protein and determined that the TIM23-translocase mediates membrane insertion(Tatsuta et al., 2005). Additionally, they analysed purified prohibitin complexes by single particle electron microscopy and found that these complexes are ring-shaped(Tatsuta et al., 2005), which indicates a possible scaffolding

function for the yeast prohibitins in the mitochondrial membrane. Importantly, the Phb1/2 complex was found to directly interact with the mitochondrial AAA-protease which mediates degradation of misfolded mitochondrial membrane proteins(Steglich et al., 1999), also supporting a role for the prohibitins in the modulation of membrane protein proteolysis.

Prohibitin-1 was identified in a yeast two-hybrid screen as an interaction partner for the retinoblastoma (Rb) protein, which inhibits E2F transcriptional activation(Wang et al., 1999a). Further studies indicated that prohibitin-1 can directly interact with E2F and the kinase Raf-1(Wang et al., 1999b). To increase confusion, prohibitin-1 and Rb were shown to co-localize in the nucleus, and prohibitin-1 was shown to recruit other proteins (e.g. HDAC1) for transcriptional repression(Wang et al., 2002). Another study showed that prohibitin can also interact with the p53 tumor suppressor protein in vitro and in vivo and appears to induce p53 –mediated transcription(Fusaro et al., 2003). This study also showed a substantial nuclear localization for prohibitin-1 in breast cancer cells, which is reduced upon induction of apoptosis. The 3' UTR RNA of prohibitin1 has recently received much attention in cancer research, because it was shown to suppress tumor formation in nude mice when introduced into the MCF7 breast cancer cell line(Manjeshwar et al., 2003) and because a polymorphism in this region was described, which increased breast cancer susceptibility(Jupe et al., 2001). The results on the increased breast cancer susceptibility, though, could not be confirmed in another study(Campbell et al., 2003). Additionally, the 3'UTR was shown to decrease breast tumor cell motility (Manjeshwar et al., 2004). Independently, prohibitin-2 was identified as an interaction partner for the estrogen receptor(Montano et al., 1999). Recently, it was reported that prohibitin-1 is recognized by a monoclonal antibody raised against the SV40 Large T antigen. The antigenic epitope is necessary for immortalization of cells by the SV40 Large T, and the authors speculate that the Virus could thereby overcome cell cycle repression by prohibitin(Darmon and Jat, 2000).

The data presented here for the prohibitin proteins seem conflicting. There are several unsolved questions concerning the subcellular localization and function. The subcellular localization seems to be different in different cell types (plasma membrane in B lymphocytes(Terashima et al., 1994); mitochondria in HeLa cells(Coates et al., 1997), BHK cells(Ikonen et al., 1995) and in yeast(Nijtmans et al., 2000; Tatsuta et al., 2005); nucleus in MCF7 and T47D breast cancer cells(Fusaro et al., 2003)). One open question is how prohibitin-1, which is widely regarded as a type-I transmembrane protein of the inner mitochondrial membrane, can alternatively be targeted to the nucleus or the plasma membrane under different conditions. It should be noted that the N-terminal, putative membrane-spanning hydrophobic domain of prohibitin-1 is not found in the yeast homologue. Of course, the interaction of prohibitin-1 with key regulators of the cell cycle like Rb and p53 and its regulation by c-myc(Menssen and Hermeking, 2002) is very interesting and also fits well to its anti-proliferative function. Also, mitochondrial integrity is critical for cell proliferation and survival, which could also explain the importance of prohibitin for cell proliferation. Finally, the anti-proliferative effect of the prohibitin 3'UTR is still enigmatic. Based on our current knowledge, one can conclude that the prohibitins seem to be very versatile proteins with

important functions. Further research will eventually shed light on the underlying mechanisms which are responsible for the puzzling variety of prohibitin functions. For readers who are interested in more details, I would like to mention two reviews on the prohibitin proteins, one by Nijtmans et al(Nijtmans et al., 2002), which critically discusses the relevance of non-mitochondrial functions for the prohibitins, and a second one by Mishra et al.(Mishra et al., 2006), which cleary promotes the importance of extra-mitochondrial functions for these proteins and adds even a new facette by mentioning the observation that prohibitins are also detected in human serum (probably they are released into the circulation via lipid droplets), and that prohibitin-1 strongly binds complement component C3.

2.3.2 Flotillins/Reggies

Flotillins/Reggies have been identified independently by 3 different groups. First, a cDNA encoding a N-terminally truncated version of flotillin-2 was identified and sequenced in an approach to identify the antigen of the antibody ECS-1, which recognized a protein on the surface of skin cells(Schroeder et al., 1994b). The gene product (which essentially was a large fragment of flotillin-2) was named ESA (epidermal surface antigen), and it was considered to play a role in epidermal structure and maintainance, but later, it was recognized that the ECS-1 antibody did not recognize this protein(Hazarika et al., 1999). Several years later, Schulte et al. identified two related proteins, which were strongly upregulated in regenerating nerve cells of zebrafish, and named them reggie-1 (= flotillin-2) and reggie-2(flotillin-1)(Schulte et al., 1997). In the same year, Bickel et al identified two novel proteins in the floating lipid raft fractions from mouse lung tissue and named them flotillin-1 and flotillin-2(Bickel et al., 1997). The name flotillins nowadays is most commonly used, so I will stick to this designation. Flotillin proteins are widely used as marker proteins for lipid rafts, because they are particularly strongly enriched in these low-density, cholesterol-enriched fractions, but the exact function of the proteins is still not known. Nevertheless, the flotillins can now be considered the best–studied members of the SPFH superfamily. Well-conserved homologues are found in drosophila, and related proteins are found in some bacteria, plants and fungi. Flotillins have been shown to participate in important cellular processes in human and zebrafish. Recently, the 3D structure of a soluble fragment of mouse flotillin-2 has been determined (see Figure 5).

A small outline of the flotillin structure and proposed functions is given below.

Flotillins do not contain a very long, hydrophobic domain at their N-termini like stomatin. They are quite hydrophobic at their N-terminus, but these hydrophobic stretches are thought

Figure 5: 3D structure of a fragment of flotillin-2
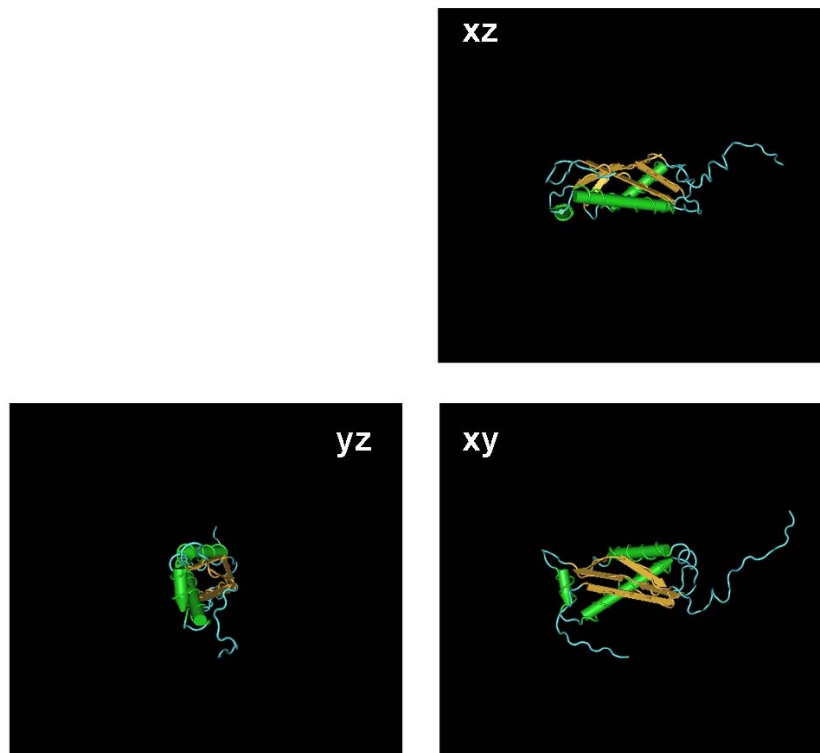
Figure 5: Schematic 3D structure of a soluble fragment of flotillin-2/reggie-1. PDB accession number 1WIN. The structure was visualized with the Cn3D programme. Alpha-helical regions are shown in green, beta sheets are shown in yellow.

not to span the bilayer, but to associate with it. Anchoring to the cytoplasmic leaflet is mediated by myristoylation and palmitoylation (flotillin-2)(Neumann-Giesen et al., 2004) or only by palmitoylation (flotillin-1)(Morrow et al., 2002). At their C- termini, both flotillins contain a flotillin domain which is characterized by numerous EA (glutamic acid-alanine) repeats. This domain is necessary for homo-oligomerization(Neumann-Giesen et al., 2004), which is probably mediated by formation of coiled coils in the EA-rich region.

Proposed functions of flotillins/reggies:

The zebrafish reggie proteins were found to be co-immunoprecipitated with zebrafish Thy-1, and this association is also conserved in different mammalian cell types like PC12 cells and lymphocytes(Deininger et al., 2003; Lang et al., 1998). Flotillins/reggies can also be co-immunoprecipitated with other GPI-anchored proteins like F3/contactin(Stuermer et al., 2001) and the Prion Protein (PrP^c)(Stuermer et al., 2004), which suggests a role for the proteins in signal transduction through GPI-anchored proteins. The flotillins also seem to be closely associated with the Src-family kinases lck and fyn, as revealed by co-immunoprecipitation and co-localisation (LM and ELMI). Two further transmembrane proteins, the ABCA1 transporter and the thrombin receptor PAR-1, have been co-immunoprecipitated with flotillin-2. The proposed function as a regulator of cytoskeletal dynamics is supported by the induction of filopodia by over-expression of flotillin-2 in several cell types(Hazarika et al., 1999) and

by the interaction of the sorbin homology (SoHo) domain of adaptor proteins of the vinexin family and flotillin-1(Kimura et al., 2001). The vinexin family of adaptor proteins includes vinexin alpha and beta, CAP/ponsin and ArgBP2(Kioka et al., 2002). These proteins are characterized by a N-terminal SoHo domain and a C-terminal SH3 domain. The SoHo domain is proposed to mediate membrane association via the interaction with flotillin-1, whereas the SH3 domain can interact with a variety of proteins (c-Cbl, vinculin, afadin, Grb4 and Sos). Flotillin-1-dependent recruitment of a CAP/c-Cbl complex was shown to be essential for insulin-stimulated translocation of the GLUT4 glucose transporter from cytoplasmic vesicles to the plasma membrane in adipocytes(Baumann et al., 2000). Flotillins also seem to play an essential role in T-cell activation. They are thought to control the assembly of signalling complexes and cytoskeletal rearrangements necessary for prolonged TCR-signalling via interaction with lck, fyn and the adaptor protein LAT. Furthermore, flotillin-1 and -2 show a polarized localization in resting lymphocytes, forming a so-called "preformed cap". Recently, it was demonstrated that flotillin-2 is practically immobile in this cap structure, whereas it is highly mobile in the rest of the plasma membrane(Rajendran et al., 2003). Stimulation of the cells by cross-linking of cell surface components leads to the accumulation of the TCR signalling machinery in this pre-formed cap, which underscores the importance of flotillins in T cell activation. Flotillins could also be involved in the pathogenesis of neurodegenerative disorders like Alzheimer and BSE/CJD/scrapie. Both flotillins are highly expressed in the brain, and lipid rafts are thought to play a role in the formation of amyloid beta(Aß) protein, the major constituent of senile plaques. Primitive senile plaques showed strong flotillin-2 labeling, and in AD patients, staining for flotillin-2 in the cortex was increased. Progression of AD seems to be accompanied by an accumulation of flotillins at sites of Aß production(Kokubo et al., 2000). Likewise, the accumulation of the disease form of the Prion protein (PrP) probably takes place in lipid rafts, and the flotillins seem to be closely associated with the GPI-anchored PrP. Of course, the direct involvement of the flotillins in the pathogenesis of these disorders is not proved yet and further investigations will be necessary to reveal their exact role in these processes.

For me, the most interesting publication on the flotillin proteins in the last years was published by Glebov et al. in 2006. This paper describes a novel, non-clathrin and non-caveolin-dependent endocytic pathway, which is defined by the presence of flotillin-1 in the endocytic structures(Glebov et al., 2006). The authors could show that the non-clathrin and non-caveolar uptake of Cholera-toxin B is strongly reduced upon depletion of flotillin-1 by siRNA, which suggests a role for flotillin-1 in the endocytic pathway. Nevertheless, the article also shows that the endocytic pathway is rather complex and that the same cargo can utilize different uptake pathways. Down-regulation of one pathway may then be compensated by up-regulating another one and thereby, overall uptake might not be different. The authors admit that they can not rule out the possibility that flotillin might be a cargo instead of a component of the transport machinery, but most likely, flotillin-1 participates in the formation and transport of non-clathrin- and non-caveolin-coated endocytic structures. A mechanism for the formation of "permanently coated" caveolin transport vesicles in the endocytic system has

recently been proposed by Bauer et al.(Bauer and Pelkmans, 2006), and similar flotillin-1 transport intermediates might also exist. For us, these reports offer the fascinating possibility that stomatin might also define a separate endocytic pathway, which could directly connect the plasma membrane and the late endocytic compartment.

2.3.3 HflK/C proteins in bacteria

HflK/C are two polypeptides, which are encoded by genes in the *hflA* (high frequency of lysogenization) locus of *E. coli*, which governs the lysis-lysogeny decision of bacteriophage λ by controlling the stability of the phage cII protein. The two proteins HflK and HflC have molecular weights of 46 and 37 kDa, respectively, and were found to be membrane proteins with putative transmembrane helixes close to the N-terminus(Noble et al., 1993). It was already recognized in 1993 that the two proteins share sequence homology with each other and with stomatin(Noble et al., 1993). Additionally, HflC was shown to contain a domain distantly related to the catalytic domain of bacterial and chloroplast ClpP proteases, which gave rise to the theory that the HflK/C complex itself might be able to proteolytically cleave cII. Indeed, cleavage of cII by a purified HflA protein complex had been described several years ago(Cheng et al., 1988). But Kiahara et al. could show later that the HflK/C proteins form a complex with the AAA-Protease FtsH (encoded by the *hflB* locus) and inhibit the degradation of mutant, uncomplexed SecY by FtsH(Kihara et al., 1996). In further experiments, it was shown that both HflK and HflC are typeII transmembrane proteins, with their short N-termini being cytoplasmatically oriented and with their larger C-termini protruding into the periplasmic space of *E. coli*, which strongly argues against proteolytic processing of cytoplasmic cII by the HflK/C complex(Kihara et al., 1997). Additionally, the authors could not reproduce the proteolytic cleavage of cII by a purified HflK/C complex and concluded that the described purified HflA complex probably also contained traces of either an unknown protease or of FtsH, thereby explaining the observed cII degradation in vitro. Consequently, it is now widely accepted that a complex of HflK/C and FtsH exists in the plasma membrane of *E. coli*, with the HflK/C complex modulating the degradation of polypeptides mediated by FtsH(Ito and Akiyama, 2005). The degradation of mutated/misfolded membrane proteins by the AAA-protease FtsH and the negative regulation of the proteolytic function by HflK/C is very similar to the prohibitins in mitochondria, which also interact with an AAA-protease and protect newly synthesized, unassembled polypeptides from degradation. This similarity has led Tavernarakis et al. and others to the suggestion that the other SPFH family members could also have a function in the regulation of membrane-associated protein degradation(Tavernarakis et al., 1999). In my opinion, this speculation is not backed up by any experimental data. Recently, a number of interaction partners have been described for other member s of the SPFH family like flotillin-1, podocin and stomatin. No associations with AAA-proteases have been described, and a "membrane chaperone" activity for these family members is also purely speculative. More work is necessary to clarify the precise function of the SPFH domain. Additionally, the level of sequence conservation is

generally low between different branches of the SPFH family, which, together with the ancient origin of the different subfamilies, makes a deduction of the protein function from the comparison of sequence data very unreliable. During evolution, the core fold of the SPFH domain may have been conserved, but the functionally important regions for protein-protein interactions may have been subject to big changes, leading to widely different functions for the different family members. Still, the functional similarities between HflK/C and the prohibitins are very interesting and will help to gain more insights into the functional determinants of the SPFH domain.

2.4 Lipid rafts: A controversial concept for membrane organisation

A detailed description of the basic concept of lipid rafts was already given in my diploma thesis(Mairhofer, 2001). I would not like to fully reproduce this summary here, but instead would like to focus on the relevant contributions made since 2001. Nevertheless, I would like to start with a short introduction to the topic.

2.4.1   The lipid raft hypothesis

Pioneering studies on lipid sorting in epithelial cells were performed in the laboratory of Kai Simons at the EMBL in Heidelberg. First, Simons and Gerrit van Meer noticed that enveloped viruses, which either bud from the apical (foul paque virus, an avian influenza virus) or basolateral (vesicular stomatitis virus) membrane of polarized MDCK cells, have a different lipid composition in their envelopes(van Meer and Simons, 1982). Next, they made use of a fluorescently labeled phospholipid analogue (NBD-ceramide), which is metabolically converted either into NBD-glucosylceramide or NBD-sphingomyelin in the golgi apparatus. This lipid probe proved to be especially valuable, because both NBD-glucosylceramide and NBD-sphingomyelin were found to be enriched at the apical surface(van Meer et al., 1987). From these experiments, they deduced a model where lipid sorting was proposed to happen in the golgi apparatus or in post-golgi carriers and where lateral segregation of the lipids in the plane of the membrane was the key step, with the subsequent formation of apical or basolateral carriers enriched in certain lipids(Simons and van Meer, 1988). Other groups reported at the same time that several GPI-anchored proteins also followed the apical transport pathway(Lisanti et al., 1988). In 1992, a crucial paper by Brown and Rose revealed that apically destined lipids and a GPI-anchored protein get detergent-insoluble after they leave the golgi apparatus and introduced the method of Triton-X-100 lysis and sucrose density gradient centrifugation for the isolation of glycolipid- and cholesterol-enriched membrane domains(Brown and Rose, 1992). In such a sucrose gradient, a detergent-insoluble membrane fraction enriched in certain lipids and proteins "floats" to the top of the gradient. The method for the preparation of detergent-resistant membranes (DRMs) was easy to

perform and led to the characterization of the major protein constituents of the DRM fractions in the following years. Another important paper drew a connection between model membranes and cultured cells and described that saturated acyl chains are crucial for detergent insolubility of GPI-anchored proteins and lipids(Schroeder et al., 1994a). All these results led to the formation of the lipid raft hypothesis, a term coined by Simons and Ikonen in 1997(Simons and Ikonen, 1997). The lipid raft hypothesis states that certain proteins and lipids are specifically targeted to sphingolipid- and cholesterol-enriched membrane domains, which are in a more ordered state than the rest of the surrounding bilayer. This liquid-ordered (l_o) domain is resistant to solubilization by cold detergent and was proposed to "float" in a sea of membrane in the liquid-disordered (l_d) state. The co-existence of l_o and l_d membrane domains had already been described in model membranes, and detergent-resistance was shown to correlate well with targeting to ordered or disordered domains(Ahmed et al., 1997; Schroeder et al., 1994a).

2.4.2   Lipid raft "proliferation and growth"

The isolation of numerous signalling proteins in detergent-resistant membranes strongly raised the interest for these freshly introduced lipid raft domains(Simons and Toomre, 2000). In the next years, DRM isolation and disruption of lipid rafts by cholesterol depletion were the major tools for cell biologists and led to the proposal that important cellular processes depend on lipid raft microdomains(Brown and London, 1998; Simons and Toomre, 2000; van der Goot and Harder, 2001). Cholesterol depletion can be performed by treating cells with agents like methyl-beta-cyclodextrin (mβCD), which removes cholesterol from the plasma membrane, with agents which complex cholesterol in the lipid bilayer (filipin, digitonin) or by prolonged incubation with inhibitors of cholesterol biosynthesis(Simons and Toomre, 2000). Acute cholesterol depletion by treatment with mβCD developed into the most commonly used method. It was recognized that especially proteins which possess a saturated lipid anchor (palmitoylation, myristoylation or GPI-anchor) are enriched in DRM fractions, whereas proteins with unsaturated lipid anchors (for example a geranyl-geranyl-group) are excluded from lipid rafts. Additionally, some integral membrane proteins were detected in the lipid raft fractions. The lipid-anchored proteins include Src-family kinases (like lck, lyn, fyn and others), subunits of hetero-trimeric G proteins ($G_{\alpha i}$, $G_{\alpha s}$), H-ras and GPI-anchored proteins like PLAP, the folate receptor, CD59 and CD55. Integral membrane proteins detected in the lipid raft fractions were the untypical hydrophobic hairpin-loop proteins caveolin and stomatin, LAT, influenza hemagglutinin (HA) and neuraminidase and CD36. Caveolin and the flotillins developed into the most important marker proteins for lipid rafts, because these proteins show a very strong enrichment in the DRM fractions and high-quality antibodies are commercially available from Transduction Laboratories. These "early" lipid raft proteins all show strong enrichment in biochemically isolated DRMs. As non-raft markers, integral transmembrane proteins like the transferrin receptor (CD71, TfR) are most widely used. The most important examples for lipid raft function were, besides apical sorting in epithelial cells,

signalling through the T-cell receptor (Moran and Miceli, 1998; Viola et al., 1999) and the B-cell receptor (Aman and Ravichandran, 2000; Petrie et al., 2000). Of course, although the basic concept soon turned popular, the idea of lipid rafts was highly controversial. Inside the "lipid raft community", it was clear that one can not rely on detergent resistance as the sole criterion for lipid raft association and that more sophisticated methods, which should be able to prove the existence of lipid rafts in vivo and elucidate the important questions regarding lipid raft size and dynamics, are necessary. Advanced light microscopy methods like single particle tracking, FRET and FRAP were considered to be the methods of choice for the examination of lipid rafts in vivo. In the meanwhile, based on DRM isolation, also many of the low-abundance constituents of lipid rafts were identified, which often showed very weak enrichment in lipid raft fractions, leading to the state that we now have hundreds of potentially lipid-raft associated proteins. Of these proteins, many fulfil important functions in the cells, and these functions have often been inhibited by cholesterol depletion, leading to the situation that virtually every process in the cell is dependent on lipid raft microdomains according to published literature. In my opinion, the lipid raft hypothesis, which, most importantly, raised the attention for the function of lipid domains in cellular transport- and signalling-processes, had somehow been hi-jacked to explain many enigmatic processes without careful examination of the biochemical and cell biological evidence. In addition, although the hypothesis stresses the importance of lipids for sorting and phase separation in the lipid bilayer, the analysis of lipid constituents was neglected in favour of an analysis of the DRM protein constituents. Together with the flood of published papers on lipid rafts, some major drawbacks in attempts to analyse lipid rafts in vivo led to the current situation, where major doubts are cast on the significance of the lipid raft hypothesis in vivo(Edidin, 2001; Lai, 2003; Munro, 2003).

2.4.3 Shrinking rafts back to a "healthy" size

As already mentioned above, lipid rafts have proven difficult to be detected in vivo. Based on solubilization with cold Triton X-100, a major proportion of the plasma membrane was found to be detergent resistant. This behaviour was most commonly not reflected by examination of live cells with advanced methods. In an early single particle tracking study, Pralle et al. concluded that lipid raft associated GPI-anchored proteins diffuse as stable, small entities of approximately 26 nm diameter(Pralle et al., 2000). This size is clearly beyond the limit of resolution of light microscopy. Diffusion of a fluorescent lipid probe was analysed in muscle cells by Schütz et al(Schutz et al., 2000). This study stated that a lipid probe with saturated acyl chains occupied much larger domains (0.7 μm in diameter), but these results may be cell-type specific, because they could not be reproduced in other studies. Generally, most single-particle tracking studies gave results which are only consistent with the model of pre-existing rafts if these rafts are 1) small/short-lived and/or 2) their constituents exchange rapidly with the bulk membrane (for a review, see Kusumi et al.(Kusumi et al., 2005)). Other techniques like FRET also failed to detect stable clusters of GPI-anchored proteins(Kenworthy et al.,

2000). On the contrary, Zacharias et al., who used raft probes tagged with monomeric GFP-variants targeted to the inner leaflet of the plasma membrane, could show that these probes are clustered in a cholesterol-dependent manner and also co-cluster with caveolin in a FRET assay (Zacharias et al., 2002). This assay made use of the different dependence of FRET efficiency on acceptor density when the fluorophores are clustered or randomly organized(Kenworthy, 2002; Zacharias et al., 2002). The large scatter in the results by Zacharias et al. makes a precise determination of cluster size impossible, but also suggests that cluster size could be quite heterogenous(Kenworthy, 2002). Interestingly, a non-raft probe also showed clustering, but in a cholesterol-independent manner(Zacharias et al., 2002). A specialized FRET-technique, homo-FRET, which monitors changes in signal anisotropy, was used together with theoretical modeling by Sharma et al. and revealed clustering of 20-40% of GFP-tagged GPI-anchored proteins, but again, the clusters were proposed to be very small (< 5nm) and to contain only four GPI-anchored proteins(Sharma et al., 2004). This nanoscale clustering was sensitive to cholesterol depletion, which indicates that the observed clusters could be very small lipid rafts(Sharma et al., 2004). This deduced small size of lipid rafts already comes close to the lipid shell-model proposed by Anderson and Jacobson(Anderson and Jacobson, 2002), which states that membrane proteins (or membrane-anchored proteins) can be encased in a shell of cholesterol and sphingolipids. These small lipid shells determine if a protein partitions into DRMs or not and can coalesce into large lipid rafts dependent on protein interactions. This model is still different from the concept of boundary lipids, because the proposed lipid shells should be much more stable than boundary lipids (boundary lipids are only detected by electron spin resonance measurements). A big caveat of this model is that it is hard to imagine how a single lipid anchor (consisting of two fatty acids) could organize the surrounding lipids in a way to induce a relatively stable lipid shell(London, 2005). For membrane proteins, this model is even more problematic, because in model membranes, transmembrane domains are excluded from liquid-ordered domains and are thought to disturb the formation of ordered domains(London, 2005). A FRAP study by Kenworthy et al. also failed to detect diffusion of raft proteins in stable structures(Kenworthy et al., 2004). Instead, the type of membrane anchor (transmembrane, GPI-anchor, palmitoylation) was found to be most important(Kenworthy et al., 2004). Cholesterol depletion and temperature variation affected both raft- and non-raft proteins in a similar manner. The authors concluded that rafts can not be stable, mobile structures (which diffuse as stable entities on the cell surface and should dominate the diffusion coefficient of raft-associated proteins), but either are very dynamic structures or do not exist at all(Kenworthy et al., 2004). Another set-back for the field of lipid rafts was the observation that Triton X-100 itself can induce domain formation in model membranes(Heerklotz, 2002; Heerklotz et al., 2003). Although the results by Heerklotz and colleagues are not undisputed(Brown, 2006; London, 2005) and the technique of detergent solubilization had been critisized before(Edidin, 2001), these studies had a big impact on the field. Before, most researchers were aware that detergent solubilization can induce artefacts and that DRMs are surely different from native rafts in living cells. Nevertheless, based on observations in model

membranes, most people were confident that the DRMs might at least give a good hint for the composition of rafts in living cells. With the observation that the detergent itself can promote domain formation in a up-to-then homogenous mixture, doubt was cast on all these results(Heerklotz, 2002). Now, all researchers agree that detergent-resistant membranes should not be identified with lipid rafts in living cells(Brown, 2006; Hancock, 2006; Lichtenberg et al., 2005; Mayor and Rao, 2004). Detergent resistance is still considered to yield important information by some researchers(Brown, 2006), while others state that only sophisticated imaging techniques can provide information about the lipid raft association of certain molecules. In addition to the possibility that detergent might induce domain formation, the other key biochemical technique to determine if a process is dependent on cholesterol-enriched rafts, cholesterol depletion, also was discredited recently. As Kwik and colleagues showed, depletion of cellular cholesterol by treatment of cells with mβCD had a profound effect on the cytoskeleton(Kwik et al., 2003). Additionally, cholesterol depletion was shown to induce domain segregation in living cells, an effect which is also inconsistent with the usage as a raft-disrupting agent(Hao et al., 2001). The third major drawback for the lipid raft hypothesis came from studies on the prototype of lipid raft-dependent signalling, the T-cell receptor: First, Glebov and Nichols, using FRET analysis, showed that GPI-anchored lipid raft probes have a random distribution during activation of Jurkat T-cells with antibody-coated beads(Glebov and Nichols, 2004). Second, Douglass and Vale performed single-molecule microscopy on Jurkat T cells activated on antibody-coated glass coverslips and found evidence for membrane microdomains. But these microdomains were shown to be dependent on protein-protein interactions rather than on lipid rafts(Douglass and Vale, 2005). On the contrary, using Jurkat T-cells and peripheral blood CD4+ T-cells stimulated by Antigen-Presenting Cells (APCs), Tavano et al. could show an enrichment of lipid raft markers at the immunological synapse, whereas non-raft markers were not enriched(Tavano et al., 2006). They also showed that the co-stimulatory molecule CD28 and FilaminA are essential for raft accumulation at the immunological synapse. This recent paper almost certainly reflects the in-vivo situation better than activation with antibody-coated beads or by plating. Gaus et al. used the Laurdan lipid probe, whose emission spectrum changes when it encounters an ordered lipid environment, to show that the plasma membrane at the site of T-cell activation is in a more ordered state compared to the rest of the membrane, which also supports a function for lipid rafts in TCR signalling(Gaus et al., 2005). Nevertheless, the results by Douglass et al. confirm that protein-protein interactions are essential for the formation of microdomains at the T-cell synapse. These publications clearly show that the concept of raft-mediated signalling has to be carefully re-examined without pre-conceived ideas. Despite these drawbacks, the last few years have also seen some very positive developments in the field of lipid rafts. For example, Prior et al. have developed an electron microscopy technique to visualize lipid rafts with the help of spatial point pattern analysis(Prior et al., 2003a; Prior et al., 2003b). They found that lipid raft probes and ras proteins are clustered on the plasma membrane, and that raft clustering is sensitive to cholesterol depletion. Another highlight was the definitive identification of a clathrin- and

caveolin-independent endocytic pathway, which clearly is cholesterol-dependent(Glebov et al., 2006; Kirkham et al., 2005). Additionally, in a pioneering systems biology approach, Pelkmans et al. have investigated the function of hundreds of kinases, many of them poorly characterized, in either clathrin- or caveolae/raft-mediated endocytosis(Pelkmans et al., 2005). This screen identified almost all kinases which were already known to regulate endocytotic events and a plethora of new kinases, which had not been implicated in endocytosis yet. The most important finding was that there are quite many kinases which influence both pathways simultaneously or differentially. Of course, only an in-depth characterization of newly identified kinases can reveal their precise mode of action. Nevertheless, this study gives a hint on the complex regulation of endocytosis, and one can expect that other cellular processes are also subject to complex regulation. Yet another highlight of the last years was the refined analysis of ordered and disordered domains in model membranes.

Figure 6: Induction of lipid domains in GUVs by addition of cholera toxin B

Figure 6: Lipid domains induced by addition of cholera toxin B subunit (CTB) to Giant Unilamellar Vesicles (GUVs) of a certain lipid composition. Reprinted from ((Hammond et al., 2005). (A) Addition of CTB to previously homogenous vesicles triggers domain formation. (B) Domain size is determined by the lipid composition before CTB addition.
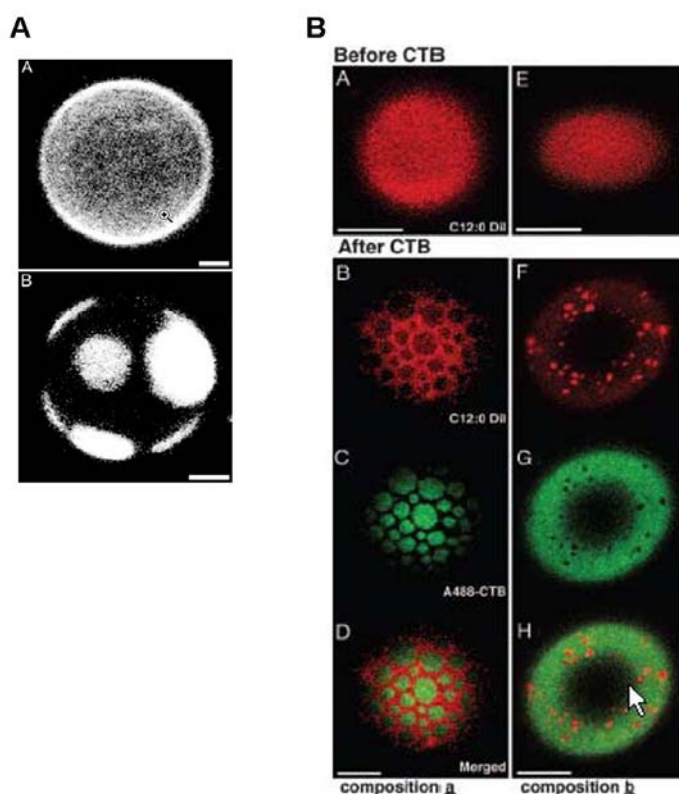
One example is the study by Baumgart et al., which shows, using two fluorescent lipid probes either prefering ordered and disordered domains and directly observing these probes in giant unilammellar vesicles (GUVs), that membrane domains may differ in their intrinsic curvature(Baumgart et al., 2003). These experiments visualizing distinct membrane domains produced very impressive pictures.

Similarly, Roux et al. showed that the lipid composition of tubes pulled from GUVs is significantly different from the vesicles(Roux et al., 2005). Precisely, disordered domain preferring lipids were enriched in the tubes. Additionally, phase separation induced in the

tubes by photoactivation led to fission events(Roux et al., 2005). Another important contribution came from Hammond et al., who could show that addition of cholera toxin B subunit to GUVs triggered the phase-separation of ordered and disordered domains(Hammond et al., 2005) (see Figure 6).

Milhiet et al. used atomic force microscopy (AFM) to visualize phase separation and followed the fate of alkaline phosphatase (AP) added to supported phospholipid bilayers containing ordered domains. When AP was added to bilayers without cholesterol, the protein was preferentially inserted at the periphery of the gel phase. In bilayers containing cholesterol, AP was homogenously distributed throughout the gel phase(Milhiet et al., 2002). These results from model membranes might have important consequences for the analysis of membrane sorting events in living cells, too. For example, tubular transport intermediates are characteristic of recycling endosomes and might (at least in part) be driven by similar domain separation events. The internalization of lipid raft constituents might also be induced by the crosslinking of pre-existing rafts or by the local induction of phase separation. This pathway is hijacked by numerous pathogens and could therefore be of therapeutic interest(Gruenberg and van der Goot, 2006; Reig and van der Goot, 2006; van der Goot and Harder, 2001). Although the value of the results obtained on model membranes has recently been doubted because cellular membranes are, of course, much more complex than model systems and, most importantly, are not in equilibrium with the surroundings but are actively maintained (in an energy-dependent fashion; e.g. "flippases", transporters, vesicular transport and endocytosis) in a non-equilibrated state(Mayor and Rao, 2004), in my opinion, similar mechanisms for the formation, fusion and fission of membrane domains might also operate in living cells. It is particularly intriguing that cells might use transient, local inhomogenities and the energy derived from phase separations for the formation of, for example, non-clathrin-dependent endocytic carriers. This could explain the importance of certain lipids (e. g. PIP2) and lipid-binding proteins/domains in endocytosis. Additionally, the cellular membrane might have a composition (which is actively maintained) close to a critical point of the system. In such a system, minor changes in the lipid composition could have large effects on the phase behaviour and could again be used to drive certain cellular processes(Hancock, 2006; London, 2005). In a recent review by John Hancock, he also outlined several interesting theoretical results from computational approaches(Hancock, 2006). Such a recent study showed that inter-protein-collisions were maximal when rafts were small (6-14 nm), mobile and when the diffusion rate of proteins was two-fold slower than outside rafts(Nicolau et al., 2006). Additionally, another computational approach revealed that, if small l_o domains might eventually coalesce to form larger domains, endocytosis might be the process that limits raft-domain size(Turner et al., 2005). In conclusion, the last few years have seen a revision of the "classical" lipid raft model(Simons and Ikonen, 1997). Lipid rafts are now seen as extremely small, dynamic inhomogenities of the plasma membrane (see Figure 7).

Figure 7: Different models for lipid raft structure
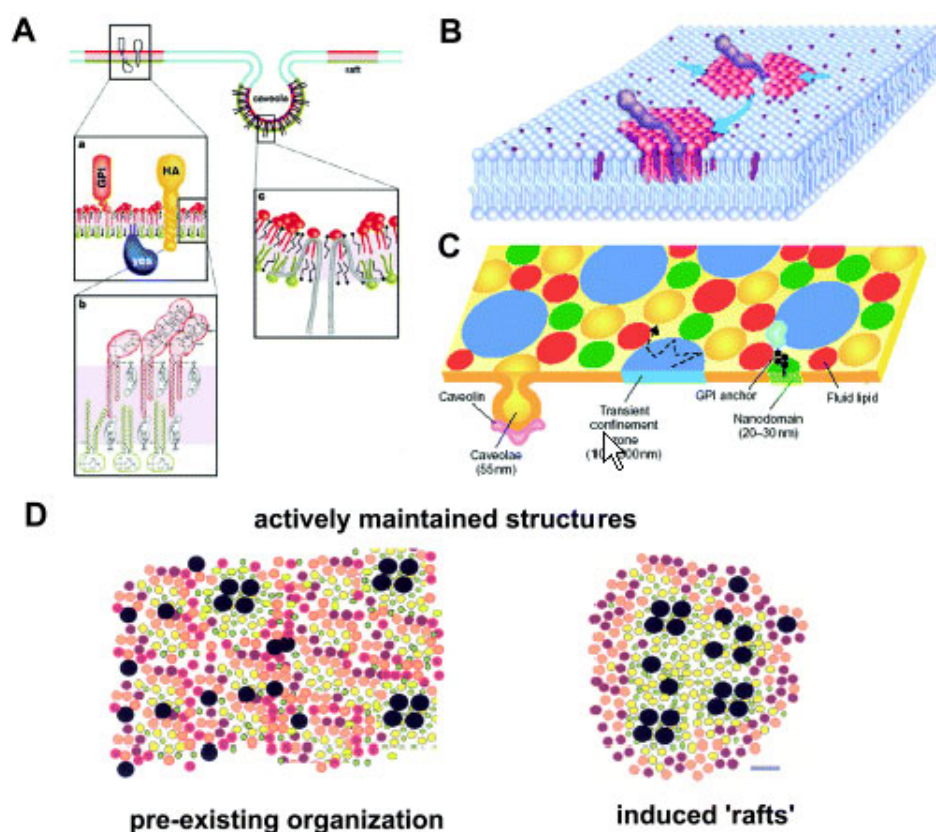
Figure 7: Current models for membrane organization. Reprinted from (Mayor and Rao, 2004)

The most commonly cited hypothesis for membrane rafts (Simons and Ikonen, 1997) depicts rafts that are relatively large structures (~50 nm), enriched with cholesterol and sphingolipid (SL), with which proteins are likely to associate. Anderson & Jacobson (Anderson and Jacobson, 2002) visualize rafts as lipid shells that are small, dynamic molecular-scale assemblies in which raft proteins preferentially associate with certain types of lipids. The recruitment of these "shells" into functional structures could be a dynamic and regulated process. (C) Another point of view is that a large fraction of the cell membrane is raft-like and exists as a "mosaic of domains"; cells regulate the amount of the different domains via a cholesterol-based mechanism (Maxfield, 2002). (D) Actively generated spatial and temporal organization of raft components. A different picture, which is consistent with data from GPI-anchored protein studies in living cells (Sharma et al., 2004), suggests that preexisting lipid assemblies are small and dynamic, and coexist with monomers. They are actively induced to form large-scale stable "rafts". Black circles, GPI-anchored proteins; red and pink circles, nonraft associated lipids; yellow circles, raft-associated lipids; green, cholesterol. Scale bar ~5 nm.

Additionally, it became clear that protein constituents of lipid rafts might have more important functions than previously anticipated. Lipid raft proteins are not passively compartmentalized, but are essential for the stabilization of small, dynamic rafts, for cholesterol-dependent signalling and transport processes and perhaps also for the maintenance of the small lipid rafts. This view is now accepted by most researchers in the field(Hancock, 2006; Mayor and Rao, 2004; Rajendran and Simons, 2005).

The lipid raft hypothesis has, without doubt, stimulated research on membrane structure and function. Even when no stable lipid rafts exist in cells in a resting state, membrane inhomogenities have been shown to be crucial for many events after stimulation. Novel methodologies will certainly enable us to draw a more precise picture of lateral membrane organisation in living cells and its consequences for membrane protein function.

An essential point is that, only because lipid rafts have proven hard to "pin down" in vivo, this must not mean that they do not exist or are not important for cellular functions. The situation is surely more complex than anticipated several years ago, and it can be that lipid rafts only comprise a few molecules and only exist on a nano-second timescale(Kusumi et al., 2005). These dynamic processes might be ideal for tight regulation, although they are, of course, more difficult to understand than a simple phase separation, with rafts floating on a sea of non-rafts and signalling proteins either associated with or excluded from the rafts. For our work, which deals with the functional characterization of stomatin and stomatin-like proteins, the novel focus on protein function in the lateral membrane organization is surely positive. As already proposed several years ago, several properties of stomatin make it a candidate scaffolding protein on the cytoplasmic leaflet(Snyers et al., 1999a).

2.5 Stomatin and SLP-1 structure

2.5.1 Stomatin structure

Because of its hydrophobic character, bacterial expression of stomatin and stomatin fragments was found to be problematic (E. Umlauf, unpublished results). Therefore, all attempts to express and purify sufficient amounts of stomatin fragments for structural analyses like X-ray diffraction or NMR were not successful. The only high-quality NMR structure available is one of a fragment of the distantly related mouse flotillin-2 protein (PDB accession 1win). This fragment contains the SPFH domain signature and one could assume that a similar structure represents the core fold in stomatin. Figure 4 shows a schematic representation of the structure. A comparison of the amino acid sequence of flotillin-2 and stomatin reveals that a big part of the central fold consisting of 4 beta-sheets and two alpha helices could also be present in stomatin, whereas the loops connecting these elements are less conserved. For a second distantly related molecule, human prohibitin-1, a computed structural model is available, which also shows a compact central domain of 6 beta-sheets which is followed by several alpha-helices. Based on secondary structure predictions with the programme JPRED, we assume that the tertiary structure of stomatin could be similar to the prohibitin model. After the long hydrophobic region, several beta-sheets and alpha-helices probably form a compact, tightly membrane-associated fold (amino acids 63 to 195), which is followed by alpha-helical structural elements, which dominate the rest of the stomatin C-terminus. No data is available for the perhaps most interesting part of stomatin, the long, hydrophobic integral membrane domain. Based on the localization of stomatin to lipid droplets, one can assume that the putative hairpin loop is only embedded into the cytoplasmic leaflet of the lipid

bilayer. Secondary structure prediction programs indicate an alpha-helical structure for this hydrophobic region, but the significance of this prediction is not clear, because alpha-helices of about 12 amino acids are long enough to span the bilayer. At present, the stomatin hydrophobic domain is thought not to span the bilayer at all. Perhaps we will be able to get more insights into the structure by circular dichroism measurements of hydrophobic peptides in collaboration with the department of structural biology in the future.

2.5.2   SLP-1

No structure is available for the SPFH domain of SLP-1 as well, but the central region can also be assumed to have a similar fold as flotillin-2 and prohibitin-1. For the SCP-2 domain, several high-quality structures are available. Cytoplasmic SCP proteins are of small size and well soluble, so they were successfully expressed in bacteria, crystallized and subjected to X-ray diffraction analysis by several groups. Although only about 25% of the amino acids are conserved between SCP-2 and the SCP-2 domain in SLP-1, a comparison of the determined structures and a structure prediction for the SLP-1 SCP-2 domain reveals an almost identical sequence of structural elements. Recently, a group has solved the structure of an insect SCP protein in complex with a fatty acid and could determine the amino acids which line out the hydrophobic binding site. These positions are all occupied by hydrophobic amino acids in the SLP-1 sequence, which also supports the thesis that the SCP-2 domain of SLP-1 could be functional and bind and/or transfer lipids. Bacterial expression of the C-terminal SCP-2 domain of SLP-1 is a future project and could enable us to determine if the domain is functional in established in-vitro lipid transfer assays. If we were lucky, we could also purify enough material for 3D structure analysis.

2.6 The SCP-2 protein

The SCP-2 protein was initially isolated and purified from rat liver cytosol as a soluble factor, which enhances the conversion of sterol precursors to cholesterol in rat microsomal fractions(Noland et al., 1980).

The same protein had been purified independently by another group(Bloj et al., 1978) and designated non-specific lipid transfer protein (nsLTP), because it was shown to stimulate the transfer of a broad range of lipids including sterols between donor and acceptor membranes in vitro(Bloj and Zilversmit, 1977; Crain and Zilversmit, 1980; Nichols and Pagano, 1983). The protein was found to contain a low-affinity lipid binding site, which can accomodate a variety of different lipids(Gadella and Wirtz, 1991). Transfer of cholesterol was found to be enhanced dramatically by acidic lipids (Butko et al., 1990). There was a big debate on the mode of action of SCP-2, if it is actually a carrier-protein (Butko et al., 1990) or if it interacts with membranes to enhance the desorption rate of lipids into the aqueous phase (Gadella and

Wirtz, 1991). Nowadays, the carrier function is widely accepted, and cytosolic SCP-2 is considered to play an important role in non-vesicular sterol transport as well as cellular uptake of cholesterol and lipids(Gallegos et al., 2001; Wirtz, 2006).

2.7 Aims of this study

Stomatin is widely expressed in different human cells and tissues. The function of this ubiquitous membrane protein is still unclear. The aims of my studies were to get more insights into the function of the stomatin family protein SLP-1 and stomatin. Several different approaches were used to perform this task:

1) I undertook a first cell biological and biochemical characterization of SLP-1, which is prone to play a role in lipid transport due to its unique combination of a SPFH domain and a SCP-2 domain and which is a potential interaction partner for stomatin based on data from *C. elegans*.

2) The dynamic behaviour of stomatin and SLP-1 was analysed by live cell imaging studies of GFP-fusion proteins. During the course of the work, we established a FRAP assay to analyze the plasma membrane dynamics of stomatin and stomatin mutants.

3) Point mutations of human stomatin were constructed in analogy to several mutations described in the *C. elegans* MEC-2 and UNC-1 proteins to get non-functional stomatin variants. Based on our mass spectroscopy results (see 4), we also targeted amino acids which potentially carry post-translational modifications.

4) Lipid raft fractions of platelets and neutrophils were analysed by 2D-PAGE, silver staining and mass spectroscopy to identify post-translational modifications of stomatin and possible binding partners in the lipid raft fractions.

In my opinion, this work adds some interesting pieces to the puzzle of stomatin family protein function (which is still far from completion).

3 METHODS

3.1 Biochemical Methods

3.1.1 SDS-PAGE

Equipment: Hoefer Vertical Slab Gel Unit SE400
                       power supply: BioRad PowerPack 1000 or 3000
                       precision syringe

solutions for SDS-PAGE (all in milliQ-H_2O):

5x sample buffer: 0.1 M Tris.HCl, pH 6,8
                                  5% SDS
                                  17% glycerol
                                  5% mercaptoethanol
                                  1/100 volume of a 0.5 % bromophenolblue solution

running buffer: 0.19 M glycine
                                  25 mM Tris
                                  0.1% (w/v) SDS

solution A: 30% acrylamide
                                  0.8% bis-acrylamide
buffer B: 1 M Tris.HCl, pH 8,8
buffer C: 1 M Tris.HCl, pH 6,8

10% (w/v) SDS
TEMED (Tetramethylethylendiamine)
10% (w/v) APS (Ammonium-peroxodisulfate)

polyacrylamide gels were prepared as follows:
          stacking gel: 2,4 mL solution A
                                          2 mL of buffer C
                                          11,2 mL milliQ-H_2O
                                          160 µl 10% SDS
                                          24 µl TEMED
                                          80 µl 10% APS

separating gel: 11 ml of solution A

11.2 ml of buffer B

7 ml milliQ H_2O

300 µl 10% SDS

20 µl TEMED

150 µl 10% APS

- the components were thoroughly mixed in glass beakers, the respective amount of 10% APS was added immediately before pouring the gel; I routinely used 11% acrylamid gels for my work, other concentrations can be achieved by changing the volumes of solution A and H_2O, e .g. 10 ml solution A and 8 ml H_2O yield a 10% acrylamide gel
- glass plates and spacers were thoroughly rinsed with tap water, cleaned with ethanol, air-dried, assembled in the clamps and mounted in the pouring stand, the lower edge was sealed with vacuum grease to prevent leakage
- the separating gel was poured to a height of 11 cm, then 1 ml of water was carefully added to be able to monitor complete polymerization
- after the separating gel was completely polymerized (15-30 minutes), the water was poured off and the stacking gel was added on top of the separating gel, with an appropriate comb for the number and volume of samples to be analyzed (combs with 10, 15 or 20 slots available)
- when polymerization of the stacking gel was complete (30 minutes), the comb was removed and the gel was inserted into the Hoefer Vertical Slab Gel Unit, the two buffer chambers were filled with running buffer and the samples and markers were filled into the slots with a precision syringe (Hoefer)
- gels were either run over night at 50 V or for approximately 4 hours at 200 V and were stopped shortly before the running front reached the lower edge of the gel

3.1.2   2D-PAGE of lipid raft fractions

The method for isoelectric focusing of lipid raft fractions was based on a protocol recently published by Sprenger et al. (Sprenger et al., 2004), with some modifications to adopt the method for our equipment.

Equipment: IPGphor IEF apparatus (Amersham/Pharmacia)

ceramic strip holders 13 cm

Immobiline DryStrips pH 3-10, 13 cm (Amersham)

Servalyt carrier ampholytes pH 3-10 for IEF, stock solution 40% w/v (Serva)

Hoefer Vertical Slab Gel Unit SE400

Solutions: all compounds were of ultra-pure quality to avoid contaminations and were

prepared with milliQ-water!

Rehydration Stock Solution (RSS):	7 M Urea
	2 M Thiourea
	4% Triton X-100
	2% carrier ampholytes pH 3-10
	20 mM Tris-base
	55 mM DTT
	0.003 % w/v bromophenol blue

a concentrated solution of thiourea was prepared first and was incubated for 1 hour with ampholyte ion exchange resin to remove contaminating salts, this solution was then diluted to a concentration of 2 M in the solution containing the other compounds;

SDS-Equilibration buffer (SDS-EB):	50 mM Tris.HCl, pH 8.8
	6 M Urea
	30% v/v glycerol
	2% w/v SDS
	0.002 %bromophenol blue

Agarose sealing solution (ASS):	25 mM Tris.HCl, pH 8.8
	200 mM Glycine
	0.1 % w/v SDS
	0.002 % bromophenol blue

- Platelet lipid rafts were isolated as described in 3.1.11. Lipid raft fractions (fractions 1-4) were collected from the gradients and diluted with 10 mL of pre-cooled TBS, pH 7,4 in Beckman SW40 centrifuge tubes
- the tubes were centrifuged for 1h at 100.000xg (20.000 rpm) in a SW40 rotor in a Beckman Ultracentrifuge
- the supernatant was discarded and the lipid raft pellet was resuspended in approximately 10-15µl of a 1% SDS solution in milliQ-H_2O for 15 minutes at RT
- a protein determination was carried out with a 1 µl-aliquot of this suspension, especially if different lipid raft fractions were compared
- total protein concentration for individual 2D-PAGE runs varied from approximately 10 to 30 µg of total protein, equal amounts of different samples were loaded and run simultaneously
- 3-10 µl of the lipid raft suspension was mixed with 280 µl of Rehydration Stock Solution (RSS) and rotated at RT for 1 hour
- this mixture (280 µl) was transferred into a 13 cm strip holder cassette, and a

dehydrated Immobiline DryStrip was carefully mounted on top of the sample (gel side down, plus-end at the pointed end of the strip holder, avoid air bubbles under the gel strip!!!)

- then, approximately 1 ml of DryStrip cover fluid is layed on top of the IEF strip to prevent leakage of the sample
- the cassette is covered with a plastic lid, transferred to the IPGphor apparatus and placed on the gold electrodes
- sample loading by in-gel-rehydration was performed for 12 hours
- the temperature was set to 20°C and the current per strip was limited to 50 μA
- after rehydration was complete, a focusing program was started:

Step 1:	200 V for 30 minutes (step-n-hold)
Step 2:	500 V for 45 minutes (step-n-hold)
Step 3:	750 V for 1 hour (step-n-hold)
Step 4:	gradual increase from 750 V to 3500 V for 2,5 hours (gradient)
Step 5:	3500 V for 9 hours (step-n-hold)
Step 6:	100 V until the run is stopped (step-n-hold)

- after the completion of Step 5, the run is stopped, and the IEF strip is carefully removed from the strip holder cassette
- the strip is then incubated in 5 ml of SDS-Equilibration buffer supplemented with 10 mg/ml DTT for 15 minutes, followed by an incubation in SDS-Equilibration buffer with 25 mg/ml Iodoacetamide
- while the strips are equilibrated, a vertical separating gel is prepared as described in chapter 3.1.1, with the difference that it is not poured to a height of 11 cm, but to approximately 15 cm
- the separating gel is overlaid with 1 ml of Isopropanol to get a very smooth gel boundary
- after polymerization is complete, the isopropanol is removed and the equilibrated gel strip is mounted on top of the separating gel between the glass plates with the plus end (pH 3) at the left and the minus end (pH 10)at the right side of the second dimension gel (only touch the plastic support of the gel strip, avoid air bubbles between the gel strip and the separating gel!!!)
- if needed, a filter paper with molecular weight marker or/and a 1D-PAGE sample can be included on each side of the strip
- the strip is then overlaid with 1-2 ml of Agarose sealing solution (ASS), which has to be melted before use (when cooling down, a gel is formed, which fixes the position of the IEF strip and the markers/1D-samples)
- the second dimension SDS-PAGE is run normally (run time has to be increased to 5-6 hours at 200 V if it is run along the full length for silver staining, for western blotting,

also short run times (1,5-2 hours at 200 V) can be used)
- silver staining and/or western blotting is performed as described below

3.1.3 Silver staining of proteins on polyacrylamide gels (standard protocol)

All incubations were performed on a shaker at room temperature!
- gels were fixed for 1h in fixing solution (50 % methanol, 12 % acetic acid, 0.5 ml/l formaldehyde (37% solution))
- washed 3 times for 20 min in 50 % ethanol
- pretreated for 1 min with 0.2 g/l $Na_2S_2O_3$.5 H_2O
- washed 3 times for 20 sec. with dest. H_2O
- incubated for 20-30 minutes in the dark with staining solution (2g/l $AgNO_3$, 0.75 ml/l formaldehyde (37%))
- washed 2 times, 20 sec. with dH_2O
- developed for 1-5 minutes in developing solution (60 g/l Na_2CO_3, 4 mg/l $Na_2S_2O_3$.5 H_2O,0.5 ml/l formaldehyde (37%))
- development was stopped with stop solution (50 % methanol, 12 % acetic acid)
- gels were stored at 4°C in 20 % methanol, 1 % glycerine until they were scanned and dried between cellulose sheets for long-term-storage;

3.1.4 Silver staining for mass spectroscopy

- for the purpose of identifying proteins by MALDI-TOF peptide mapping, a special protocol was used and all solutions were prepared with high-quality milliQ-water to minimize contaminations;
- the solutions for this protocol are:

  fixing solution: 50 % methanol, 5 % acetic acid

  washing solution 50 % methanol

  sensitizing solution 0.2 g/l $Na_2S_2O_3$.5 H_2O

  silver solution 1 g/l $AgNO_3$

  developing solution 20 g/l Na_2CO_3, 0.4 ml/l formaldehyde

  stop solution 5 % acetic acid
- the staining procedure is as follows:
  - fix the gel (20 min, fixing solution)
  - wash the gel (10 min, washing solution)
  - wash the gel (2 h or over night, milliQ-H_2O)
  - sensitize the gel (1 min, sensitizing solution)
  - wash the gel (2x 1 min, milliQ-H_2O)
  - incubate the gel (20 min, silver solution, at 4°C!!!, in the dark!!!)
  - wash the gel (2x 1 min, milliQ-H_2O)

- develop the gel (0.5-5 min, developing solution)
- stop the color development (3x 1 min, stop solution)

- gels can be stored for several weeks in 1% acetic acid at 4°C
- protein bands of interest are excised with a clean scalpel, digested by trypsin, and identified by mass spectrometry (Bruker Reflex III MALDI-TOF-MS, peptide mapping);
- the identity of the respective proteins should be (if an antibody is available) confirmed by Western blotting;

3.1.5 Western blotting

Equipment/Materials: Hoefer TE 50X wet blotting unit;
AGFA Curix 60 developing machine;
SuperSignal West Pico Chemiluminescence Detection reagent (Pierce)
CL Xposure films (Pierce)
blotting buffer: 0.19 M glycine, 25 mM Tris, 10% methanol

- after SDS-PAGE, the gel is incubated in blotting buffer for ~1min, then the gel sandwich is assembled (black side of map, sponge, whatman paper, gel, nitrocellulose membrane, whatman paper, sponge, grey side of map; all compounds soaked in blotting buffer), inserted into the blotting chamber (anode - nitrocellulose membrane - gel - cathode), and blotted over night at setting 100 mA, 10 V;
- after blotting, the membrane is either stained with Ponceau S (staining of protein markers, control for blotting efficiency) or immediately blocked
- blocking of non-specific binding sites on the membrane is performed with blocking buffer (150 mM NaCl; 20 mM Tris·HCl, pH 8.0; 1% non-fat dry milk, 1% PVP) for 1 hour
- then incubations with primary antibodies are performed for 1 h; antibodies are diluted in washing buffer (150 mM NaCl; 20 mM Tris·HCl, pH 8,0; 0.1 % Tween 20)
- the blots are washed 3x 5 min with washing buffer
- incubation with secondary antibodies (horseradish peroxidase (HRP) conjugates from Pierce) diluted 1:5000 for 1 h;
- washing step 3x 5 min, washing buffer
- blots are mounted on transparent plastic foil in an autoradiography map and incubated with the Pierce West Super Signal Chemiluminescence Detection reagent (approximately 1 ml for a full-size blot) according to the manufacturer's instructions
- protein bands are visualized by exposure of X-ray films (exposure times from ~ 15 seconds to 1 h or overnight, depending on the antibody and the amount of protein)

3.1.6   Isolation of platelets and neutrophil granulocytes from whole blood

- whole blood (45 mL) is obtained from healthy donors by venipuncture and collected into heparinized tubes;

- red cells and leukocytes are pelleted (15 minutes, $200xg$=900 rpm, Heraeus Varifuge 3.0R, room temperature = RT), the platelet rich plasma is removed from the tubes and 9 parts are mixed with 1 part ACD-solution (25 g/L Na_3-citrate, 13.7 g/L citric acid, 20 g/L glucose) as anticoagulant

- platelets are pelleted from this solution (12 minutes, $2000xg$≡3200 rpm, Heraeus Varifuge 3.0R, RT) and resuspended in 2 ml wash buffer (90 mM NaCl, 5 mM KCl, 36 mM Na_3citrate, 10 mM EDTA, pH 6,5)

- this platelet suspension is transferred to Eppendorf tubes, the platelets are pelleted by centrifugation (10 minutes, $2000xg$=2000 rpm, Eppendorf bench-top centrifuge, RT) the supernatant is discarded and the platelet pellets are resuspended in 2 ml wash buffer; remaining erythrocytes are removed by 2-3 quick spins (quick spin: the button is pressed for approx. 3-5 seconds, shortly released, pressed again for 3-5 seconds, released and finally pressed a third time for 3-5 seconds, this procedure is used to prevent too big g-forces),

- the supernatants after the quick spins are transfered to new Eppendorf tubes, the quick spins are repeated 2-3 times, then the platelets are again pelleted (10 minutes,$2000xg$=2000 rpm, Eppendorf bench-top centrifuge, RT)

- the final platelet pellet is resuspended in the appropriate buffer for following experiments

- for the isolation of neutrophils, the leukocyte-rich buffy coat is removed from the top of the erythrocyte layer after the collection of the PRP and transferred into a 15 ml Falcon tube

- the buffy coat (approximately 5 ml) is then mixed with 1/9 volume of ACD-solution, and 2 ml of a 6% dextran solution (average MW ~ 168000 kDa) are added

- the suspension is mixed well by inverting several times, and then is left at RT for 1 hour, during this period, most erythrocytes, which are crosslinked by the dextran, sediment to the bottom of the tube

- next, the yellow plasma layer is carefully removed from the erythrocyte pellet, transferred into a fresh 15 ml Falcon tube and precooled to 4°C on ice

- then, the leukocytes are pelleted by centrifugation (Heraeus Varifuge 3.0R, 700 rpm, 12 min, 4°C), the supernatant is discarded and the pellet is resuspended in 100 µl DPBSE (Dulbecco's Phosphate Buffered Saline+5mM EDTA, pH 7,4)

- 3 ml dH_2O are added (to lyse residual erythrocytes)

- after 30 seconds, 1 ml of 0.6 M KCl is added to again yield an isotonic suspension

- the leukocytes are pelleted (Heraeus Varifuge 3.0R, 900 rpm, 4 min, 4°C), the supernatant is discarded and the pellet again resuspended in 100 µl of DPBSE

- the lysis and pelleting step are repeated
- the leukocytes are resuspended in 8 ml of DPBSE
- this suspension is carefully layered on top of a cushion of 4 ml Ficoll-Paque in a 15 ml Falcon tube
- the tube is centrifuged (Heraeus Varifuge 3.0R, 2000 rpm, 30 minutes, 4°C)
- after centrifugation, a band is visible at the DPBSE/Ficoll phase border; this band consists of lymphocytes and some residual platelets
- the granulocytes are recovered from the pellet at the bottom of the tube, this pellet is resuspended in 1 ml DPBSE, and a cell count with a CASY cell counter is performed to analyse the number of isolated cells and the homogenity of the preparation (the cell counter also yields the mean diameter and mean volume of the cells)
- the cells are pelleted (Eppendorf desk-top centrifuge, 2000 rpm, 5 min, 4°C) and finally resuspended in the appropriate volume of HBSS (Hank's balanced salts solution) for further experiments

3.1.7 Preparation of HeLa PNS

solutions: Dulbecco´s PBS

                  PBS+PI: +5µg/ml aprotinin
                                               +5 µg/ml leupeptin
                                               +0.5 µg/ml pepstatin A
                                               + 0.4 mM AEBSF

     Homogenization Buffer (HB):   250 mM sucrose
                                           3 mM imidazole, pH 7.4

                  HB+PI: +5µg/ml aprotinin
                                               +5 µg/ml leupeptin
                                             +0.5 µg/ml pepstatin A
                                             + 0.4 mM AEBSF

                  HB+PI/EC: +1 mM EDTA
                                          +15 µg/ml cycloheximide
                                        +10 µg/ml aprotinin
                                        +10 µg/ml leupeptin
                                        +1 µg/ml pepstatin A
                                        + 0.8 mM AEBSF

- HeLa cells were cultured on 150 mm culture dishes
- at confluency, cells were removed from the incubator and washed twice with 5 ml ice-

cold PBS per culture dish

- the cells were scraped off the dish on ice with a rubber policeman in 5 ml PBS+PI
- the cells were pelleted by centrifugation at 1000 rpm in a refrigerated Heraeus Varifuge 3.0R
- the supernatant was discarded and the cell pellet was resuspended in 5 ml of HB+PI
- the suspended cells were pelleted at 2500 rpm and resuspended in 2 ml HB+PI/EC
- the cells were homogenized on ice with a syringe by seven passages through a 23-gauge needle, efficiency of homogenization was checked with a drop of the lysate mounted on a coverslip and viewed on a microscope
- the homogenate was centrifuged at 3000 rpm to pellet nuclei and unbroken cells, the supernatant was recovered carefully and used for further experiments

3.1.8 Subcellular fractionation of detergent lysates on linear density gradients

- cells were grown to confluency on 150mm cell culture dishes and a PNS was prepared as described in 3.1.7.
- the PNS was diluted with cold TBS, pH 7.4 to a final volume of 4 mL, transferred to a SW50 centrifuge tube and centrifuged at 100.000xg (25000 rpm, 1 hour, 4°C) to pellet cellular membranes
- the membrane pellet was resuspended in 500 µl of ice-cold TNET lysis buffer (10 mM Tris.HCl, pH 7.4, 150 mM NaCl, 5 mM EDTA, 1% TritonX-100 + protease inhibitors) and incubated for 20-30 minutes on ice (vortexing was performed every 5-10 minutes to ensure proper mixing)
- then, the lysates were centrifuged (10 minutes, $15.000xg$=14.000 rpm, Eppendorf centrifuge, 4°C), the supernatants were removed and layed on top of preformed, precooled (4°C) sucrose gradients
- the linear sucrose gradients were formed with a gradient mixer connected to a peristaltic pump (Gilson Minipuls 3, speed set to 12-16) and a long syringe needle at room temperature;
- 6 ml 5% sucrose solution in TBEST (10 mM Tris·HCl, pH 7,4; 150 mM NaCl; 5 mM EDTA; 1% TX100) were pipetted into the first chamber, the second (mixing) chamber was filled with 6 ml 25% sucrose in TBEST, a magnetic stirrer was placed in the second chamber, and a linear sucrose gradient was formed in SW40 polycarbonate centrifuge tubes (the needle is always kept close above the liquid meniscus to prevent excessive mixing) and precooled to 4°C (alternatively, one can also pipet the lower density solution into the mixing chamber and the higher density solution into the second chamber; then, the needle is always kept at the bottom of the tube, and the mixture gets more and more dense and displaces the lighter solution upward;)
- 400 µl of the different supernatants were loaded on top of the 5-25% sucrose gradients and centrifuged over night in a Beckman SW40 swing-out rotor ($200.000xg$=36.000 rpm, 4°C, 20 h)

- 19 fractions of 650 µl were taken from the top of the gradient, pelleted material was resuspended in the 19th fraction
- the fractions were mixed with 165 µl of 5xR, boiled for 3 min, and aliquots of 100 µl of each fraction were then analyzed by SDS-PAGE, silver staining or western blotting; the rest of the fractions was stored at –20°C

3.1.9 Subcellular fractionation of HeLa cell lysates on sucrose step gradients

solutions: HB

                                 HB+PI/EC

                                 25 % w/w sucrose solution   0.806 M sucrose
                                                            3 mM imidazole, pH 7.4
                                                             1 mM EDTA

                                 35 % w/w sucrose solution   1.177 M sucrose
                                                            3 mM imidazole, pH 7.4
                                                             1 mM EDTA

                                 62 % w/w sucrose solution   2.351 M sucrose
                                                            3 mM imidazole, pH 7.4
                                                             1 mM EDTA

- a PNS is prepared as described above; all subsequent steps are performed at 4°C;
- 2 ml of PNS is adjusted to a sucrose concentration of 40.6 % (w/w) by addition of 2.4 ml of 62% sucrose solution; the suspension is thoroughly mixed and the sucrose concentration is be checked with a refractometer (everything between 40 and 41 % is acceptable)
- 4 ml of the diluted PNS is transferred to the bottom of a SW40 centrifuge tube and sequentially overlaid with 4.5 ml of 35 % sucrose solution and 3.5 ml of HB
- the tubes aremounted in a SW40 rotor and centrifuged for 1 hour with 35.000 rpm at 4°C
- the interphases between the HB and 35 % sucrose phase and between the 35 % and 40.6 % sucrose phase are collected (equal volumes, should be as small as possible, approximately 500 µl!), the rest of the gradient is fractionated in 1 ml steps, the pellet is resuspended in 1 ml of HB, these fractions are included in cholesterol and protein determinations; the HB/35% interphase represents a crude endosomal fraction and should be enriched in early endosomal (e.g. rab5) and late endosomal/lysosomal markers (e.g. LAMP-1), whereas the 35%/40.6% interface should contain plasma membrane, ER and Golgi markers;

- equal protein amounts of a PNS aliquot, the crude endosomal fraction and the PM/ER/Golgi fraction are analysed by western blotting/silver staining;

- alternatively, a two-step gradient centrifugation can be performed; therefore, the volume of the 35% sucrose solution is reduced to 3.5 ml, then, 2.5 ml of 25% sucrose solution are carefully overlaid, and the tube is subsequently filled by addition of 2 ml HB;

- centrifugation is performed analogous to the one-step-gradient

- the HB/25% interface should be enriched in late endosomal markers, whereas the 25%/35% interface should be enriched in early endosomal proteins;

- we were unable to obtain fractions enriched in late endosomal markers with this protocol, either because we did not use sufficient starting material or because the endosomes of HeLa cells behave differently in such gradients (the protocol was originally developed for BHK cells/MDCK cells)

3.1.10 Subcellular fractionation of HeLa cell lysates on linear optiprep gradients

Fractionation of HeLa cell lysates on Optiprep gradients was performed as described (Meyers and Prekeris, 2002), with some modifications.

Solutions:	HB+E:	Homogenization Buffer (HB) + 1 mM EDTA

Optiprep stock solution: 60% iodixanol

Optiprep working solution (OWS):   50 % w/v iodixanol
                                   250 mM sucrose
                                   3 mM imidazol
                                   1 mM EDTA

5 % Optiprep solution: mix 1 vol. OWS with 9 vol. HB+E
20 % Optiprep solution: mix 2 vol. OWS with 3 vol. HB+E

- one 150 mm-dish containing confluent cells was used for preparing lysates
- a PNS was prepared as described above
- one ml of this supernatant was loaded on top of a precooled 11 ml linear density gradient from 5% to 20% Optiprep repared in a SW40 centrifuge tube (the gradient was prepared with a gradient mixer connected to a peristaltic pump (Gilson Minipuls 3) and a long syringe needle in a SW40 centrifuge tube; the 5% Optiprep solution was pipetted in the front chamber of the gradient mixer, therefore, the density increases during the process; the syringe needle is kept at the bottom of the tube, the density gradually increases and the gradient is formed; this method was found to be superior

to the inverse protocol, where one has to move the needle up in the tube, in respect to gradient reproducibility)

- the gradients were centrifuged at 100 000xg for 14-16 hours
- nineteen fractions of 580 µl were taken from the top and analyzed by SDS-PAGE and Western blotting.
- aliquots were assayed for alkaline phosphatase content as described (Lowry, 1957).

3.1.11 Isolation of lipid rafts/DRMs

Isolation of lipid raft/DRM fractions was performed with different cells during my work. I established a protocol for the isolation of DRMs (as they should be called, but lipid rafts just sounds nicer) from platelets during my diploma thesis, which was continuously improved during the next years(Mairhofer et al., 2002). This protocol was then adapted for the isolation of DRMs from cultured cell lines. The basic centrifugation procedure is the same, only the starting material and the lysis buffers are different. For platelets, I used the cells isolated from ~50 ml of fresh blood for 2-4 experiments, whereas I used the membrane pellet from 1-2 150mm cell culture dishes for adherent cell lines.

- Platelets (~1x10^9 cells/mL) were resuspended in 250 µL Tyrode´s buffer and lysed by addition of a same volume of ice-cold lysis buffer (2% Triton X-100 or CHAPS, 100 mM Tris.HCl, pH 7.4, 10 mM EGTA, protease inhibitors)
- lysis was performed on ice for 20 minutes
- for cell culture cells, a detergent lysate was prepared by lysing a membrane pellet (prepared as in section 3.1.8) in 500 µl ice-cold lysis buffer (1% Triton X-100, 150 mM NaCl, 10 mM Tris-Cl, pH 7.4, 5 mM EGTA, and protease inhibitors)
- the lysate was then brought to 50% sucrose by addition of 800 µL 80% sucrose in TBS containing 1% detergent
- 1,2 mL of the 50%-sucrose-layer was pipetted onto the bottom of a SW50-Beckman centrifuge tube
- this layer was overlaid with 0.8 mL 40% sucrose in TBS, followed by 2 mL of 35% and 0.5 mL 5% sucrose in TBS
- the gradient was centrifuged at 48.000 rpm (230.000 xg) for 17 to 18 hours in a Beckman Ultracentrifuge at 4°C
- nine fractions of 0.5 mL were collected from the top of the gradient, the pellet was resuspended in 0.5 mL of TBS, pH 7.4; fractions were analysed by SDS-PAGE, silver staining and western blotting

3.1.12 Immunoprecipitation

The protocol for immunoprecipitation was adapted from *"Current Protocols in Cell Biology"* (Bonifacino and Dell'Angelica, 1998).

Solutions: PBS

TX-100 Lysis-Buffer: 1% w/v Triton X-100
                              50 mM Tris.HCl, pH 7.4
                              300 mM NaCl
                              5 mM EDTA
                              0.02 % w/v sodium azide
(this mixture can be stored for several months at 4°C)
                              5 μg/ml aprotinin
                              5 μg/ml leupeptin
                              0.5 μg/ml pepstatin A
                              0.4 mM AEBSF
                              10 mM iodoacetamide
(add protease inhibitors and iodoacetamide directly before use)

RIPA-Lysis-Buffer: 1% w/vNP-40
                              1% sodium-deoxycholate
                              50 mM Tris.HCl, pH 7.4
                              150 mM NaCl
                              1 mM EDTA
                              5 μg/ml aprotinin
                              5 μg/ml leupeptin
                              0.5 μg/ml pepstatin A
                              1 mM PMSF or 0.4 mM AEBSF
Phosphatase Inhibitors: 1 mM sodium vanadate
                              1 mM NaF
(alternatively, Phosphatase Inhibitor cocktails I and II from Sigma can be used at a dilution of 1/100)

wash buffer TX: 0.1% w/v Triton X-100
                              50 mM Tris.HCl, pH 7.4
                              300 mM NaCl
                              5 mM EDTA
                              0.02% w/v sodium azide

wash buffer RIPA: 0.1% NP-40

0.1% sodium deoxycholate

50 mM Tris.HCl, pH 7.4

300 mM NaCl

5 mM EDTA

0.02% w/v sodium azide

10% w/v BSA stock solution in milliQ-H$_2$O

50% v/v slurry of ProteinA-Agarose beads in phosphate buffer (20 mM phosphate, pH 8, 150 mM NaCl)

- HeLa cells (stably expressing the tagged protein of interest) were cultivated on 100mm cell culture dishes;
- at confluency, the plates were removed from the incubator, washed twice with 3 ml ice-cold PBS and the cells were lysed by addition of 1 ml of ice-cold lysis buffer (either TX-100 or RIPA-lysis buffer);
- the cells were scraped off with a rubber policeman and were transfered to an 1.5 ml Eppendorf tube, vortexed thoroughly and left on ice for 20-30 minutese
- the lysates were cleared by centrifugation (15 min, 16.000xg, 4°C), the supernatant was transferred to a new tube
- a preclearing step was performed by adding 30 µl of the ProteinA-Agarose to the lysate and rotating for 30 minutes, the beads were spun down after the pre-clearing step and the supernatant was then combined with the antibody-ProteinA-Agarose complexes;
- ProteinA-Agarose-antibody complexes were prepared as follows:
    - 30 µl of the ProteinA-Agarose slurry were diluted with 500 µl PBS, and the respective amount of primary antibody was added:

        1-5 µl of polyclonal antiserum

        1µg of purified polyclonal/monoclonal antibody

        50 µl of hybridoma culture supernatant

    - the suspension was mixed thoroughly and tumbled end-over-end for 1-2 hours at 4°C;
    - then, the beads were recovered by centrifugation (15-30 seconds), the supernatant was discarded and the beads were washed twice with the respective lysis buffer;
    - finally, the beads were spun down again, the lysis buffer was aspirated and the antibody-Protein-A-Agarose complexes were ready for immunoprecipitation;

- per immunoprecipitation, 10 µl of 10% BSA and 500 µl of pre-cleared lysate were added to the antibody-ProteinA-Agarose complexes, the suspensions were carefully

mixed and tumbled end-over-end for 1-2 hours at 4°C;

- after this incubation, the beads were spun down, and the supernatant was removed and transferred to a fresh tube (an aliquot of this IP-supernatant can also be analysed by western blotting, alternatively, a second IP can be performed with a different antibody)
- the beads were washed 4 times with 1 ml of the respective wash buffer and finally with 1 ml of PBS;
- the beads were spun down and the PBS was aspirated as completely as possible;
- the precipitated proteins were eluted from the beads by rotating with 50-100 µl of SDS sample buffer for 1 hour at RT, the beads were spun down again and the immunoprecipitate was recovered from the beads and transfered to a new tube; alternatively, the beads can be directly boiled in the respective volume of SDS sample buffer; sometimes, it can be useful to use SDS sample buffer without mercaptoethanol or DTT (non-reducing sample buffers) to avoid strong bands from the antibodys at 55 and 25 kDa;
- IPs were analysed by SDS-PAGE and western blotting or silver staining;
- as controls, IPs were performed with either pre-immune serum (for rabbit antiserum) or with irrelevant hybridoma supernatants/purified antibodies

3.2 Molecular biological techniques

3.2.1 Bacterial strains, media and solutions for bacteria culture

Bacteria:

DH5α, chemically competent, subcloning efficiency (Invitrogen)
DH10B
BL21

The DH5α strain was used as a host for all standard cloning procedures.
The genotype of this strain is: F⁻ φ80d*lac*ZΔM15 Δ(*lac*ZYA-*arg*F) U169 *rec*A1 *end*A1 *hsd*R17(r_k^-, m_k^+) *pho*A *sup*E44 λ⁻ *thi*-1 *gyr*A96 *rel*A1.

The purchased cDNA clones (STOML-1, STOML-2, STOML-3) were provided in the DH10B *E. coli* strain.
This strain was optimised for the construction of cDNA libraries and has the following genotype: F⁻ *mcr*A Δ(*mrr-hsd*RMS-*mcr*BC) φ80*lac*ZΔM15 Δ*lac*X74 *rec*A1 *end*A1 *ara*Δ139 Δ(*ara*, *leu*)7697 *gal*U *gal*K λ⁻ *rps*L (Str^R) *nup*G.

The BL21 strain was planned to be used for bacterial expression and subsequent purification of the SCP-2 domain of SLP-1 cloned into the pET28a vector. Due to lack of time, only one transformation of BL21 cells with the pET28a constructs was performed, and proper

expression of the protein domain was not verified yet.

The genotype of the BL21 strain is: F⁻ *omp*T *hsd*S$_B$ ($r_B^-m_B^-$) *gal dcm rne1*31.

Media and solutions:

LB medium: 1% w/v NaCl

1% w/v BactoPeptone (Difco)

0.5% w/v yeast extract

pH adjusted to 7.5 and autoclaved

LB agar: 15 g agar are solubilized in 1 l of LB medium,

the solution is autoclaved and stored at 4°C;

Antibiotics:

Antibiotic	stock solution	final concentration
Ampicillin (AMP)	50 mg/ml in H_2O	50 µg/ml
Kanamycin (KAN)	10 mg/ml in H_2O	30 µg/ml
Chloramphenicol (CAM)	34 mg/ml in EtOH	25 µg/ml

LB agar plates:

LB agar is melted in the microwave oven (low power setting, 150 W, takes about 30 minutes), then the solution is cooled down to 65°C in a heated water bath, the respective amount of antibiotic is added from a stock solution and the plates are poured in 10cm culture dishes, cooled down to RT and stored at 4°C until use;

3.2.2   Polymerase chain reaction (PCR)

Equipment:

RoboCycler Gradient 40 (Stratagene)

Composition of a single reaction:

1.5 µl forward Primer (50 ng/µl)

1.5 µl reverse Primer (50 ng/µl)

1 µl DNA-template (100-250 ng)

2 µl 10 mM dNTPs (dATP, dCTP, dGTP, dTTP, 10 mM each)

5 µl 10x Pfu buffer (Stratagene)

0.5 µl Pfu Polymerase (Stratagene)

H_2O-PCR ad 50 µl

- the   different   PCR-reactions   were   prepared   in   0.5   ml   PCR   tubes   at   4°C,   the

proofreading-competent Pfu-Polymerase was added last;

- the following standard PCR protocol was used (unless indicated) and found appropriate for our cloning needs (inserts in the size range from 800-1500 base pairs):

Step 1:	94°C	1 minute	1 cycle
Step 2:	94°C	1 min 30 sec	
	55°C	1 min 30 sec	35 cycles
	72°C	3 min	
Step 3:	72°C	5 min	1 cycle

- the PCR reactions were stored at 4°C until further use, an aliquot (1-2 µl) was diluted to 10 µl with a 1/5 mixture of 6x loading buffer and H_2O and analysed on 1-1.5% agarose gels

Figure 8: PCR mutagenesis

Figure 8**:** Schematic overview of the method used for the introduction of defined point mutations into proteins. Reprinted from the on-line version at the NCBI bookshelf of "Human Molecular Genetics 2"by Tom Strachan and Andrew P. Read, Garland Publishing Ltd.
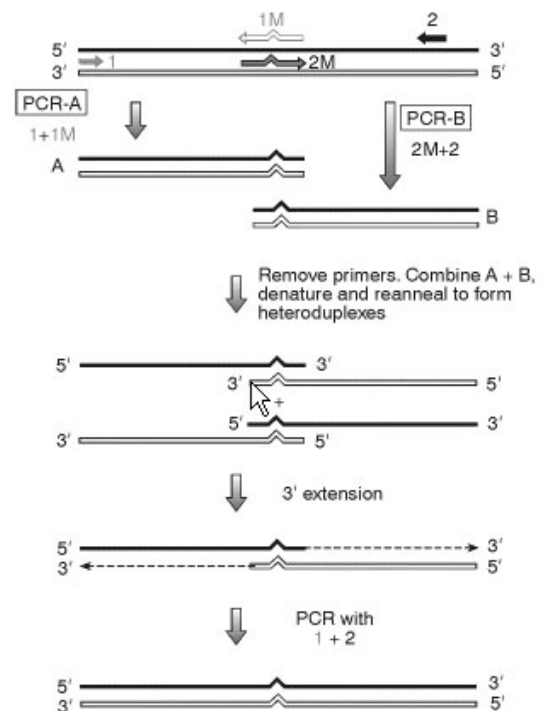
3.2.3   Site-directed mutagenesis (oligonucleotide-directed PCR mutagenesis)

- to introduce point-mutations in the coding sequence of stomatin or SLP-1, forward and reverse oligonucleotides carrying the desired mutant codons were designed
- on both sides of the introduced mismatch, approximately 18 matching bases were included

- a schematic representation of the mutagenesis procedure is given in Figure 8.
- first, 2 separate PCRs are performed, with a N-terminal forward primer and the mutagenic reverse primer, and the complementary reaction, with the mutagenic forward primer and a C-terminal reverse primer;
- the PCR products were then separated on low-melting agarose gels (NuSieve GTG agarose from BioWhittaker, 2-3%), the bands of correct size were excised, the agarose was melted at 50-60°C, and the fragments were used as "Megaprimers" for the subsequent second PCR step; the N- and C-terminal primers were included in the reaction mix to get strong amplification of the mutagenic full-length construct;
- the mutagenic insert was then purified, digested and ligated into the vector of choice
- the mutations were verified by sequencing of the inserts after cloning

3.2.4   DNA sequencing

- DNA sequencing was performed by capillary electrophoresis of fluorescently end-labelled, prematurely terminated PCR products with an ABI PRISM 310 automated sequencer.

Sequencing PCR: (V=20µl)   1 µl sequencing primer (4-10 pmol/µl)
2 µl BigDye terminator Mix (ABI, contains Taq Polymerase, dNTPs and ddNTPs labelled with different fluorophores in an optimal ratio)
3 µl 5X sequencing buffer (100 mM Tris·HCl, pH 9, 10 mM MgCl$_2$
0.2-0.5 µg Plasmid-DNA
H$_2$O ad 20 µl

PCR protocol:	Step 1:	96°C	5 minutes	1 cycle
	Step 2:	96°C	1 min 30 sec	
		50°C	1 min 30 sec	30 cycles
		60°C	4-5 min	

- excess fluorescent ddNTPs must be removed prior to capillary electrophoresis by Sephadex G-50 minicolumn purification
- Sephadex G-50 (Amersham-Pharmacia, DNA grade) was swollen o/n in milliQ-water (1 g Sephadex G-50 in 15 ml of H$_2$O)
- 650 µl of this G-50 slurry were pipetted into a UltrafreeMC column (Millipore) in an Eppendorf tube, and the tube was centrifuged for 3 minutes at 2500 rpm
- the flow-through was discarded and the column was placed in a fresh tube
- the product of the sequencing PCR (~20 µl) was loaded on top of the G-50 column

- the tube was again spun for 3 minutes at 2500 rpm
- the flow-through should have approximately the same volume as the added PCR reaction (~20 µl) and can be directly used for sequencing

3.2.5 Purification of DNA from PCR reactions

Phenol-chloroform extraction of PCR fragments:

- the PCR reaction was diluted with 100µl H_2O-PCR to 150 µl
- an equal volume of equilibrated phenol/chloroform/isoamylalcohol (25:24:1, Fluka) was added and the mixture was vortexed;
- after centrifugation (14.000 rpm, 2 minutes), the aqueous (upper) phase was transferred to a new tube, and the organic phase was mixed with 150 µl of TE, vortexed and centrifuged again
- the aqueous phases were combined and re-extracted with an equal volume of chloroform/isoamylacohol (24:1), vortexed and centrifuged again
- the aqueous phase was carefully removed from the organic phase, mixed with 1/9 volume of 3 M sodium acetate (vortex!) and 2.5 volumes of 96% EtOH (vortex!) and kept at -20°C o/n to precipitate the DNA
- the precipitate was pelleted by centrifugation (14.000 rpm, 30 minutes, 4°C), the supernatant was discarded and the pellet was washed once with 150 µl 70% EtOH (vortex!), and centrifuged (14.000 rpm, 3 minutes)
- the supernatant was discarded and the DNA pellet was air-dried and resuspended in 20 µl of H_2O-PCR

Purification of PCR fragments with the Wizard SV Gel and PCR Clean-Up system (Promega):

- the PCR reaction was combined with an equal volume of Membrane Binding Solution (acidic solution (pH 5) containing a high concentration (4.5 M) of guanidine isothiocyanate), mixed thoroughly, transferred into the DNA binding columns and incubated for 1 minute
- the column was centrifuged (14.000 rpm, 1 minute), the flow-through was discarded and the column was washed with 700 µl Membrane Wash Solution (an acidic buffer containing 80% EtOH, add wash solution, incubate for ~1min, centrifuge (14.000 rpm, 1 min.))
- the washing step was repeated with 500 µl Membrane Wash Solution, centrifugation time 5 minutes!
- finally, the collection tube was emptied again, and the empty column was centrifuged for 1-2 minutes with the centrifuge lid open (to allow evaporation of any residual EtOH)
- the DNA binding column was then transferred to a clean 1.5 ml tube and the DNA is

eluted with 20 µl H$_2$O-PCR or TE

3.2.6 Restriction digestion of PCR fragments and vector DNA

- restriction enzymes used were from New England Biolabs, and the recommended RE buffers were used for single- and double digests; in case of a total incompatibility of the two buffers for a digest, sequential digestion was performed;

control digests: (V=10µl) 1 µl 10x NEBuffer (NEB 1, 2, 3,4, EcoRI, BamHI)
0.2 µl restriction enzyme (s)
2 µl Mini-Prep-DNA/vector DNA
H$_2$O ad 10 µl

preparative digests:

for vectors: (V=50µl) 5 µl 10x NEBuffer (NEB 1, 2, 3,4, EcoRI, BamHI)
1 µl restriction enzyme (s)
~ 3 µg vector DNA
H$_2$O ad 50 µl

for inserts: (V=25µl) 2.5 µl 10x NEBuffer (NEB 1, 2, 3,4, EcoRI, BamHI)
0.5 µl restriction enzyme (s)
20 µl purified insert-DNA
H$_2$O ad 25 µl

- control and preparative digests were analysed by agarose gel electrophoresis
- preparative digests were purified from the alarose gels as described in 3.2.11

3.2.7 Dephosphorylation of (vector) DNA

- for cloning of inserts into vectors via a single restriction site (non-directional cloning), the vector DNA was dephosphorylated after the restriction digest

(restriction digest, V=50µl) +5 µl 10x Alkaline Phosphatase buffer (Promega)
+0.5 µl Alkaline Phosphatase (1 U/µl, Promega)

- the reaction mix was incubated for 30 minutes at 37°C
- then, another 0.5 µl of Alkaline Phosphatase was added, followed by further incubation for 30 minutes at 37°C
- the reaction was processed for Agarose gel electrophoresis and the vector DNA was

isolated as described

3.2.8 Phosphorylation of insert DNA/oligonucleotides

- for cloning methods where the inserts are directly used without a restriction digest (e.g. blunt-end cloning after PCR, insertion of oligonucleotide linkers etc.), the inserts/oligonucleotides/Primers have to be phosphorylated prior to use
- phosphorylation was done with the T4 polynucleotide kinase from Promega, the reaction mix was as follows:

> 300-350 ng insert DNA / 10 μg of oligonucleotide/Primer
> 5 μl 10 mM ATP
> 5 μl 10x One-Phor-All buffer (Promega)
> 2 μl T4 Kinase (Promega)
> H_2O-PCR to 50 μl

- the reaction mix was incubated for 1 hour at 37°C, then, the reaction was stopped by adding 2 μl of 0.5 M EDTA
- purification of the DNA was either done by Phenol extraction/ethanol precipitation or with the Promega Wizard SV Gel and PCR Clean-Up system;

3.2.9 Creation of blunt end DNA with Klenow Polymerase fragment

- for some cloning purposes, it was necessary to convert DNA containing "sticky" ends (5´ or 3´ overhangs) to blunt end DNA
- the optimal buffer for the Klenow Polymerse is NEB Buffer 2, but according to the manufacturer, the enzyme should be active in all restriction enzyme buffers
- after the restriction digest of the vector/insert DNA, 33 μM of dNTPs were added to the restriction enzyme digest from a 1 mM stock solution
- approximately 1U Klenow polymerase (5U/μl) was added per μg of DNA
- incubation was performed for 15 minutes at 25°C
- Klenow polymerase fills in 5´overhangs (polymerase activity) and removes 3´overhangs (3´-5´exonuclease activity)
- after the 15 minute incubation, the Klenow polymerase is inactivated by adding 10 mM EDTA and heating to 75°C for 20 minutes
- the vector/insert DNA is the purified as described

3.2.10 Agarose Gel Electrophoresis

Equipment: MINNIE submarine agarose gel unit HE33 (Hoefer)

Mighty Bright power supply, Model UVTM 25 (Hoefer)

Microwave

UV screen

GenXpress Doc-Print Video system and Mitsubishi P91 thermal printer

Solutions:	running buffer (0.5x TBE)	50 mM Tris
		45 mM boric acid
		1 mM EDTA
	6x loading buffer	0.25% bromophenol blue
		0.25% Xylene Cyanol FF
		15 % Ficoll (Type 400, Amersham)
	ethidium bromide stock	10 mg/ml in milliQ-H_2O

- Agarose (GibcoBRL) was weighed in an Erlenmeyer (to yield a 0.7-1.5 % w/v solution in 60 ml 0.5x TBE), TBE was added, the suspension was mixed thoroughly and the agarose was solubilized by boiling in the microwave
- the agarose solution was cooled down to approximately 50°C , 6 µl of the ethidium bromide stock was added and the solution was thoroughly mixed
- the agarose solution was poured into the horizontal gel holder with the appropriate comb and let stiffen (~20 min)
- the comb was carefully removed, the gel was transferred to the agarose gel unit, overlaid with running buffer, and the samples (mixed with 1/5 vol. of 6xloading buffer) were loaded together with a DNA size standard (1kb DNA ladder from GibcoBRL or Fermentas)
- electrophoresis was performed at 90 V for 30-45 minutes
- DNA was visualized under UV light, and pictures of the gel were taken

3.2.11 Purification of DNA from Agarose gels

Purification of DNA from gel slices with the QIAEX II Gel Extraction Kit (Qiagen)

Solutions: 10 mM Tris.HCl, pH 8.5

- insert and vector bands were excised from agarose gels on the UV screen, and purification of DNA from the gel slices was done exactly according to the manufacturer´s instructions;
- vector DNA was eluted from the QIAEX beads with 50 µl of Tris.HCl, whereas insert DNA was eluted with 20 µl of Tris.HCl

(this method was most frequently used for purification, and yielded good results)

Purification of DNA bands from DEAE-membrane:

Materials: NA45 DEAE membrane (0.45 µm), Schleicher&Schuell

Solutions: low-salt washing buffer   50 mM Tris.HCl, pH 8
                                                 150 mM NaCl
                                                 10 mM EDTA, pH 8

                 high-salt washing buffer   50 mM Tris.HCl, pH 8
                                                 2 M NaCl
                                                 10 mM EDTA, pH 8

                 10 M ammonium acetate

- after separation of DNA fragments by agarose gel electrophoresis, the band of interest was identified
- the gel was cut exactly below the band, and a piece of DEAE membrane was inserted in the cleft
- the gel was put back into the apparatus, and electrophoresis was performed for another 5 minutes (then, the gel was checked under the UV screen; the band of interest should have disappeared, and the EtBr staining should be detectable on the DEAE membrane; if transfer was still incomplete, electrophoresis was continued for 2-3 minutes)
- the piece of DEAE membrane was transfered to a tube and was washed 6 times with 1 ml low-salt washing buffer
- the DNA was eluted from the membrane by incubation with 150 µl high-salt buffer at 65°C for 30 minutes
- the elution step was repeated, the eluates were combined
- DNA was precipitated by adding 1/5 volume (60µl) 10 M ammonium acetate (vortex!) and 2 volumes (600 µl) 96% EtOH (vortex!), the mixture was incubated for at least 30 minutes at -20°C
- the DNA was pelleted (14.000 rpm, 30 minutes, 4°C), the supernatant was discarded
- the pellet was washed with 150 µl of 70% EtOH (vortex, centrifuge 14.000 rpm, 3 minutes, remove supernatant)
- the pellet was air-dried, resuspended in 7-10 µl of H_2O-PCR and DNA was stored at -20°C
  (with this method, stronger concentration of digested insert-DNA can be achieved)

Isolation of DNA from gel slices with the Wizard SV Gel and PCR purification kit:
- gel bands were excised as described above
- the bands were weighed and mixed with 10 µl of Membrane Binding Solution per 10

µg gel slice

- the mixture was vortexed and incubated at 50-60°C until the gel slice was completely dissolved
- the solution was transferred to the DNA binding column, incubated for 1 minute and the rest of the procedure was identical to the purification of PCR reactions (Verweis) (this is the fastest method, which was only used if time was short, this kit is best used for purification from PCR reactions; vector bands from gels can be problematic because of their weight!)

3.2.12 Ligation of DNA fragments into vector DNA

Materials: T4 DNA ligase 1U/µl (Invitrogen)

Ligation reaction:

- for a ligation with "sticky ends", approximately a 3-fold molar excess of insert over vector DNA should be used; the amounts of vector and insert DNA were estimated on an Agarose gel prior to ligation;

a typical ligation reaction was as follows:

> insert DNA 5-7.5µl
> vector DNA 0.5-1µl
> 2 µl 5x ligase buffer
> 0.5 µl T4 DNA Ligase (diluted to 0.1 U/µl in 1x Ligase buffer)
> H_2O-PCR to 10 µl

- a control ligation reaction (insert DNA replaced with H_2O) was always included
- the reactions were mixed gently and incubated for 1-2 hours at room temperature (for sticky ends; for blunt-end cloning, incubation o/n at 16°C is necessary, and 1 µl of undiluted T4 ligase should be used)
- the ligation reaction was diluted 1:5 in H_2O-PCR, and 5 µl of this dilution were used for transformation of chemically competent E. coli; the remainder of the ligation reaction was stored at 4°C
-

3.2.13 Transformation of chemically competent E. coli with the heat-shock method

Materials: chemically competent E. coli, strain DH5α, subcloning efficiency (Invitrogen)
water bath at 37°C

- chemically competent E. coli were thawed upon arrival, aliquoted and stored at -80°C until use
- aliquots were thawed on ice directly before use
- the competent cells were mixed with 5µl of the respective ligation reaction and

incubated for 30 minutes on ice

- transformation was performed by a brief heat-shock (transfer the cells to the 37°C-water bath for 30 seconds)
- cells were incubated for further two minutes on ice, then mixed carefully with 1 ml of LB-medium, transferred to a 14ml round-bottom polypropylene tube (Falcon) and incubated in a shaker for 1 hour (recovery)
- then, 1/10 and 9/10 of the cells were plated on the respective selective LB plates and incubated over night in an incubator at 37°C
- grown colonies were counted, numbers were compared with the control plates;
- single colonies were picked, single colony streaks were produced on fresh plates and the colonies were analyzed for the presence of the correct plasmid DNA (Mini-Prep or single-colony PCR)

3.2.14 Plasmid Mini-Prep (boiling Prep)

Equipment: Lab-Therm Shaker (Adolf Kühner AG)
              Eppendorf desk-top centrifuge
              sterile toothpicks/yellow pipette tips

Solutions: STET lysis buffer: 8% w/v sucrose
                                            0.5% Triton X-100
                                            50 mM EDTA pH 8
                                            50 mM Tris.HCl pH 8
                                            sterile filter, store at -20°C;

              Lysozyme stock solution: 50 mg/ml in 250 mM Tris.HCl, pH 8

              RNAse A stock solution: 10 mg/ml in milliQ-H_2O

              70% EtOH

              TE buffer: 10 mM Tris.HCl, pH 8
                                            1 mM EDTA, pH 8

- 6 colonies per agar-plate were picked in case of directional cloning (2 different restriction enzymes), whereas 12 colonies were picked when the insert was not cloned directionally;
- the colonies were picked with sterile toothpicks or sterile yellow pipette tips
- the colonies were streaked out on fresh agar plates before inoculating the medium (these plates are grown o/n and can then be used to inoculate cultures for Midi-Preps)
- 4 ml of LB medium supplemented with the respective antibiotic were inoculated with the toothpicks/tips and grown over night at 37°C in a shaker
- 2 ml of these o/n cultures were transferred to 2 ml Eppendorf tubes and the bacteria

were pelleted by centrifugation (Eppendorf desk-top centrifuge, 5000 rpm, 5 minutes)

- the supernatant was sucked off and the pellet was resuspended in 500 µl ice-cold STET buffer by rigorous vortexing
- 4 µl of Lysozyme stock solution were added and the lysate was incubated for 10 minutes on ice
- the lysates were then heated to 95°C for 3 minutes
- debris was pelleted by centrifugation (13.000 rpm, 15 minutes)
- the pellet was removed with a toothpick, and 4 µl of RNAseA stock solution were added
- the lysate was incubated for 30 minutes at RT
- then, 500 µl isopropanol were added to precipitate plasmid DNA, the solution was vortexed and centrifuged (13.000 rpm, 15 minutes)
- the supernatant was discarded and the pellet was washed once with 150 µl 70% EtOH, pelleted again (13.000 rpm, 15 minutes) and finally resuspended in 80 µl of TE buffer

3.2.15 Single-colony-PCR

- single colonies grown after transformation and plating o/n were picked with a sterile yellow tip, a single-colony streak was produced on a new LB-antibiotic plate
- the tip was then transferred to a sterile tube with 50 µl H_2O-PCR, the tube was vortexed vigorously and the tip was discarded
- the tubes were heated to 95°C for 5 minutes and centrifuged (14.000 rpm, 1 minute)
- 10 µl of the supernatant were used as template for a PCR reaction, the primers were chosen to reveal the orientation of the insert (e.g. the forward primer was slightly upstream of the MCS, and the reverse primer was somewhere in the coding sequence; correct insertion leads to a fragment of known length)

PCR reaction: 10 µl template DNA
1 µl 10 mM dNTPs
5 µl 10x Taq buffer
2 µl 25 mM MgCl2 solution (final: 1 mM)
1 µl forward primer (50 ng/µl)
1 µl reverse primer (50 ng/µl)
0.5 µl Taq-Polymerase (Promega)
to 50 µl with H_2O-PCR

- PCRs were done as described, and 1-2 µl aliquots of the PCRs were analysed by Agarose gel electrophoresis
- colonies with correct inserts were chosen and used for Midi-Preps

3.2.16 Plasmid Midi-Prep

Qiagen Plasmid Midi Kit:

Equipment: Lab-Therm Shaker (Adolf Kühner AG)
RC5C preparative centrifuge (Sorvall Instruments)
sterile toothpicks/yellow pipette tips
QIAGEN Plasmid Midi Kit

- a fresh o/n single colony streak from a LB agar plate was used for inoculation, bacteria were picked with a sterile inoculation loop
- approximately 100 ml of LB-medium (+antibiotic) were inoculated and cultivated o/n at 37°C in a shaker
- 100 µl of each culture were transferred into an Eppendorf tube, mixed with 400 µl of sterile glycerol and stored at -80°C (Glycerol-stocks)
- the rest of the cultures was transferred to Sorvall GSA beakers and the bacteria were pelleted by centrifugation (GSA rotor, 3000 rpm, 10 minutes, 4°C)
- the supernatant was discarded and the pellet was used to isolate the plasmid DNA according to the QIAGEN Plasmid Preparation handbook (basically, the bacteria are lysed in an alkaline SDS lysis buffer, the lysate is filtered and the plasmid DNA is bound to an anion exchanger, washed bound to the column and eluted at high salt concentrations)
- after elution of the plasmid DNA from the anion exchanger with 5 ml of elution buffer into a corex tube, 3.5 ml of isopropanol were added to precipitate DNA, the solution was vortexed thoroughly and then centrifuged for 30 minutes (Sorvall centrifuge, HB-4 swing-out rotor, 12.000 rpm, 4°C)
- the supernatant was discarded, and the pellet was washed with 2 ml of 70% ethanol (add washing solution, vortex, discard washing solution)
- the pellet was then air-dried, finally resuspended in 150 µl of sterile H_2O and stored at -20°C
- the plasmid´s concentration and purity was analysed as follows:
  - the optical density (OD) of a 1:100 dilution of the plasmid DNA is determined at 260 and 280 nm
  - concentration: 1 OD corresponds to   50µg/ml double-stranded DNA
    40µg/ml single-stranded DNA or RNA
    30µg/ml single-stranded oligonucleotides
  - purity: the ratio between OD_{280} and OD_{260} should be 2/3 to 3/4

Plasmid Midi-Prep with the PureYield Plasmid Midiprep system (Promega):

Equipment: Lab-Therm Shaker (Adolf Kühner AG)
RC5C preparative centrifuge (Sorvall Instruments)

> Heraeus Varifuge 3.0R
>
> Vac-Man Jr. Laboratory Vacuum Manifold
>
> sterile toothpicks/yellow pipette tips

- approximately 100 ml over-night culture and a glycerol stock was prepared as described above
- the rest of the cultures was transferred to Sorvall GSA beakers and the bacteria were pelleted by centrifugation (GSA rotor, 3000 rpm, 10 minutes, 4°C)
- the pellet was used to isolate plasmid DNA according to the technical manual of the PureYield plasmid MidiPrep system from Promega (similar system, filtration column and DNA binding column can be used by centrifugation of the lysate or by use of a vacuum manifold; sterile H_2O is used for elution of the DNA)
- due to the presence of EtOH in the final eluate when using the original protocol, a precipitation step was included
- the DNA was eluted from the Promega column with the elution buffer from the Qiagen Kit, DNA precipitation, washing and resuspension in sterile H_2O was done as described (this procedure yielded plasmid DNA of higher purity)

3.2.17 Isolation of the SLP-1 coding sequence from the IMAGE clone

Image clone Nr. 5185908 was purchased from the RZPD (German Resource Center for Genome Research), RZPD Clone ID: IRATp970H0745D;

The full coding sequence of SLP-1 (gene name STOML-1) was inserted into the multiple cloning site of the pCMV-Sport6 vector (Invitrogen) via the 5´EcoRV and the 3´NotI
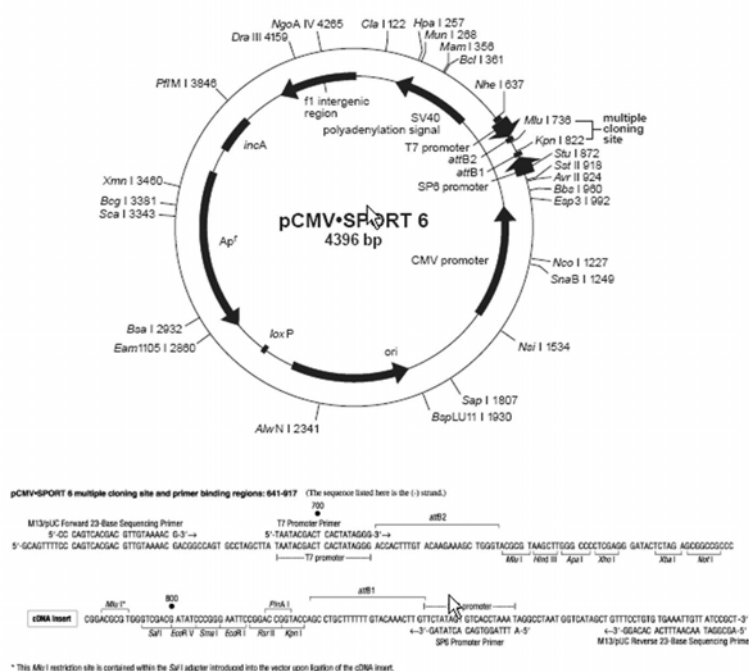
restriction sites.

Some DH10B bacteria were picked with an inoculating loop, streaked on a LB-AMP agar plate and incubated over night at 37°C. Then, single colonies were picked, streaked out on a

fresh LB-AMP plate and used to inoculate 100 ml LB-AMP for over-night cultures for Midi-Preps.

Midi-Preps were performed as described, the isolated vector DNA was resuspended in 150 μl of sterile H_2O and stored at -20°C. The vector DNA was digested with EcoRV and NotI and digested and undigested vector were analyzed by Agarose gel electrophoresis. The insert of the Midi-Prep vector DNA was sequenced with the SP6 promotor primer and was found to be identical to the SLP-1 cDNA sequence from the database. With the expression vector pCMV-Sport6, it should be possible to express untagged SLP-1 protein, but as we did not have an antibody recognizing the untagged SLP-1 protein, we had to construct tagged SLP-1 constructs. Therefore, we used the vector DNA as template for PCR reactions with the primers specified below, purified the PCR-products, performed restriction digests of the insert and vector DNA and ligated the coding region of SLP-1 into the described vectors, yielding in-frame fusions to either the short myc-tag, the GFP-tag or a 3xHA-tag.

Image clone Nr. 3346384 (SLP-2/STOML2) (RZPD Clone ID: IRALp962M085Q) and Image clone Nr. 5204252 (SLP-3/STOML3) (RZPD Clone ID: IRATp970D0742D) were also purchased. The coding sequence for SLP-3 was also present as EcoRV/NotI insert in pCMV-Sport6, whereas the coding sequence for SLP-2 was inserted into the MCS of the pOTB7 vector (CAM resistance) via a 5´EcoRI and 3´XhoI restriction site. The vector DNA was isolated as described above and the inserts were sequenced with the SP6 promotor primer. No further experiments were performed with these cDNAs, but they are ready for the preparation of tagged constructs and could be used in the future.

3.2.18 Cloning of tagged SLP-1 constructs

SLP-1-GFP:

Primers:	
forward: SLP-1 GFP NT EcoRI	CGGAATTCGCCATGCTCGGCAGGTCT
reverse: SLP-1 GFP CT SacII	TCCCCGCGGCTGCGCCCTTCAAGGCCCTGAGGAC

- the insert spanning the entire coding region of SLP-1 was prepared by PCR as described, digested with EcoRI and SacII and ligated into the pEGFP-N3 vector (BD Biosciences Clontech) digested with the same restriction enzymes
- this procedure leads to an in-frame fusion of the GFP coding sequence to the C-terminus of SLP-1, a linker sequence (GAAAAGSIAT) connects the final amino acid of SLP-1 and the start methionine of GFP

GFP-SLP-1:

Primers:	
forward: C/G/YFP-SLP1	ATCTCGAGCTCTCGGCAGGTCTGGG
reverse: SLP-1 myc CT SpeI	GGACTAGTCTTCAAGGCCCTGAGGAC

- the XhoI and XbaI restriction sites were used for cloning of GFP-SLP-1; the reverse primer for the SLP-1-myc construct was re-used, the insert was digested with XhoI and SpeI; SpeI and XbaI digestion creates compatible ends;

Restriction Map and Multiple Cloning Site (MCS) of pEGFP-N3 (Unique restriction sites are in bold). The *Not* I site follows the EGFP stop codon. The *Xba* I site (*) is methylated in the DNA provided by BD Biosciences Clontech. If you wish to digest the vector with this enzyme, you will need to transform the vector into a *dam*‾ host and make fresh DNA.
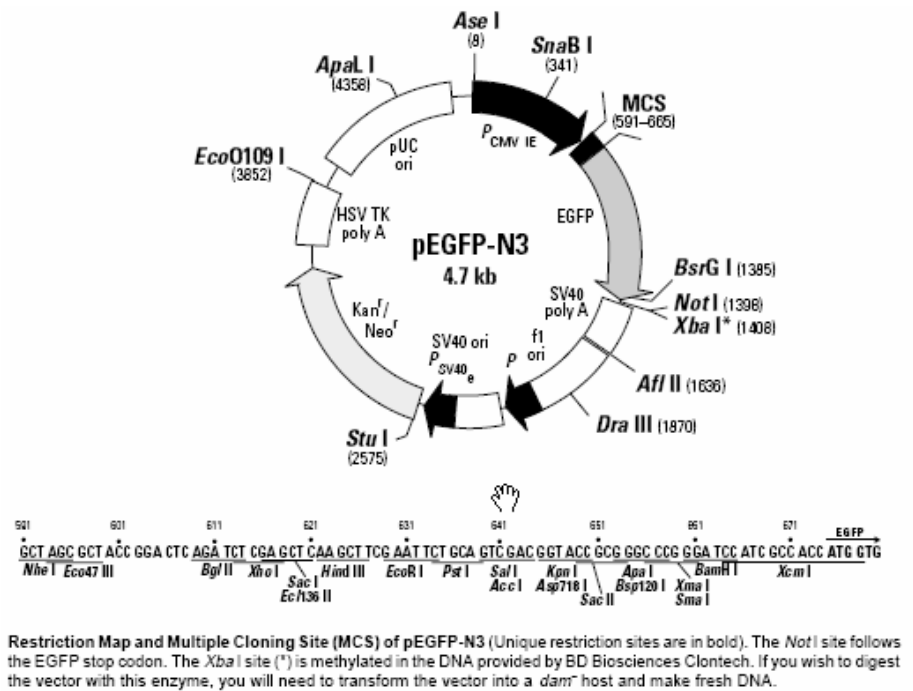
pEGFP-C1 Vector Information   PT3028-5

GenBank Accession #: U55763   Catalog #6084-1

Restriction Map and Multiple Cloning Site (MCS) of pEGFP-C1. All restriction sites shown are unique. The *Xba* I and *Bcl* I sites (*) are methylated in the DNA provided by BD Biosciences Clontech. If you wish to digest the vector with these enzymes, you will need to transform the vector into a *dam*‾ host and make fresh DNA.
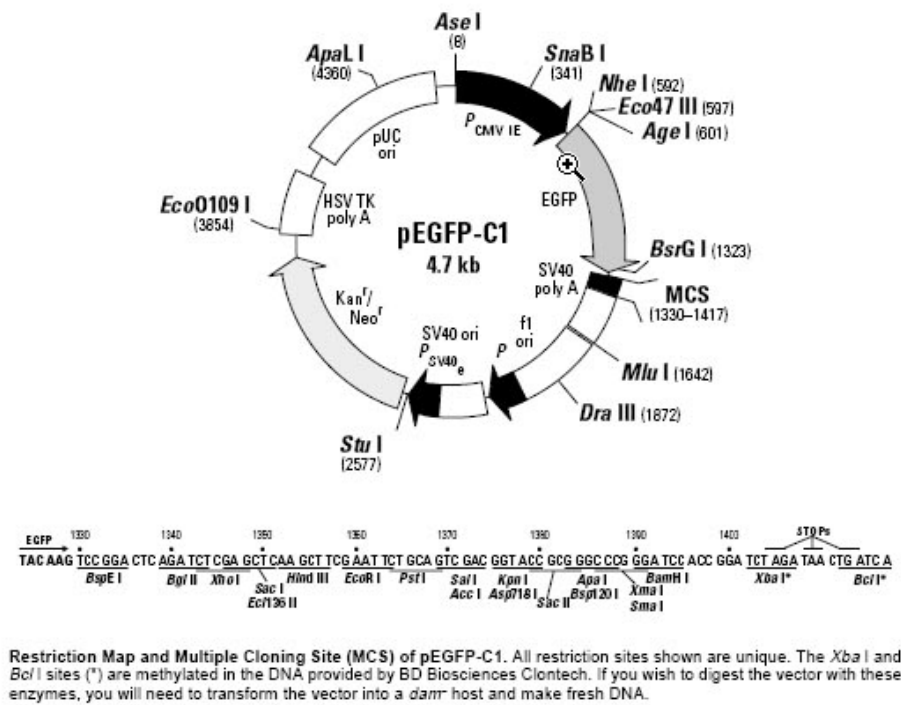
SLP-1-myc:

- to get a myc-tagged SLP-1 construct, the vectors used in our group had to be modified, because the SLP-1 coding region contains a KpnI restriction site, the use of the pEFKmyc vector constructed by Luc Snyers in our laboratory was not possible.

- therefore, a novel vector containing the myc tag and a stop codon in frame with a SpeI restriction site was constructed from the pEFBOSpuro vector (pEFBOSpuro is a 6.1 kb mammalian expression vector with the following features: the gene of interest is constitutively expressed through an EF1α promotor, for selection in bacteria, the vector contains an ampicillin resistance gene and for selection in mammalian cell lines a puromycin resistance gene as well as an ori for replication in E. coli)

eukaryotischer Expressionsvektor pEFBOS puro (~6.1 kb)
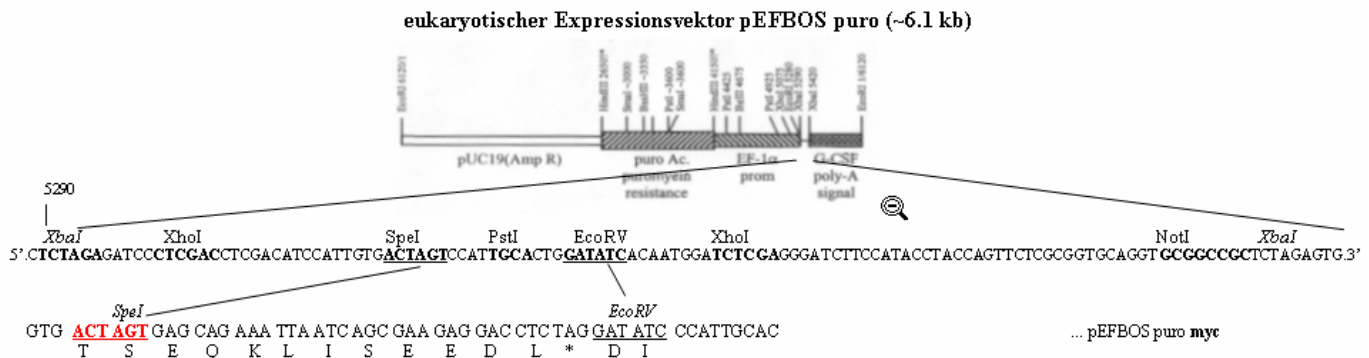
- forward and reverse oligonucleotides were designed, which code for the myc-tag (EQKLISEEDL) followed by a stop-codon; at the 5´end of the resulting double-stranded oligonucleotide, an overhang equal to digestion with SpeI was included, whereas the 3´overhang was designed to be blunt-ended

Oligonucleotides:	
Myc fwd SpeI/EcoRV	CTAGTGAGCAGAAATTAATCAGCGAAGAGGACCTCTAGGAT
Myc rwd SpeI/EcoRV	ATCCTAGAGGTCCTCTTCGCTGATTAATTTCTGCTCA

- the oligonucleotides were solubilized in water at a concentration of 2 µg/µl, the concentration was checked by measuring the $OD_{260/280}$ of a 1/400 dilution

- 10 µg of each oligonucleotide were used for a phosphorylation reaction:

> 10 µg Myc fwd (3.3 µl)/Myc rwd (5.1 µl)
> 5 µl 10 mM ATP
> 5 µl 10x One-Phor-All buffer (Promega)
> 2 µl T4 Kinase (Promega)
> H_2O-PCR to 50 µl

- the phosphorylation reaction was incubated for 1 hour at 37°C

- for the annealing of the oligos, the phosphorylation reactions Myc fwd and Myc rwd were mixed and transferred in a styrofoam floater to a beaker with boiling water, which was let cool down to RT (destruction of T4 kinase and annealing of the oligos)

- the double-stranded oligo was then purified with Sephadex G-50 nick columns

(Amersham/Pharmacia) as follows: the column was equilibrated with TE-buffer, then the annealing reaction (100 µl) was loaded on the column, the column was washed with 400 µl of TE and the ds-oligo was eluted with another 400 µl of TE

- 100 µl of this eluate were diluted with 400 µl of H₂O and the OD260/280 was measured (the concentration of the phosphorylated ds-oligo was ~72 ng/µl)
- a 1:60 dilution of the phosphorylated ds-oligo was made (~1.2 ng/µl) and used for the subsequent ligation reaction:

> (V=5µl) 2.5 µl phosphorylated ds-Myc-oligo
> 1.5 µl pEFBOSpuro, digested with SpeI and EcoRV
> 0.5 µl 10x Ligase buffer (Promega)
> 0.5 µl T4 Ligase

- the ligation was performed as described (3.2.12), and chemically competent E. coli (DH5α) were transformed as described (3.2.13)
- full-length SLP-1 inserts for cloning into this new myc-tag vector were prepared with the following primers:

Primers:	
forward: SLP-1 myc NT SpeI	GGACTAGTGCCATGCTCGGCAGGTCT
reverse: SLP-1 myc CT SpeI	GGACTAGTCTTCAAGGCCCTGAGGAC
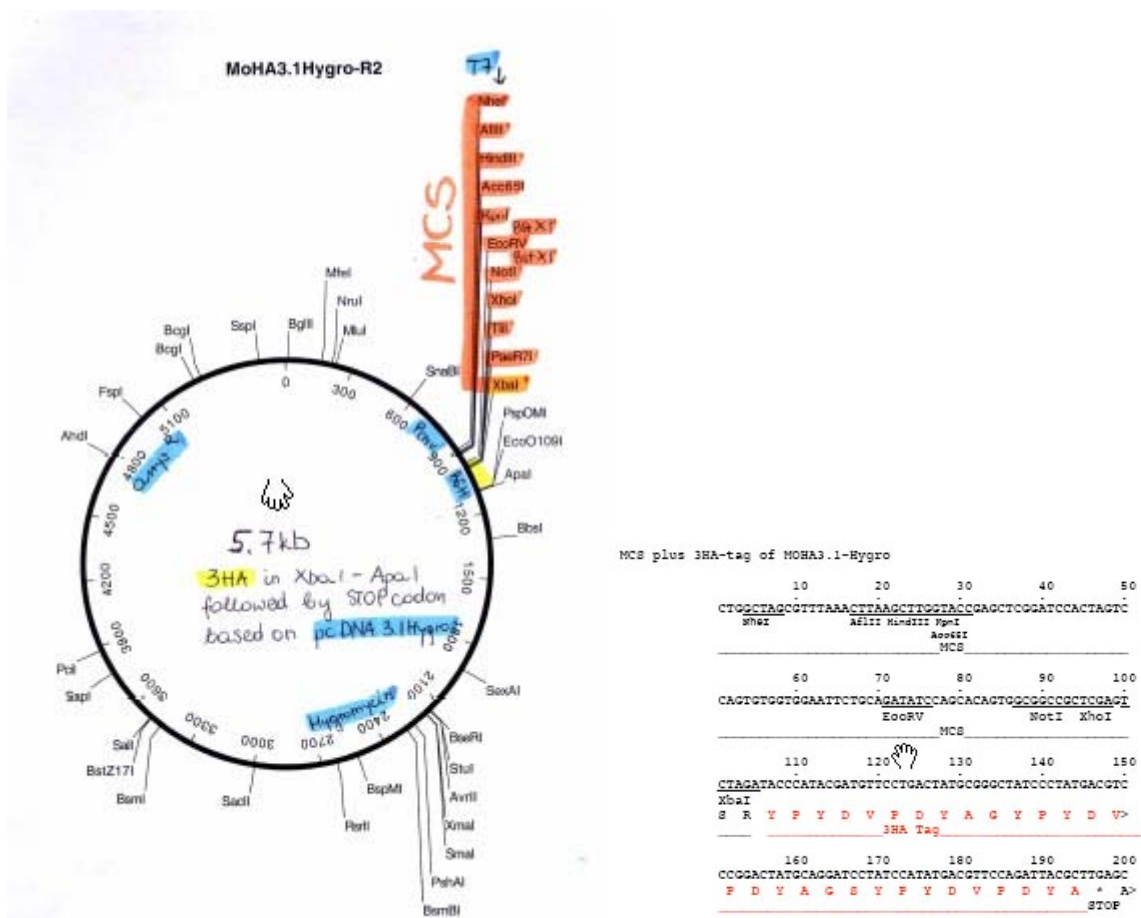
SLP-1-3HA:

- the vector pC3HA (based on pcDNA3.1hygro, with a triple HA-tag (YPYDVPDYAG) inserted) was a kind gift of Dr. Christoph Thiele (Max-Planck-Institute for Molecular Cell Biology and Genetics, Dresden); see vector map above!
- for cloning into pC3HA, I used the XbaI site (see vector map); because XbaI and SpeI restriction digestion produces compatible ends for ligation, I could use the primers for the myc-tagged constructs for PCR or prepare the inserts by digestion of the existing myc-tagged constructs with SpeI

Primers:	
forward: SLP-1 myc NT SpeI	GGACTAGTGCCATGCTCGGCAGGTCT
reverse: SLP-1 myc CT SpeI	GGACTAGTCTTCAAGGCCCTGAGGAC

3.2.19 SLP-1 truncation mutants

- N- and C-terminal truncations were prepared by performing PCR-reactions with primers which bound internally in the coding region and contained appropriate initiator/terminator codons and restriction sites for cloning into the vectors to yield GFP- or myc-tagged truncation mutants

SLP-1(1-288)-GFP:

Primers:	
forward: SLP-1 GFP NT EcoRI	CGGAATTCGCCATGCTCGGCAGGTCT
reverse: SLP-1 dnsLTP GFP	TCCCCGCGGCTGCGCCAGGCTGCTTCGGACTGG

SLP-1(1-224)-GFP:

Primers:	
forward: SLP-1 GFP NT EcoRI	CGGAATTCGCCATGCTCGGCAGGTCT
reverse: SLP-1 T225 GFP	TCCCCGCGGCTGCGCCCGGCTGGAGCACGGCCT

SLP-1(1-96)-GFP:

Primers:	
forward: SLP-1 GFP NT EcoRI	CGGAATTCGCCATGCTCGGCAGGTCT
reverse: SLP-1 T96 GFP	TCCCCGCGGCTGCGCCGATCCGGCCCAGGCGG

SLP-1(1-288)-myc:

Primers:	
forward: SLP-1 myc NT SpeI	GGACTAGTGCCATGCTCGGCAGGTCT
reverse: SLP-1 dnsLTP myc	GGACTAGTAGGCTGCTTCGGACTGG

SLP-1(1-224)-myc:

Primers:	
forward: SLP-1 myc NT SpeI	GGACTAGTGCCATGCTCGGCAGGTCT
reverse: SLP-1 T225 myc	GGACTAGTCGGCTGGAGCACGGCCTC

SLP-1(43-397)-myc:

Primers:	
forward: SLP-1 dNT myc	GGACTAGTCCACCATGGCCGATGTACCCCAGAGC
reverse: SLP-1 myc CT SpeI	GGACTAGTCTTCAAGGCCCTGAGGAC

SLP-1(43-288)-myc:

Primers:	
forward: SLP-1 dNT myc	GGACTAGTCCACCATGGCCGATGTACCCCAGAGC
reverse: SLP-1 dnsLTP myc	GGACTAGTAGGCTGCTTCGGACTGG

SLP-1(43-224)-myc:

Primers:	
forward: SLP-1 dNT myc	GGACTAGTCCACCATGGCCGATGTACCCCAGAGC
reverse: SLP-1 T225 myc	GGACTAGTCGGCTGGAGCACGGCCTC

SLP-1(11-397)-myc:

Primers:	
forward: SLP-1 dGYRAL	GGACTAGTCCACCATGCTGGGTGATTTTGACCGC
reverse: SLP-1 myc CT SpeI	GGACTAGTCTTCAAGGCCCTGAGGAC

SLP-1(1-384)-myc:

Primers:	
forward: SLP-1 myc NT SpeI	GGACTAGTGCCATGCTCGGCAGGTCT
reverse: SLP-1 T385 rwd	GGACTAGTCAGGTCGCCCTTCACC

SLP-1(1-288)-3HA:

Primers:	
forward: SLP-1 myc NT SpeI	GGACTAGTGCCATGCTCGGCAGGTCT
reverse: SLP-1 dnsLTP myc	GGACTAGTAGGCTGCTTCGGACTGG

SLP-1(1-224)-3HA:

Primers:	
forward: SLP-1 myc NT SpeI	GGACTAGTGCCATGCTCGGCAGGTCT
reverse: SLP-1 T225 myc	GGACTAGTCGGCTGGAGCACGGCCTC

SLP-1(1-49)-GFP:

Primers:	
forward: SLP-1 GFP NT EcoRI	CGGAATTCGCCATGCTCGGCAGGTCT
reverse: SLP-1 1-50 rwd SacII	TCCCCGCGGCTGCGCCGCTCTGGGGTACATCGG

- the same primers were used with the mutagenised Y7A and L10S constructs as templates, giving rise to SLP-1(Y7A,1-50)-GFP and SLP-1(L10S,1-50)-GFP constructs!

GFP-SLP-1(278-397):

Primers:	
forward: GFP-LTP fwd BglII	GGAAGATCTGCCCCTCAAGTTGGTGC
reverse: HIS/GFP LTP rwd BamHI	CGGGATCCCTACTTCAAGGCCCTGAGG

GFP-SLP-1(278-384):

Primers:	
forward: GFP-LTP fwd BglII	GGAAGATCTGCCCCTCAAGTTGGTGC
reverse: HIS/GFP LTPT385 rwd BamHI	CGGGATCCCTACAGGTCGCCCTTCACC

6xHIS-SLP-1(278-397):

Primers:	
forward: HIS LTP fwd NdeI	GGAATTCCATATGGCCCCTCAAGTTGGTGC
reverse: HIS/GFP LTP rwd BamHI	CGGGATCCCTACTTCAAGGCCCTGAGG

6xHIS-SLP-1(278-384):

Primers:	
forward: HIS LTP fwd NdeI	GGAATTCCATATGGCCCCTCAAGTTGGTGC
reverse: HIS/GFP LTPT385 rwd BamHI	CGGGATCCCTACAGGTCGCCCTTCACC

- for cloning of the HIS-tagged constructs, which were constructed for future bacterial expression and purification of the SCP-2/nsLTP-domain of SLP-1, the pET28a+ vector was used

pET-28a-c(+) cloning/expression region
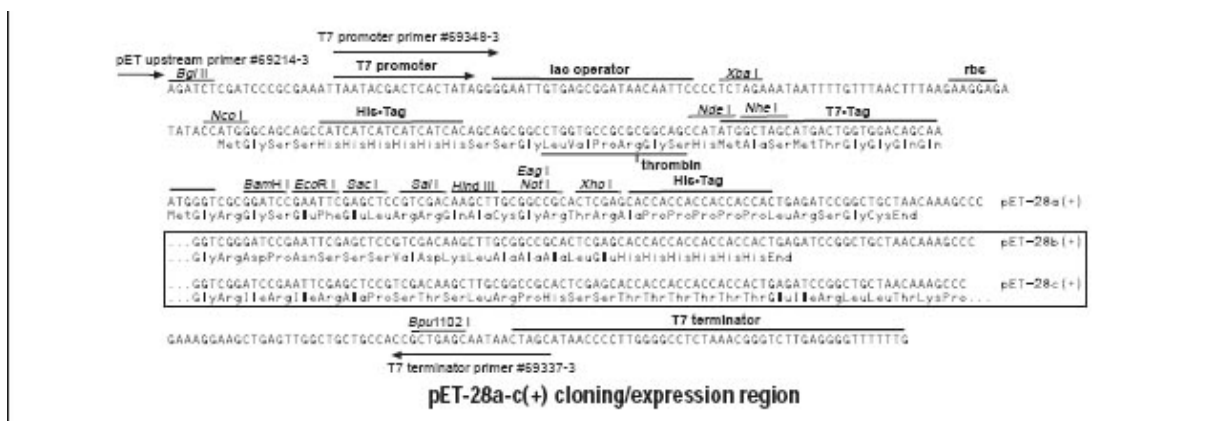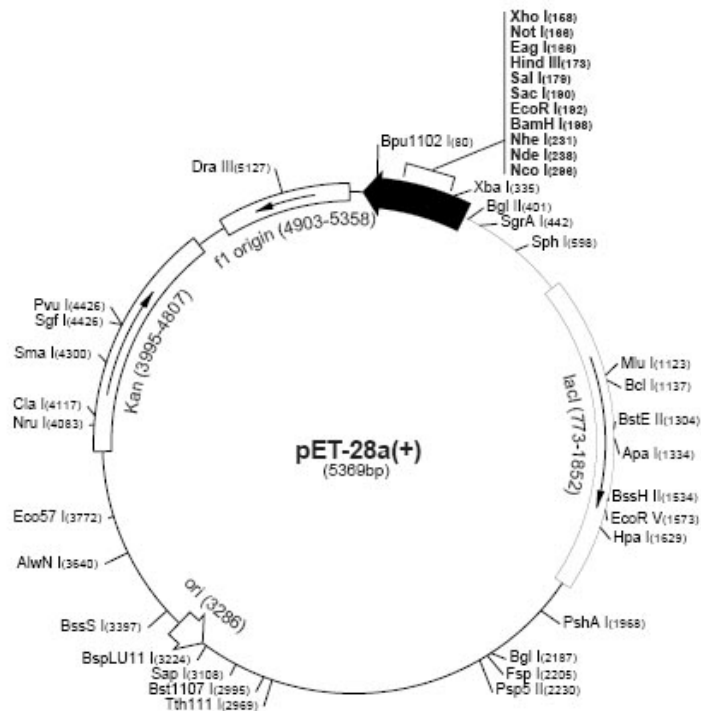
3.2.20 SLP-1 point mutations

SLP-1(Y7A)-3HA:

- a long oligo covering the 5´end of the coding region and bearing the desired point-mutation along with a SpeI restriction site was used for mutagenesis; the 5´KpnI restriction site in the coding region is destroyed by the mutation and can be used for analysis of clones;

forward: SLP1 Y7A	GGACTAGTCCACCATGCTCGGCAGGCTTGGGGCCCGGGCGCTGCC
reverse: SLP-1 myc CT SpeI	GGACTAGTCTTCAAGGCCCTGAGGAC

SLP-1(Y7A)-GFP:

- the mutated SLP-1(Y7A)-3HA construct was used as template for a PCR with primers for cloning into pEGFP-N3!

forward: SLP-1 GFP NT EcoRI	CGGAATTCGCCATGCTCGGCAGGTCT
reverse: SLP-1 GFP CT SacII	TCCCCGCGGCTGCGCCCTTCAAGGCCCTGAGGAC

SLP-1(L10S)-myc:

- the region between the KpnI and BamHI restriction site within the coding region of SLP-1 was amplified with a mutagenic 5´primer and a non-mutagenic 3´primer, and this mutagenised fragment was then inserted into the SLP-1-myc construct via these restriction sites;

forward: SLP1 L10S fwd	GGTCTGGGTACCGGGCGTCCCCCCTGGGTGATTTTGACC
reverse: SLP-1 L10S rwd	GCGGATCCGGCCCAGG

3.2.21 Stomatin point-mutations

STOM (S231A)-myc/GFP:

forward: MM S231A	GAAATGAATGCAGCCAGGGCTCTGAAAG
reverse: MM S231A as	CTTTCAGAGCCCTGGCTGCATTCATTTC

STOM (S231E)-myc/GFP:

forward: MM S231E	GGAGAAATGAATGCAGAGAGGGCTCTGAAAGAAGCC
reverse: MM S231E as	GGCTTCTTTCAGAGCCCTCTCTGCATTCATTTCTCC

- the following forward and reverse primers from Ellen Umlauf were used in the PCR mutagenesis reaction to enable cloning into the pEFKmyc-vector (also kindly provided by Ellen (Snyers et al., 1998; Umlauf et al., 2004)) via the unique KpnI site

forward: STCt Kpn1	CGGGGTACCATGGCCGAGAAGCGGCACACA
reverse: STCt Kpn2	CGGGGGTACCGCCTAGATGGCTGTGTTTTGC

- for cloning the point mutations and wt stomatin into the pEGFP-N3 vector, the constructs were excised with KpnI and ligated into the unique KpnI site in the MCS of pEGFP-N3

STOM (E210K)-GFP:

forward: StomE210Kfwd	GAGAGCTATGGCTGCAAAAGCAGAAGCGTCCCG
reverse: StomE210Krwd	CGGGACGCTTCTGCTTTTGCAGCCATAGCTCTC

STOM (E212K)-GFP:

forward: StomE212Kfwd	CTATGGCTGCAGAAGCAAAAGCGTCCCGCGAGGC
reverse: StomE212Krwd	GCCTCGCGGGACGCTTTTGCTTCTGCAGCCATAG

STOM (E210,212K)-GFP:

forward: StomE210,212Kfwd	GAGAGCTATGGCTGCAAAAGCAAAAGCGTCCCGCGAGGC
reverse: StomE210,212Krwd	GCCTCGCGGGACGCTTTTGCTTTTGCAGCCATAGCTCTC

STOM (S214A)-GFP:

forward: StomS214Afwd	CTGCAGAAGCAGAAGCGGCCCGCGAGGCCCGCGCCAAG
reverse: StomS214Arwd	CTTGGCGCGGGCCTCGCGGGCCGCTTCTGCTTCTGCAG

STOM (S214E)-GFP:

forward: StomS214Efwd	GCTGCAGAAGCAGAAGCGGAGCGCGAGGCCCGCGCCAAG
reverse: StomS214Erwd	CTTGGCGCGGGCCTCGCGCTCCGCTTCTGCTTCTGCAGC

- the 5´ and 3´primers used for PCR mutagenesis were (also from Ellen Umlauf(Umlauf et al., 2006)) as follows:

forward: ST1Kozak.EcoRI	TACGGAATTCCGCCACCATGGCCGAGAAGCGGCACACAC
reverse: ST287Ala.BamHI	TGCGGGATCCGGCGGCAGCGGCTCCGCCTAGATGGCTGTGTTTTGCC

- mutated fragments were cloned into pEGFP-N3 via EcoRI and BamHI sites
- for the construction of the C-terminal truncation mutant (S231A,T262), a different reverse primer was used in a normal PCR with STOM (S231A)-myc as template: ST262Ala.BamHI: TGCGGGATCCGGCGGCAGCGGCTCCTTTCTCAGCAGCAATGGTGGTC
- double mutants S214,231A and S214,231E were constructed by using the STOM (S231A/E)-myc constructs as templates for a second PCR mutagenesis step

3.2.22 Fusion of the N-terminus of SLP-1 to STOM (21-287)-GFP

- the constructs SLP-1(1-50)-GFP (see 0) and STOM (21-287)-GFP (kindly provided by Ellen Umlauf) were used as starting material
- the vector containing STOM (21-287)-GFP was digested with EcoRI and subsequently incubated with Klenow Polymerase (see 3.2.9)
- Klenow enzyme was heat-inactivated by incubation at 75°C for one hour, and subsequently, the vector was digested with BglII
- the insert containing amino acids 1-50 of SLP-1 (or of the point mutations Y7A or L10S) was prepared by digestion of SLP-1(1-50)-GFP by digestion with SacII, followed by Klenow incubation, heat-inactivation of Klenow enzyme and subsequent digestion with BglII
- the ligation of this insert into the STOM (21-287)-GFP vector yields an in-frame fusion of the wild-type or point-mutated N-terminus of SLP-1 to the N-terminally truncated stomatin construct, with an 8 amino acid linker (GAANSATM) between the two sequences

3.2.23 Construction of pECFP-N3 and pEYFP-N3

- as only the vectors pECFP-C1 and pEYFP-C1 (a kind gift from J. Weghuber) were available and due to the fact that N-terminal tagging of stomatin (and also SLP-1, as we found out during our work) is problematic even with small tags, we decided to create the C-terminal CFP- and YFP-tag-vectors corresponding to pEGFP-N3, which we had used successfully for tagging of stomatin and SLP-1, by ourselves
- the CFP/YFP coding sequence was amplified from the pECFP-C1/pEYFP-C1 vectors with the following primers:

| C/G/YFP fwd BamHI | CGCGGATCCATCGCACCATGGTGAGCAAGG |
| C/G/YFP rwd NotI | TTTTCCTTTTGCGGCCGCTTTACTTGTACAGCTCGTCCATGC |

- the PCR products were purified, digested with BamHI and NotI and ligated into the pEGFP-N3 vector digested with BamHI and NotI, thereby exchanging the GFP-coding region with CFP/YFP, preserving almost the entire MCS of the vector (only the XcmI site was lost) and creating a novel STOP-codon after the CFP/YFP (which was of

course not present in the C1 vectors)
- both vectors were successfully used for the creation of STOM-CFP/YFP as well as SLP-1-CFP/YFP and showed good expression of the fluorescent fusion proteins

3.3 Methods in cell culture

3.3.1 Cell lines used during my work:

- HeLa cells (human cervical cancer cells) were routinely used for stable expression of tagged proteins because of their fast growth and unproblematic maintainance.
  Medium: DMEM, 5% FCS, Penicillin/Streptomycin, L-Glutamine

- COS7 cells (african green monkey kidney cells, immortalized with SV40 largeT) were used for transient transfections and live microscopy because of their large, flat shape.
  Medium: DMEM, 5% FCS, Penicillin/Streptomycin, L-Glutamine

- MDCK cells (adult dog kidney cells) were used because they polarize when grown to confluency on Costar filters and form distinct apical and basolateral domains.
  Medium: DMEM, 5% FCS, Penicillin/Streptomycin, L-Glutamine

- HepG2 cells (human hepatic carcinoma cells) were used because they polarize when they approach confluency and form apical domains without the need for filter wells.
  Medium: DMEM, 10% FCS, Penicillin/Streptomycin, L-Glutamine

- HL-60 cells (acute myeloid leukemia cells) were used because they can be induced to differentiate along the neutrophil lineage with DMSO (our HL-60 cells did not differentiate properly!!!-fresh cells from ATCC should be purchased)
  Medium: RPMI medium, 10% FCS, Penicillin/Streptomycin

3.3.2 Passaging of cells/subculture

Adherent cells:
- cells were grown to confluency, Medium was changed every 2-3 days or when yellow
- cells were washed 1x with PBS
- a small volume (just enough to wet the entire surface, excess liquid was removed!) of 10x Trypsin/EDTA solution was added to the dish/flask, and the dish/flask was incubated for 3-5 minutes at 37°C; (alternatively, a larger volume of 1x trypsin/EDTA,

e.g. 500 µl per 25 cm² flask can be used, especially for cells which detach easily)

- cells were briefly inspected under the microscope for proper detachment; if cells were not rounded up and cell-cell contacts were not broken, further incubation at 37°C was necessary
- trypsinisation was stopped by addition of Medium with FCS, cells were singled and washed off the surface by pipetting the suspension up and down several times
- the desired subcultivation ratio was achieved by mixing the cell suspension with fresh medium and seeding them into a fresh dish/flask; (a washing step after trypsinisation was routinely performed every 2nd to 3rd passage)

Suspension cells:

- cell number was routinely analysed by CASY counting (CASY 2, Schärfe System) every 2-3 days
- cell number was re-adjusted to 2×10^6 cells/ml by a partial medium change
- a total medium change was performed once a week

3.3.3 Freezing of cells/thawing of cells

Freezing:

- cells were trypsinized as described (adherent cells) or resuspended by pipetting (suspension cells) and counted (manual count with hemocytometer or CASY count)
- the cells were pelleted by centrifugation (1200 rpm, 3 minutes, RT)
- the cell pellets were resuspended in 800 µl cell freezing medium (Sigma C-6295) and transferred into cryotubes
- the cryotubes were put on ice, transferred to an isopropanol container ("Mr. Frosty", Nunc) and put into a -80°C freezer (this yields a slow cooling rate of -1°C/minute)
- the next day, the cryotubes were transferred to a N_2-storage tank (liquid phase storage)

Thawing:

- cryotubes were removed from the liquid nitrogen tanks and incubated for approximately 5 minutes at 37°C until the cell suspension is completely thawed (use a closed container due to the risk of cryovial disruption)
- the cells were transferred to a 50 ml Falcon tube and pre-warmed medium was added drop-wise (first 3-4 ml) while swirling the tube frequently;
- further medium was added to a final volume of 10 ml, and the cells were then pelleted (1200 rpm, 3 minutes, RT)
- the pellet was resuspended in the desired volume and the cells were seeded into the appropriate flasks
- after several hours/over-night incubation, the cells were inspected under the microscope for proper attachment/growth and a medium change was performed

3.3.4 Transient/stable transfection

Transfection with Lipofectamine 2000 (Invitrogen) or Nanofectin (PAA):

- approximately 300.000 cells were seeded into 6-well plates the day before transfection
- 2-3 hours before addition of plasmid DNA, the cells were washed with PBS and Medium without antibiotics was added
- the Lipofectamin (Nanofectin)-DNA complexes were prepared as follows:
    - 4 μg of plasmid DNA was diluted with 250 μl of serum-free DMEM
    - 10 μl of Lipofectamin 2000(Nanofectin) were diluted with 250 μl of serum-free DMEM
    - DNA and Lipofectamin (Nanofectin) dilutions were combined, mixed well and incubated for 20-30 minutes at RT
    - the transfection mixture was added dropwise to the cells
    - after 4-6 hours, a medium change can be performed, fresh medium with antibiotics can be added
    - if transfection efficiency is very low, the ratio of DNA/Lipofectamine can be varied to optimize the outcome; this was rarely necessary for our purposes;
- cells were analysed for expression of the transfected construct by western blotting/immunofluorescence after 48-72 hours
- for immunofluorescence, the transfected cells were trypsinized, resuspended in fresh medium and seeded at the appropriate density onto glass coverslips 24 hours after transfection
- for stable transfections, an aliquot (typically 1/3 of the cells) was seeded onto a 10 cm-dish and, after letting the cells adhere overnight, selection for stable genomic integration of the transfected vector was performed by addition of the respective antibiotic to the culture medium
    - antibiotic concentrations have to be tested and optimised for every new cell line
    - routinely used antibiotic concentrations for our cell lines:
        - G418 (neomycin resistance): 500-700 μg/ml
        - Puromycin: 2 μg/ml
        - Hygromycin: 10 μg/ml
- medium was changed every 2nd day during the first week and every 2-4 days afterwards
- after 2-4 weeks (depending strongly on the proliferation rate of the cells), colonies of antibiotic resistant cells were visible with the bare eye
- single colonies were picked with cloning cylinders, trypsinized inside the cylinders, with one drop of 10X trypsin/EDTA, resuspended in 100 μl of medium and transferred to a 96well plate
- single colonies were (if possible) expanded from the 96-wells to 24-wells and finally 6-wells

- expression of the protein of interest was analysed by western blotting
- several clones (if possible) with varying expression levels were further expanded in culture flasks or dishes and finally frozen down as working aliquots in liquid nitrogen

Transfection with the calcium phosphate method:

- the cells were seeded the day before transfection at approximately 30-50% density in 100 mm plates
- on the day of transfection, the medium was changed and the cells were incubated in fresh medium without antibiotics (Pen/Strep) for 3 hours
- the 2M CaCl$_2$ and 2x HBS solutions were thawed, 500 µl of 2xHBS were pipetted in a sterile tube
- 20 µg of vector DNA were combined with sterile water (mix!) and 62 µl of the 2M CaCl$_2$ solution (final volume 500 µl, mix again!) in a second tube
- calcium phosphate-DNA complexes were prepared by slowly adding the CaCl$_2$-DNA solution to the 2xHBS solution and continuously mixing the solution by bubbling air through it (good mixing is essential for the formation of a fine DNA-calcium phosphate precipitate, which then is essential for good transfection efficiency!!!)
- the mixture appeared slightly opaque when addition of the DNA-solution was complete and was then incubated for 30 minutes at RT
- the mixture was then vortexed and added dropwise to the plates
- after over-night incubation, the medium was changed and the cells were incubated for another 24-36 hours
- after this period, the plates were trypsinised and several dilutions (in the range from 1:10 to 1:100, depending on the number of cells on the plate) were seeded in 100mm plates; after the cells had adhered, the proper antibiotic for selection was added (the calcium phosphate method was only used for stable transfection!)
- clones were picked and analysed as described above

3.3.5 Indirect immunofluorescence

- cells were grown to approximately 50% confluency on glass coverslips (No.1 thickness) in 6-well dishes
- the cells were washed twice with 1.5 ml PBS
- then, the cells were fixed by incubation with 1 ml 4% paraformaldehyde (PF) in PBS for 15 minutes
  - a 16% paraformaldehyde (PF) stock was incubated at 65°C for 5 minutes and then combined with an equal volume of 2X PBS and 2 volumes of PBS, yielding a 4% PF solution
  - the 16% PF stock was prepared as follows: 8 g PF were solubilized in ~40 ml milliQ-H$_2$O; the solution was heated to ~60°C, and several drops of 1 M NaOH were added until the solution was almost clear; then, the solution was

cooled down to RT, brought to 50 ml, aliquoted and stored frozen at -20°C;

- the 4% PF-solution was aspirated, and excess fixative is quenched by incubation with 50 mM NH$_4$Cl in PBS for 10 minutes
- the cells were washed 3X with 1.5 ml PBS (time: 5 minutes total)
- the cells were permeabilized with 1 ml 0.1% Triton X-100 in PBS for 5 minutes
- the cells were washed 3X with 1.5 ml PBS (time: 5 minutes total)
- while the 3rd washing solution was added, a small plastic plate was placed under the coverslip and the plate and the coverslip were arranged in a staggered fashion
- the coverslip was then blocked by addition of 0.1 ml 5% FCS in PBS for 10 minutes
- the blocking solution was aspirated, and 50-100 µl of the primary antibody solution (diluted in PBS containing 1% FCS) were added
- a moist paper towel was placed on the lid of the 6-well to ensure a moist atmosphere and to prevent evaporation of the antibody solutions
- the cells were incubated with the primary antibody for 1 hour (o/n incubation is also possible)
- the cells were washed 3X with 2 ml PBS (time: 15 minutes total)
- then, they were incubated for 1 hour with the secondary antibody diluted in PBS, 1 % FCS (for our AlexaFluor-488 and -596 conjugated antibodies, a standard dilution of 1:600 was used)
- the cells were washed 3X with 2 ml PBS (time: 15 minutes total)
- to remove salts, the coverslip was finally dipped briefly into milliQ-H$_2$O, excess water was removed with a paper towel and the coverslip was inversely mounted on a drop of Vectashield mounting medium on a clear glass slide
- the coverslip was immobilised with nail polish and let dry
- cells were analsyed at high magnification (63X, 100X) with a fluorescence microscope (Zeiss Axiovert) or a confocal microscope (LeicaTCS-NT or ZeissLSM 5)

3.3.6 Fluorescence Recovery After Photobleaching (FRAP)

- HeLa cells were transiently transfected with pEGFP-N3-Stomatin or pEGFP-N3-ST (1-262) as described using Lipofectamine 2000 (Invitrogen)
- 12 hours after transfection, cells were seeded on 35mm glass-bottom dishes (MatTek Corp., Ashland, MA) and FRAP analysis was performed after another 24 hours, essentially as described (Goodwin and Kenworthy, 2005; Kenworthy et al., 2004)
- Cells were washed with HBSS medium and mounted in prewarmed HBSS (supplemented with 25mM Hepes, pH 7.4) on a Zeiss LSM 510 Meta confocal microscope equipped with a stage heater (37°C)
- Cells were imaged with a 63x NA1.4 Plan-Apochromat oil-immersion lens at 4-fold magnification
- for quantitative FRAP, pre- and postbleach images were monitored with the 488 nm laser line of a 30mW Argon Laser set to 60% laser power at 1% transmission and a

confocal pinhole of 1.5 Airy units

- photobleaching of a circular region of interest (ROI) with a diameter of 1.8 μm was performed by 12 bleach iterations with all Argon Laser lines set to 100% transmission
- images were recorded with 2 s time lapse at a scan time of about 0.8 s
- fluorescence intensity data of the whole cell ROI, the bleached ROI and a background ROI were quantified using the Physiology Evaluation Software Package (Carl Zeiss Microscopy, Jena, Germany)
- recovery curves were bleach- and background-corrected and mobile fractions were calculated as described(Goodwin and Kenworthy, 2005)
- for the calculation of the recovery halftime $t_{1/2}$, the normalized and bleach-corrected recovery data were fitted to the following formula to estimate recovery kinetics:

$$I(t) = a(1-\exp(-kt))$$

The recovery half-time was then calculated as $t_{1/2}=\ln2/k$.

- for qualitative FRAP, the diameter of the bleach ROI was increased to 3.4 μm, the pinhole was set to 1 Airy unit and laser transmission was increased to 2-3% for pre- and postbleach images
- postbleach images were acquired with 30 seconds time lapse,and 4-line-averaging was used to get high-quality pictures; the other settings were identical to those used in the quantitative experiments

3.3.7 Live cell imaging

Live cell imaging was performed as described in the FRAP method, with different settings for time lapse/laser intensity/pinhole, depending on the desired temporal resolution and quality of the single pictures and on the fluorescence of the analysed samples.

In some experiments, lysosomes/late endosomes were stained with LysoTracker Red (Invitrogen) according to the manufacturer´s instructions. To increase the signal intensity and to enable reduction of laser power, the pinholes for green and red channel fluorescence were increased to 2 airy units if necessary.

3.3.8 Induction of lipid droplets

HeLa cells transiently transfected with the indicated GFP-fusion proteins were seeded onto glass coverslips 24 hours after transfection. The cells adhered overnight, subsequently 0.4 mM oleic acid in 66.7 μM fatty-acid-free BSA (Brasaemle et al., 1997) were added to the medium to induce the formation of lipid droplets (LDs). After 24 hours, the cells were fixed with 4% paraformaldehyde and stained with NileRed as described (Umlauf et al., 2004).

3.3.9 Blocking intracellular cholesterol transport with the aminosteroid U18666A

A mixture of control HeLa cells and HeLa cells stably expressing the respective fusion

protein was seeded onto glass coverslips at about 50% density. Cells were adhering overnight and the indicated concentrations of U18666A were added from a 2 mg/ml stock solution in water. Accumulation of cholesterol in perinuclear vesicles was assessed by filipin staining as described (Kobayashi et al., 1999). The filipin stock solution was always prepared fresh, filipin was solubilized in DMSO at a concentration of 10 mg/mL. This stock was added to the primary and secondary antibody solution during the immunofluorescence staining prcedure at a dilution of 1/200.

3.3.10 Uptake of fluorescent dextran

- for uptake of fluorescent dextran, cells stably expressing SLP-1-GFP were seeded onto glass coverslips, let adhere and incubated in Medium with 1% FCS over night
- the cells were incubated with Medium containing 5 mg/ml TRITC-Dextran (Sigma) for 10 minutes at 37°C
- the TRITC-dextran was removed, and the cells were chased for the indicated time-points with Medium without TRITC-dextran
- then, the cells were immediately fixed with 4% paraformaldehyde and analysed by immunofluorescence

3.3.11 Immunoelectron microscopy

Only the seeding and fixing of the cells were done by me, the rest of the procedure, from embedding to sectioning to immunostaining were done by our collaboration partner Marianne Fliesser!

- HeLa cells stably expressing SLP-1-GFP were grown on gridded Cellocate-coverslips (Eppendorf)
- Cells strongly expressing SLP-1-GFP were selected and phase contrast and fluorescence images were recorded. Subsequently, the cells were fixed for 1 hour in 0.1 M sodium phosphate buffer, pH 7.4, containing 4% paraformaldehyde and 0.2% glutaraldehyde, washed for 30 minutes with 0.1 M phosphate buffer and then incubated for 2 hours in 0.1 M phosphate buffer containing 50 mM glycine.
- Embedding in LR white, trimming and thin-sectioning was essentially performed as described (Steiner et al., 1994).
- Thin sections were blocked for 1 hour in phosphate buffered saline (PBS), pH 7.4, containing 0.05% Tween-20, 5% bovine serum albumin, and 1% goat serum.
- Rabbit anti-GFP (Abcam) was diluted 1/500 in blocking buffer and thin sections were incubated for 2-3 hours at room temperature.
- After washing 3 times with PBS, 0.05% Tween-20, the thin sections were incubated with a 10nm gold-conjugated goat anti-rabbit antibody (Biocell, diluted 1/40 in PBS,

pH 8.0, 0.05% Tween-20) for 2 hours.

- Finally, the thin sections were washed 3 times with PBS, pH 8.0, 0.05% Tween-20, stained with 2% uranyl acetate for 1 hour and then analyzed with a Jeol 1200 EXII microscope. Anti-GFP signal was virtually eliminated by staining of thin sections with antibody saturated with a 10-fold excess of recombinant GFP (incubated for 2 hours at 37°C), confirming the specificity of the observed signal.

In a different set of experiments, the cells were fixed as described, but then embedded in Epon resin instead of LR white. This different embedding method allows for the use of OsO_4 as contrasting agent, but is not feasible for immunostaining. Pictures with superior resolution of vesicle internal membranes and cytoskeletal structures were obtained from thin sections prepared with this method.

4 RESULTS

4.1 SLP-1

4.1.1   Subcellular localization of SLP-1

The presented work represents the first detailed characterization of the SLP-1 protein. Because no antibody was available against human SLP-1 (although several attempts have already been made to obtain polyclonal antibodies against SLP-1 in our group; the reason for these failures could lie in the extremely good conservation of SLP-1 in mammals (see Figure 7), I started with the construction of tagged SLP-1 protein fusions. We chose the small myc-epitope to minimize the effects of the tag in respect to protein trafficking and the GFP-tag to enable live cell imaging of SLP-1. Because we were not successful in cloning a N-terminally tagged stomatin construct, we thought that N-terminal tagging of SLP-1 might also be problematic and started with C-terminal tags. We analysed several different cell types by transient and stable transfection. The results for HeLa cells, HepG2 cells and MDCK cells are shown in Figure 9A.

The tagged SLP-1 protein was localized to perinuclear vesicles. No PM localization was observed in all tested cell types. In contrast to stomatin, SLP-1 did not translocate to the apical membrane upon polarization of MDCK cells (data not shown). The strictly perinuclear localization was observed in transient transfections and in stably transfected cell lines. Several clones expressing different amounts of either SLP-1-myc or SLP-1-GFP were analysed and all showed perinuclear staining. ELMI analysis showed that SLP-1 is predominantly found on the limiting membrane of multivesicular structures, already indicating that the perinuclear vesicles could be late endosomes (Figure 9B).

4.1.2   SLP-1 is localized to the late endosomal compartment

We next analysed the colocalization of SLP-1 with different marker proteins for subcellular compartments. Figure 10 shows the results for several late and early endosomal markers. SLP-1 showed good colocalization with the LE markers LAMP-2, Rab7, Rab9 and CI-M6PR, whereas there was only little colocalization with the early endosomal markers TfR and Rab5. No colocalization was observed with a golgi marker, GM130, and a peroxisomal marker, PMP70 (Figure 11). The next question was if the SLP-1-positive perinuclear structures are accessible to endocytosed TRITC-dextran as expected for late endosomes. Indeed, we observed co-localization of SLP-1-GFP with TRITC-dextran after a 30 minute chase after labeling, but no colocalization after 10 minutes of labeling (Figure 12).

Figure 9: SLP-1 is localized to perinuclear vesicles
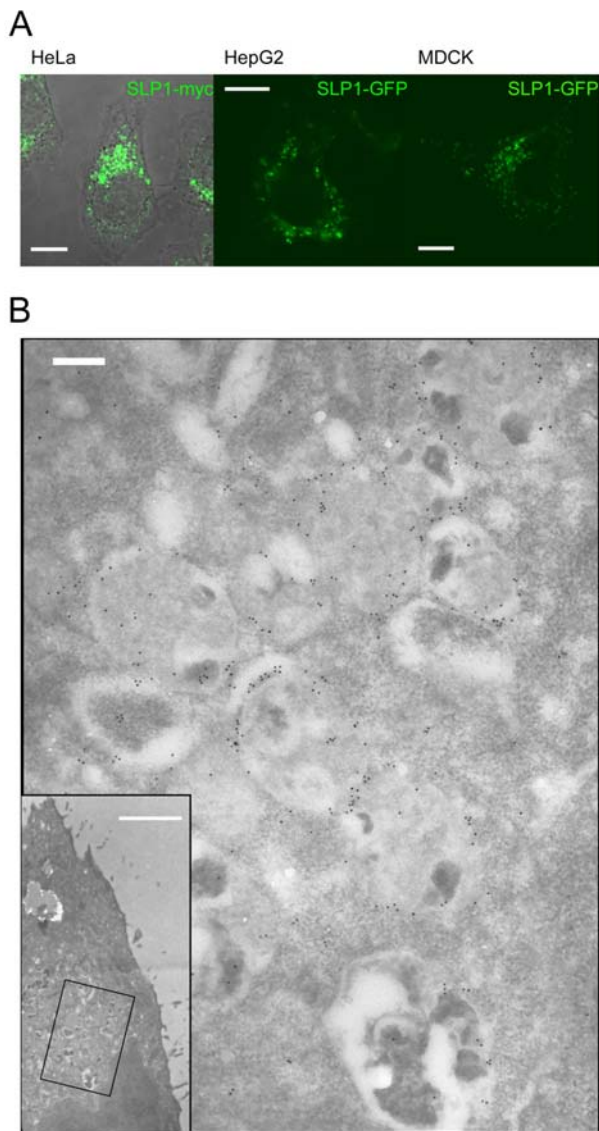
Figure 9: (A) Localization of SLP-1-myc and SLP-1-GFP to perinuclear vesicles in different cell types (HeLa, HepG2, MDCK) Scale bar 10µm. (B) Electron microscopy image of a HeLa cell stably expressing SLP-1-GFP. The insert shows a part of the cell at lower magnification, the position of the high magnification image is marked by the box. SLP-1 is detected on the limiting membrane of multivesicular structures around the nucleus. Scale bars: 200 nm, 1 µm (insert).

Subcellular fractionation experiments confirmed the localization of SLP-1 to endosomal fractions (Figure 13), but we were unable to properly separate early from late endosomes with these step gradient protocols. The colocalization with different markers was never perfect, we always observed a fraction of SLP-1 positive vesicles, which were negative for the marker. Co-localization was best with Rab7 and Rab9, where more than 50% of the vesicles were positive for both proteins. The late endosomal compartment is rather complex and heterogenous, as exemplified by the different staining pattern for LAMP-1/2 and CI-M6PR. All three proteins are widely used as LE markers, but they show only little overlap. CI-M6PR cycles between the Golgi apparatus and the LEs and stains a very restricted vesicle population around the MTOC, whereas LAMP-1/2 stains more peripheral LE vesicles and also lysosomes. The situation gets even more difficult when one considers the inhomogenous staining for SLP-1 on many vesicles (see Figure 32, Figure 36). This makes an unambiguous determination of colocalization difficult. SLP-1 seems to be broadly expressed on all late endosomal sub-compartments.

Figure 10: Late/early endosomal markers
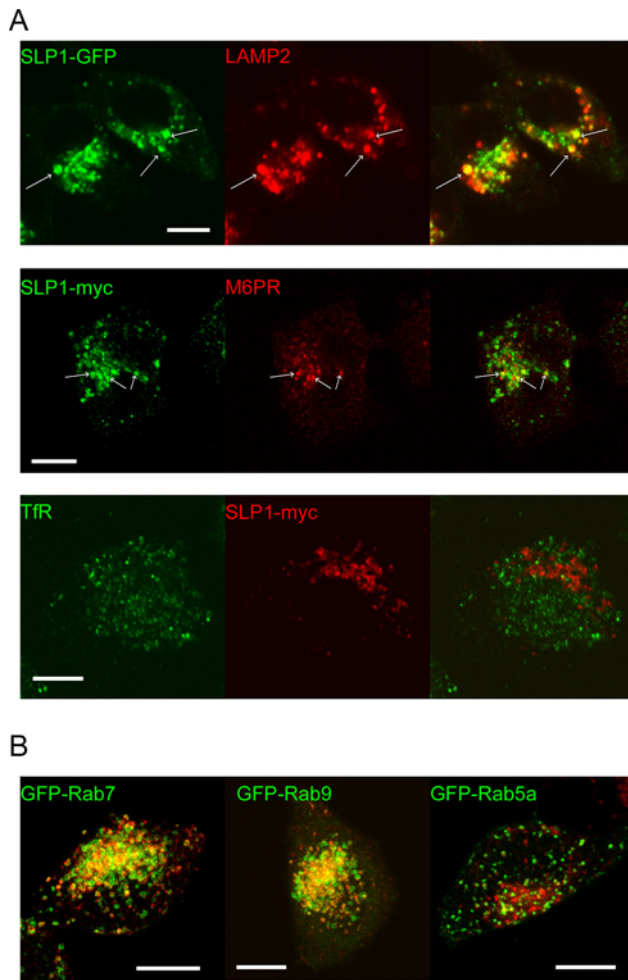
Figure 10: SLP-1 colocalizes with LE markers but not with EE markers. (A) HeLa cells stably expressing either SLP-1-GFP or SLP-1-myc were stained for different markers for late (LAMP-2, M6PR) or early endosomes (TfR). Significant colocalization was observed for LE markers only. (B) HeLa cells stably expressing SLP-1-myc were transfected with the indicated GFP-Rab constructs. Colocalization with the LE markers GFP-Rab7 and GFP-Rab9 was observed, whereas the EE marker GFP-Rab5 showed only minimal overlap. Scale bars 10 μm.

Figure 11: Golgi and peroxisome markers
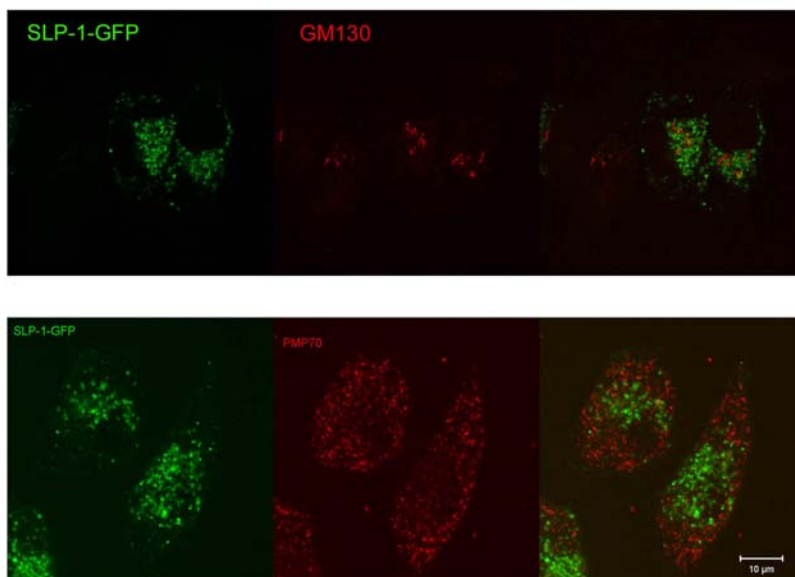
Figure 11: Double-staining with other organelle markers. HeLa cells stably expressing SLP-1-GFP were co-stained with either the Golgi marker GM130 (upper panel) or the peroxisomal marker PMP70. No colocalization was observed for both markers.

4.1.3   Over-expressed SLP-1 interacts with endogenous stomatin

As endogenous stomatin is also partially localized to LEs in different cell types, we next wanted to investigate if over-expressed SLP-1 co-localizes with endogenous stomatin. We performed transient transfections of HeLa cells with either SLP-1-GFP or SLP-1-myc and did double-stainings with the mouse monoclonal stomatin antibody GARP50 (Figure 14 A). We observed co-localization between SLP-1 and stomatin on late endosomes, and, importantly, we observed that the localization of endogenous stomatin changes if SLP-1 is over-expressed in the cells. Strong expression of SLP-1 results in reduced PM staining and increased LE staining for endogenous stomatin. This result could also be verified biochemically. We compared control HeLa cells with a clone stably expressing SLP-1-myc in subcellular fractionation experiments on Optiprep-gradients. As a marker for PM, we used alkaline phosphatase activity, and as LE marker, we performed western blotting with anti-LAMP-1 antibody. The results are shown in Figure 14 B. In the clone stably expressing SLP-1-myc, stomatin is clearly reduced in the low-density fractions. Interestingly, SLP-1 and stomatin are detected in high-density endosomal fractions, but their distribution does not overlap perfectly. This indicates that the two proteins could occupy different subsets of late endosomes, but it could also be due to contamination of the endosomal fraction with PM components. The results that SLP-1 overexpression causes a redistribution of stomatin further indicated an interaction between SLP-1 and stomatin. We next performed co-immunoprecipitation experiments with an anti-GFP antibody to analyse if endogenous stomatin could be co-precipitated with SLP-1. We also included two C-terminal truncations of SLP-1 to map the region of SLP-1, which is responsible for the interaction. Figure 15 shows the results of one such co-immunoprecipitation experiment.

Endogenous stomatin is clearly co-precipitated with SLP-1-GFP and also with the two C-terminal truncation mutants SLP-1(1-288)-GFP and SLP-1(1-224)-GFP. Therefore, the SPFH domain or the N-terminus of SLP-1 must be responsible for the interaction with stomatin, whereas the SCP-2/nsLTP domain and the linker region between the SPFH domain and the SCP-2 domain are not required for the interaction. The strongly reduced amount of co-precipitated stomatin for SLP-1(1-224)-GFP is probably caused by the fact that this truncation mutant is mis-targeted to cytoplasmic aggregates and does barely reach the late endosomal compartment where it can interact with stomatin (see Figure 16).

4.1.4   C-terminal truncation mutants

To identify the regions which cause the targeting of SLP-1 to late endosomes, I constructed C-terminal truncation mutants. The first construct, SLP-1(1-288), where the entire C-terminal SCP-2 domain had been deleted, showed no difference compared to the full-length protein regarding its subcellular distribution. Further deleting the amino acids 225-288, however, had a strong impact on the localization (Figure 16+17).

This SLP-1(1-224) construct seemed to be mis-targeted to cytoplasmic aggregates and filamentous structures and did not co-localize with LE markers any more. No colocalization

was observed with ER and Golgi markers, either (Figure 17).

Staining of cells expressing high amounts of SLP-1(1-224)-GFP with Nile Red revealed that the cytoplasmic aggregates strongly stain with this neutral lipid stain even in the absence of oleic acid (data not shown).

Figure 12: Endocytosis of fluorescently labeled dextran
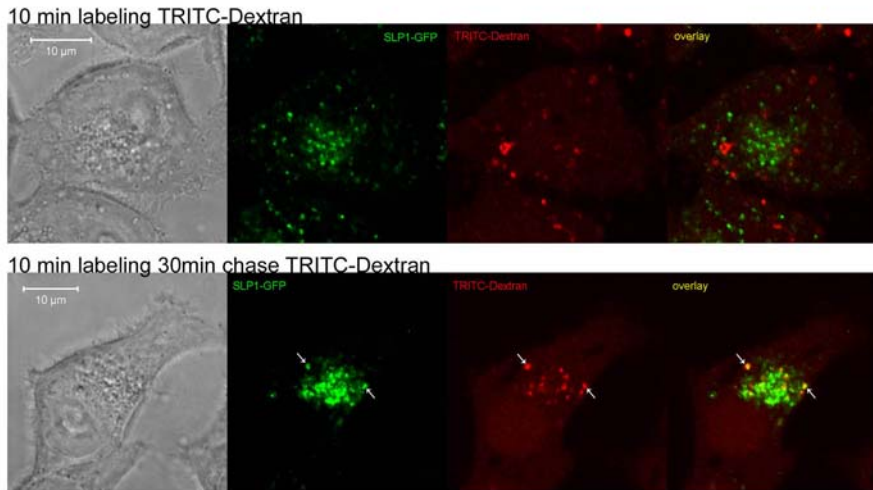
Figure 12: The LEs containing SLP-1 are accessible to endocytosed fluid phase markers. HeLas stably expressing SLP-1-GFP were incubated with fluorescently labeled dextran (TRITC-Dextran) for 10 minutes and either fixed directly after the incubation or subjected to a 30 minute chase with medium without dextran. After the 30 minute chase, TRITC-Dextran was clearly detected in SLP-1-GFP positive vesicles (arrows in lower panel). Scale bar 10 μm.

Figure 13: Subcellular fractionation
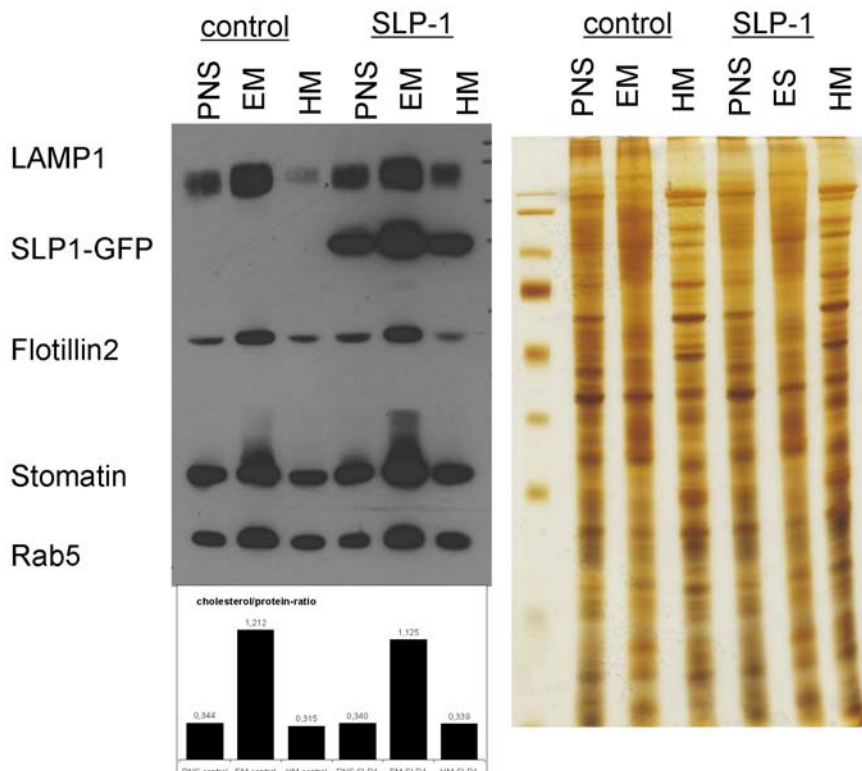
Figure 13 (previous page): SLP-1 is enriched in a crude endosomal fraction. Control HeLas and HeLas stably expressing SLP-1-GFP were grown in 15cm culture dishes and subjected to subcellular fractionation on sucrose step gradients as described in the Methods section. Aliquots of the PNS, the endosomal membrane fraction (EM) and the heavy membrane fraction (HM) were analysed by western blotting, silver staining and cholesterol/protein determination as described. SLP-1, stomatin, LAMP-2, flotillin-2 and Rab5 were all found to be enriched in the EM fractions. Silver staining revealed the different overall protein composition of the fractions. By analysing the cholesterol/protein ratio, the EM fraction was fount to be strongly enriched in cholesterol. Comparison of LAMP-1 in control HeLas and SLP-1-GFP expressing HeLas reveals that over-expression of SLP-1 could affect the distribution of LEs in the subcellular fractionation experiment, probably by an effect on the cholesterol content.

4.1.5 SLP-1 is excluded from lipid droplets (LDs) induced by feeding with oleic acid

As it was recently shown that stomatin is targeted to LDs and because of the potential of SLP-1 to function in lipid transfer/transport, we were interested if SLP-1 is also targeted to LDs. We transiently transfected HeLa cells with stomatin-GFP, SLP-1-GFP or with the truncation mutants SLP-1(1-288)-GFP and SLP-1(1-224)-GFP and induced the formation of LDs by addition of oleic acid. The results are shown in Figure 18.

As expected, stomatin is targeted to LDs. Full-length SLP-1 and SLP-1(1-288)-GFP are not targeted to LDs and show no colocalization with NileRed-positive droplets, but instead retain their normal LE localization. The SLP-1(1-224)-GFP construct, however, is efficiently targeted to the membrane of LDs. These results show that the SPFH domain of SLP-1 has the potential to gain access to LDs, but the C-terminal region between amino acid 224 and 288 inhibits this translocation. Of course, the LD localization of the SLP-1(1-224)-GFP construct could also be a consequence of the mistargeting, and correct targeting to LEs could make the translocation to LDs impossible. Nevertheless, these data strongly support the hydrophobic hairpin structure we assumed for the N-terminus of SLP-1 in analogy to stomatin. Additionally, I frequently observed that cells expressing high amounts of full-length SLP-1 only contained rather small LDs compared to non-expressing cells. This indicates that SLP-1 could act as a negative regulator of LD formation (possibly by mediating lipid transfer out of the LDs), but more quantitative data are necessary to confirm this notion.

Figure 14: Overexpression of SLP-1 decreases PM stomatin
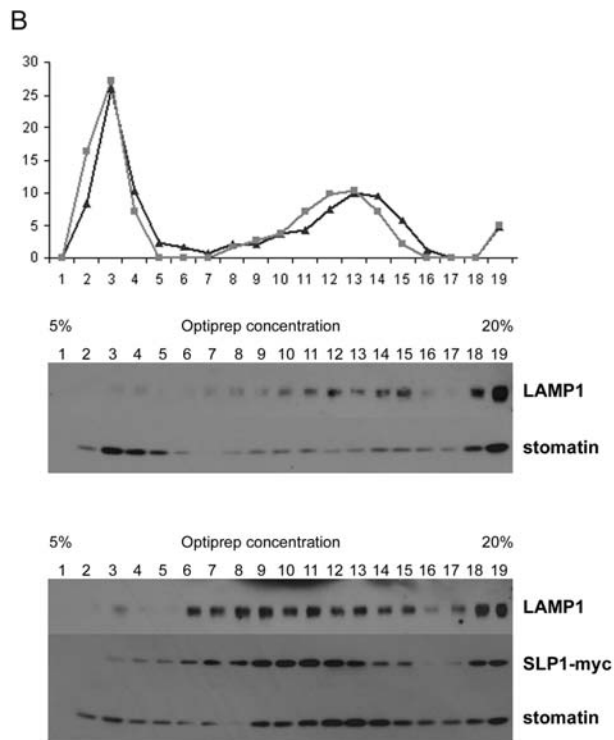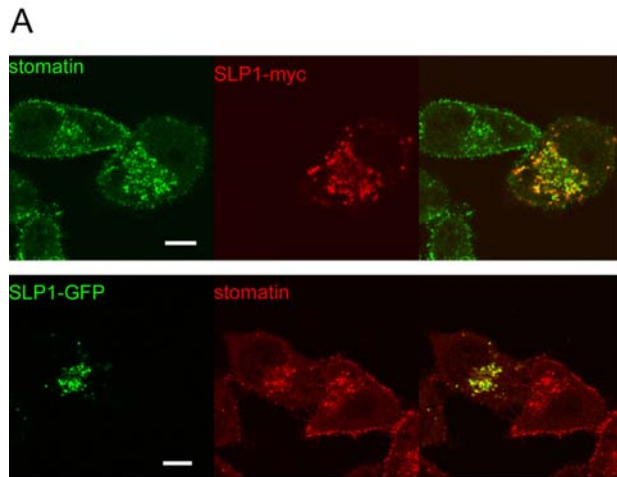
Figure 14: Over-expression of SLP-1 causes a shift in stomatin localization from the plasma membranes to late endosomes. (A) HeLa cells were transiently transfected either with SLP-1-GFP or SLP-1-myc and co-stained for stomatin. Cells expressing SLP-1 showed a reduction of stomatin signal at the PM compared to cells not expressing SLP-1. (B) Confirmation of this shift by subcellular fractionation on Optiprep gradients. Lysates of control HeLas and HeLas stably expressing SLP-1-myc were subjected to subcellular fractionation as described. Nineteen fractions were collected and analysed for alkaline phosphatase content (upper panel; black: control, grey: SLP-1-myc clone) as a PM marker and for the distribution of LAMP-1, stomatin and SLP-1-myc by western blotting. Over-expression of SLP-1 causes a reduction of the PM pool of stomatin and an increase in the more dense fractions.

4.1.6 The SLP-1(1-224) construct is targeted to lipid droplets

A dominant-negative caveolin-3 (cav3DGV) mutant has been described, which is capable of disrupting cholesterol trafficking and is localized to small, cytoplasmic lipid droplets (Pol et al., 2001). We analysed if this protein colocalized with our myc-tagged SLP-1 constructs and observed almost perfect co-localization with SLP-1(1-224)-myc (Figure 17). The major difference was that ER staining was frequently observed for GFP-cav3DGV, but not for SLP-1(1-224)-myc. As already outlined above, we did not observe ER localization for SLP-1(1-224). Instead, we observed some colocalization of SLP-1(1-224) with the early endosomal marker Rab4 in the filamentous structures. Addition of oleic acid lead to the formation of large lipid droplets, which also contained GFP-cav3DGV.

Figure 15: Co-immunoprecipitation experiments
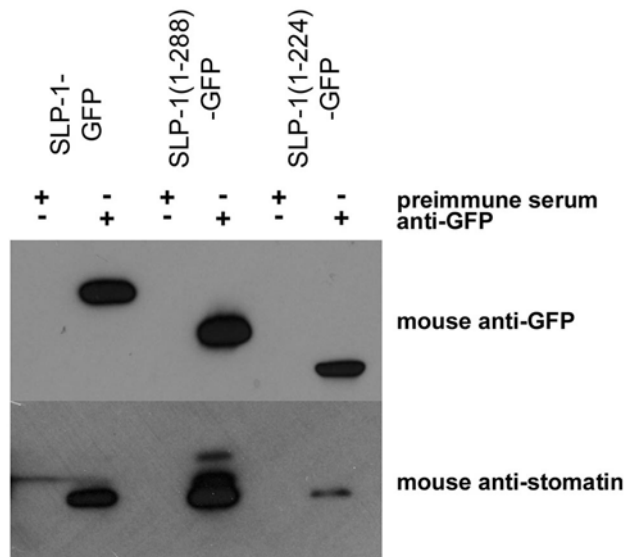
Figure 15: Stomatin is co-precipitated with SLP-1 and two C-terminal truncation mutants.

SLP-1-GFP and the two truncation mutants, SLP-1(1-288)-GFP and SLP-1(1-224)-GFP, were stably expressed in HeLa cells. Immunoprecipitations were performed with an anti-GFP antibody, and the samples were analysed for co-precipitation of endogenous stomatin by western blotting. As controls, HeLa cells and cells stably expressing EGFP were also analysed and did not yield a signal for stomatin under identical conditions (data not shown).

Figure 16: Vesicular aggregates and tubular structures of SLP-1(1-224)-GFP
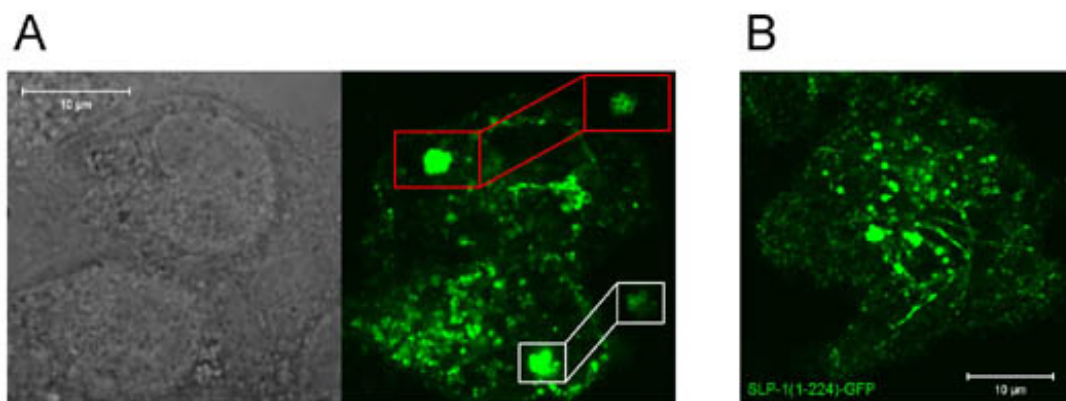
Figure 16: HeLa cells stably expressing SLP-1(1-224)-GFP were analysed by confocal microscopy. A subset of cells showed very strong GFP-fusion protein expression, which was found on large cytoplasmic aggregates of smaller vesicles (A). Cells with a lower expression level frequently displayed tubular GFP-positive structures in the cytoplasm (B). Scale bars 10 µm.

In double transfections of HeLa cells with GFP-cav3DGV and either SLP-1-myc, SLP-1(1-288)-myc or SLP-1(1-224)-myc, which were treated with oleic acid to induce the formation of large lipid droplets, we observed perfect colocalization of SLP-1(1-224)-myc with the cav3DGV construct (Figure 19). Full-length SLP-1 and SLP-1(1-288) were excluded from these structures, STOM-GFP was not tested yet.

Figure 17: Co-staining of SLP-1(1-224) with different organelle markers
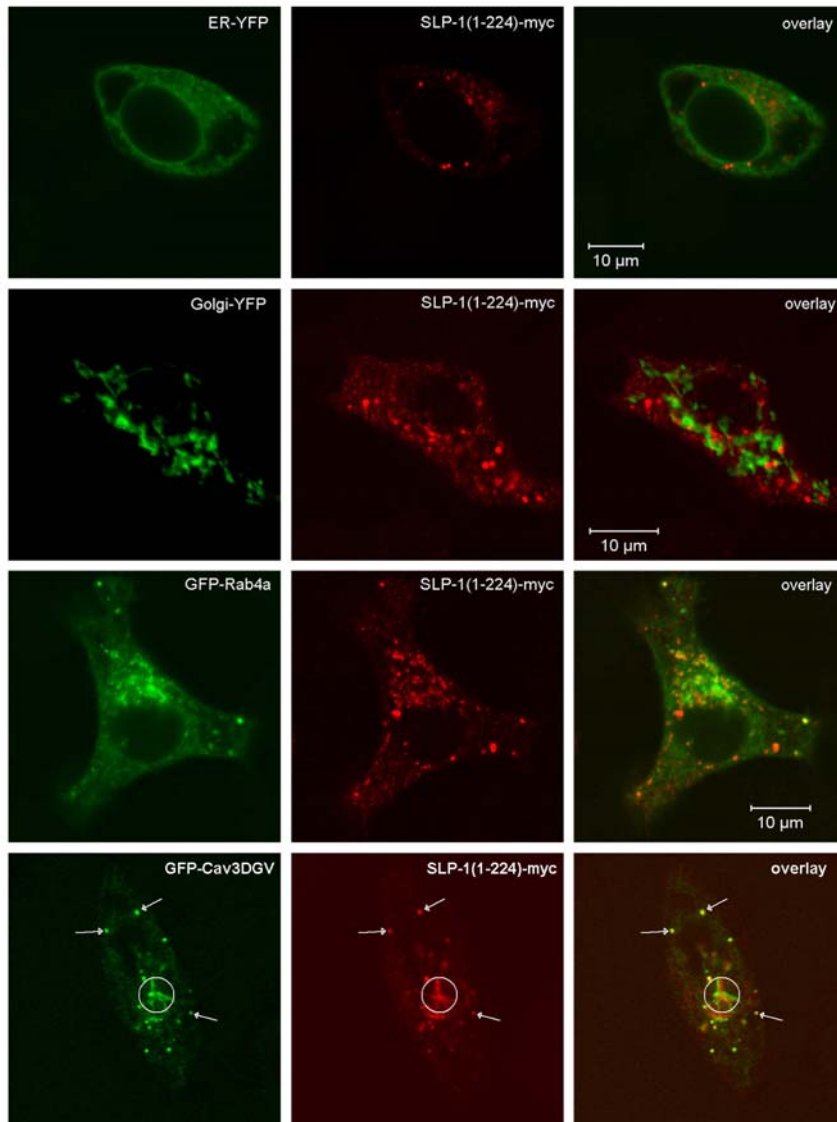
Figure 17: Co-staining of SLP-1(1-224) with different organelle markersFigure 17: Hela cells stably expressing SLP-1(1-224)-myc were transiently transfected with different organelle markers (pEYFP-ER and pEYFP-Golgi from Clontech, GFP-Rab4a and GFP-Cav3DGV (Pol et al., 2001). Only little colocalization was observed with ER-YFP and Golgi-YFP. Overlap was higher with the GFP-Rab4a construct and almost perfect with GFP-Cav3DGV.

Figure 18: SLP-1 on lipid droplets?
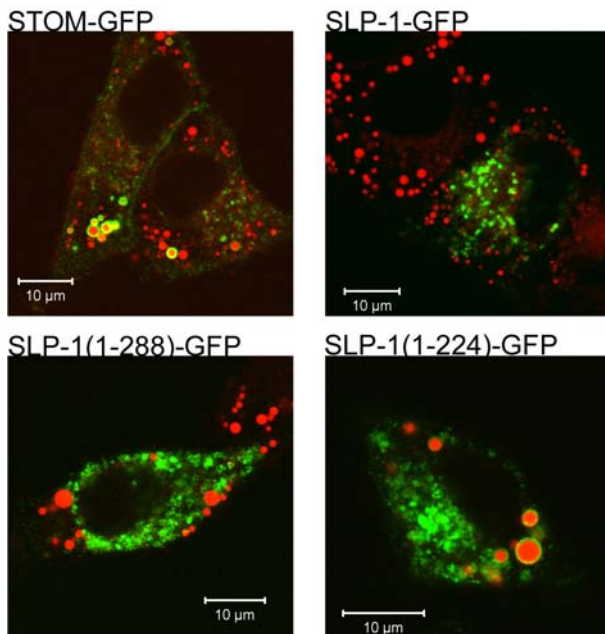
Figure 18: Different GFP-tagged constructs were transiently expressed in HeLa cells and formation of large lipid droplets/bodies was induced by addition of oleic acid to the medium for 18-24 hours (Brasaemle et al., 1997). Lipid bodies were stained with NileRed. Full-length SLP-1-GFP and SLP-1(1-288)-GFP do not localize to lipid bodies, whereas the truncation mutant SLP-1(1-224)-GFP is clearly detected on the surface of large lipid droplets (visible as yellow rings). Scale bars: 10 µm.

Figure 19: Co-localization with Cav3DGV
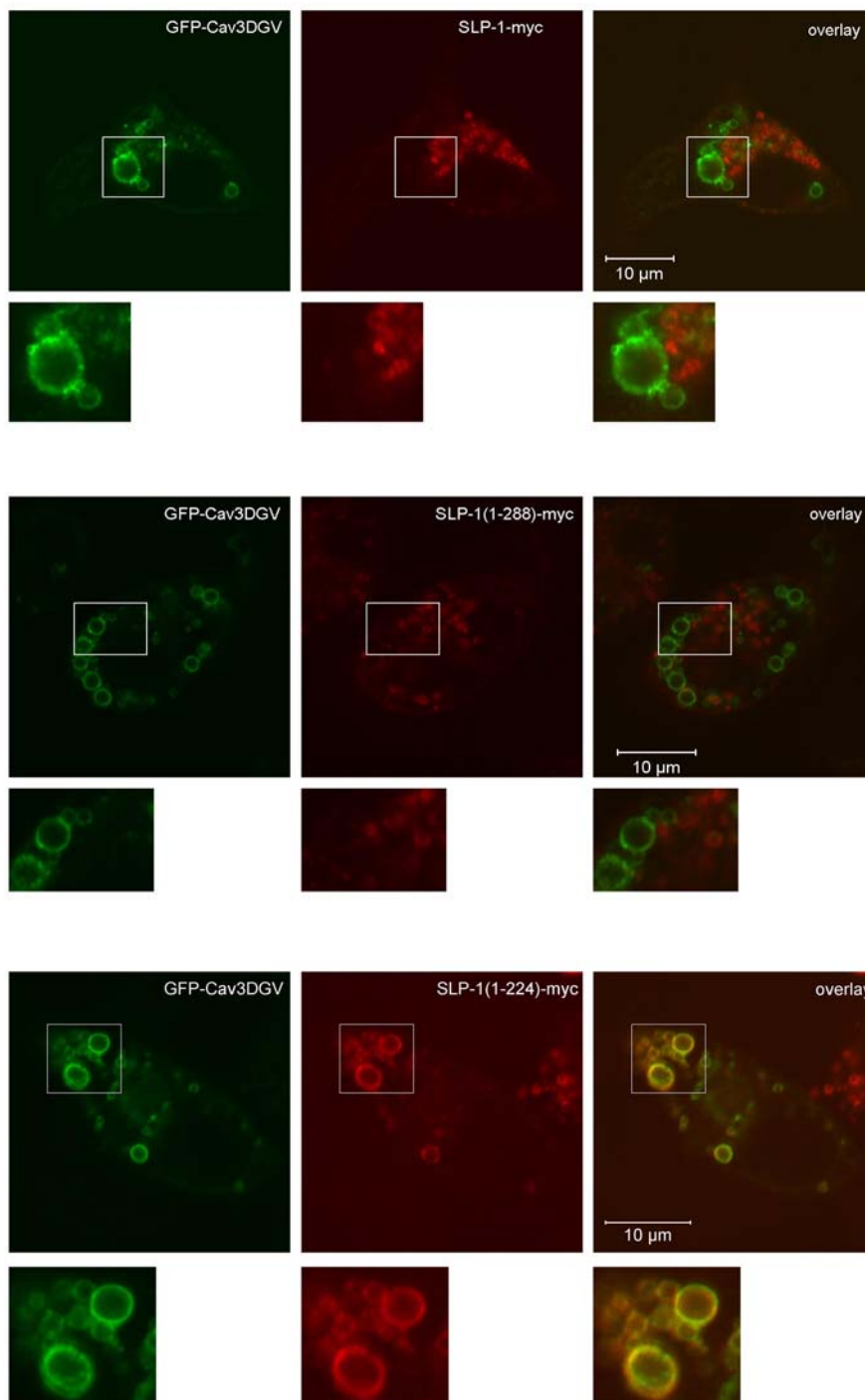
Figure 19: Co-localization of SLP-1(1-224)-myc and GFP-Cav3DGV on the surface of lipid droplets. HeLa cells stably expressing the indicated myc-tagged constructs were transiently transfected with GFP-Cav3DGV, and formation of lipid bodies was induced by treatment with oleic acid. GFP-Cav3DGV co-localizes with SLP-1(1-224)-myc, but not with SLP-1-myc or SLP-1(1-288)-myc, as expected. Scale bars 10 μm.

4.1.7 ELMI analysis of a clone stably expressing SLP-1(1-224)-GFP

To gain further insights in the localization and trafficking of this mutant, we analysed cells by ELMI. As shown in Figure 20, we observed very strong signal in vesicular and tubular

structures.

These pictures were taken from ultra-thin sections of cells embedded in LR white resin. This procedure allows efficient immunostaining, but the ultra-structure is not very well conserved. Several of the SLP-1(1-224)-GFP positive vesicles were found to have an "empty" appearance characteristic for lipid droplets, but a real identification was not possible. We therefore analysed the cells after embedding in Epon and staining with OsO_4. This procedure yielded a superior conservation of the ultrastructure, but immunostaining was not possible (we tried de-osmiation and also to do a pre-embedding labeling, but were not successful up to now).

Analysis of the Epon sections revealed that the SLP-1(1-224)-GFP clone contains many small LD structures. These structures often were aggregated and strongly reminded us of the cytoplasmic vesicle aggregates observed in fluorescence microscopy. In our opinion, these structures are induced by the over-expression of SLP-1(1-224)-GFP, although of course, we can not definitely proof that they are positive for SLP-1(1-224)-GFP. But this conclusion is supported by the fact that SLP-1(1-224)-GFP colocalizes with the LD markers NileRed and cav3DGV already in the absence of oleic acid and localizes to large LDs when oleic acid is added. During the analysis of the Epon sections, we found very interesting structures (Figure 21).

Figure 20: ELMI of SLP-1(1-224)-GFP I: immunolabeling
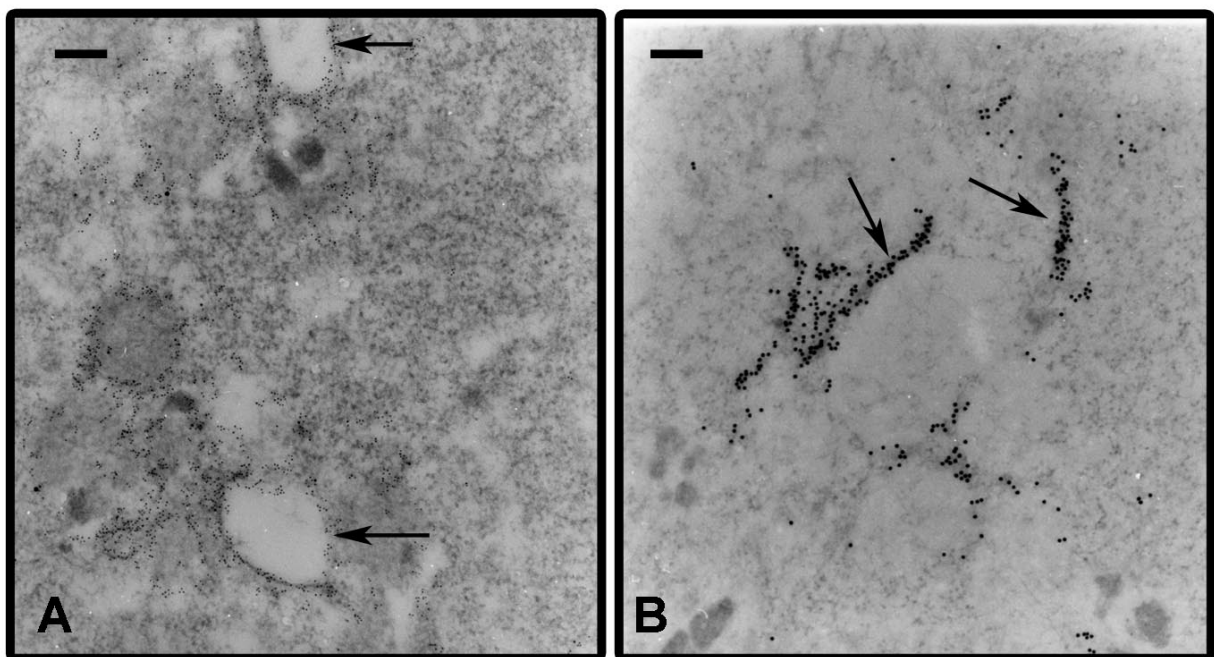
Figure 20: Analysis of HeLa cells stably expressing SLP-1(1-224)-GFP by immuno-electron microscopy. Cells were fixed and processed for ELMI as described in the Methods section. Thin sections were immuno-stained with a polyclonal anti-GFP antibody and with gold-conjugated secondary antibodies (A: 5 nm, B: 10 nm gold). SLP-1(1-224)-GFP was detected in tubular structures and on the surface of larger vesicles, often with an "empty", electron-translucent appearance. Scale bars: 200 nm.

Small vesicles were often observed close to the LD aggregates, which could represent transport intermediates on their way to/from LDs (Figure 21A). The formation and turn-over of LDs still remains enigmatic up to date. One theory is that LDs form from the ER membrane. Even less is known about the turn-over of this organelle. We observed some LDs, which seem to be surrounded by a vesicle containing electron-dense material (Figure 21B).

Figure 21: ELMI II: Epon embedding
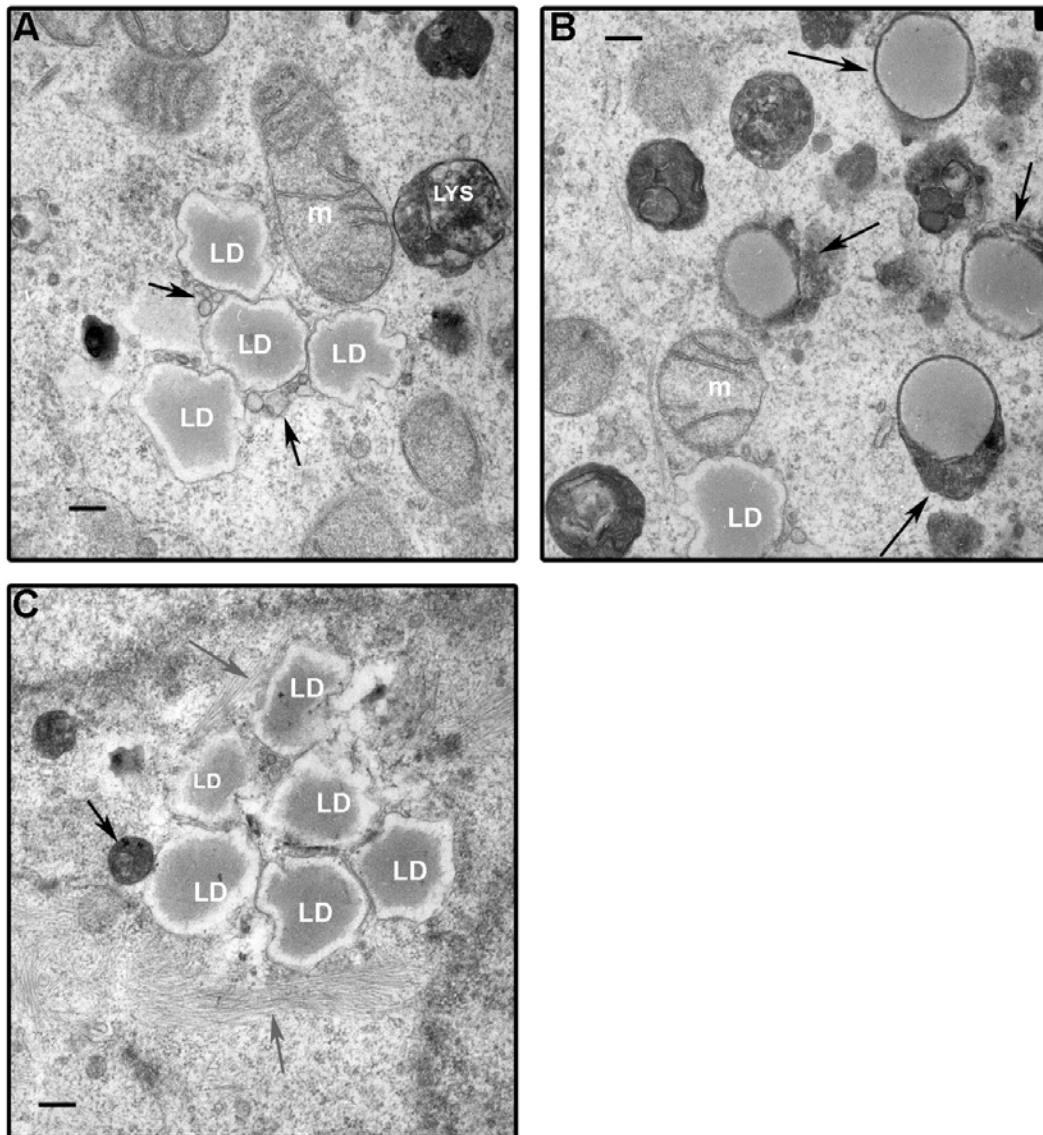
Figure 21: ELMI analysis of HeLa cells stably expressing SLP-1(1-224)-GFP embedded in Epon resin. To achieve better conservation of vesicular ultra-structure, fixed cells were embedded in Epon, thin sections were cut and analysed under the electron microscope. Cells expressing SLP-1-GFP were also analysed, but no similar droplet aggregates or "enveloped" droplets were observed (data not shown). Scale bars: 200 nm.

These structures could either represent LDs engulfed by e.g. lysosomes, or they could represent a LD which is forming in the interior. Our pictures could represent one of the first examples, where the digestion of a small LD structure inside a lysosome/late endosome is captured. The second possibility is also fascinating. If these structures represented LDs which

form out of a late endosomal/lysosomal structure, such a mechanism would be totally new. It is now well established that LDs are active organelles, which are connected not only to the ER, but also to other organelles by vesicular transport. Further work with this truncation mutant could clarify this issue. In a first step, it would be necessary to establish a proper pre-embedding labeling procedure to be able to unambiguously identify the SLP-1(1-224)-GFP positive structures in Epon thin sections. With this information, we then could try to establish the mechanism, which leads to the formation of the observed, peculiar structures.

4.1.8   SLP-1 and the C-terminal truncation mutants are localized to lipid rafts:

As it is well established that stomatin and other proteins with SPFH domains are enriched in lipid rafts, we analysed if SLP-1 is also detected in these cholesterol-rich membrane domains. Figure 22 shows the results for flotation experiments with cells stably expressing SLP-1-GFP (A), SLP-1(1-288)-GFP and SLP-1(1-224)-GFP (B).

Figure 22: SLP-1 is enriched in DRMs

Figure 22: Lipid rafts/DRMs were isolated from the indicated stable clones as described in the Methods section. Cholesterol content was determined with the Infinity cholesterol reagent from ThermoElectron, protein content was determined with the D_c-Protein assay kit from BioRad. Equal volumes of the fractions were analysed by western blotting.

Full-length SLP1 and both truncations are strongly enriched in the low-density buoyant fractions compared to total protein content. The deletion of the SCP-2 domain does not have an effect on lipid raft association. This is in contrast to the situation regarding stomatin, where the outmost C-terminus is essential for lipid raft association(Umlauf et al., 2006). Surprisingly, also the SLP-1(1-224)-GFP construct, which shows defects in subcellular trafficking, is also strongly lipid raft associated. These data show that lipid raft association of SLP-1 must be mediated by its SPFH domain. A similar result has been obtained for flotillin-1, where the isolated SPFH/PHB domain was also found to be raft-associated(Morrow and Parton, 2005). The distribution of stomatin in the gradients was not affected by the presence of SLP-1 (data for control HeLa cells not shown), which indicates that stomatin is a DRM-protein independent of its subcellular localization.

4.1.9 SLP-1 forms homo-oligomers

To determine if SLP-1 also forms high-order oligomers like the related stomatin protein, we performed an equivalent equilibrium density gradient centrifugation assay as described for stomatin (Snyers et al., 1998). We prepared membranes from HeLa cells stably expressing SLP-1-GFP, lysed the membranes in a buffer containing 1% TX100 and loaded the detergent-extract on top of a linear sucrose gradient from 5-25% sucrose. The whole gradient contained 1% TX100 to keep the proteins properly solubilized. Figure 23 shows the results of a representative experiment for SLP-1-GFP.

Figure 23: Analysis of SLP-1 oligomerization

Figure 23: Analysis of SLP-1 oligomers by equlibrium density gradient centrifugation. Detergent extracts of HeLa cells and of the clone A2 stably expressing SLP-1-GFP were loaded on top of linear density gradients from 5-25% sucrose and centrifuged at 200.000xg for 16-18 hours. Fractions were collected from the top and analysed by western blotting.

Similar to stomatin, we observed a pool of SLP-1-GFP in the low-density fractions, which probably represents monomeric SLP-1-GFP or dimers. The shift between the monomeric stomatin pool and the monomeric SLP-1 pool can be explained by the GFP-tag, which almost

doubles the molecular weight of the monomers. Additionally, a very intense band was detected in the bottom fraction of the gradient. This fraction most probably represents a high-molecular weight oligomeric complex of SLP-1. This complex is too heavy to be properly fractionated in the 5-25% gradient and therefore accumulates in the bottom fraction or gets pelleted. Protein aggregation could also be responsible for the observed signal in this fraction, but this should in principle also affect a similarly hydrophobic protein like stomatin. As seen in Figure 23, only a faint band is observed for stomatin in the bottom fraction in an analogous assay performed with control HeLa cells. The signal for stomatin in the bottom fraction slightly increases in the SLP-1-GFP expressing cells, but is in no relation to the fraction of SLP-1.

Figure 24: Further evidence for oligomerization: Double transfections I
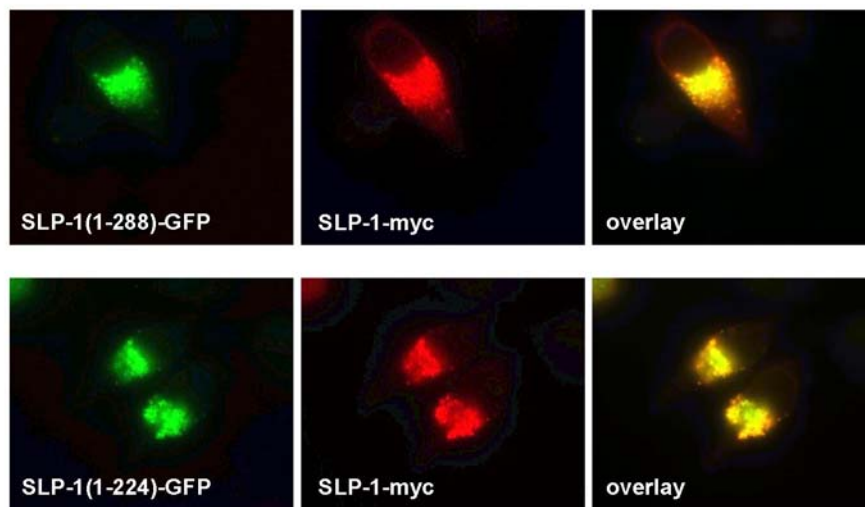
Figure 24: Full-length SLP-1 co-localizes with the truncation mutants SLP1(1-288) and SLP-1(1-224) and corrects the trafficking defect observed with SLP-1(1-224). HeLa cells were transiently transfected with the indicated constructs and analysed by immunofluorescence microscopy. Almost perfect co-localization of SLP-1 is observed with both truncation mutants. Cells expressing SLP-1(1-224)-GFP and SLP-1-myc at similar strength showed no filamentous structures and vesicle aggregates (see lower panel), but these structures were observed in cells only expressing the SLP-1(1-224)-GFP construct (data not shown).

This result could also indicate the formation of hetero-oligomers. Further evidence for the formation of SLP-1 homo-oligomers comes from double-transfection experiments with different SLP-1 constructs. As already described, the SLP-1(1-224) truncation mutant is mis-localized. Co-expression of wild-type SLP-1 can restore normal LE localization of this mutant (Figure 24). Perfect colocalization between SLP-1(1-224)-GFP or SLP-1(1-288)-GFP and wild-type SLP-1-myc was observed.

4.1.10 N-terminal deletions of SLP-1 are targeted to the plasma membrane (PM)

In addition to the previously described C-terminal truncations, we next analysed the effect of a deletion of the first 42 amino acids of SLP-1. As figure 25 shows, such a truncation mutant

is efficiently transported to the PM, whereas wild-type SLP-1 and the C-terminal truncations practically do not show PM localization.

Figure 25: N-terminal deletions/point mutations of SLP-1
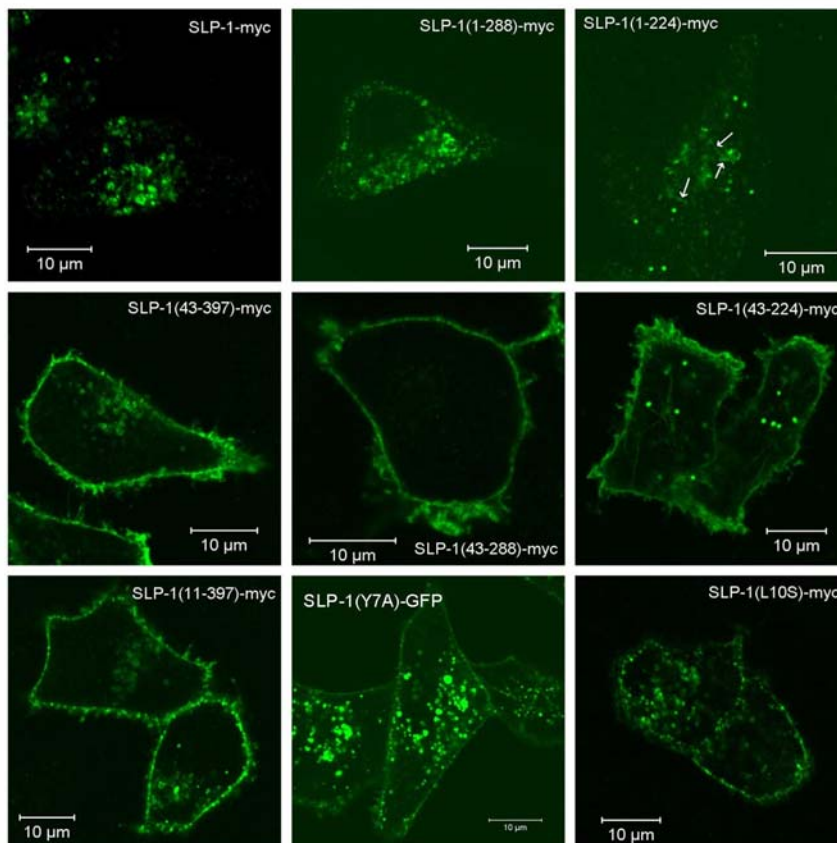
Figure 25: Comparison of different N- and C-terminal SLP-1 truncations/point mutations. HeLa cells were transiently transfected with the indicated constructs and analysed by confocal microscopy. N-terminal deletions of amino acids 1-42 or 1-10 cause targeting of SLP-1 to the plasma membrane. Point mutations in the GYXXΦ motif (Y7→A and L10→S) have a similar effect. Scale bars: 10 μm.

Next, we analysed this sequence for putative subcellular targeting signals and found that it contains a GYXXΦ motif (GYRAL), which is well known in the context of late endosomal/lysosomal targeting of LAMP-1, LAMP-2 and CD63. This motif is highly conserved in mammalian SLP-1 homologues (see Figure 2). In a next step, we combined our C- terminal truncations with the N-terminal deletion and analysed the localization of the constructs. All constructs with the N-terminal deletion showed plasma membrane staining, and the SLP-1(43-224)-myc construct showed cytoplasmic aggregates and PM staining. These data clearly show that the N-terminus of SLP-1 is necessary for the targeting of the protein to internal membranes. We then sought to determine if it is really the tyrosine-based signal at the outmost N-terminus, which is responsible for the internal localization. We first constructed a deletion mutant where only the first 10 amino acids were missing (SLP-1(11-397)-myc). Indeed, this construct also showed strong PM localization, which often appeared inhomogenously distributed. Finally, we targeted the tyrosine residue and mutated it to an alanine (SLP-1(Y7A)-GFP construct), and converted the hydrophobic amino acid at positon +2 after the tyrosine into a polar amino acid (SLP-1(L10S)-myc construct). These point mutations also caused a PM localization of the protein, which confirmed that the N-terminal GYRAL motif is indeed required for LE targeting of SLP-1. Three mechanisms could principally exist to direct SLP-1 to late endosomes: 1) the protein is directly transported to

LEs from the TGN; 2) SLP-1 is first delivered to the PM and is efficiently endocytosed to LEs; 3) a combination of both mechanisms is operating.

Figure 26: Inhibition of endocytosis and SLP-1 localization I: dynK44A
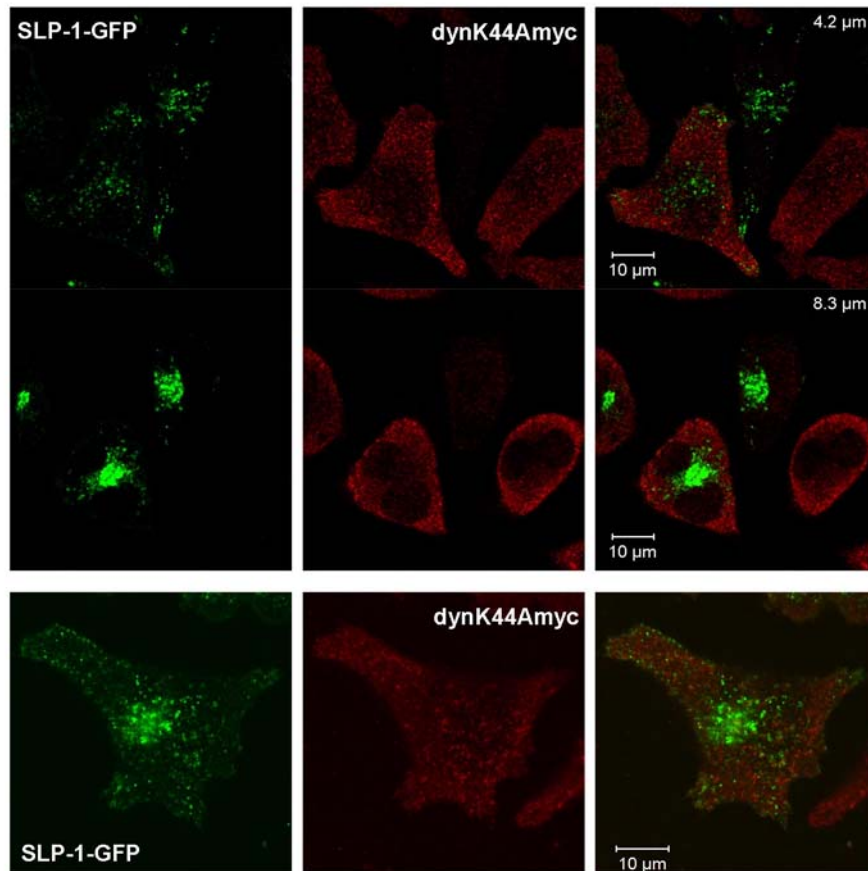
Figure 26: Inhibition of clathrin-mediated endocytosis by expression of a dominant-negative dynamin mutant does not redirect SLP-1 to the plasma membrane. HeLa cells stably expressing dynK44A under the control of a tet-off promotor were transiently transfected with SLP-1-GFP. Expression of the mutant dynamin was induced 12 hours after transfection by removal of tetracycline from the medium. Cells were analysed by confocal microscopy. No strong accumulation of SLP-1 at the plasma membrane was observed, although some changes in the distribution of SLP-1 were observed. The signal appeared more dispersed throughout the cytoplasm (section at 4.2 μm and lower panel), and very weak plasma membrane staining was observed in basal sections (lower panel). Scale bars 10 μm.

To adress this question, we inhibited endocytosis from the PM by expression of dominant-negative constructs. We either used a HeLa cell line, which stably expresses a dominant-negative dynamin mutant (DynK44A) under the control of a tetracyclin-responsive promotor, or transiently over-expressed either the C-terminus of AP180 (AP180C construct) or the SH3 domain of amphiphysin (AMPH-SH3). All these constructs target clathrin-mediated endocytosis(Snyers et al., 2003). No big effect (in regard to a strongly increased PM expression) was observed for all three experiments (see Figure 26 and 27).

Figure 27: Inhibition of endocytosis II: Amph-SH3, AP180C
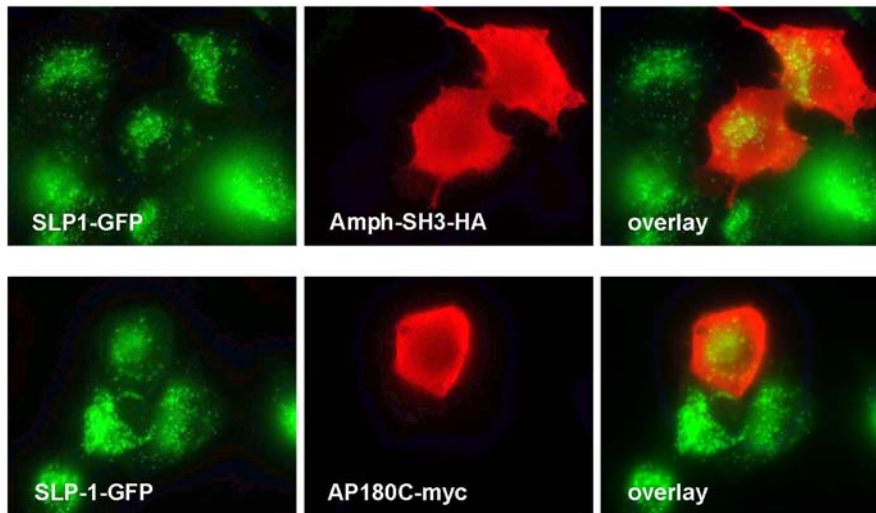
Figure 27: Inhibition of clathrin-dependent endocytosis with other constructs shows little effects on the subcellular distribution of SLP-1. HeLa cells stably expressing SLP-1-GFP were transiently transfected with the HA-tagged SH3 domain of amphiphysin or with the myc-tagged C-terminus of the adaptor protein AP180. Both constructs were previously shown to strongly inhibit clathrin dependent endocytosis. SLP-1 localization to perinuclear endosomes was not affected by expression of both constructs.

Figure 28: Inhibition of endocytosis III: Cyclodextrin
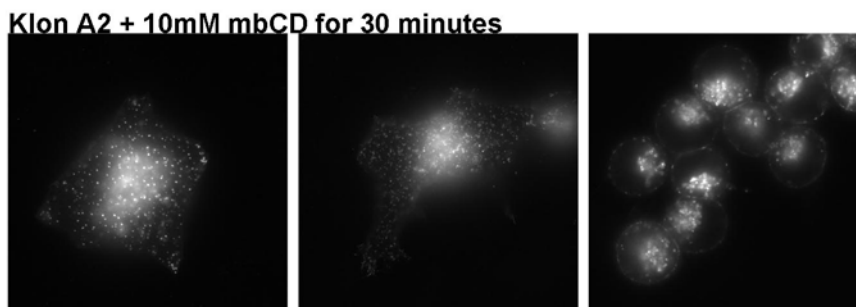
Figure 28: HeLa cells stably expressing SLP-1-GFP were treated with 10 mM methyl-beta-cyclodextrin for 30 minutes at 37°C and were then analysed by immunofluorescence. MβCD had a strong effect on the distribution of SLP-1 and caused the dispersal of the signal throughout the cytoplasm and the appearance of weak plasma membrane staining. Treatment with mβCD caused rounding and detachment of a large proportion of the cells (right picture).

These data rule out that the late endosomal localization of SLP-1 is caused by very efficient endocytosis via the clathrin-mediated "classic" endocytic pathway. As several clathrin-independent pathways have recently been described especially for raft-associated proteins (Glebov et al., 2006), we still can not rule out that SLP-1 trafficks to LEs via the PM.

In a different experiment, we treated SLP-1-GFP expressing cells with mβCD to achieve cholesterol depletion, which is known to inhibit both clathrin-dependent and –independent endocytosis. This treatment led to the detection of a clearly visible signal for SLP-1-GFP at

the PM (see Figure 28). But the treatment of the cells with ~10mM mβCD for 30 minutes also dramatically affected cell adherence and viability. Most cells remained only loosely attached to the substrate. Therefore, it is doubtable if this PM staining is only due to the inhibition of endocytosis. Treatment with lower doses of mβCD did not show this effect in SLP-1 localization. Additionally, in most cells, the perinuclear signal still strongly dominated over the PM signal. In an independent experiment, we inhibited protein synthesis with cycloheximide and analysed if this treatment has any effect on the localization of the protein (data not shown). We found that the GFP-tagged SLP-1 protein is very stable in LEs and is still detected in strongly expressing cells after 72 hours of cycloheximide treatment. No PM localization was observed, although the amount of SLP-1-GFP was strongly reduced. This result indicates that LE targeting is not a mere consequence of a high expression level, which was also shown by the fact that we did not observe PM localization in transient transfections, also not in cells which show a low expression level.

4.1.11 N-terminally GFP-tagged SLP-1 is partially localized to the PM

During my work, I also cloned a N-terminally GFP-tagged SLP-1 variant to confirm the results obtained for the C-terminally tagged construct. Interestingly, this construct showed a clearly detectable PM signal besides a stronger LE signal in immunofluorescence (see Figure 29).

Figure 29: GFP-SLP-1 is mis-targeted to the PM
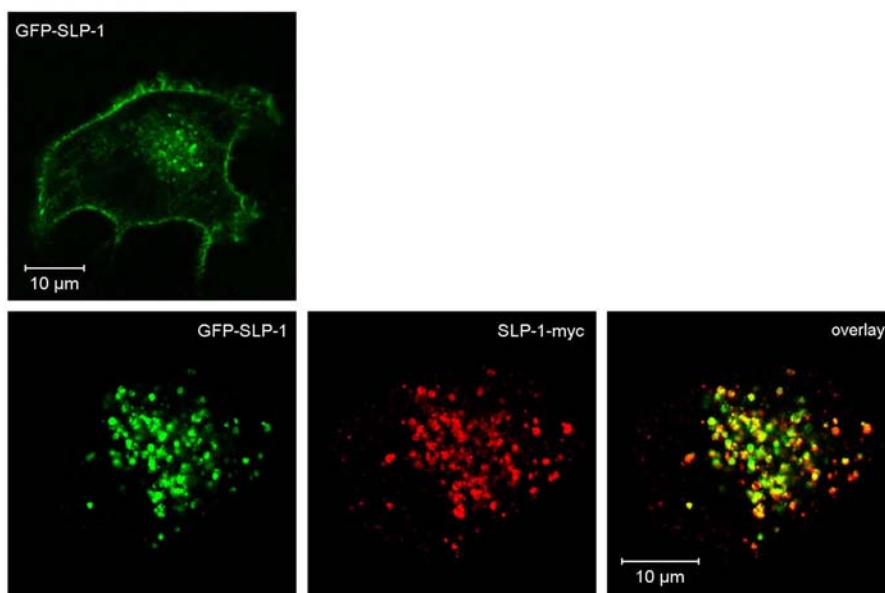
Figure 29: The GFP-SLP-1 construct was transiently expressed in HeLa cells and surprisingly showed PM localization (upper picture). Co-expression of C-terminal tagged SLP-1-myc abolished the PM localization of GFP-SLP-1 (lower panel), which again indicates that SLP-1 forms oligomers. Scale bars 10 μm.

Based on our results, which show the importance of the GYXXΦ signal at the outmost N-terminus, we concluded that the bulky N-terminal GFP-tag probably reduces the accessibility

of this signal for adaptor proteins which mediate transport/sorting to LEs and cause a proportion of GFP-SLP-1 to be transported to the PM with the bulk flow. Co-expression of SLP-1-myc caused the PM signal for GFP-SLP-1 to vanish, therefore restoring normal LE localization (Figure 29) and almost perfect colocalization with SLP-1-myc. This result again indicates the formation of SLP-1 oligomers during biosynthesis.

We next made use of the different SLP-1 constructs, which show at least partial PM localization to explore if SLP-1 also is inserted into the membrane via a hydrophobic hairpin as described for stomatin. If the hydrophobic hairpin conformation was correct, N- and C-terminus of SLP-1 should reside in the cytoplasm.

Figure 30: Both N- and C-termini of SLP-1 are cytoplasmic
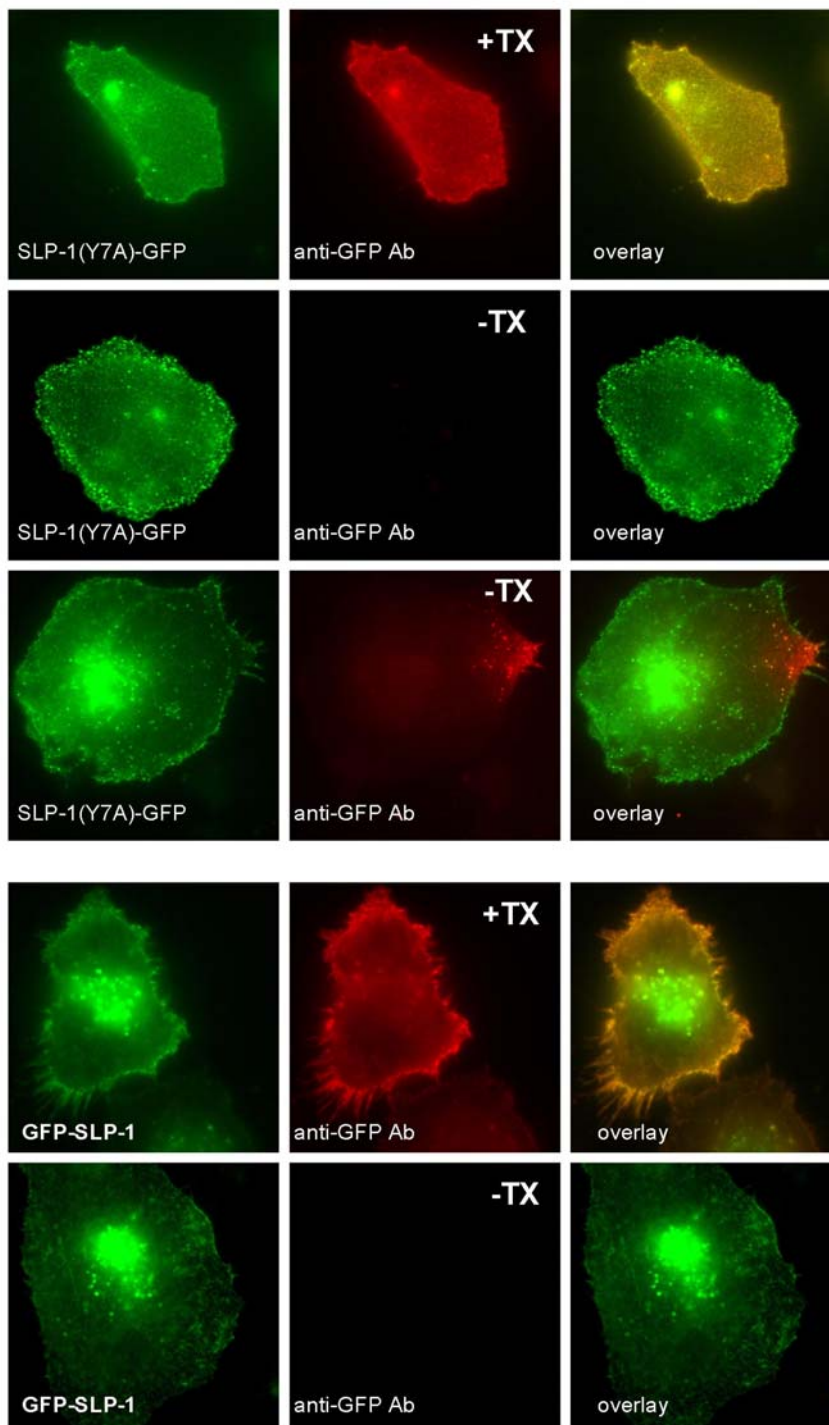
Figure 30: Analysis of N- and C-terminally tagged SLP-1 constructs with PM localization. The SLP-1(Y7A)-GFP and GFP-SLP-1 constructs were transiently expressed in HeLa cells. Cells were analysed by indirect immunofluorescence with an anti-GFP antibody either with or without permeabilization. Without detergent, only the GFP-signal was observed (except for some leaky cells, see middle panel), confirming the cytoplasmic localization of both termini.

The constructs which show PM localization should therefore only be detected after permeabilization of the cells and not without permeabilization. We used the GFP-SLP-1 construct and the SLP-1(Y7A)-GFP construct, transiently transfected COS7 cells and then performed indirect immunofluorescence with an anti-GFP antibody on TX100-permeabilized and non-permeabilized cells (Figure 30).

No signal was observed for both experiments without TX100 permeabilization (some "leaky" cells were observed, where some antibody could diffuse into the cytoplasm without TX100, see figure). These results confirm that the GFP-tag at the N-terminus and at the C-terminus is not exposed at the cell surface and rules out the possibility that SLP-1 could be a typeI transmembrane protein. Based on the similarities between the long hydrophobic membrane domains (same size, adjacent cysteine residues which can be palmitoylated, short strongly charged cytoplasmic N-terminus) and the already described possibility to localize to lipid droplets (transmembrane proteins are excluded from LDs), we conclude that SLP-1 is anchored to the membrane by an equivalent hydrophobic hairpin loop.

4.1.12 Chimeric SLP-1/stomatin fusions confirm the LE targeting function of the N-terminus

Finally, I decided to construct a chimeric protein consisting of the N-terminus of SLP-1 (amino acids 1-49) fused to the hydrophobic domain and the C-terminus of stomatin. The STOM (21-287)-GFP construct where the N-terminus of stomatin is deleted was cloned by Ellen Umlauf of our group recently. This construct was practically indistinguishable from the full-length stomatin-GFP construct in respect to subcellular localization, oligomerization and lipid raft association (Umlauf et al., 2004; Umlauf et al., 2006). Therefore, the N-terminus of stomatin is not essential for proper subcellular targeting of the protein. If I added the N-terminus of SLP-1 to this construct, I would expect to see enhanced LE targeting of the resulting fusion protein. As a control, I also constructed fusions of STOM (21-287)-GFP with the point-mutated N-termini (Y7A, L10S) already described.

The resulting fusion proteins were analysed by western blotting with an anti-GFP antibody and showed the expected sizes, with the expected size difference between the STOM (21-287)-GFP construct and the SLP-1(1-49)STOM (21-287)-GFP construct. The two point-mutated fusions had the same size as the wild-type SLP-1-STOM fusion (Figure 31 A). Transient transfections were analysed for the localization of the constructs (Figure 31 B), cells were co-stained with LysoTrackerRed to reveal acidic endosomes/lysosomes. The results were really striking. The STOM (21-287)-GFP construct showed the known distribution typical for stomatin (PM+LE staining). The fusion SLP-1(1-49)STOM (21-287)-GFP, however, did not show any PM localization any more and only showed perinuclear, vesicular staining as observed with SLP-1.

Figure 31: Fusion of the SLP-1 N-terminus to stomatin
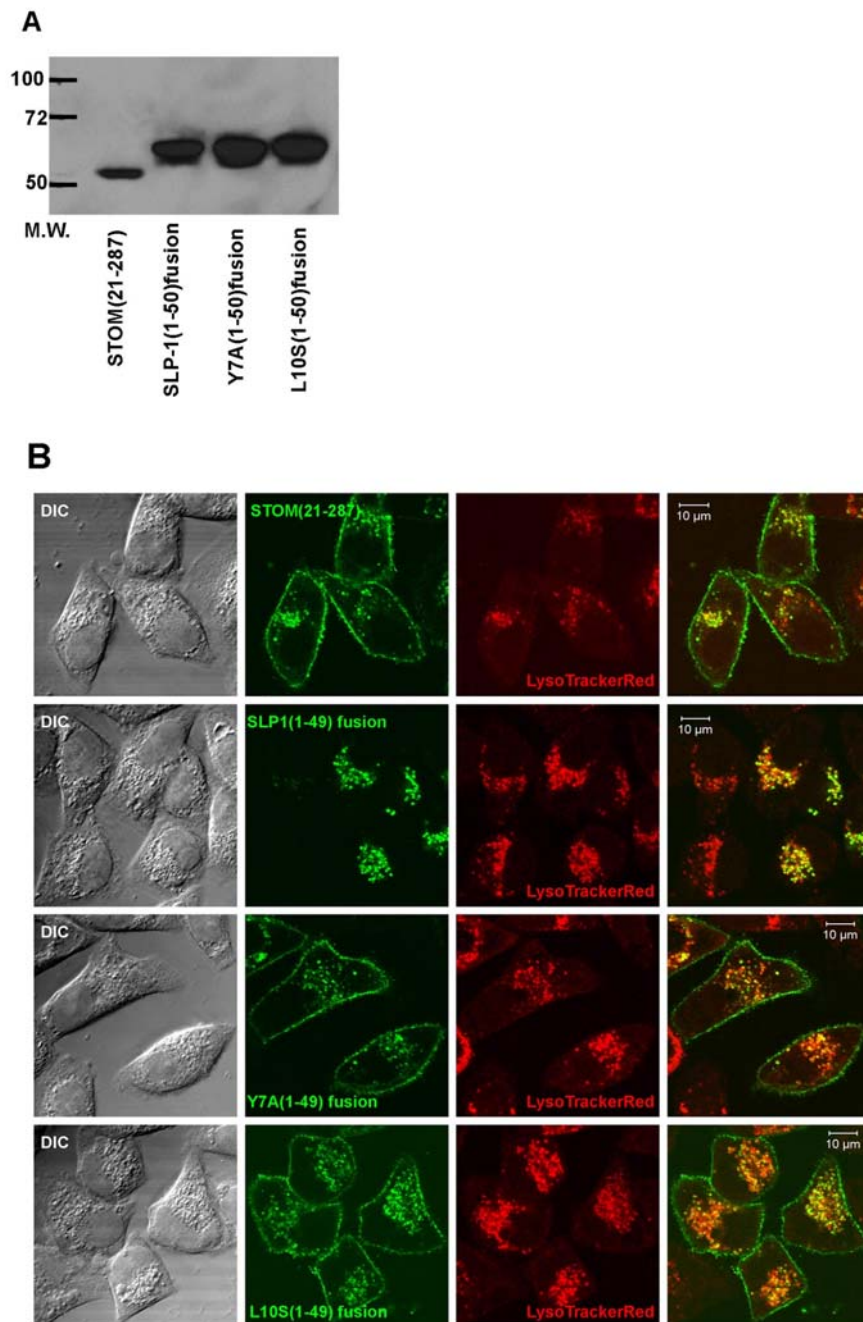
Figure 31: Fusion of the N- terminus of SLP-1 to stomatin. Deletion of the N-terminus of stomatin does not have an effect on the subcellular localization of the protein (PM and LE localization indistinguishable from wt stomatin, (Umlauf et al., 2004)). We constructed fusions of the entire N-terminus of SLP-1 (1-49) or of the N-terminus carrying point mutations (Y7→A and L10→S) in frame with STOM (21-287)-GFP, transiently expressed them in HeLa cells and analysed expression by western blotting and immunofluorescence. The wild type N-terminus abolished PM localization of stomatin, which was restored when the GYRAL motif was mutated. Scale bars 10 μm.

Introduction of point mutations in the N-terminus of SLP-1 abolished the stringent LE targeting and restored the normal pattern for stomatin, with PM and LE signal. This result confirms that the N-terminus of SLP-1 is an efficient LE targeting signal. Targeting to LEs is most probably accomplished by direct trafficking from the TGN to LEs, because we did not observe cells with PM signal for the SLP-1(1-49)STOM (21-287)-GFP fusion. Alternatively, very efficient and quick internalization from the PM might also operate. The amino acids Y7 and L10 are essential for proper function of the N-terminus as an endocytic targeting signal. This suggests that the N-terminus might also directly interact with a subunit of an adaptor complex as had already been described for other GYXXΦ motifs (Gough et al., 1999; Ihrke et al., 2004; Ohno et al., 1998). The analysis of interaction partners with this short, cytoplasmic stretch could yield interesting results on the transport machinery which is responsible for LE targeting of SLP-1.

4.1.13 Live cell imaging reveals that SLP-1 on late endosomes is highly dynamic

With our SLP-1-GFP construct, we were able to analyse the dynamics of SLP-1 in living cells. We used HeLa cells stably expressing high amounts of SLP-1-GFP and subjected the cells to time-lapse confocal microscopy. Most of the SLP-1-GFP-positive vesicles were found to reside close to the nucleus and to show brownian motion. But we also observed some vesicles which clearly showed directed movement to/from the cell periphery (Figure 32 A, Movie 1). In addition to the typical, perinuclear staining pattern known from fixed cells, we noted smaller vesicles, which moved at higher speed. These vesicles could either represent TGN-derived carriers or early endosomal carriers, which interact with the late endosomes. We frequently observed fusion events between these small SLP-1-GFP positive structures and large, LysoTrackerRed stained, larger structures (Figure 32 B, Movie 2).

This population of small vesicles is probably missed in fixed cells, because these structures are indistinguishable from larger vesicles with an inhomogenous staining pattern for SLP-1. This inhomogenous, "patchy" staining of SLP-1 on large late endosomes was clearly confirmed by live cell imaging studies (Figure 32 A,B) and complicates the quantification of the degree of colocalization of SLP-1 with other marker proteins. Nevertheless, most of the SLP-1-GFP signal clearly resides on large, LysoTrackerRed-stained acidic vesicles, in line with a localization to late endosomes.

The next step in the analysis of SLP-1 dynamics must clearly be to identify the origin/nature of the small, highly dynamic SLP-1-GFP vesicles, because these could be essential for the proposed function in lipid transport.

Figure 32: Live cell imaging of SLP-1-GFP
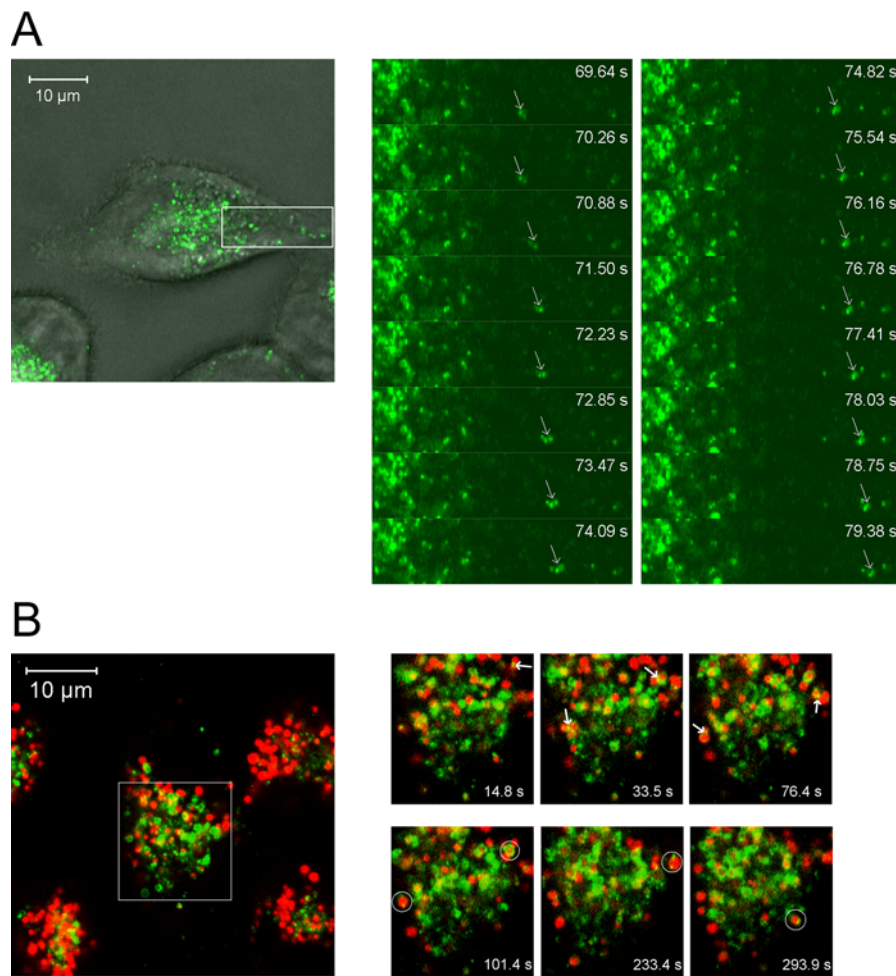
Figure 32: Live cell imaging reveals the dynamic behavior of SLP-1-GFP. (A) HeLa cells stably expressing SLP-1-GFP were processed for live cell imaging as described in the Methods section. A freeze image of a cell is shown in the left panel. The boxed region was zoomed in and GFP-images were acquired every 0.65 seconds for about 3 minutes. The right panel shows images from the movie from time point 69 to 79 seconds. A large vesicle rapidly moving towards the cell periphery is marked by arrows. Please note the dotted distribution of the SLP-1-GFP signal on the vesicle. In the complete movie, several vesicles rapidly moving to and from the cell periphery were observed. (B) Cells were co-stained with LysoTracker Red and analyzed by confocal live cell imaging. The left panel shows a freeze image of the cells, with the region analysed by live microscopy marked. The left panel shows overlays for SLP-1-GFP and LysoTrackerRed staining at different time points. Several big vesicles with small, dynamic SLP-1-GFP dots on their surface can be observed in the complete movie. Scale bar: 10 μm.

4.1.14 SLP-1 induces the formation of enlarged, cholesterol-enriched vesicles if cholesterol efflux from LEs to the PM is blocked with the amino-steroid U18666A

The unique domain structure of SLP-1 indicates that it could function in lipid transport/transfer. After we had discovered that the protein is localized to LEs, we decided to investigate if it could help the cells to overcome a blockade in cholesterol transport induced by U18666A when overexpressed. U18666A induces the accumulation of cholesterol in late

endosomes and is frequently used to artificially cause a so-called Niemann-Pick phenotype. This phenotype, which was first observed in fibroblasts derived from patients with the Niemann-Pick syndrome, a disease which affects the central nervous system, is characterized by the accumulation of cholesterol in late endosomes. Overexpression of MLN64, a cholesterol-binding late endosomal protein, inhibits cholesterol accumulation at low concentrations of U18666A(Alpy et al., 2001). We therefore wanted to analyse if SLP-1 has a similar effect. We treated control HeLa cells and HeLa cells stably expressing SLP-1-GFP with different concentrations of U18666A and analysed cholesterol accumulation by staining with filipin. No reduction of cholesterol accumulation was observed in cells over-expressing SLP-1-GFP (data not shown). Instead, we frequently observed the formation of enlarged, strongly filipin-stained structures in cells expressing SLP-1-GFP (Figure 33 A). These structures often had a diameter of up to 3 μm and were even visible in phase contrast. We next analysed if these enlarged vesicles were also present if the SCP-2 domain of SLP-1 is deleted. In cells expressing the SLP-1(1-288)-GFP construct, these enlarged structures were not observed. These data strongly indicate that SLP-1 might have a function in cholesterol transport and that the SCP-2 domain is required for this function. To get a quantitative picture of the situation, we analysed the SLP-1-GFP/SLP-1(1-288)-GFP and filipin-positive structures for maximal vesicle diameter. The results are shown in Figure 33 B. Cells expressing SLP-1-GFP contain significantly larger cholesterol-filled structures compared to cells expressing SLP-1(1-288)-GFP. These enlarged structures are not caused by the GFP-tag, because they were also observed in cells expressing SLP-1-myc (Figure 34).

We next wanted to determine if these enlarged structures represent late endosomes/lysosomes as expected. We therefore performed a triple staining of filipin, SLP-1-GFP/SLP-1(1-288)-GFP and the late endosomal marker LAMP-2. The results are shown in Figure 35.

Because there are numerous reports that U18666A induces the accumulation of cholesterol in LAMP-1/2 positive late endosomes, we expected that the enlarged structures should be positive for LAMP-2. We were rather surprised to find that these structures only contain very little LAMP-2 (Figure 35A). In cells expressing SLP-1-GFP, the signal for filipin and LAMP-2 was largely separated, and the structures with the strongest filipin staining showed only very little LAMP-2 signal (see arrows). Almost no colocalization of all 3 markers was observed. In cells expressing SLP-1(1-288)-GFP, however, we observed much better colocalization of filipin and LAMP-2 and also observed a higher fraction of vesicles clearly positive for all 3 markers (Figure 35B). In control HeLa cells treated with U18666a, filipin and LAMP-2 clearly co-localized, although not perfectly (Figure 36A). We then repeated the triple staining with SLP-1-GFP expressing cells and essentially got the same results. We could confirm that the enlarged structures contain only tiny amounts of LAMP-2 (Figure 36B). This means that they should be part of the late endosomal system, but they could represent a subcompartment, which is rather devoid of LAMP-2. In a live cell imaging experiment, we induced cholesterol accumulation and co-stained the cells with LysoTrackerRed. We again observed the enlarged structures in response to U18666A treatment in SLP-1-GFP positive cells.

Figure 33: Influence on cholesterol distribution upon U18666A treatment
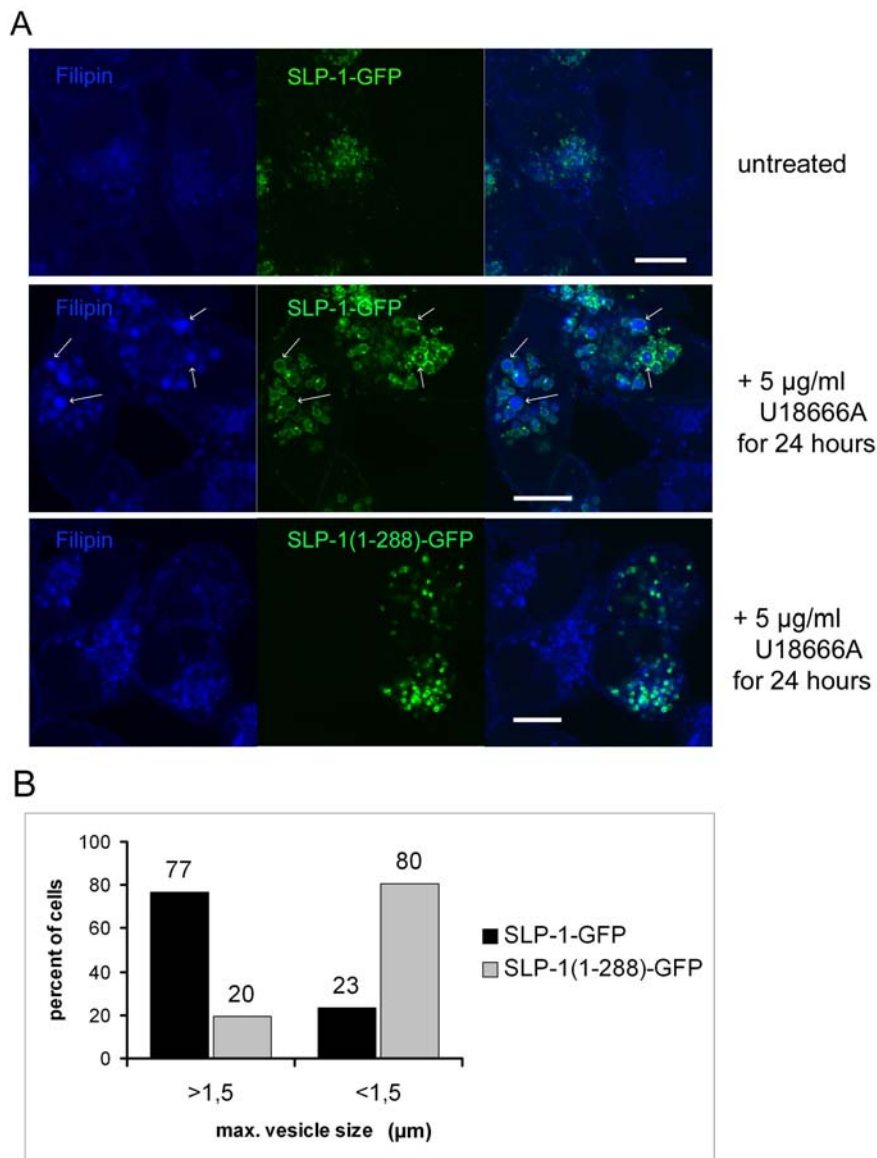
Figure 33: Treatment of SLP-1-GFP expressing cells with the aminosteroid U18666A results in the formation of enlarged, cholesterol-rich vesicles. (A) Upper panel: Mixed SLP-1-GFP expressing and normal HeLa cells were grown in the absence of U18666A and stained with filipin to visualize cholesterol distribution. Weak filipin-staining was detected on the plasma membrane and in the perinuclear region. Middle panel: Mixed SLP-1-GFP expressing and normal HeLa cells were treated with U18666A as indicated. In cells expressing SLP-1-GFP, enlarged, filipin-stained vesicles can be seen (arrows) that are surrounded by SLP-1-GFP. These filipin-stained vesicles are clearly larger than in normal, SLP-1-GFP-negative HeLa cells. Lower panel: Cells expressing SLP-1(1-288)-GFP were treated with U18666A and analyzed equally. Small, filipin- stained, SLP-1(1-288)-GFP-positive vesicles can be observed but not the enlarged vesicles. Scale bars: 10 μm. (B) Comparison of the maximum vesicle size of cells either expressing SLP-1-GFP or SLP-1(1-288)-GFP after treatment with 5 μg/mL U18666A for 24 hours. The diameter of the largest vesicular structures positive for the respective GFP-fusion protein and filipin was measured with the software of the Zeiss LSM microscope in 50 different cells, for each cell type. Diameters larger or smaller than 1.5 μm were scored. The relative results are shown in the diagram.

Figure 34: U18666A II
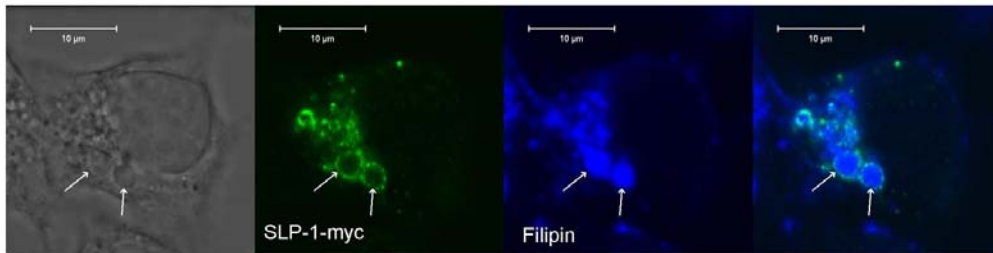
Figure 34: Enlarged vesicles are also detected in cells expressing SLP-1-myc. Cells stably expressing SLP-1-myc were treated with 3 µg/ml U18666A for 24 hours and analyzed by filipin staining. Two enlarged structures containing SLP-1-myc (green channel) and filipin (blue channel) were marked by arrows. These vesicles were also clearly visible in the phase contrast image. Scale bar: 10 µm.

Figure 35: U18666A III
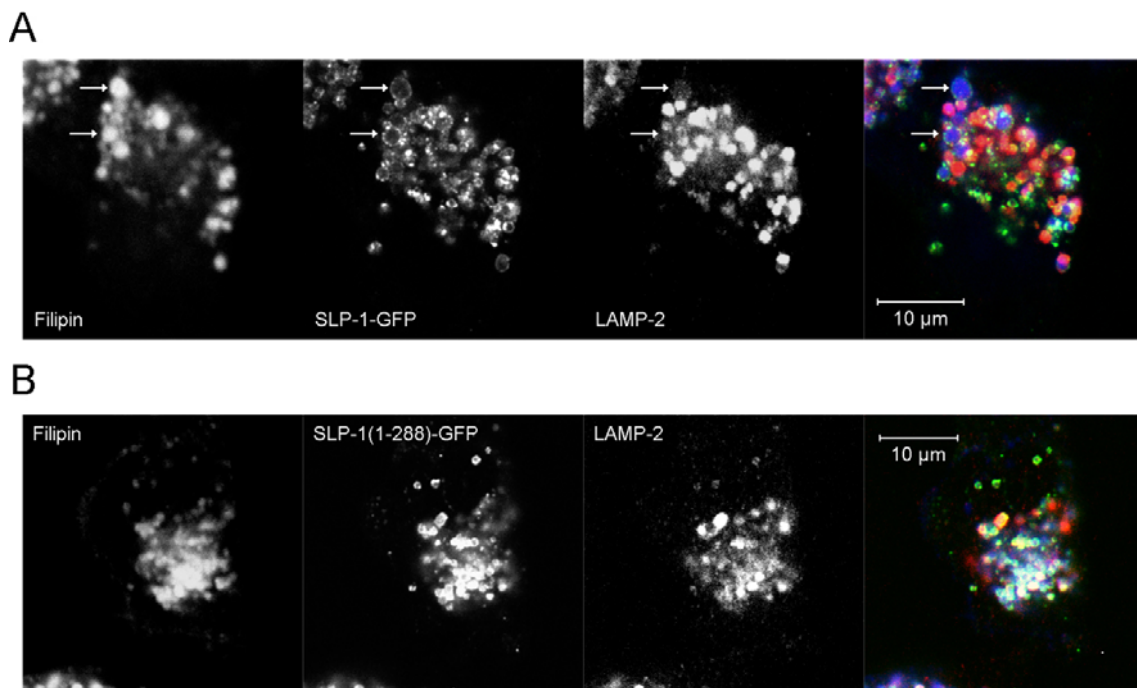
Figure 35: Triple staining of cells treated with U18666A reveals a reduced co-localization of LAMP-2 with filipin and SLP-1-GFP in the large, cholesterol-rich vesicles. Cells stably expressing either (A) SLP-1-GFP or (B) SLP-1(1-288)-GFP were treated with 3 µg/ml U18666A for 24 hours. The cells were fixed and stained with filipin and anti-LAMP-2-antibody. (A) The enlarged, filipin-positive vesicles that are observed in cells expressing SLP-1-GFP (arrows) contain very little LAMP-2. (B) Co-localization of filipin, SLP-1(1-288)-GFP, and LAMP-2 can be clearly seen in a large part of the late endosomal compartment. Please compare the triple overlays in A and B. Scale bars: 10 µm.

These large structures were clearly positive for LysoTrackerRed (Figure 36C), confirming their late endosomal origin. Several unanswered questions remain: 1) Why are the enlarged structures devoid of LAMP-2? Do they represent a LAMP-2-poor subcompartment of LEs?. 2) Do these LAMP-2 poor structures exist before U18666A treatment? Do they specifically accumulate cholesterol stronger than other LEs? 3) Or is LAMP-2 sorted from the SLP-1-

GFP-positive structures upon U18666A treatment? 4) Alternatively, the LAMP-2 signal could also simply be "diluted" when the vesicle gets bigger and bigger.

At first, it would be important to find other marker proteins, which are enriched in these SLP-1-GFP positive structures. This could help to precisely define the relationship of these giant vesicles to the late endosomal compartment. Next, analysis of the ultrastructure of these structures could provide interesting results (What is the ultrastructure of the interior of these vesicles? Are they MVBs or vacuoles?).

Figure 36: U18666A IV
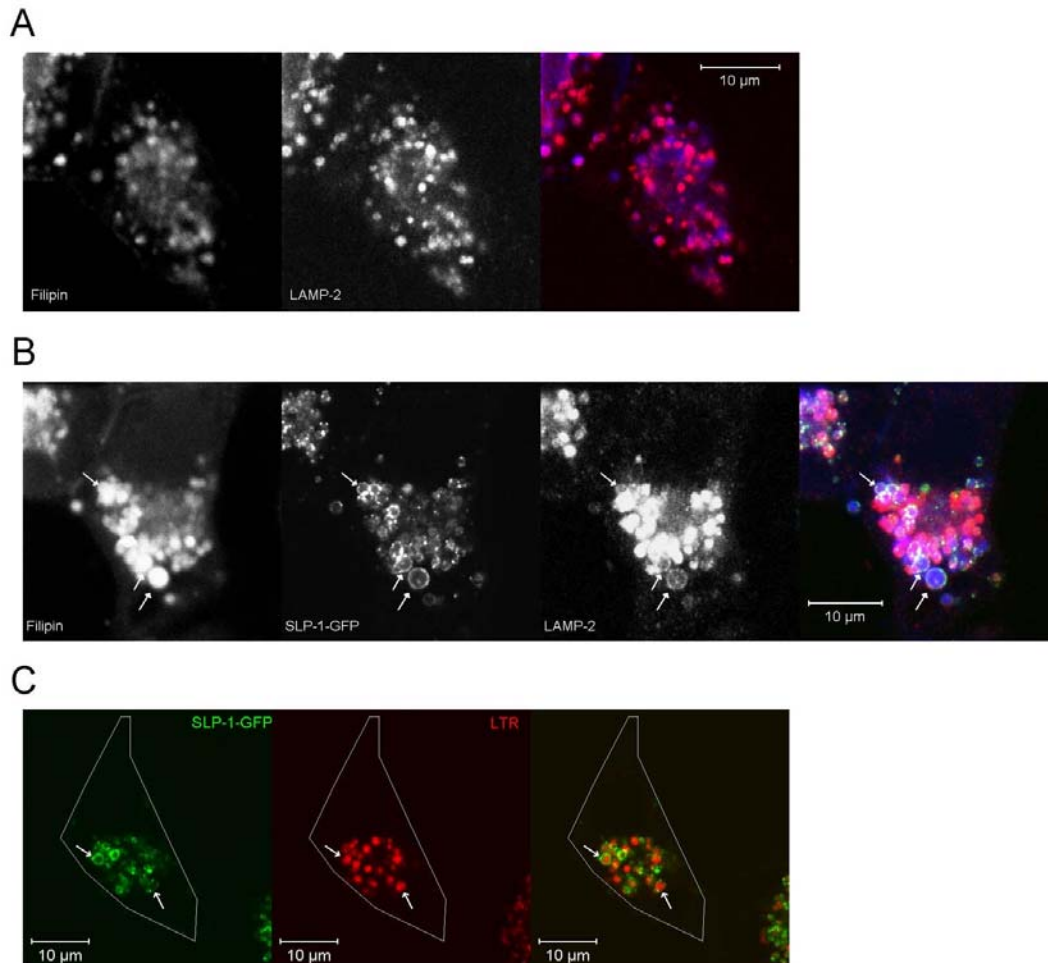
Figure 36: The enlarged vesicles do contain small amounts of LAMP-2 and are acidic.(A) HeLa cells were incubated with 3 μg/ml U18666A for 24 hours and stained with filipin (blue) and anti-LAMP-2 antibody (red). LAMP-2 was detected in virtually all filipin-positive vesicles. (B) HeLa cells stably expressing SLP-1-GFP were treated equally and analyzed for filipin (blue), SLP-1-GFP (green), and LAMP-2 (red) staining. Three enlarged, SLP-1-GFP-positive vesicles were marked with arrows. These structures contained small but clearly detectable amounts of LAMP-2, indicating that they were derived from late endosomes. (C) Live cells expressing SLP-1-GFP were treated with 10 μg/ml U18666A for 24 hours and stained with LysoTracker Red (LTR) as described. A cell showing the typical, enlarged structures is shown. Two enlarged, acidic vesicles clearly stained with LTR are marked with arrows. Scale bars: 10 μm.

4.2 Stomatin

The function of stomatin, the founder member of the stomatin protein family, still remains enigmatic. Before I started with the project of the characterization SLP-1, I have tried to elucidate the function of stomatin in platelets and neutrophilic granulocytes. I decided to include these in large part biochemical data in my thesis because of the now apparent association of SLP-1 and stomatin in a high molecular weight complex. Because this complex formation is relevant for both proteins, the stomatin data will also be relevant for SLP-1. Additionally, I extended the work of the previous lab member and colleague, Ellen Umlauf, who had started the cell biological characterization of stomatin and constructed numerous stomatin point mutants and deletions with the aim of characterizing the oligomerization domain and possibly producing dominant-negative mutants which could reveal the function of the protein. She had clearly identified a region necessary for oligomerization and lipid raft association, but all her mutants did not show a clear phenotype in cell culture. In parallel to the characterization of SLP-1, I also constructed several stomatin point mutants, with a focus on amino acids conserved between the *C. elegans* homologue MEC-2 and stomatin, which were mutated in *mec-2* alleles. Due to limitations in time, these novel constructs are not characterized in detail, but I am convinced that they will be very useful for the study of the function of stomatin in the future. Interestingly, two of these novel point mutations (S231A and S231E) apparently affect the interaction of stomatin with SLP-1.

4.2.1 Immunofluorescence analysis of resting and activated platelets and PMNs reveals major changes upon activation

Platelets and PMNs were isolated from whole blood as described, either activated or directly seeded onto coated coverslips. The distribution of stomatin was analysed by indirect immunofluorescence. The upper panel of Figure 37 shows the results for resting and activated platelets. In resting platelets, stomatin is detected in cytoplasmic puncta of variable size, which represent alpha-granules(Mairhofer et al., 2002). Activation with thrombin causes platelet spreading and fusion of alpha-granules with the plasma membrane. Stomatin is detected on the plasma membrane. The signal is strong at the tips of filopodia. A similar staining pattern was recently described for a toxin which binds to cholesterol(Heijnen et al., 2003). This staining pattern is also interesting, because we have observed an enrichment of stomatin in platelet-derived microvesicles, and these microvesicles could form by shedding from the tips of the filopodia. Activation with a peptide mimicking the effect of thrombin action (TRAP peptide) showed the same results. The lower panel of Figure 37 shows the results for isolated PMNs.

Figure 37: Immunofluorescence images of platelets and neutrophils
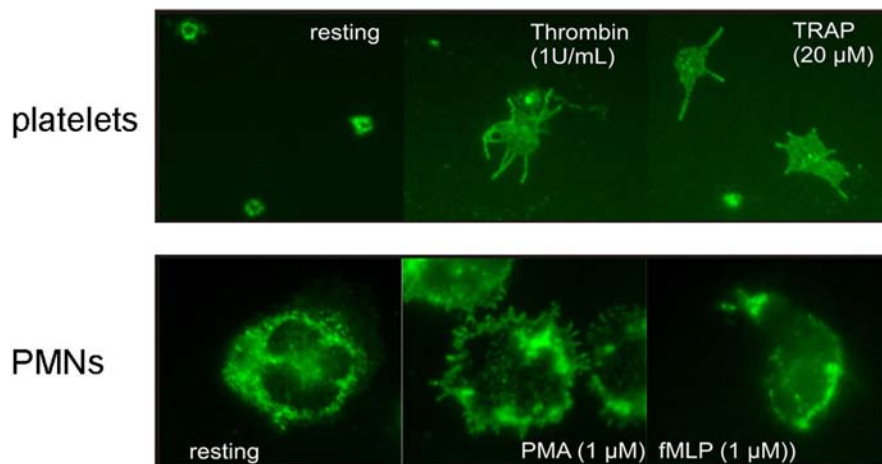
Figure 37: Immunofluorescence images of platelets and neutrophils. Platelets and Neutrophils were isolated from whole blood as described in the Methods section and seeded onto poly-L-lysine–coated coverslips. Cells were either fixed immediately or activated with the indicated agonists for 5 minutes at 37°C. Immunofluorescence was performed with the anti-stomatin-antibody GARP50. Please note the dramatic shape change of platelets and the characteristic filopodia seen after activation.

In resting PMNs, stomatin is detected in cytoplasmic granules as expected(Feuk-Lagerstedt et al., 2002). Please note the lobes of the nucleus, which are clearly visible. No plasma membrane staining was observed in resting PMNs. Activation with PMA caused a translocation of stomatin to the plasma membrane. Again, stomatin staining was visible in tiny filopodia. Activation with the chemotactic peptide fMLP caused random polarization of the adherent PMNs. The outer right picture in the lower panel of Figure 37 shows a polarized neutrophil cell with the leading edge and the trailing edge strongly stained for stomatin. This staining may not represent true polarization of the stomatin signal, but could also be caused by an accumulation of stomatin-positive granules close to the membrane.

4.2.2 2D-PAGE analysis of platelet lipid rafts reveals major differences between raft fractions isolated with different detergents

During my diploma thesis, we established a method for the isolation of lipid rafts from platelets with the detergent CHAPS instead of Triton X-100, which is routinely used for this purpose. For the hydrophobic membrane protein stomatin, detergent lysis with CHAPS leads to an increased proportion of total stomatin in the low-density, buoyant lipid raft fractions. Several other proteins were also detected in the CHAPS lipid raft fractions, but not in the Triton X-100 lipid raft fractions (GLUT3, CD9, CD36). Figure 38 shows a comparison of TX100 and CHAPS flotation assays analysed by 1D-PAGE and western blotting/silver staining.

Figure 38: Platelet lipid rafts isolated with different detergents: 1D PAGE
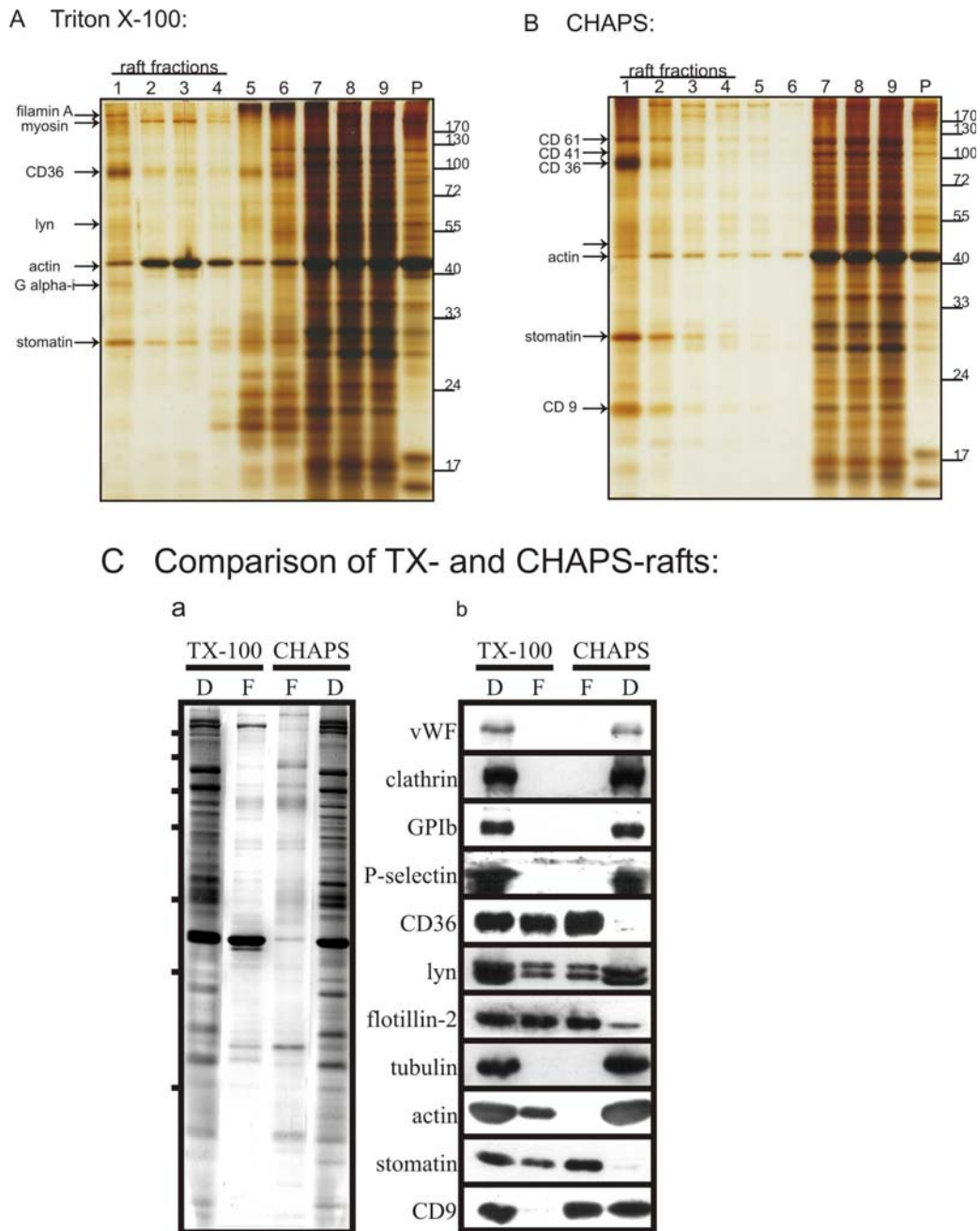
Figure 38: Comparison of platelet lipid rafts/DRMs isolated with different detergents. Platelets were lysed with either 1% TritonX-100 or 1% CHAPS as described, and DRMs were isolated by step density gradient centrifugation. Equal volumes of density gradient fractions were analysed by silver staining (A, B). (C) represents a comparison of the pooled raft fractions (label F) and the non-floating dense fractions (label D). Differences in protein content are clearly visible. The most striking difference is the reduction of actin in the CHAPS raft fractions.

We then developed a 2D-PAGE method suitable for lipid raft fractions to be able to analyse these differences in more detail. Figure 39 shows a comparison of TX100 and CHAPS lipid raft fractions analysed by 2D-PAGE. Major differences are clearly visible in the two spot patterns. Most striking is the strong reduction of actin (and actin-associated cytoskeletal proteins) in the CHAPS raft fractions. But although the cytoskeleton content of the raft fractions is decreased, the complexity is increased compared to the TX100 raft fractions. This means that CHAPS lysis is less stringent and probably results in the isolation of much more proteins in the low-density buoyant fractions.

Figure 39: Platelet lipid rafts isolated with different detergents: 2D PAGE
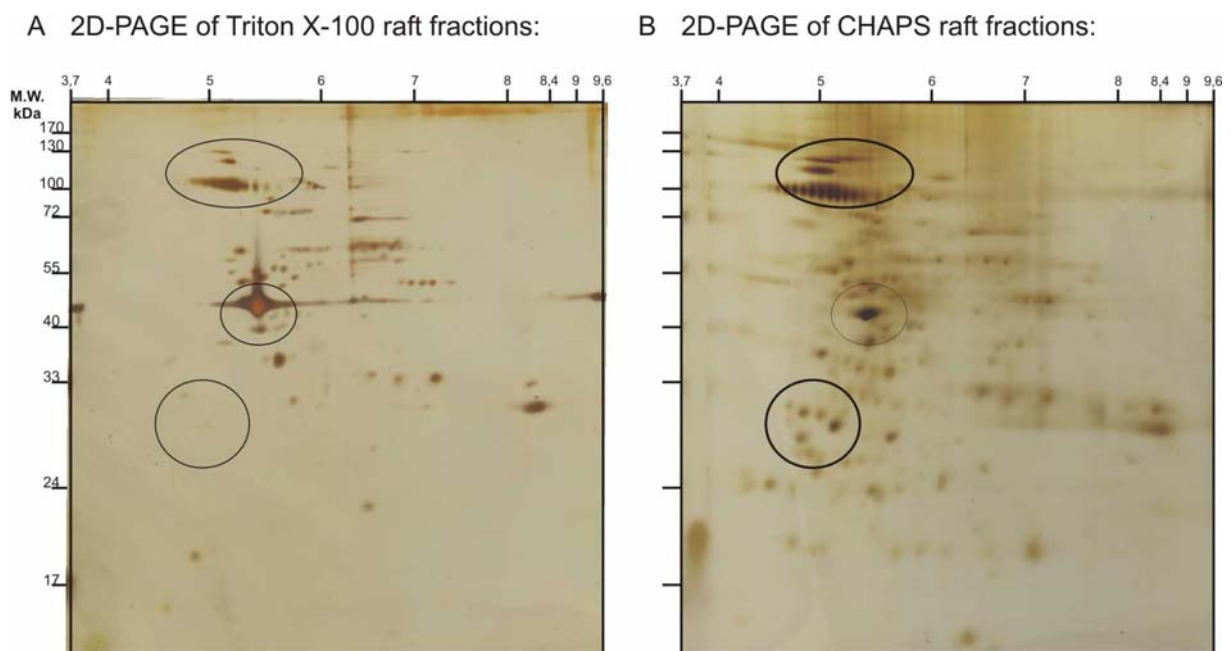
Figure 39: Analysis of TritonX-100 and CHAPS lipid rafts by 2D-PAGE. Lipid raft fractions were isolated and 2D-PAGE was performed as described in the Methods section. 2D-PAGE analysis revealed that CHAPS rafts contain much more different proteins than TritonX-100 rafts. Regions with the biggest differences are encircled.

As the value of the isolation of detergent-resistant membranes was strongly doubted recently (see introduction), we decided to return to the more stringent TX100 raft isolation procedure for a more detailed proteomic analysis of platelet lipid rafts. We therefore compared lipid raft fractions isolated either from resting platelets or from thrombin-activated platelets and looked for differences in the protein patterns. Figure 40 shows the silver-stained polyacrylamide gels. Regions with big differences in the spot pattern are encircled.

Figure 40: 2D-PAGE analysis of resting and activated platelets
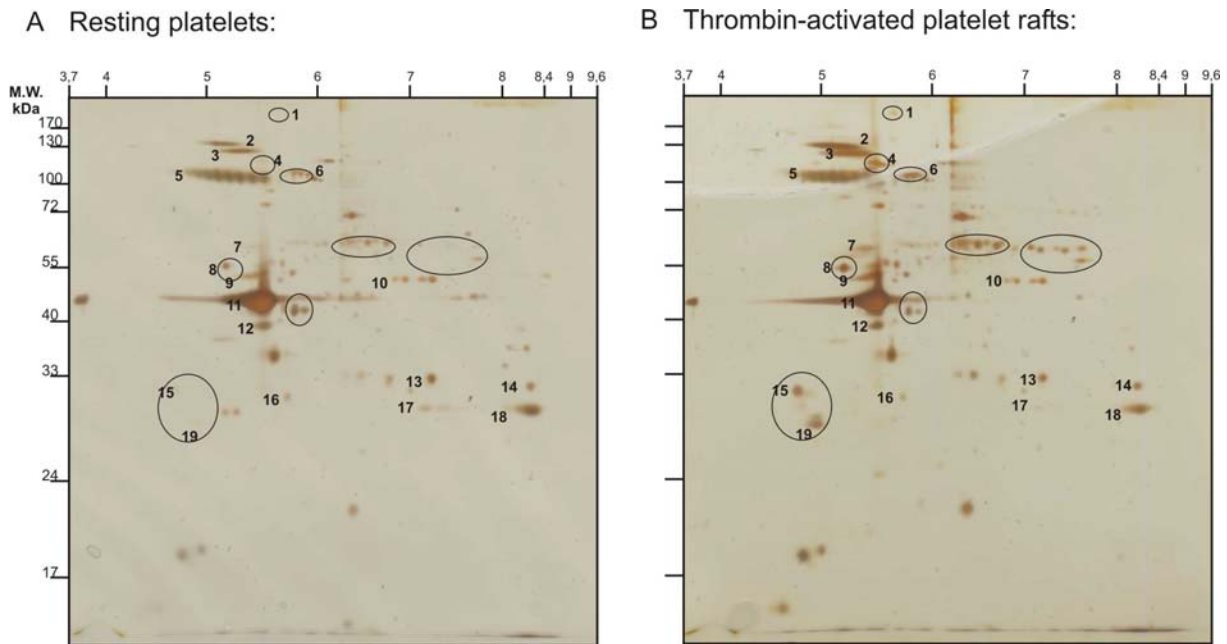
Figure 40: Comparison of TritonX-100 rafts from resting and activated platelets. Lipid raft fractions of resting and activated platelets were analysed by 2D-PAGE and silver staining for mass spectroscopy. Regions with big changes are encircled. Spot numbers refer to

Table 1 on the next page summarizes the results from this analysis. Due to the high costs of mass spectroscopic protein identification on a service basis, only a subset of spots was analysed by MALDI-TOF or MS^2-ESI. As expected, numerous cytoskeletal proteins were identified in the lipid raft fractions. These cytoskeletal proteins also account for the major differences between resting and activated platelets, which probably only reflects the changes in actin-associated proteins in response to platelet activation. Therefore, these changes probably do not represent activation-induced changes in lipid raft composition, which we were looking for. But in addition to these cytoskeletal proteins, we also identified several new platelet lipid raft proteins which could be involved in cellular signalling (InsP4 binding protein, zinedin, 14-3-3 subunits, Galpha i).

Additionally, there must without doubt be some connection between lipid rafts and the cytoskeleton, which is sensitive to CHAPS lysis but remains intact when TX100 is used. Due to the small proportion of signalling proteins, we did not procure this proteomic approach any further. Instead, we focused on the analysis of the stomatin protein by 2D-PAGE.

Table 1: **Platelet lipid raft proteins identified in this work:**

Spot #	Increase with activation	Protein (s)	Identification	remarks
1	yes	talin	MALDI	
2	yes	CD 61	MALDI	glycosylated
3	yes	CD 41	MALDI	glycosyl.
		gamma-Fibrinogen	MALDI	secreted upon activation
		InsP4 binding protein	MS/MS	GTPase activating
		alpha-actinin	MS/MS	actin bundling protein
4	yes	zinedin	MS/MS	
5	no	CD 36	MALDI, WB	glycosyl.
		filamin A	MS/MS	only fragment
6	yes	gelsolin	MS/MS	
		vimentin	MS/MS	intermediate filament
7	no	tubulin	MS/MS	
8	yes	ATP synthase beta subunit	MALDI	mitochondrial
9	no	flotillin-2	WB	
10	no	flotillin-1	WB	3 spots
11	decrease	beta-actin	WB	major spot
12	no	G alpha i	WB	
13	no	VDAC2	MS/MS	mitochondrial protein
14	no	VDAC1	MS/MS	mitochondrial protein
		tropomyosin 4	MS/MS	
15	yes	beta-tropomyosin	MS/MS	
16	no	CapZ beta	MS/MS	actin filament capping
17	no	stomatin	MALDI, WB	focuses poorly
18	no	VDAC3	MS/MS	mitochondrial protein
		14-3-3 zeta	MALDI, MS/MS	
		14-3-3 eta	MS/MS	
		14-3-3 tau	MS/MS	
		14-3-3 gamma	MS/MS	
19	yes	14-3-3 beta	MS/MS	

4.2.3   Stomatin phosphorylation in response to platelet activation?

To analyse if stomatin is modified in response to platelet activation, we analysed lipid raft fractions from resting or activated platelets by western blotting. As a positive control, we included the lyn tyrosine kinase, which is strongly phosphorylated upon platelet activation. Figure 41A shows the western blots for lyn in resting and activated lipid raft samples. A shift towards the more acidic end of the gradient is clearly visible.

Figure 41B shows a comparison of the spot pattern of stomatin in resting or activated platelets. In resting platelets, we observed 3 major spots for stomatin. The outer right spot is close to the theoretical pI (7.81) for stomatin. The two other spots are shifted to the more acidic region. The increments perfectly match the expected shift for two additional negative charges. These shifts could be explained by two phosphorylation events, but also de-amination of basic amino acids could account for it. In activated platelets, we clearly observed a shift of stomatin to the more acidic region of the gel. This clearly supports a possible phosphorylation of stomatin in response to platelet activation. The three spots in resting platelets could be explained by slight activation of the platelets during the isolation procedure, which is frequently observed.

Figure 41: Western blot analysis of 2D-PAGE gels
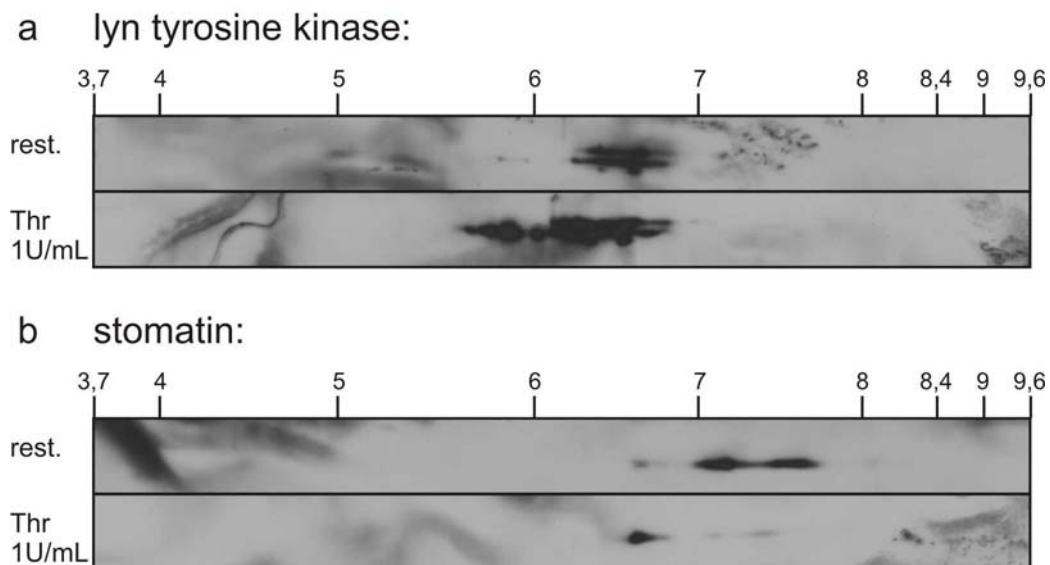
Figure 41: Lipid raft fractions of resting and thrombin-activated platelets were analysed by 2D-PAGE and western blotting with anti-lyn kinase and anti-stomatin antibodies. The lyn kinase shows a strong shift of the signal to the acidic region, which fits well to the described phosphorylation of the protein upon platelet activation. Stomatin also shows a shift to the acidic region.

4.2.4 Mass spectroscopic analysis of stomatin from platelet lipid rafts for post-translational modifications

Because we were unable to get properly focused stomatin spots in silver-stained 2D-gels (increasing the sample amount resulted in poor focusing and smears of stomatin instead of sharp, discrete spots), we went back to 1D-PAGE to prepare samples for mass spectroscopy. Lipid rafts of resting and activated platelets were prepared as described, the lipid raft fractions were analysed by 1D-PAGE and silver staining. The stomatin bands were excised, trypsin digested and analysed by LC-MS/MS. Neutral loss scanning was performed to identify peptides which could be phosphorylated. During this work, the described phosphorylation of stomatin on Ser-9 could be confirmed (Salzer et al., 1993), but no further phosphorylation sites could be detected. Instead, three peptides were identified, which show a neutral loss as observed for phosphopeptides, but the characteristic dehydroalanine residues which are observed after elimination of H_3PO_4 from the peptide were not found. The post-translational modification observed was characterized by addition of a molecular mass of ~96 to the peptide, which was lost in MS^2. The MS^2 and MS^3 spectrum of the unmodified and modified peptide were virtually identical. No PTM with these characteristics has been described up to now. Recently, O-sulfonation of serine and threonine has been described(Medzihradszky et al., 2004). This modification is characterized by the neutral loss of SO_3 and does not leave a "mark" on the backbone. But the mass difference to the unmodified peptide also should be +80 and not +96 as in our case. Therefore, we could not identify the nature of the PTM on the three stomatin peptides. It could either be a novel, yet uncharacterized modification, which of course would be very interesting. Additionally, either non-covalent, tightly bound H3PO4 or covalently bound persulfonate could explain the observed behaviour. The detailed MS data are given in Appendix 2. As these cryptic PTMs were observed in samples from resting and activated platelets, they do not account for the observed shift in the 2D-PAGE experiments. We aim at a collaboration with an expert in PTMs to resolve these issues. In addition to these LC-MS/MS data, we also got some hints on possible PTMs from MALDI-TOF data. Two peptides with a mass difference of +80 characteristic of phosphorylation were observed. One contained the well-known serine-9, whereas the other contained serine-231 as the only possible phosphorylation site. These data were the starting point for the generation of stomatin point mutants, which either inhibit phosphorylation (S231A) or mimick phosphorylation (S231E). Although the phosphorylation of stomatin at position 231 is still only hypothetic, these point mutations showed very interesting effects.

4.2.5 Point mutations at serine-231 show effects on stomatin trafficking

Because serine-231 was identified as a potential new phosphorylation site in a MALDI-TOF experiment, I constructed point mutations which either abolish a possible phosphorylation (S231A) or should mimick permanent phosphorylation (S231E). Independent of the putative phosphorylation, this region of stomatin seems to be very important for the function of the

protein because numerous point mutants at conserved positions have been described for the C. elegans homologues MEC-2 and UNC-1. Therefore, I decided to construct numerous different point mutants and started with serine-231. At first, both the S231A and S231E mutant seemed to show no difference to wild-type stomatin. A more detailed analysis revealed that the myc-tagged S231A mutant was reduced in the perinuclear region compared to wild-type stomatin and the S231E mutant. This was very obvious when we transiently transfected cells stably expressing SLP-1-GFP with these constructs. As seen in Figure 42, wild-type stomatin is detected on the PM and in late endosomes, where it colocalizes with SLP-1. The S231E mutant was barely detectable at the PM and colocalized perfectly with SLP-1-GFP, whereas the S231A mutant did not colocalize with SLP-1 at all, but remained exclusively at the PM. In cells stably expressing only the respective myc-tagged constructs, the situation was as follows: wt stomatin and S231E were practically indistinguishable, both showing PM and LE staining. The S231A mutant, however, only showed PM staining, which indicates a reduced rate of internalization of this point mutant. As a next step, I re-cloned these constructs into the pEGFP-N3 vector. With these GFP-tagged constructs, I created stably expressing cell lines. When I analysed the resulting stable clones by immunofluorescence, I got very surprising results. The S231A mutant showed ER localization in one of the stable clones, whereas it showed normal PM localization in others. The localization was correlated with the level of expression, the clone with the strongest expression showed the ER labeling.

Figure 42: Stomatin point mutations I
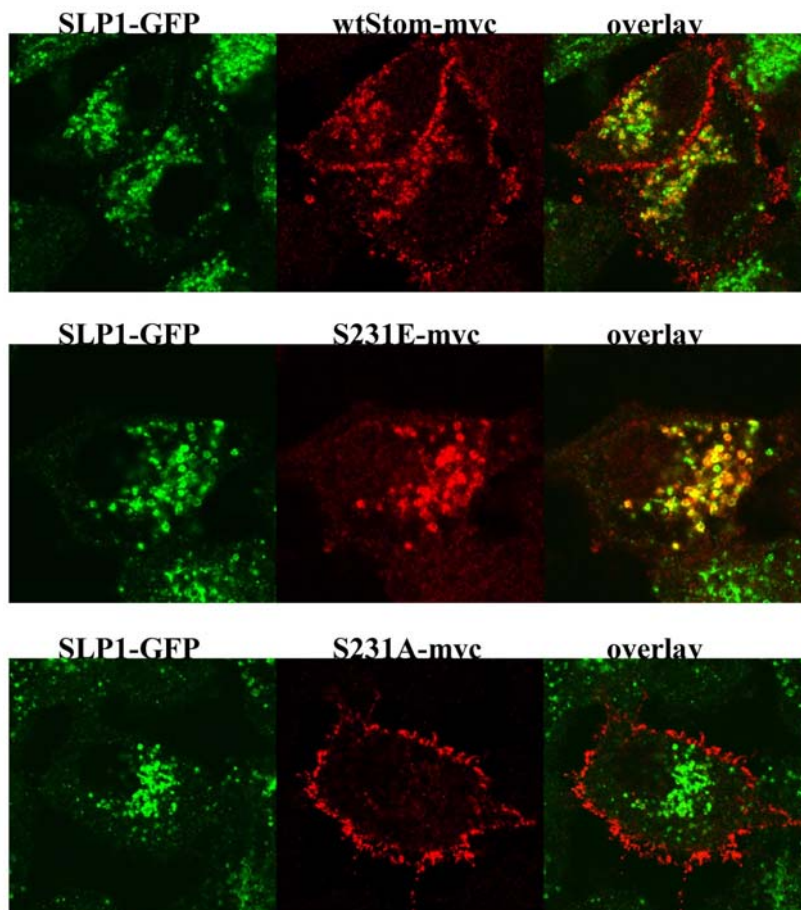
Figure 42: Point mutations at serine 231 strongly influence co-localization of stomatin with SLP-1. HeLa cells stably expressing SLP-1-GFP were transiently transfected with wt stomatin-myc (upper panel), with ST (S231E)-myc (middle panel) or with ST (S231A)-myc (lower panel). The wild-type stomatin construct partially co-localizes with SLP-1, the S231E mutant almost perfectly co-localizes with SLP-1 and shows practically no PM localization, whereas the S231A construct shows only PM localization and does not co-localize with SLP-1.

I then repeated transient transfections with the S231A-myc construct and also observed obvious ER staining in cells with a very high expression level of the construct. Therefore, we concluded that the targeting of the S231A construct to the PM can probably be rescued by the endogenous stomatin protein at moderate expression levels of the mutant. Consequently, we performed transient transfections in A431 cells, which only express minimal amounts of stomatin. We observed ER localization of the S231A-GFP construct in virtually all cells.

Figure 43: ER localization of S231A
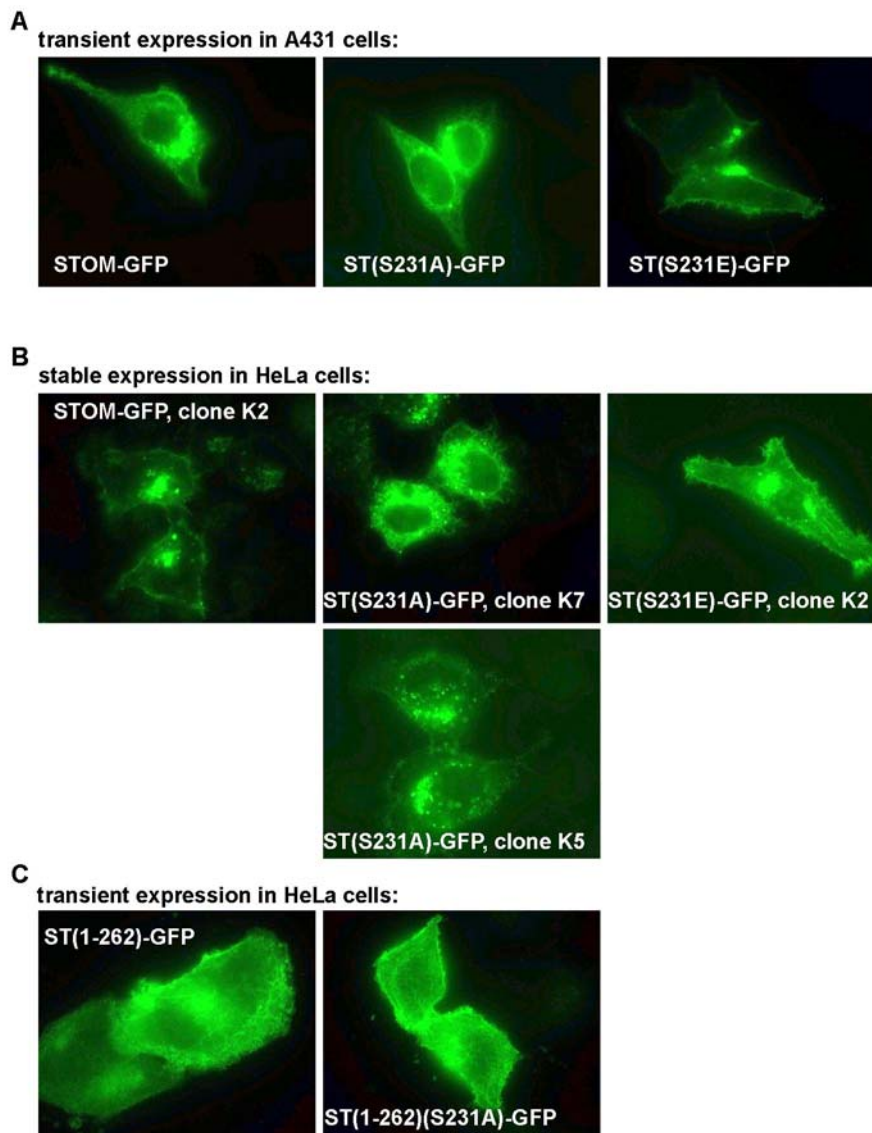
Figure 43: GFP-tagged wild type stomatin and point mutants at S231 were either transiently or stably expressed in A431 and HeLa cells and analysed by immunofluorescense. In A431 cells, which express no endogenous stomatin, the S231A mutant accumulates in the ER. In HeLa cells, the subcellular localization depends on the expression level of the mutant. At high expression, we observe ER localization, whereas we observe perinuclear and weak PM staining at lower expression levels. The C-terminally truncated point mutant ST (1-262)(S231A), which should be unable to oligomerize (Snyers et al., 1998), does not show ER localization even at high expression levels.

Figure 43 shows the described results from stable and transient transfections of the GFP-tagged constructs in HeLa and A431 cells. Additionally, I also combined the S231A point mutation with a truncation after amino acid 262. This construct, ST (1-262)(S231A)-GFP, differed from the full length construct, because it was transported to the PM without any problem. No ER localisation was observed in contrast to the full-length ST (S231A)-GFP construct. The truncation after amino acid 262 abolishes the formation of high-order stomatin oligomers and lipid raft association of stomatin (Umlauf et al., 2006). In my opinion, the formation of oligomers between mutant stomatin (S231A) and endogenous wild-type stomatin is responsible for the observed, apparently contradictory results. If enough endogenous stomatin is present, the mixed oligomers of mutant and wt stomatin can be transported to the plasma membrane. If the mutant form dominates, the oligomers are not transport-competent and accumulate in the ER. Additionally, the mutant form seems to inhibit the endocytosis of stomatin oligomers. A truncated, monomeric variant is transported to the PM without any problems. This truncation probably is not functional and is transported with the bulk of other membrane proteins, whereas the transport of stomatin oligomers seems to be regulated. The question if oligomers already form in the ER will be addressed with the stable clone which shows ER localisation.

The S231E mutant also showed some special characteristics when tagged with GFP. In many cells, we observed filamentous structures of S231E-GFP, often several μm in length. These structures are aligned along actin filaments as shown by costaining with fluorescent phalloidin (Figure 44), whereas they did not colocalize with tubulin.

These filamentous structures could represent linear arrays of vesicles, which are transported along actin filaments. The questions, which remain are: Are these vesicles transported to the cell periphery/PM or are they internalized? Are these filaments a mere consequence of the strong overexpression of the GFP-tagged construct or do they represent functional transport intermediates? Live cell imaging and FRAP analysis can perhaps help to clarify these questions in the future.

4.2.6 A non-oligomeric, not raft associated stomatin truncation mutant shows enhanced plasma membrane motility in a FRAP assay

With the possibility to do live cell imaging with the newly acquired Zeiss LSM Meta confocal microscope, we decided to analyse the motility of full-length stomatin-GFP and compare it to the truncation mutant ST (1-262)-GFP. Both GFP fusions were cloned by Ellen Umlauf. FRAP was performed with transiently transfected HeLa cells as described. The results are depicted in Figure 45.

Figure 44: Tubular structures of S231E
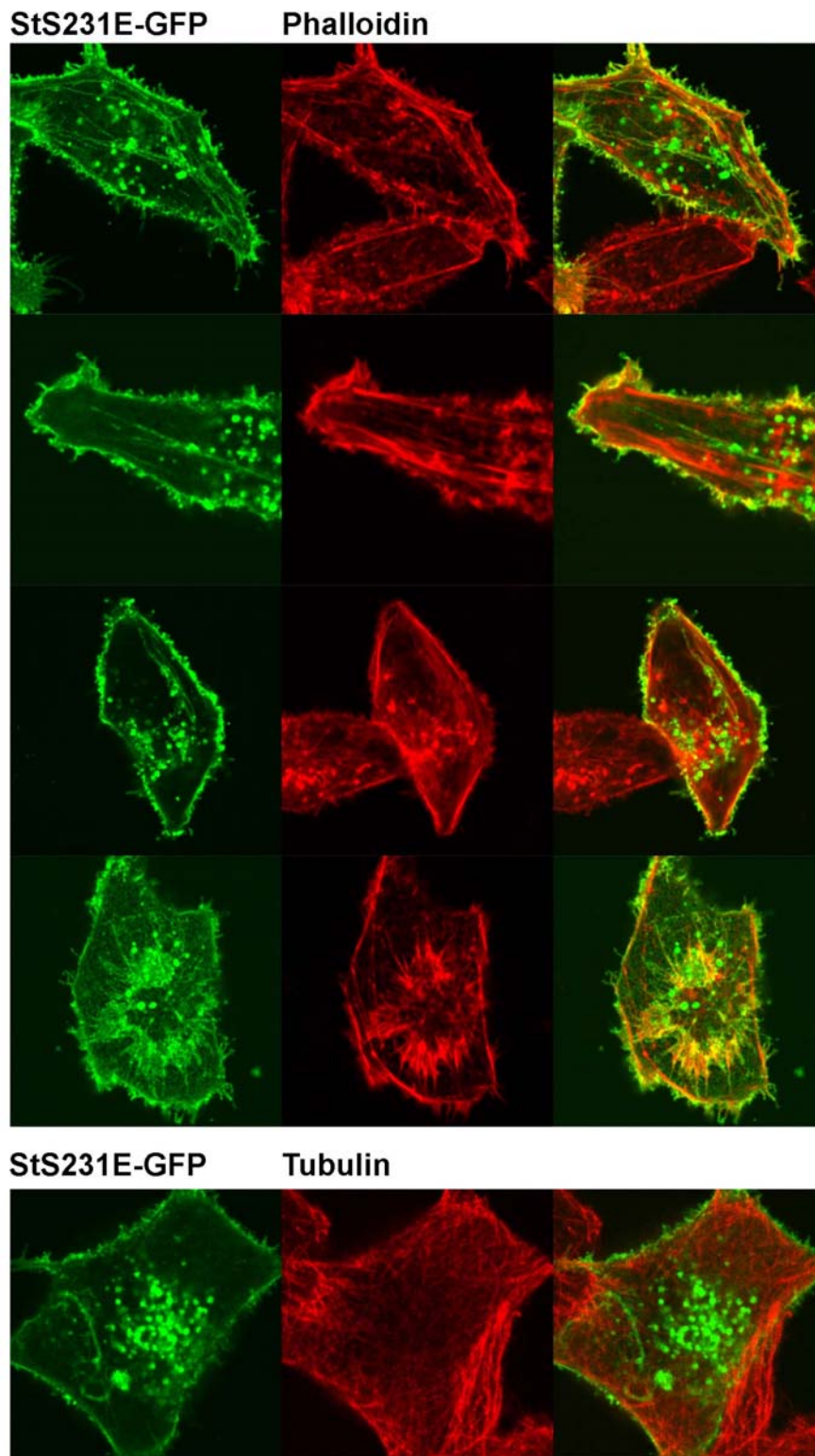
Figure 44: Transient transfections of HeLa cells with St (S231E)-GFP show filamentous, GFP-positive structures. HeLa cells were transiently transfected with St (S231E)-GFP and were co-stained with AlexaFluor596-conjugated phalloidin to stain actin filaments or with an anti-tubulin antibody.

Figure 45: FRAP analysis of stomatin mobility
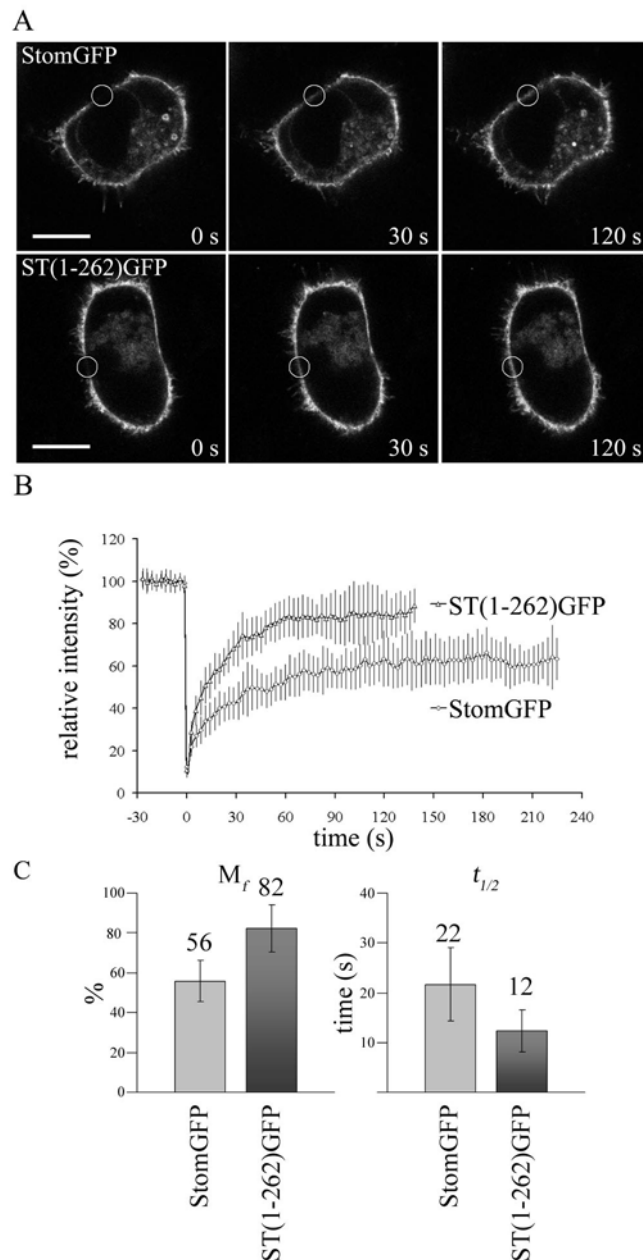
Figure 45: HeLa cells transiently expressing full-length StomGFP and the truncation mutant ST (1-262)GFP, respectively, were subjected to FRAP analysis. (A) Qualitative FRAP. A ROI of 3.4 µm diameter was bleached and the recovery of StomGFP or ST (1-262)GFP in the plasma membrane after 30 and 120 s is shown. Bars = 10 µm. (B) Quantitative FRAP. The recovery curves show the mean intensity ± SD from 7 cells, each. (C) Comparison of the mobile fractions M_f and the recovery halftimes $t_{1/2}$ for StomGFP and ST (1-262)GFP calculated from the recovery data as described in Materials and Methods. Mean values for M_f and $t_{1/2}$ (n=7, respectively), error bars represent +/- one standard deviation. The paired Student's *t* test was used to assess the statistical significance of the differences between the results for StomGFP and ST (1-262)GFP.

Wild-type stomatin diffuses relatively slow, and a large fraction is immobilised, probably through an interaction with the cytoskeleton. The truncation mutant ST (1-262)-GFP shows faster diffusion as revealed by the reduced recovery half-time $t_{1/2}$, and the mobile fraction is

also significantly higher. Because ST (1-262)-GFP is non-oligomeric and not raft associated, we cannot determine precisely if raft association or oligomerization is responsible for the slow diffusion velocity and high immobile fraction. During her PhD thesis, Ellen Umlauf constructed several point mutations, which have different effects on oligomerization and raft association. Some of these mutants were already cloned as GFP fusion proteins, but the expression and localization of the fusion proteins had not be verified yet. I analysed several of these mutants by transient transfection into HeLa cells. The results are shown in Figure 46.

Figure 46: Further candidates for FRAP analysis
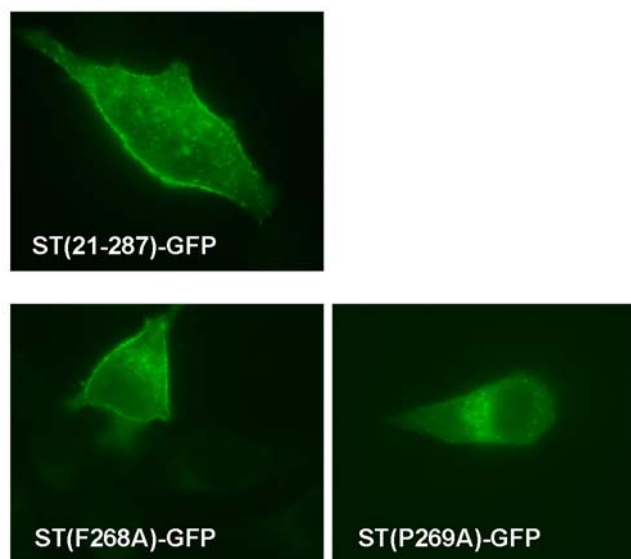
Figure 46: Three mutated GFP-tagged constructs, which had been constructed by E. Umlauf, were tested for proper expression and PM localization to find out if they are feasible for FRAP analysis. All 3 constructs work and show PM localization, although the PM staining is weak in the P269A construct.

All three tested constructs showed PM and LE localization and can therefore be used for FRAP analysis in the future. The PM signal for the P269A mutant, however, was rather low and LE localization dominated. The F268A and P269A point mutations could be very interesting, because F268A is monomeric and not raft-associated, whereas P269A is also monomeric, but localized to lipid rafts (Umlauf et al., 2006).

If these constructs showed differences in respect to diffusion speed and immobile fraction (compared to each other and wt stomatin), one should be able to separate the contributions of oligomerization and lipid raft association to the diffusional behaviour of stomatin-GFP. Another issue for future FRAP experiments would be the comparison of the lateral mobility of stomatin at the PM and in the ER (S231A-GFP construct).

Figure 47: Alignment of the human stomatin family, MEC-2 and UNC-1

```
STOMATIN   25  ----GLGPCGWIIVAESFLFTVITFPISIWMCIKIIKEYERAIIFRLGRILQGGAKGPGL
SLP-3      24  ----RLGVCGWIIFSLSFLLVIITFPISIWMCLKIIKEYERAVVFRLGRIQADKAKGPGL
PODOCIN    93  TKSSGLGACEWLIVLISLLFIIMTFPFSIWFCVKVVQEYERVIIFRLGHLLPGRAKGPGL
SLP-1      50  ---WPSCLCHGLISFLGFLLLLVTFPISGWFALKIVPTYERMIVFRLGRIRTP--QGPGM
SLP-2      22  ---------------GRAPRRASSGLPRNTVVLFVPQQEAWVVERMG--RFHRILEPGL

MEC-2     115  ------GVCGWIITILSYLLIFFTLPISACMCIKVVQEYERAVIFRLGRLMPGGAKGPGI
UNC-1      29  -------IFGYAIQALSWILIIVTFPFSMCVCLKVIKEYERVVIFRIGRLVFGGARGPGM


STOMATIN   81  RFILPCIDSFIKVD-MRTISEDIPPQEILTKDSVTISVDGVVYYRVQNATLAVANITNAD
SLP-3      80  ILVLPCIDVFVKVD-LRTVTCNIPPQEILTRDSVTTQVDGVVYYRIYSAVSAVANVNDVH
PODOCIN   153  RFFLPCLDTYHKVD-LRLQILEIPFHEIVTKDMFIMEIDAICYYRMENASLLLSSLAHVS
SLP-1     106  VLLLPFIDSFQRVD-LRTRAFNVPECKLASKDGAVLSVGADVQFRIWDPVLSVMTVKDLN
SLP-2      65  NILIEVLDRIRYVQSLKEIVINVPEQSAVTLDMVTLQIDGVLYLRIMDPYKASYGVEDPE

MEC-2     169  RFIVPCIDTYRKVD-LRVLSFEVPPQEILSKDSVTVAVDAVVYFRISNATISVTNVEDAA
UNC-1      83  IFIIPCIDTYRKID-LRVVSYAVPPQEILSKDSVTVSVDAVVYFRTSDPIASVNNVDDAI


STOMATIN  140  SATRLLAQTTLRNVLGTKNLSQILSDREEIAHNMQSTLDDATDANGIKVERVEIKDVKLP
SLP-3     139  QATFLLAQTTLRNVLGTQTLSQILAGREEIAHSIQTLLDDATELWGIRVARVEIKDVRIP
PODOCIN   212  KAVQFLVQTTMKRLLAHRSLTEILLERKSIAQDAKVALDSVTCIWGIKVERIEIKDVRLP
SLP-1     165  TATRMTAQNAMTKALLKRPLREIQMEKLKISDQLLLEINDVTRAWGLEVDRVELAVEAVL
SLP-2     125  YAVTQLAQTTMRSELGKLSLDKVFRERESLNASIVDAINQAADCWGIRCLRYEIKDIHVP

MEC-2     228  RSTKLLAQTTLRNILGTKTIAEMLSDREAISHQMQTTLDEATEPWGVKVERVEVKDVRLP
UNC-1     142  YSTKLLAQTTLRNALGMKTLTEMLTEREAIAQLCETILDEGTEHWGVKVERVEVKDIRLP


STOMATIN  200  VQLQRAMAAEAEASREARAKVIAAEGEMN-------ASRALKEASMVITESPAALQLRYL
SLP-3     199  VQLQRSMAAEAEATREARAKVLAAEGEMN-------ASKSLKSASMVLAESPIALQLRYL
PODOCIN   272  AGLQHSLAVEAEAQRQAKVRMIAAEAEKA-------ASESLRMAAEILSGTPAAVQLRYL
SLP-1     225  QPPQDSPAGPNLDSTLQQLAIHFLGGSMNSMAGGAPSPGPADTVEMVSEVEPPAPQVGAR
SLP-2     185  PRVKESMQMQVEAERRKRATVIESEGTRESAIN---VAEGKKQAQILASEAEKAEQINQA

MEC-2     288  VQLQRAMAAEAEAAREARAKVIVAEGEQK-------ASRALKEAAEVIAESPSALQLRYL
UNC-1     202  QQLTRAMAAEAEAAREARAKVVAAEGEQK-------ASRALKEAADVIQANPVALQLRHL


STOMATIN  253  Q-----TLTTIAAEKNSTIVFPLPIDMLQGIIGA----KHSHLG----------------
SLP-3     252  Q-----TLSTVATEKNSTIVFPLPMNILEGIGGV----SYDNHKKLPNKA----------
PODOCIN   325  H-----TLQSISTEKPSTVVLPLFFDLLNCLSSP----SNRTQGSLPFPSPSKPVEPLNP
SLP-1     285  S-----SPKQPLAEGLLIALQEFLSEALVSQVGA----CYQFNVVLPSGTQSAYFLDLTT
SLP-2     242  AGEASAVLAKAKAKAEAIRILAAALTQHNGDAAASLTVAEQYVSAFSKLAKDSNTILLPS

MEC-2     341  Q-----TLNSISAEKNSTIIFPFPIDLLSAFLQR----TPPKVEEPPSLPKKIRSCCLYK
UNC-1     255  Q-----ALNSIAAEHNSTIVFPVPVEMFGAFMKK----DQ--------------------
```

Figure 47: Multiple sequence alignment of human stomatin family proteins and of *C. elegans* MEC-2 and UNC-1 proteins. The alignment was computed with the ClustalW programme (http://www.ebi.ac.uk/clustalw/). Identical and similar amino acids were coloured with boxshade (http://www.ch.embnet.org/software/BOX_form.html). Point mutations identified in functional screens in C. elegans or in steroid resistant nephrotic syndrome patients or created in-vitro through site-directed mutagenesis are coloured in red. Details about the point mutations are given in Table 2.

Table 2: **Point mutations in the SFPH domain of stomatin family proteins**

Table 1: Point mutations in the PHB domain of stomatin family proteins:

	mutation	commentary	origin	reference
STOMATIN	W184→A	defective oligomerization	in vitro mutation, overexpression	Ellen Umlauf (E.U), unpublished data
	P199→G			
	E209→K	defective PM targeting		Mario Mairhofer, unpublished data
	E211→K			
	S230→A	defective targeting → ER		
	Y251→A	defective oligomerization		E. U., unpublished
	T265→A			
	I266→A	defective oligomerization and lipid raft association		Umlauf et al., 2006
	V267→A			
	F268→A			
	P269→A	defective oligomerization		
	L270→A			
PODOCIN	P118→L	defective targeting → ER	steroid-resistant nephrotic syndrome	Roselli et. al., 2004
	R138→Q			
	D160→G			
	R168→H			
	V180→M			
	R238→S			
	R291→W	defective targeting → LEs		
MEC-2	P134→S	abolishes cholesterol binding	C. elegans mec-allele u274	Huber et. al., 2006
	R184→C	touch sensitivity ---	mec-allele u64	Zhang et al., 2004
	V190→M	touch sensitivity --	mec-allele u224	
	S200→F	touch sensitivity -	mec-allele u306	
	A204→T		mec-alleles e75 + u284	Gu et al., 1996
	A207→T	touch sensitivity ---	mec-allele u28	Zhang et al., 2004
	A234→V	touch sensitivity --	mec-allele u227	Huang et al., 1995
	R239→H		mec-allele e1608	
	G243→E		mec-allele u7	
	T246→I		mec-allele u750	
	A296→V	touch sensitivity ---	mec-allele u144	Zhang et al., 2004
	E297→K		mec-allele u318	
	E299→K	touch sensitivity -	mec-allele e1514	Huang et al., 1995
	A304→T		mec-allele u243	Zhang et al., 2004
	A306→T		mec-allele u24	
	E314→K		mec-allele u217	
	A320→V		mec-allele u311	
	A325→T		mec-allele u43	
	P357→L	touch sensitivity ---	mec-allele u130	
	P357→S	touch sensitivity ---	mec-allele u132	
UNC-1	E60→K	loss of function	C. elegans unc-allele n774	Rajaram et al., 1998
	A121→T		unc-allele e114	
	T183→R	dominant negative allele	unc-allele n494	Park & Horvitz, 1986 Rajaram et al., 1998
	G187→E		unc-allele e580	Rajaram et al., 1998
	K189→R+ A212→V	intragenic revertant of the dominant e1598 allele	unc-allele e1598n1201	Park & Horvitz, 1986 Rajaram et al., 1998
	R252→C	cold-sensitive alleles	unc-alleles hs1+hs4	Rajaram et al., 1998 Hecht et al., 1996
	L257→I		unc-allele hs5	
	T267→I		unc-allele hs2	
	P273→S		unc-allele hs3	

Abbreviations: ER...endoplasmatic reticulum; PM...plasma membrane

4.2.7 Further point mutations introduced into stomatin

As outlined in Figure 47 and

Table 2, a great number of point mutations in the PHB domain of stomatin are known, either from unc- and mec-alleles in C. elegans or from patients with steroid-resistant nephrotic syndrome, which is caused by alterations in the podocin protein. The majority of these point mutations affect amino acids conserved from the C. elegans protein to human stomatin or from podocin to stomatin. Based on these findings, I began to construct several novel point mutations in the human stomatin sequence, with the hope that these mutants would cause a defect either in stomatin localization or function. The aim was to create a dominant-negative mutant, which would show a distinct phenotype when introduced to cultured cells. This aim proved difficult, because the precise function of the protein is still not clear and the point mutations did not directly affect the vitality or appearance of the cells. Nevertheless, I think that this approach can yield valuable results in the future. I identified two mutations (E210K and E212K) which apparently affect the subcellular trafficking of stomatin and cause an accumulation in intracellular compartments (Figure 48).

Figure 48: Stomatin point mutants II

ST(E210K)-GFP   ST(E212K)-GFP

ST(S214A)-GFP   ST(S214,231A)-GFP

ST(S214E)-GFP   ST(S214,231E)-GFP
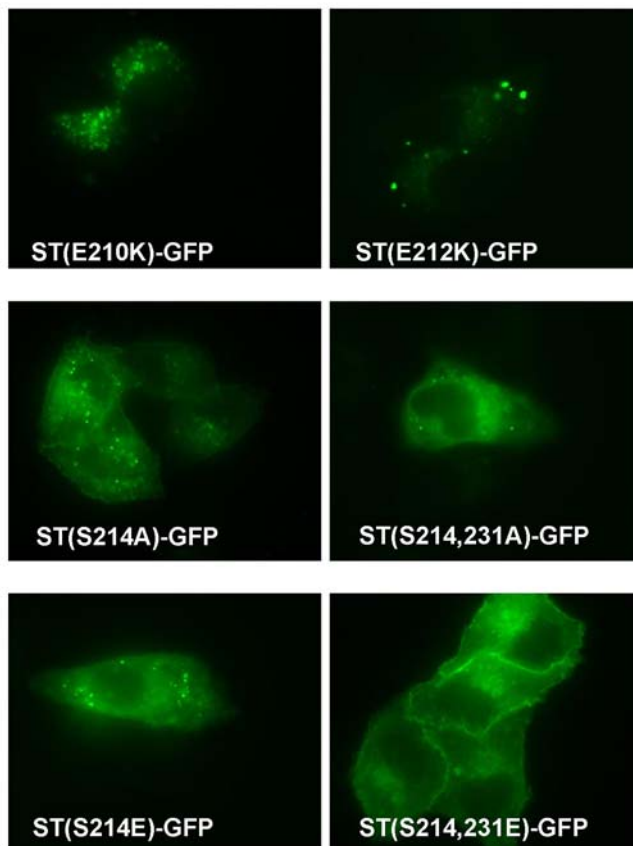
Figure 48: Point mutations in stomatin, which correspond to mutations found in the *mec-2* gene, show effects on the subcellular targeting of stomatin. The region around amino acid 212, which is well conserved between MEC-2 and stomatin and seems to be important for MEC-2 function, was targeted by site-directed mutagenesis in the human stomatin protein. Double serine mutants (S214, S231) were also cloned. Pictures represent the results from transient transfections into HeLa cells. St (E210K) and St (E212K) show no PM labeling.

Recently, a point mutation in MEC-2, which abolishes cholesterol binding, was

described(Huber et al., 2006). As already mentionned in the introduction, results from Ellen Umlauf (in collaboration with Dr. Christoph Thiele, MPL Dresden) confirmed that stomatin also binds a photo-activatable cholesterol derivative efficiently. This point mutation would be the next target if I were able to continue with this strategy. For the analysis of functional consequences of the point mutations, it would be important to seek collaborations with groups which are able to analyse the activity of cation channels by patch-clamp analysis or the activity of the GLUT-1 glucose transporter, as a function for stomatin in the regulation of cation channels and glucose transport seems very likely in the light of recent results (Price et al., 2004; Zhang et al., 2001; Huber et al., 2006).

5 DISCUSSION

5.1 SLP-1 function

As already outlined in the introduction, the SLP-1 protein had been identified and cloned several years ago by our group based on its similarity to the stomatin protein (Seidel and Prohaska, 1998). After compiling its complete sequence (and although there had been a mistake in sequencing, which led to a wrong stretch of ~35 amino acids), it was quickly realized that SLP-1 is the human orthologue of the *C. elegans* UNC-24 protein, sharing the unique, bipartite structure with a SPFH-domain and a SCP-2/nsLTP domain. When the *unc-24* locus had been sequenced by Barnes et al. in 1996(Barnes et al., 1996), they already postulated a function for UNC-24 in lipid transport, but further evidence for this function had not been presented yet. Meanwhile, several members of the SPFH protein family had been implicated in the formation/stabilization/organization of cholesterol- and sphingolipid-enriched membrane domains, so-called "lipid rafts"(Bickel et al., 1997; Lang et al., 1998; Mairhofer et al., 2002; Salzer and Prohaska, 2001). Interesting new findings from *C. elegans* (Sedensky et al., 2004; Sedensky et al., 2001) led us to the conclusion that the human SLP-1 protein could also function in a complex with stomatin analogous to the UNC-1/UNC-24 complex in the worm and that a detailed characterization of the human SLP-1 could also help to shed light on the function of stomatin. We therefore attempted a first cell biological characterization of the human SLP-1 protein. Based on the *C. elegans* data, we expected SLP-1 to be localized to the PM and were really surprised to find this protein to be exclusively localized to perinuclear organelles (Figure 9). Different constructs with C-terminal tags (GFP, myc, HA) all yielded identical results and showed this late endosomal localization, in transient as well as stable expression. Also, variation of the expression level did not show an effect on the subcellular distribution of SLP-1, therefore we can out-rule that the LE localization is an artefact caused by the over-expression of the protein. To identify the essential regions for this targeting, we started with the construction of an array of truncation mutants. Quickly, we realized that the C-terminal SCP-2/nsLTP domain is not required for the transport to LEs (truncation mutant SLP-1(1-288) was indistinguishable from the wild type protein in respect to subcellular localization), whereas deletion of the linker region between the SPFH domain and the SCP-2/nsLTP-domain (a sequence with no detectable homology to any other human protein, and also only poorly conserved between C. elegans and human) clearly showed an effect (SLP-1(1-224), see Figure 16). This truncation most probably gets mis-localized to early endosomes and cytoplasmic lipid aggregates (some co-localization with Rab4a, co-localization with cav3DGV and NileRed staining of the cytoplasmic aggregates, see Figure 17).

The late endosomes play a crucial role in subcellular cholesterol trafficking, but the precise

mechanisms, which are responsible for the release of LDL-derived cholesterol and subsequent transport to the plasma membrane are very incompletely understood. Some "key players" have been identified (NPC-1 and 2), but the whole picture is incomplete. Because cholesterol homeostasis is very important for cell survival, one also has to be aware that several different mechanisms of cholesterol transport from/to late endosomes might co-exist and be partially redundant. Based on the enrichment of SLP-1 in cholesterol-rich lipid rafts and on its localization to late endosomes, we hypothesized that it could also take part in cholesterol efflux from LEs to the PM. For another late endosomal cholesterol-binding protein named MLN64, which is also an integral membrane protein with a C-terminal cholesterol binding domain, it was recently shown that over-expression of the protein released the block of cholesterol efflux from LEs in Niemann-Pick fibroblasts as well as in U18666A-treated cells (Alpy et al., 2001). The synthetic amino-steroid U18666A causes cholesterol accumulation in LEs similar to the phenotype observed in Niemann-Pick fibroblasts (Kobayashi et al., 1999; Liscum and Faust, 1989). Because we did not have NPC fibroblasts, we decided to explore the potential effect of SLP-1 on cholesterol efflux from LEs in cells treated with U18666A. We soon realized that SLP-1 does not seem to mediate cholesterol efflux from LEs because we could not reduce the accumulation of cholesterol by (transient or stable) over-expression of SLP-1. Instead, we observed that over-expression of SLP-1 rather induces the formation of enlarged, cholesterol-rich LEs (Figure 33), but only when normal cholesterol efflux from LEs was blocked. The observed structures were clearly bigger than in control HeLa cells, and the cells expressing SLP-1 contained numerous of these enlarged organelles. The SCP-2/nsLTP domain of SLP-1 was required to trigger this effect, because deletion of this domain abolished the formation of the enlarged vesicles. So, insted of having a function in cholesterol efflux from LEs (as was our initial hypothesis), SLP-1 could rather mediate cholesterol accumulation. When we tried to characterize these cholesterol-rich, enlarged structures in more detail, we observed that they were only weakly stained with the LE marker LAMP-2, although it was described that U18666A triggers cholesterol accumulation in LAMP-1 and LAMP-2-positive vesicles (Umeda et al., 2003; Watari et al., 2000). In cells expressing the truncation mutant SLP-1(1-288)-GFP, we observed the expected accumulation of cholesterol in LAMP-2 positive vesicles. SLP-1 is broadly distributed throughout the late endosomal compartment, partially co-localizing with different markers. If cholesterol efflux from late endosomes is blocked, cholesterol accumulation is enhanced in LE vesicles which carry full-length SLP-1 compared to untransfected cells and cells carrying C-terminal truncation mutants. These enlarged structures only contain low amounts of LAMP-2, which indicates that a shift of the cholesterol accumulation away from strongly LAMP-2 positive vesicles takes place. The SCP-2 domain is essential for this redistribution. As already mentioned above, this effect of SLP-1 on cholesterol distribution was only observed under conditions where the efflux of cholesterol from LEs was blocked. Nevertheless, we think that SLP-1 could have a function in cholesterol transport in unperturbed cells as well.

Because of its unique, bipartite structure, SLP-1 is a candidate for a role in lipid transport. Recently, stomatin was found to localize to lipid droplets under certain conditions, especially

when the protein was overexpressed or when newly synthesized proteins were accumulated in the ER by treatment with brefeldin A(Umlauf et al., 2004). We hypothesized that SLP-1 could also be targeted to LDs and probably act in lipid transfer to/from these organelles. Surprisingly, over-expressed SLP-1 was strictly excluded from the LDs (see Figure 18 and Figure 19). Only the C-terminal truncation mutant SLP-1(1-224)-GFP could be detected on LDs. This finding confirms that SLP-1 is anchored to the cytoplasmic leaflet of the membrane via its long hydrophobic domain at the N-terminus (and probably a lipid anchor like palmitate). Nevertheless, it also raises the question why this certain truncation can be translocated to LDs. The biogenesis of LDs is still a matter of controversy. Several different theories exist, the most popular being the idea that LDs form in the cytoplasmic leaflet of the ER as lipids and certain proteins accumulate in bulges and finally pinch off , forming an organelle surrounded only by a lipid monolayer. ELMI analysis has revealed that also "mature" LDs still are in tight contact with the ER. When we first observed the tubular structures positive for SLP-1(1-224) in the cells, we immediately thought that these might represent ER tubules and that the truncation gets somehow stuck in biosynthetic transport. But we never observed co-localization of SLP-1(1-224) with ER markers (neither with ER-YFP nor with calnexin). We also compared the localization of SLP-1(1-224) with Cav3DGV, a mutated caveolin construct, which localizes to LDs and induces imbalances in intracellular lipid transport. In double transfections, we observed almost perfect co-localization of SLP-1(1-224) and Cav3DGV, in cells fed with/without oleic acid (without oleic acid: Figure 18, lowest panel, Figure 19 with oleic acid). The only difference was that Cav3DGV often was clearly detected on the ER around the nucleus, whereas this localization was not observed for SLP-1(1-224). In our opinion, this data suggests that SLP-1(1-224) is not transported to the LD surface via the ER, but probably via a different organelle system. ELMI analysis of cells stably expressing SLP-1(1-224)-GFP revealed numerous interesting ultrastructures in these cells. Of special interest are the structures in the Epon-embedded samples. There, we could luckily depict intermediates in the formation/degradation of LDs (see Figure 21). These structures look like hybrid organelles between lysosomes and LDs and could represent either LDs which were engulfed by lysosomes or LDs budding from electron-dense multi-vesicular organelles (the latter would be my favourite option, but the first option would be interesting as well). We also observed later/earlier stages, where the LD is only surrounded by a distinct bilayer. Comparison of light and electron microscopy results strongly indicates that the LD aggregates observed in ELMI are positive for SLP-1(1-224). The definitive proof is still missing, because our attempts to perform immunodetection on the Epon-embedded cells (preembedding immunolabeling or removal of OsO_4 prior to immunolabeling) were not successful. For me, it is clear that SLP-1(1-224) is on the surface of the characteristic LD aggregates. For the "intermediates", the evidence is not so compelling. But a point is that these structures were only observed in the cells expressing SLP-1(1-224) and not in cells expressing full-length SLP-1 (data not shown). This indicates that these structures could be induced by the overexpression of this construct. As already mentioned, overexpression of Cav3DGV disturbes intracellular cholesterol homeostasis(Pol et al., 2001). The SLP-1(1-224)

construct could have a similar effect. Therefore, it could be interesting to follow the subcellular transport of (radio- or fluorescence-)labelled lipids in control cells and in cells expressing SLP-1(1-224). Because the vesicular aggregates induced by SLP-1(1-224) are likely to be somehow related to LDs (ELMI results and results after induction of LDs with oleic acid), we think that there is a good chance that this truncation will affect lipid trafficking.

A more detailed analysis of the tubular structures and the vesicle organelles will be necessary to pin down such an effect. And, of course, cooperation with Marianne Fliesser on ELMI of cells expressing these constructs should be continued to improve our understanding of these interesting ultrastructures.

5.2 Subcellular targeting of SLP-1

During my PhD thesis, I could show that the overexpressed SLP-1 protein is exclusively localized to late endosomes in different cell types (see Figure 9 and Figure 10). This LE localization was found in transient and stable transfection experiments, at variable expression levels and with different tags (GFP, myc-tag, HA-tag). The next step was to investigate which regions of SLP-1 are responsible for this LE targeting. For stomatin, which is localized to the PM and to LEs, a specific LE targeting signal might exist, but is not absolutely necessary. The LE localization could also be the consequence of bulk membrane endocytosis. For LE localization without PM localization, as is the case for SLP-1, it is necessary that a trafficking signal is present, which specifically directs transport to LEs and not to the PM via the constitutive biosynthetic/secretory pathway. Analysis of the protein sequence of SLP-1 revealed a tyrosine-based GYXXϕ motif at the N-terminus of SLP-1. Similar motifs at the cytoplasmic C-terminus of LAMP proteins are necessary for the targeting of the LAMPs to LEs/lysosomes (Gough et al., 1999; Guarnieri et al., 1993). We constructed several truncations at the N-terminus and found out that N-terminal deletions cause that SLP-1 is transported to the PM (Figure 25). Similar to stomatin, a combined localization to perinuclear vesicles and the PM was observed in deletions of amino acids 1-50 and 1-10. Therefore, we could conclude that the first 10 amino acids are required for correct LE targeting (amino acid sequence MLGRSGYRAL). In the next step, we introduced point mutations into the GYXXϕ-motif and replaced tyrosine 7 with an alanine (Y7A construct) and the hydrophobic amino acid at position +2, leucine-10, with a more polar serine (L10S construct). Both point mutations caused transport of the protein to the PM (see Figure 25) and therefore confirmed the functionality of the GYRAL motif at the N-terminus of SLP-1. In a different experiment, we exchanged the N-terminus of stomatin for amino acids 1-50 of SLP-1. The resultant chimeric protein showed exclusive localization to perinuclear organelles and colocalized with LysoTrackerRed (see Figure 31). When the point mutations (Y7A and L10S) were present in the SLP-1 N-terminus, the localization changed to PM and LEs and was practically indistinguishable from wt stomatin or from the original ST (21-287)-GFP construct. In the

SLP-1 protein, however, other sequences also seem to be necessary for proper subcellular targeting. As already outlined, the region between amino acid 224 and 288 also is necessary for correct LE targeting. Combinations of N- and C-terminal truncations revealed that N-terminal truncations always induced PM localization of the construct, independent of the C-terminal truncations. This suggests that the GYRAL motif at the N-terminus of SLP-1 is necessary, but not sufficient for LE targeting (because SLP-1(1-224) truncations are also mislocalized), although it was shown to be sufficient in a SLP-1/stomatin chimeric protein. Finally, I tried to clarify if SLP-1 is transported to LEs via very efficient endocytosis from the PM or via a direct transport pathway from the TGN. I tried to inhibit clathrin-dependent endocytosis by expressing either a dynamin mutant (dynK44A), a fragment of AP-180 (AP180-C) or the SH3 domain of amphiphysin (Amph-SH3), but I could not observe big effects on the subcellular localization of SLP-1. Therefore, I can conclude that SLP-1 is not transported to LEs via clathrin-dependent endocytosis from the PM. A non-clathrin-dependent mechanism would still be possible. Direct transport of proteins to LEs has been described to be mediated by the AP-3 complex. The μ-subunits of different AP complexes have been shown to interact directly with short tyrosine-based sorting signals(Ihrke et al., 2004; Ohno et al., 1998; Rous et al., 2002). Our current working hypothesis is that the GYRAL motif could directly interact with AP-3 and therefore mediate direct targeting to LEs. This putative interaction could be confirmed by yeast two-hybrid screens or immunoprecipitation assays. In my opinion, there must be an interaction partner, which binds to/recognizes the GYRAL motif in the N-terminus.

5.3 The interaction between SLP-1 and stomatin

As already outlined, we started with the hypothesis that human SLP-1 and stomatin could form a complex as described for *C. elegans* UNC-24 and UNC-1. This assumption was found to hold true, because we could show that endogenous stomatin is co-immunoprecipitated with over-expressed SLP-1 (Figure 15) and that SLP-1 causes a change in stomatin localization (Figure 14). Based on these results, we assume that hetero-oligomeric complexes of SLP-1 and stomatin can form. A future goal is to confirm the existence of hetero-oligomers in vivo by FRET experiments, but this method still has to be established in our laboratory. CFP- and YFP-tagged SLP-1 and stomatin constructs were cloned, and the FRET analysis can perhaps be done in collaboration with experts in this field. A very important question to be solved is: Are the hetero-oligomers of SLP-1 and stomatin also present in unperturbed cells (without overexpression of one or both binding partners)? To adress this question, it is necessary to first get a good antibody against endogenous SLP-1. Then, different cell lines and tissues can be investigated, and the relative amounts of SLP-1 and stomatin can be compared. From microarray and northern blot data, we must expect that the expression level of SLP-1 is considerably low compared to stomatin in most tissues. Nevertheless, a non-stoichiometric incorporation of SLP-1 into bigger oligomeric complexes could still have a profound impact

on the subcellular localization of the complex. Another question is where these hetero-oligomers might form. For stomatin, we know that oligomer formation starts early in the biosynthetic pathway, probably at the ER membrane shortly after biosynthesis. Further experiments will be necessary to adress these interesting questions.

5.4 FRAP experiments with stomatin

As shown in Figure 45, deletion of the outmost C-terminus of stomatin has an impact upon the diffusional properties of the protein. The mobile fraction M_f as well as the diffusion speed (as measured by the recovery half-time $t_{1/2}$) both increase when amino acids 263-287 are deleted. This region of the protein is also essential for both oligomerization(Snyers et al., 1998) and lipid raft association(Umlauf et al., 2006) of stomatin. During her work, my colleague Ellen Umlauf has constructed several point mutations in this region and has shown that one of these mutants, P269A, only interferes with oligomerization and not with lipid raft association. This mutant could be used to investigate which of these two properties of stomatin has a bigger influence on the diffusion properties. Lipid raft association was recently shown not to have a big impact on the diffusional properties of several proteins(Kenworthy et al., 2004), therefore I would expect that it is the oligomerization, which causes the slow diffusional speed of the protein. Concerning the low mobile fraction of wild-type stomatin, experiments with agents which cause depolymerization of the cytoskeleton (e.g. cytochalasins or latrunculin A) could be very interesting. An interaction of stomatin with the cytoskeleton has been proposed almost ten years ago(Snyers et al., 1997), but an experimental proof is still missing. The high fraction of immobile stomatin in the plasma membrane again indicates a link to the cytoskeleton, but further experiments are necessary. The FRAP assay could be very useful for the confirmation of a (direct or indirect) link to the cytoskeleton, because depolymerization of, for example, cortical actin could result in a substantial increase of the mobile fraction of stomatin. To investigate the role of lipid raft association and oligomerization, one could immediately start with the existing, GFP-tagged point mutants (see Figure 46) and analyse them in FRAP experiments.

5.5 New stomatin point mutations

As already mentioned, I started with the construction of several new stomatin point mutants, either based on described mutations in the C. elegans MEC-2/UNC-1 protein (

Table *2*) or targeting residues with potential PTMs (eg.serine 231).

Especially the serine 231 point mutants gave very interesting results, although the putative phosphorylation still has to be confirmed. The S231A point mutant obviously gets stuck in the ER early during biosynthesis (Figure 43). This blockade can be overcome by formation of

oligomers with endogenous stomatin, depending on the expression level in HeLa, the mutated protein either localizes to the ER (high expression level) or can be transported to the PM (low expression level). In A431 cells, which only have very low levels of endogenous stomatin, I only observed ER localization. Interestingly, a combination of this point mutation with the C-terminal truncation, which abolishes oligomerization (deletion 263-287) yields a construct which can be properly transported to the PM and does not accumulate in the ER. This indicates that only the oligomeric S231A mutant is not transport-competent for exit from the ER, but the monomeric mutant can be transported. Of course, biochemical analysis of the oligomerization state of the mutants should be done to complement the cell biological data. The S231E mutant, which was designed to mimic permanent phosphorylation at this position, also showed some interesting features. Upon strong overexpression, this mutant was detected on long, filamentous structures in the cells, which most likely represent bundles of actin filaments (Figure 44). The localization of the mutant to these structures could, of course, represent an artefact of over-expression. But it could also indicate that this mutant is more efficiently recruited to transport vesicles travelling along cytoskeletal structures. Another difference to the wild-type protein was observed if this mutant was co-expressed with SLP-1. The S231E mutant showed perfect co-localization with SLP-1 on late endosomes, whereas wild-type stomatin only showed partial co-localization and also strong PM staining (Figure 42). We hypothesize that S231E can be internalized more rapidly than the wild-type stomatin protein, whereas the S231A mutant, when targeted to the PM, is only internalized to a very low extent. Irrespective of phosphorylation at serine 231, this region seems to be very important for proper function and targeting of stomatin. This is also reflected by the many point mutants discovered in this region (

Table *2*). Secondary structure prediction programs suggest a very long alpha-helical structure for this region, which could be involved in oligomerization and protein-protein interactions. The outmost 25 amino acids are necessary for oligomerization of stomatin, but a second region must also be involved to give rise to stable, large oligomers (>12 subunits). Because three consecutive peptides in this region showed the cryptic PTM described in the Results section, we decided to target S214 according to S231 and constructed the S214A and S214E mutants. A detailed analysis of these mutants and of the double mutants (S214,231A, S214,231E) is still missing, but the effects described above seem to be specific for position S231. But two other mutants, E210K and E212K, converting the negative charge to a positive one, were shown to profoundly impact stomatin trafficking. In my first transient transfection experiments with these constructs, I did not observe PM localization, but only localization to cytoplasmic vesicles or aggregates (see Figure 48). Therefore, the subcellular trafficking of these mutants seems to be defective. Further experiments are necessary to confirm this result, especially derivation of stable clones and biochemical analysis.

The stomatin mutants constructed in this thesis, in my opinion, could be very useful for the elucidation of the true function of the stomatin protein. The approach to introduce point mutants has been started several years ago in our laboratory, and the outmost C-terminus was

analysed by an alanine scanning mutagenesis approach. Several point mutants which are defective in oligomerization or lipid raft association were identified. But the subcellular localization of all these constructs was practically indistinguishable from the wild-type protein, and clearly visible phenotypes caused by the over-expression of the mutants could also not be identified. Now, we have several candidate mutants, which show effects on the subcellular trafficking of the protein. Stable over-expression in different cell lines and accurate analysis of these cells by different means (e.g. fluorescence microscopy, ELMI) will show if the expression of these mis-targeted proteins has any effect on the cells, for example in respect to lipid transport, and could help to identify the processes where stomatin is involved.

5.6 Outlook

The molecular function of the members of the human stomatin protein family still remains largely obscure. Nevertheless, a basic function can be assumed for these enigmatic membrane proteins. The kidney-specific member podocin is mutated in steroid-resistant nephrotic syndrome (NPHS2)(Boute et al., 2000), SLP-3 knockout mice show defects in mechanosensation(Wetzel et al., 2007) and SLP-2 knockout mice are not viable (data presented in poster sessions by two different groups). In my thesis, I have tried to expand our knowledge about the least characterized human family member, SLP-1. I am sure that the mouse knockout for SLP-1 will soon be reported, and I am really curious to see if there is a phenotype. Also, crossing of the newly available SLP-3 -/- animals with the stomatin -/- animals(Zhu et al., 1999) could lead to interesting insights. As we still assume an important function for the stomatin protein, it might happen that the phenotype is only apparent when SLP-3 cannot compensate for the loss of stomatin. For me, the function of the stomatin family proteins lies somewhere in the field of lipid transport, membrane domain formation and modification of membrane properties. The oligomeric properties of the stomatin family proteins and the organization in lipid rafts make them ideal candidates for scaffolding proteins on the inner leaflet of the PM. A similar function has been described for the related flotillins, which are essential for proper insulin signalling. An involvement in any signalling pathway has not yet been reported for stomatin, but this possibility should not be forgotten. With the first commercial antibodies available now, the protein might become a useful marker protein for lipid raft domains in cell types or tissues expressing low levels of other markers, and this more wide-spread use might also lead to unexpected new discoveries. Modern molecular biological methods like siRNA should be implemented as soon as possible for all family proteins, because they provide a quick method to screen for the pathways where the proteins could be involved. Of course, good antibodies for all 5 family members are needed for this task, but these reagents will hopefully be available soon. A focus must be put on the analysis of lipid/cholesterol distribution and lipid raft formation in the cells. For SLP-1, the proposed lipid binding ability of its SCP-2 domain should be tested in vitro after bacterial expression

and purification of this domain, and methods to analyse subcellular cholesterol transport have to be established to analyse SLP-1 function in vivo.

As the interest in SPFH family proteins continuously increases(Browman et al., 2007; Morrow and Parton, 2005), I am optimistic that the field will advance and draw more attention in the next years. As exemplified by podocin, which was basically unknown until Boute et al. described the mutations which cause NPHS2, a single "breakthrough paper" in a high-impact journal can persistantly boost research in a field. Up to now, more than 230 publications dealing with podocin have been published. The recent article in Nature describing *"A stomatin domain protein essential for touch sensation in the mouse"*(Wetzel et al., 2007) hopefully will promote research on stomatin and the other family members, because there are still plenty of open questions to be solved.

6 REFERENCES

Ahmed, S. N., Brown, D. A., and London, E. (1997). On the origin of sphingolipid/cholesterol-rich detergent-insoluble cell membranes: physiological concentrations of cholesterol and sphingolipid induce formation of a detergent-insoluble, liquid-ordered lipid phase in model membranes. Biochemistry *36*, 10944-10953.

Alpy, F., Stoeckel, M. E., Dierich, A., Escola, J. M., Wendling, C., Chenard, M. P., Vanier, M. T., Gruenberg, J., Tomasetto, C., and Rio, M. C. (2001). The steroidogenic acute regulatory protein homolog MLN64, a late endosomal cholesterol-binding protein. J Biol Chem *276*, 4261-4269.

Aman, M. J., and Ravichandran, K. S. (2000). A requirement for lipid rafts in B cell receptor induced Ca (2+) flux. Curr Biol *10*, 393-396.

Anderson, R. G., and Jacobson, K. (2002). A role for lipid shells in targeting proteins to caveolae, rafts, and other lipid domains. Science *296*, 1821-1825.

Barnes, T. M., Jin, Y., Horvitz, H. R., Ruvkun, G., and Hekimi, S. (1996). The Caenorhabditis elegans behavioral gene unc-24 encodes a novel bipartite protein similar to both erythrocyte band 7.2 (stomatin) and nonspecific lipid transfer protein. J Neurochem *67*, 46-57.

Bauer, M., and Pelkmans, L. (2006). A new paradigm for membrane-organizing and -shaping scaffolds. FEBS Lett *580*, 5559-5564.

Baumann, C. A., Ribon, V., Kanzaki, M., Thurmond, D. C., Mora, S., Shigematsu, S., Bickel, P. E., Pessin, J. E., and Saltiel, A. R. (2000). CAP defines a second signalling pathway required for insulin-stimulated glucose transport. Nature *407*, 202-207.

Baumgart, T., Hess, S. T., and Webb, W. W. (2003). Imaging coexisting fluid domains in biomembrane models coupling curvature and line tension. Nature *425*, 821-824.

Bickel, P. E., Scherer, P. E., Schnitzer, J. E., Oh, P., Lisanti, M. P., and Lodish, H. F. (1997). Flotillin and epidermal surface antigen define a new family of caveolae-associated integral membrane proteins. J Biol Chem *272*, 13793-13802.

Blacque, O. E., Perens, E. A., Boroevich, K. A., Inglis, P. N., Li, C., Warner, A., Khattra, J., Holt, R. A., Ou, G., Mah, A. K.*, et al.* (2005). Functional genomics of the cilium, a sensory organelle. Curr Biol *15*, 935-941.

Bloj, B., Hughes, M. E., Wilson, D. B., and Zilversmit, D. B. (1978). Isolation and amino acid analysis of a nonspecific phospholipid transfer protein from rat liver. FEBS Lett *96*, 87-89.

Bloj, B., and Zilversmit, D. B. (1977). Rat liver proteins capable of transferring phosphatidylethanolamine. Purification and transfer activity for other phospholipids and cholesterol. J Biol Chem *252*, 1613-1619.

Bonifacino, J. S., and Dell'Angelica, E. (1998). Immunoprecipitation. In Current Protocols in Cell Biology, J. S. Bonifacino, M. Dasso, J. B. Harford, J. Lippincott-Schwartz, and K. M. Yamada, eds. (New York, John Wiley & Sons, Inc.), pp. 7.2.1-7.2.21.

Boute, N., Gribouval, O., Roselli, S., Benessy, F., Lee, H., Fuchshuber, A., Dahan, K., Gubler, M. C., Niaudet, P., and Antignac, C. (2000). NPHS2, encoding the glomerular protein podocin, is mutated in autosomal recessive steroid-resistant nephrotic syndrome. Nat Genet *24*, 349-354.

Brasaemle, D. L., Barber, T., Kimmel, A. R., and Londos, C. (1997). Post-translational regulation of perilipin expression. Stabilization by stored intracellular neutral lipids. J Biol Chem *272*, 9378-9387.

Brenner, S. (1974). The genetics of Caenorhabditis elegans. Genetics *77*, 71-94.

Browman, D. T., Hoegg, M. B., and Robbins, S. M. (2007). The SPFH domain-containing proteins: more than lipid raft markers. Trends Cell Biol *17*, 394-402.

Brown, D. A. (2001). Lipid droplets: proteins floating on a pool of fat. Curr Biol *11*, R446-449.

Brown, D. A. (2006). Lipid rafts, detergent-resistant membranes, and raft targeting signals. Physiology (Bethesda) *21*, 430-439.

Brown, D. A., and London, E. (1998). Functions of lipid rafts in biological membranes. Annu Rev Cell Dev Biol *14*, 111-136.

Brown, D. A., and Rose, J. K. (1992). Sorting of GPI-anchored proteins to glycolipid-enriched membrane subdomains during transport to the apical cell surface. Cell *68*, 533-544.

Butko, P., Hapala, I., Scallen, T. J., and Schroeder, F. (1990). Acidic phospholipids strikingly potentiate sterol carrier protein 2 mediated intermembrane sterol transfer. Biochemistry *29*, 4070-4077.

Campbell, I. G., Allen, J., and Eccles, D. M. (2003). Prohibitin 3' untranslated region polymorphism and breast cancer risk. Cancer Epidemiol Biomarkers Prev *12*, 1273-1274.

Caridi, G., Perfumo, F., and Ghiggeri, G. M. (2005). NPHS2 (Podocin) mutations in nephrotic syndrome. Clinical spectrum and fine mechanisms. Pediatr Res *57*, 54R-61R.

Carroll, B. T., Dubyak, G. R., Sedensky, M. M., and Morgan, P. G. (2006). Sulfated Signal from ASJ Sensory Neurons Modulates Stomatin-dependent Coordination in Caenorhabditis elegans. J Biol Chem *281*, 35989-35996.

Chalfie, M., and Au, M. (1989). Genetic control of differentiation of the Caenorhabditis elegans touch receptor neurons. Science *243*, 1027-1033.

Chalfie, M., and Sulston, J. (1981). Developmental genetics of the mechanosensory neurons of Caenorhabditis elegans. Dev Biol *82*, 358-370.

Cheng, H. H., Muhlrad, P. J., Hoyt, M. A., and Echols, H. (1988). Cleavage of the cII protein of phage lambda by purified HflA protease: control of the switch between lysis and lysogeny. Proc Natl Acad Sci U S A *85*, 7882-7886.

Coates, P. J., Jamieson, D. J., Smart, K., Prescott, A. R., and Hall, P. A. (1997). The prohibitin family of mitochondrial proteins regulate replicative lifespan. Curr Biol *7*, 607-610.

Crain, R. C., and Zilversmit, D. B. (1980). Two nonspecific phospholipid exchange proteins from beef liver. I. Purification and characterization. Biochemistry *19*, 1433-1439.

Darmon, A. J., and Jat, P. S. (2000). BAP37 and Prohibitin are specifically recognized by an SV40 T antigen antibody. Mol Cell Biol Res Commun *4*, 219-223.

Deininger, S. O., Rajendran, L., Lottspeich, F., Przybylski, M., Illges, H., Stuermer, C. A., and Reuter, A. (2003). Identification of teleost Thy-1 and association with the microdomain/lipid raft reggie proteins in regenerating CNS axons. Mol Cell Neurosci *22*, 544-554.

Douglass, A. D., and Vale, R. D. (2005). Single-molecule microscopy reveals plasma membrane microdomains created by protein-protein networks that exclude or trap signaling molecules in T cells. Cell *121*, 937-950.

Edidin, M. (2001). Shrinking patches and slippery rafts: scales of domains in the plasma membrane. Trends Cell Biol *11*, 492-496.

Fan, Q., Xing, Y., Ding, J., Guan, N., and Zhang, J. (2006). The relationship among nephrin, podocin, CD2AP, and alpha-actinin might not be a true 'interaction' in podocyte. Kidney Int *69*, 1207-1215.

Feuk-Lagerstedt, E., Samuelsson, M., Mosgoeller, W., Movitz, C., Rosqvist, A., Bergstrom, J., Larsson, T., Steiner, M., Prohaska, R., and Karlsson, A. (2002). The presence of stomatin in detergent-insoluble domains of neutrophil granule membranes. J Leukoc Biol *72*, 970-977.

Fricke, B., Argent, A. C., Chetty, M. C., Pizzey, A. R., Turner, E. J., Ho, M. M., Iolascon, A., von During, M., and Stewart, G. W. (2003). The "stomatin" gene and protein in overhydrated hereditary stomatocytosis. Blood *102*, 2268-2277.

Fricke, B., Lints, R., Stewart, G., Drummond, H., Dodt, G., Driscoll, M., and von During, M. (2000). Epithelial Na+ channels and stomatin are expressed in rat trigeminal mechanosensory neurons. Cell Tissue Res *299*, 327-334.

Fricke, B., Parsons, S. F., Knopfle, G., von During, M., and Stewart, G. W. (2005). Stomatin is mis-trafficked in the erythrocytes of overhydrated hereditary stomatocytosis, and is absent from normal primitive yolk sac-derived erythrocytes. Br J Haematol *131*, 265-277.

Fusaro, G., Dasgupta, P., Rastogi, S., Joshi, B., and Chellappan, S. (2003). Prohibitin induces the transcriptional activity of p53 and is exported from the nucleus upon apoptotic signaling. J Biol Chem *278*, 47853-47861.

Gadella, T. W., Jr., and Wirtz, K. W. (1991). The low-affinity lipid binding site of the non-specific lipid transfer protein. Implications for its mode of action. Biochim Biophys Acta *1070*, 237-245.

Gallegos, A. M., Atshaves, B. P., Storey, S. M., McIntosh, A. L., Petrescu, A. D., and Schroeder, F. (2001). Sterol carrier protein-2 expression alters plasma membrane lipid distribution and cholesterol dynamics. Biochemistry *40*, 6493-6506.

Gaus, K., Chklovskaia, E., Fazekas de St Groth, B., Jessup, W., and Harder, T. (2005). Condensation of the plasma membrane at the site of T lymphocyte activation. J Cell Biol *171*, 121-131.

Gilles, F., Glenn, M., Goy, A., Remache, Y., and Zelenetz, A. D. (2000). A novel gene STORP (STOmatin-Related Protein) is localized 2 kb upstream of the promyelocytic gene on chromosome 15q22. Eur J Haematol *64*, 104-113.

Gillespie, P. G., and Walker, R. G. (2001). Molecular basis of mechanosensory transduction. Nature *413*, 194-202.

Glebov, O. O., Bright, N. A., and Nichols, B. J. (2006). Flotillin-1 defines a clathrin-independent endocytic pathway in mammalian cells. Nat Cell Biol *8*, 46-54.

Glebov, O. O., and Nichols, B. J. (2004). Lipid raft proteins have a random distribution during localized activation of the T-cell receptor. Nat Cell Biol *6*, 238-243.

Goldstein, B. J., Kulaga, H. M., and Reed, R. R. (2003). Cloning and characterization of SLP3: a novel member of the stomatin family expressed by olfactory receptor neurons. J Assoc Res Otolaryngol *4*, 74-82.

Goodman, M. B., Ernstrom, G. G., Chelur, D. S., O'Hagan, R., Yao, C. A., and Chalfie, M. (2002). MEC-2 regulates C. elegans DEG/ENaC channels needed for mechanosensation. Nature *415*, 1039-1042.

Goodwin, J. S., and Kenworthy, A. K. (2005). Photobleaching approaches to investigate diffusional mobility and trafficking of Ras in living cells. Methods *37*, 154-164.

Gough, N. R., Zweifel, M. E., Martinez-Augustin, O., Aguilar, R. C., Bonifacino, J. S., and Fambrough, D. M. (1999). Utilization of the indirect lysosome targeting pathway by lysosome-associated membrane proteins (LAMPs) is influenced largely by the C-terminal residue of their GYXXphi targeting signals. J Cell Sci *112 (Pt 23)*, 4257-4269.

Green, J. B., Fricke, B., Chetty, M. C., von During, M., Preston, G. F., and Stewart, G. W. (2004). Eukaryotic and prokaryotic stomatins: the proteolytic link. Blood Cells Mol Dis *32*, 411-422.

Gruenberg, J., and van der Goot, F. G. (2006). Mechanisms of pathogen entry through the endosomal compartments. Nat Rev Mol Cell Biol *7*, 495-504.

Guarnieri, F. G., Arterburn, L. M., Penno, M. B., Cha, Y., and August, J. T. (1993). The motif Tyr-X-X-hydrophobic residue mediates lysosomal membrane targeting of lysosome-associated membrane protein 1. J Biol Chem *268*, 1941-1946.

Hajek, P., Chomyn, A., and Attardi, G. (2006). Identification of a novel mitochondrial complex containing mitofusin 2 and stomatin-like protein 2. J Biol Chem.

Hammond, A. T., Heberle, F. A., Baumgart, T., Holowka, D., Baird, B., and Feigenson, G. W. (2005). Crosslinking a lipid raft component triggers liquid ordered-liquid disordered phase separation in model plasma membranes. Proc Natl Acad Sci U S A *102*, 6320-6325.

Hancock, J. F. (2006). Lipid rafts: contentious only from simplistic standpoints. Nat Rev Mol Cell Biol *7*, 456-462.

Hao, M., Mukherjee, S., and Maxfield, F. R. (2001). Cholesterol depletion induces large scale domain segregation in living cell membranes. Proc Natl Acad Sci U S A *98*, 13072-13077.

PhD thesis   *Mario Mairhofer*

Hazarika, P., Dham, N., Patel, P., Cho, M., Weidner, D., Goldsmith, L., and Duvic, M. (1999). Flotillin 2 is distinct from epidermal surface antigen (ESA) and is associated with filopodia formation. J Cell Biochem *75*, 147-159.

Heerklotz, H. (2002). Triton promotes domain formation in lipid raft mixtures. Biophys J *83*, 2693-2701.

Heerklotz, H., Szadkowska, H., Anderson, T., and Seelig, J. (2003). The sensitivity of lipid domains to small perturbations demonstrated by the effect of Triton. J Mol Biol *329*, 793-799.

Heijnen, H. F., Van Lier, M., Waaijenborg, S., Ohno-Iwashita, Y., Waheed, A. A., Inomata, M., Gorter, G., Mobius, W., Akkerman, J. W., and Slot, J. W. (2003). Concentration of rafts in platelet filopodia correlates with recruitment of c-Src and CD63 to these domains. J Thromb Haemost *1*, 1161-1173.

Hiebl-Dirschmied, C. M., Adolf, G. R., and Prohaska, R. (1991a). Isolation and partial characterization of the human erythrocyte band 7 integral membrane protein. Biochim Biophys Acta *1065*, 195-202.

Hiebl-Dirschmied, C. M., Entler, B., Glotzmann, C., Maurer-Fogy, I., Stratowa, C., and Prohaska, R. (1991b). Cloning and nucleotide sequence of cDNA encoding human erythrocyte band 7 integral membrane protein. Biochim Biophys Acta *1090*, 123-124.

Huang, M., Gu, G., Ferguson, E. L., and Chalfie, M. (1995). A stomatin-like protein necessary for mechanosensation in C. elegans. Nature *378*, 292-295.

Huber, T. B., Schermer, B., Muller, R. U., Hohne, M., Bartram, M., Calixto, A., Hagmann, H., Reinhardt, C., Koos, F., Kunzelmann, K.*, et al.* (2006). Inaugural Article: Podocin and MEC-2 bind cholesterol to regulate the activity of associated ion channels. Proc Natl Acad Sci U S A *103*, 17079-17086.

Huber, T. B., Simons, M., Hartleben, B., Sernetz, L., Schmidts, M., Gundlach, E., Saleem, M. A., Walz, G., and Benzing, T. (2003). Molecular basis of the functional podocin-nephrin complex: mutations in the NPHS2 gene disrupt nephrin targeting to lipid raft microdomains. Hum Mol Genet *12*, 3397-3405.

Ihrke, G., Kyttala, A., Russell, M. R., Rous, B. A., and Luzio, J. P. (2004). Differential use of two AP-3-mediated pathways by lysosomal membrane proteins. Traffic *5*, 946-962.

Ikonen, E., Fiedler, K., Parton, R. G., and Simons, K. (1995). Prohibitin, an antiproliferative protein, is localized to mitochondria. FEBS Lett *358*, 273-277.

Ito, K., and Akiyama, Y. (2005). Cellular functions, mechanism of action, and regulation of FtsH protease. Annu Rev Microbiol *59*, 211-231.

Jupe, E. R., Badgett, A. A., Neas, B. R., Craft, M. A., Mitchell, D. S., Resta, R., Mulvihill, J. J., Aston, C. E., and Thompson, L. F. (2001). Single nucleotide polymorphism in prohibitin 39 untranslated region and breast-cancer susceptibility. Lancet *357*, 1588-1589.

Jupe, E. R., Liu, X. T., Kiehlbauch, J. L., McClung, J. K., and Dell'Orco, R. T. (1996). The 3' untranslated region of prohibitin and cellular immortalization. Exp Cell Res *224*, 128-135.

Kenworthy, A. (2002). Peering inside lipid rafts and caveolae. Trends Biochem Sci *27*, 435-437.

Kenworthy, A. K., Nichols, B. J., Remmert, C. L., Hendrix, G. M., Kumar, M., Zimmerberg, J., and Lippincott-Schwartz, J. (2004). Dynamics of putative raft-associated proteins at the cell surface. J Cell Biol *165*, 735-746.

Kenworthy, A. K., Petranova, N., and Edidin, M. (2000). High-resolution FRET microscopy of cholera toxin B-subunit and GPI-anchored proteins in cell plasma membranes. Mol Biol Cell *11*, 1645-1655.

Kestila, M., Lenkkeri, U., Mannikko, M., Lamerdin, J., McCready, P., Putaala, H., Ruotsalainen, V., Morita, T., Nissinen, M., Herva, R.*, et al.* (1998). Positionally cloned gene for a novel glomerular protein--nephrin--is mutated in congenital nephrotic syndrome. Mol Cell *1*, 575-582.

Kihara, A., Akiyama, Y., and Ito, K. (1996). A protease complex in the Escherichia coli plasma membrane: HflKC (HflA) forms a complex with FtsH (HflB), regulating its proteolytic activity against SecY. Embo J *15*, 6122-6131.

Kihara, A., Akiyama, Y., and Ito, K. (1997). Host regulation of lysogenic decision in bacteriophage lambda: transmembrane modulation of FtsH (HflB), the cII degrading protease, by HflKC (HflA). Proc Natl Acad Sci U S A *94*, 5544-5549.

Kimura, A., Baumann, C. A., Chiang, S. H., and Saltiel, A. R. (2001). The sorbin homology domain: a motif for the targeting of proteins to lipid rafts. Proc Natl Acad Sci U S A *98*, 9098-9103.

Kioka, N., Ueda, K., and Amachi, T. (2002). Vinexin, CAP/ponsin, ArgBP2: a novel adaptor protein family regulating cytoskeletal organization and signal transduction. Cell Struct Funct *27*, 1-7.

Kirkham, M., Fujita, A., Chadda, R., Nixon, S. J., Kurzchalia, T. V., Sharma, D. K., Pagano, R. E., Hancock, J. F., Mayor, S., and Parton, R. G. (2005). Ultrastructural identification of uncoated caveolin-independent early endocytic vehicles. J Cell Biol *168*, 465-476.

Kobayakawa, K., Hayashi, R., Morita, K., Miyamichi, K., Oka, Y., Tsuboi, A., and Sakano, H. (2002). Stomatin-related olfactory protein, SRO, specifically expressed in the murine olfactory sensory neurons. J Neurosci *22*, 5931-5937.

Kobayashi, T., Beuchat, M. H., Lindsay, M., Frias, S., Palmiter, R. D., Sakuraba, H., Parton, R. G., and Gruenberg, J. (1999). Late endosomal membranes rich in lysobisphosphatidic acid regulate cholesterol transport. Nat Cell Biol *1*, 113-118.

Kokubo, H., Lemere, C. A., and Yamaguchi, H. (2000). Localization of flotillins in human brain and their accumulation with the progression of Alzheimer's disease pathology. Neurosci Lett *290*, 93-96.

Kusumi, A., Ike, H., Nakada, C., Murase, K., and Fujiwara, T. (2005). Single-molecule tracking of membrane molecules: plasma membrane compartmentalization and dynamic assembly of raft-philic signaling molecules. Semin Immunol *17*, 3-21.

Kwik, J., Boyle, S., Fooksman, D., Margolis, L., Sheetz, M. P., and Edidin, M. (2003). Membrane cholesterol, lateral mobility, and the phosphatidylinositol 4,5-bisphosphate-dependent organization of cell actin. Proc Natl Acad Sci U S A *100*, 13964-13969.

Lai, E. C. (2003). Lipid rafts make for slippery platforms. J Cell Biol *162*, 365-370.

Lang, D. M., Lommel, S., Jung, M., Ankerhold, R., Petrausch, B., Laessing, U., Wiechers, M. F., Plattner, H., and Stuermer, C. A. (1998). Identification of reggie-1 and reggie-2 as plasmamembrane-associated proteins which cocluster with activated GPI-anchored cell adhesion molecules in non-caveolar micropatches in neurons. J Neurobiol *37*, 502-523.

Lee, S. Y., and MacKinnon, R. (2004). A membrane-access mechanism of ion channel inhibition by voltage sensor toxins from spider venom. Nature *430*, 232-235.

Lichtenberg, D., Goni, F. M., and Heerklotz, H. (2005). Detergent-resistant membranes should not be identified with membrane rafts. Trends Biochem Sci *30*, 430-436.

Lisanti, M. P., Sargiacomo, M., Graeve, L., Saltiel, A. R., and Rodriguez-Boulan, E. (1988). Polarized apical distribution of glycosyl-phosphatidylinositol-anchored proteins in a renal epithelial cell line. Proc Natl Acad Sci U S A *85*, 9557-9561.

Liscum, L., and Faust, J. R. (1989). The intracellular transport of low density lipoprotein-derived cholesterol is inhibited in Chinese hamster ovary cells cultured with 3-beta-[2-(diethylamino)ethoxy]androst-5-en-17-one. J Biol Chem *264*, 11796-11806.

London, E. (2005). How principles of domain formation in model membranes may explain ambiguities concerning lipid raft formation in cells. Biochim Biophys Acta *1746*, 203-220.

Lowry, O. H. (1957). Micromethods for the Assay of Enzymes. In Methods in Enzymology, S. P. Colowick, and N. O. Kaplan, eds. (New York, Academic Press Inc.), pp. 366-381.

Mairhofer, M. (2001) Characterization of stomatin in platelets, diploma thesis, University of Vienna, Vienna.

Mairhofer, M., Steiner, M., Mosgoeller, W., Prohaska, R., and Salzer, U. (2002). Stomatin is a major lipid-raft component of platelet alpha granules. Blood *100*, 897-904.

Majewska, M. D. (1992). Neurosteroids: endogenous bimodal modulators of the GABAA receptor. Mechanism of action and physiological significance. Prog Neurobiol *38*, 379-395.

Manjeshwar, S., Branam, D. E., Lerner, M. R., Brackett, D. J., and Jupe, E. R. (2003). Tumor suppression by the prohibitin gene 3'untranslated region RNA in human breast cancer. Cancer Res *63*, 5251-5256.

Manjeshwar, S., Lerner, M. R., Zang, X. P., Branam, D. E., Pento, J. T., Lane, M. M., Lightfoot, S. A., Brackett, D. J., and Jupe, E. R. (2004). Expression of prohibitin 3' untranslated region suppressor RNA alters morphology and inhibits motility of breast cancer cells. J Mol Histol *35*, 639-646.

Mannsfeldt, A. G., Carroll, P., Stucky, C. L., and Lewin, G. R. (1999). Stomatin, a MEC-2 like protein, is expressed by mammalian sensory neurons. Mol Cell Neurosci *13*, 391-404.

Maxfield, F. R. (2002). Plasma membrane microdomains. Curr Opin Cell Biol *14*, 483-487.

Mayor, S., and Rao, M. (2004). Rafts: scale-dependent, active lipid organization at the cell surface. Traffic *5*, 231-240.

Medzihradszky, K. F., Darula, Z., Perlson, E., Fainzilber, M., Chalkley, R. J., Ball, H., Greenbaum, D., Bogyo, M., Tyson, D. R., Bradshaw, R. A., and Burlingame, A. L. (2004). O-sulfonation of serine and threonine: mass spectrometric detection and characterization of a new posttranslational modification in diverse proteins throughout the eukaryotes. Mol Cell Proteomics *3*, 429-440.

Menssen, A., and Hermeking, H. (2002). Characterization of the c-MYC-regulated transcriptome by SAGE: identification and analysis of c-MYC target genes. Proc Natl Acad Sci U S A *99*, 6274-6279.

Meyers, J. M., and Prekeris, R. (2002). Formation of mutually exclusive Rab11 complexes with members of the family of Rab11-interacting proteins regulates Rab11 endocytic targeting and function. J Biol Chem *277*, 49003-49010.

Mielenz, D., Vettermann, C., Hampel, M., Lang, C., Avramidou, A., Karas, M., and Jack, H. M. (2005). Lipid rafts associate with intracellular B cell receptors and exhibit a B cell stage-specific protein composition. J Immunol *174*, 3508-3517.

Milhiet, P. E., Giocondi, M. C., Baghdadi, O., Ronzon, F., Roux, B., and Le Grimellec, C. (2002). Spontaneous insertion and partitioning of alkaline phosphatase into model lipid rafts. EMBO Rep *3*, 485-490.

Miller, D. M., 3rd, Niemeyer, C. J., and Chitkara, P. (1993). Dominant unc-37 mutations suppress the movement defect of a homeodomain mutation in unc-4, a neural specificity gene in Caenorhabditis elegans. Genetics *135*, 741-753.

Mishra, S., Murphy, L. C., and Murphy, L. J. (2006). The Prohibitins: emerging roles in diverse functions. J Cell Mol Med *10*, 353-363.

Montano, M. M., Ekena, K., Delage-Mourroux, R., Chang, W., Martini, P., and Katzenellenbogen, B. S. (1999). An estrogen receptor-selective coregulator that potentiates the effectiveness of antiestrogens and represses the activity of estrogens. Proc Natl Acad Sci U S A *96*, 6947-6952.

Moran, M., and Miceli, M. C. (1998). Engagement of GPI-linked CD48 contributes to TCR signals and cytoskeletal reorganization: a role for lipid rafts in T cell activation. Immunity *9*, 787-796.

Morgan, P. G., Sedensky, M., and Meneely, P. M. (1990). Multiple sites of action of volatile anesthetics in Caenorhabditis elegans. Proc Natl Acad Sci U S A *87*, 2965-2969.

Morrow, I. C., and Parton, R. G. (2005). Flotillins and the PHB domain protein family: rafts, worms and anaesthetics. Traffic *6*, 725-740.

Morrow, I. C., Rea, S., Martin, S., Prior, I. A., Prohaska, R., Hancock, J. F., James, D. E., and Parton, R. G. (2002). Flotillin-1/reggie-2 traffics to surface raft domains via a novel golgi-independent pathway. Identification of a novel membrane targeting domain and a role for palmitoylation. J Biol Chem *277*, 48834-48841.

Munro, S. (2003). Lipid rafts: elusive or illusive? Cell *115*, 377-388.

Neumann-Giesen, C., Falkenbach, B., Beicht, P., Claasen, S., Luers, G., Stuermer, C. A., Herzog, V., and Tikkanen, R. (2004). Membrane and raft association of reggie-1/flotillin-2: role of myristoylation, palmitoylation and oligomerization and induction of filopodia by overexpression. Biochem J *378*, 509-518.

Nichols, J. W., and Pagano, R. E. (1983). Resonance energy transfer assay of protein-mediated lipid transfer between vesicles. J Biol Chem *258*, 5368-5371.

Nicolau, D. V., Jr., Burrage, K., Parton, R. G., and Hancock, J. F. (2006). Identifying optimal lipid raft characteristics required to promote nanoscale protein-protein interactions on the plasma membrane. Mol Cell Biol *26*, 313-323.

Nijtmans, L. G., Artal, S. M., Grivell, L. A., and Coates, P. J. (2002). The mitochondrial PHB complex: roles in mitochondrial respiratory complex assembly, ageing and degenerative disease. Cell Mol Life Sci *59*, 143-155.

Nijtmans, L. G., de Jong, L., Artal Sanz, M., Coates, P. J., Berden, J. A., Back, J. W., Muijsers, A. O., van der Spek, H., and Grivell, L. A. (2000). Prohibitins act as a membrane-bound chaperone for the stabilization of mitochondrial proteins. Embo J *19*, 2444-2451.

Nishibori, Y., Liu, L., Hosoyamada, M., Endou, H., Kudo, A., Takenaka, H., Higashihara, E., Bessho, F., Takahashi, S., Kershaw, D.*, et al.* (2004). Disease-causing missense mutations in NPHS2 gene alter normal nephrin trafficking to the plasma membrane. Kidney Int *66*, 1755-1765.

Noble, J. A., Innis, M. A., Koonin, E. V., Rudd, K. E., Banuett, F., and Herskowitz, I. (1993). The Escherichia coli hflA locus encodes a putative GTP-binding protein and two membrane proteins, one of which contains a protease-like domain. Proc Natl Acad Sci U S A *90*, 10866-10870.

Noland, B. J., Arebalo, R. E., Hansbury, E., and Scallen, T. J. (1980). Purification and properties of sterol carrier protein2. J Biol Chem *255*, 4282-4289.

Nuell, M. J., Stewart, D. A., Walker, L., Friedman, V., Wood, C. M., Owens, G. A., Smith, J. R., Schneider, E. L., Dell' Orco, R., Lumpkin, C. K., and et al. (1991). Prohibitin, an evolutionarily conserved intracellular protein that blocks DNA synthesis in normal fibroblasts and HeLa cells. Mol Cell Biol *11*, 1372-1381.

Ohashi, T., Uchida, K., Uchida, S., Sasaki, S., and Nihei, H. (2003). Intracellular mislocalization of mutant podocin and correction by chemical chaperones. Histochem Cell Biol *119*, 257-264.

Ohno, H., Aguilar, R. C., Yeh, D., Taura, D., Saito, T., and Bonifacino, J. S. (1998). The medium subunits of adaptor complexes recognize distinct but overlapping sets of tyrosine-based sorting signals. J Biol Chem *273*, 25915-25921.

Park, E. C., and Horvitz, H. R. (1986). Mutations with dominant effects on the behavior and morphology of the nematode Caenorhabditis elegans. Genetics *113*, 821-852.

Pelkmans, L., Fava, E., Grabner, H., Hannus, M., Habermann, B., Krausz, E., and Zerial, M. (2005). Genome-wide analysis of human kinases in clathrin- and caveolae/raft-mediated endocytosis. Nature *436*, 78-86.

Petrie, R. J., Schnetkamp, P. P., Patel, K. D., Awasthi-Kalia, M., and Deans, J. P. (2000). Transient translocation of the B cell receptor and Src homology 2 domain-containing inositol phosphatase to lipid rafts: evidence toward a role in calcium regulation. J Immunol *165*, 1220-1227.

Piper, P. W., Jones, G. W., Bringloe, D., Harris, N., MacLean, M., and Mollapour, M. (2002). The shortened replicative life span of prohibitin mutants of yeast appears to be due to defective mitochondrial segregation in old mother cells. Aging Cell *1*, 149-157.

Pol, A., Luetterforst, R., Lindsay, M., Heino, S., Ikonen, E., and Parton, R. G. (2001). A caveolin dominant negative mutant associates with lipid bodies and induces intracellular cholesterol imbalance. J Cell Biol *152*, 1057-1070.

Pralle, A., Keller, P., Florin, E. L., Simons, K., and Horber, J. K. (2000). Sphingolipid-cholesterol rafts diffuse as small entities in the plasma membrane of mammalian cells. J Cell Biol *148*, 997-1008.

Price, M. P., Thompson, R. J., Eshcol, J. O., Wemmie, J. A., and Benson, C. J. (2004). Stomatin modulates gating of acid-sensing ion channels. J Biol Chem *279*, 53886-53891.

Prior, I. A., Muncke, C., Parton, R. G., and Hancock, J. F. (2003a). Direct visualization of Ras proteins in spatially distinct cell surface microdomains. J Cell Biol *160*, 165-170.

PhD thesis *Mario Mairhofer*

Prior, I. A., Parton, R. G., and Hancock, J. F. (2003b). Observing cell surface signaling domains using electron microscopy. Sci STKE *2003*, PL9.

Rajaram, S., Sedensky, M. M., and Morgan, P. G. (1998). Unc-1: a stomatin homologue controls sensitivity to volatile anesthetics in Caenorhabditis elegans. Proc Natl Acad Sci U S A *95*, 8761-8766.

Rajaram, S., Spangler, T. L., Sedensky, M. M., and Morgan, P. G. (1999). A stomatin and a degenerin interact to control anesthetic sensitivity in Caenorhabditis elegans. Genetics *153*, 1673-1682.

Rajendran, L., Masilamani, M., Solomon, S., Tikkanen, R., Stuermer, C. A., Plattner, H., and Illges, H. (2003). Asymmetric localization of flotillins/reggies in preassembled platforms confers inherent polarity to hematopoietic cells. Proc Natl Acad Sci U S A *100*, 8241-8246.

Rajendran, L., and Simons, K. (2005). Lipid rafts and membrane dynamics. J Cell Sci *118*, 1099-1102.

Reig, N., and van der Goot, F. G. (2006). About lipids and toxins. FEBS Lett *580*, 5572-5579.

Riddle, D. L., and Brenner, S. (1978). Indirect suppression in Caenorhabditis elegans. Genetics *89*, 299-314.

Rivera-Milla, E., Stuermer, C. A., and Malaga-Trillo, E. (2006). Ancient origin of reggie (flotillin), reggie-like, and other lipid-raft proteins: convergent evolution of the SPFH domain. Cell Mol Life Sci *63*, 343-357.

Roselli, S., Moutkine, I., Gribouval, O., Benmerah, A., and Antignac, C. (2004). Plasma membrane targeting of podocin through the classical exocytic pathway: effect of NPHS2 mutations. Traffic *5*, 37-44.

Rous, B. A., Reaves, B. J., Ihrke, G., Briggs, J. A., Gray, S. R., Stephens, D. J., Banting, G., and Luzio, J. P. (2002). Role of adaptor complex AP-3 in targeting wild-type and mutated CD63 to lysosomes. Mol Biol Cell *13*, 1071-1082.

Roux, A., Cuvelier, D., Nassoy, P., Prost, J., Bassereau, P., and Goud, B. (2005). Role of curvature and phase transition in lipid sorting and fission of membrane tubules. Embo J *24*, 1537-1545.

Rubin, D., and Ismail-Beigi, F. (2003). Distribution of Glut1 in detergent-resistant membranes (DRMs) and non-DRM domains: effect of treatment with azide. Am J Physiol Cell Physiol *285*, C377-383.

Rubin, D., and Ismail-Beigi, F. (2004). Differential accumulation of Glut1 in the non-DRM domain of the plasma membrane in response to the inhibition of oxidative phosphorylation. Arch Biochem Biophys *431*, 224-232.

Salzer, U., Ahorn, H., and Prohaska, R. (1993). Identification of the phosphorylation site on human erythrocyte band 7 integral membrane protein: implications for a monotopic protein structure. Biochim Biophys Acta *1151*, 149-152.

Salzer, U., and Prohaska, R. (2001). Stomatin, flotillin-1, and flotillin-2 are major integral proteins of erythrocyte lipid rafts. Blood *97*, 1141-1143.

Schroeder, R., London, E., and Brown, D. (1994a). Interactions between saturated acyl chains confer detergent resistance on lipids and glycosylphosphatidylinositol (GPI)-anchored proteins: GPI-anchored proteins in liposomes and cells show similar behavior. Proc Natl Acad Sci U S A *91*, 12130-12134.

Schroeder, W. T., Stewart-Galetka, S., Mandavilli, S., Parry, D. A., Goldsmith, L., and Duvic, M. (1994b). Cloning and characterization of a novel epidermal cell surface antigen (ESA). J Biol Chem *269*, 19983-19991.

Schulte, T., Paschke, K. A., Laessing, U., Lottspeich, F., and Stuermer, C. A. (1997). Reggie-1 and reggie-2, two cell surface proteins expressed by retinal ganglion cells during axon regeneration. Development *124*, 577-587.

Schutz, G. J., Kada, G., Pastushenko, V. P., and Schindler, H. (2000). Properties of lipid microdomains in a muscle cell membrane visualized by single molecule microscopy. Embo J *19*, 892-901.

Schwarz, K., Simons, M., Reiser, J., Saleem, M. A., Faul, C., Kriz, W., Shaw, A. S., Holzman, L. B., and Mundel, P. (2001). Podocin, a raft-associated component of the

glomerular slit diaphragm, interacts with CD2AP and nephrin. J Clin Invest *108*, 1621-1629.

Sedensky, M. M., Siefker, J. M., Koh, J. Y., Miller, D. M., 3rd, and Morgan, P. G. (2004). A stomatin and a degenerin interact in lipid rafts of the nervous system of Caenorhabditis elegans. Am J Physiol Cell Physiol *287*, C468-474.

Sedensky, M. M., Siefker, J. M., and Morgan, P. G. (2001). Model organisms: new insights into ion channel and transporter function. Stomatin homologues interact in Caenorhabditis elegans. Am J Physiol Cell Physiol *280*, C1340-1348.

Seidel, G., and Prohaska, R. (1998). Molecular cloning of hSLP-1, a novel human brain-specific member of the band 7/MEC-2 family similar to Caenorhabditis elegans UNC-24. Gene *225*, 23-29.

Sharma, P., Varma, R., Sarasij, R. C., Ira, Gousset, K., Krishnamoorthy, G., Rao, M., and Mayor, S. (2004). Nanoscale organization of multiple GPI-anchored proteins in living cell membranes. Cell *116*, 577-589.

Shih, N. Y., Li, J., Karpitskii, V., Nguyen, A., Dustin, M. L., Kanagawa, O., Miner, J. H., and Shaw, A. S. (1999). Congenital nephrotic syndrome in mice lacking CD2-associated protein. Science *286*, 312-315.

Simons, K., and Ikonen, E. (1997). Functional rafts in cell membranes. Nature *387*, 569-572.

Simons, K., and Toomre, D. (2000). Lipid rafts and signal transduction. Nat Rev Mol Cell Biol *1*, 31-39.

Simons, K., and van Meer, G. (1988). Lipid sorting in epithelial cells. Biochemistry *27*, 6197-6202.

Snyers, L., Thines-Sempoux, D., and Prohaska, R. (1997). Colocalization of stomatin (band 7.2b) and actin microfilaments in UAC epithelial cells. Eur J Cell Biol *73*, 281-285.

Snyers, L., Umlauf, E., and Prohaska, R. (1998). Oligomeric nature of the integral membrane protein stomatin. J Biol Chem *273*, 17221-17226.

Snyers, L., Umlauf, E., and Prohaska, R. (1999a). Association of stomatin with lipid-protein complexes in the plasma membrane and the endocytic compartment. Eur J Cell Biol *78*, 802-812.

Snyers, L., Umlauf, E., and Prohaska, R. (1999b). Cysteine 29 is the major palmitoylation site on stomatin. FEBS Lett *449*, 101-104.

Snyers, L., Zwickl, H., and Blaas, D. (2003). Human rhinovirus type 2 is internalized by clathrin-mediated endocytosis. J Virol *77*, 5360-5369.

Sooksawate, T., and Simmonds, M. A. (2001). Influence of membrane cholesterol on modulation of the GABA (A) receptor by neuroactive steroids and other potentiators. Br J Pharmacol *134*, 1303-1311.

Sprenger, R. R., Speijer, D., Back, J. W., De Koster, C. G., Pannekoek, H., and Horrevoets, A. J. (2004). Comparative proteomics of human endothelial cell caveolae and rafts using two-dimensional gel electrophoresis and mass spectrometry. Electrophoresis *25*, 156-172.

Steglich, G., Neupert, W., and Langer, T. (1999). Prohibitins regulate membrane protein degradation by the m-AAA protease in mitochondria. Mol Cell Biol *19*, 3435-3442.

Steiner, M., Schofer, C., and Mosgoeller, W. (1994). In situ flat embedding of monolayers and cell relocation in the acrylic resin LR white for comparative light and electron microscopy studies. Histochem J *26*, 934-938.

Stewart, G. W. (1997). Stomatin. Int J Biochem Cell Biol *29*, 271-274.

Stewart, G. W., Hepworth-Jones, B. E., Keen, J. N., Dash, B. C., Argent, A. C., and Casimir, C. M. (1992). Isolation of cDNA coding for an ubiquitous membrane protein deficient in high Na+, low K+ stomatocytic erythrocytes. Blood *79*, 1593-1601.

Stuermer, C. A., Lang, D. M., Kirsch, F., Wiechers, M., Deininger, S. O., and Plattner, H. (2001). Glycosylphosphatidyl inositol-anchored proteins and fyn kinase assemble in noncaveolar plasma membrane microdomains defined by reggie-1 and -2. Mol Biol Cell *12*, 3031-3045.

Stuermer, C. A., Langhorst, M. F., Wiechers, M. F., Legler, D. F., Von Hanwehr, S. H., Guse, A. H., and Plattner, H. (2004). PrPc capping in T cells promotes its association with the lipid raft proteins reggie-1 and reggie-2 and leads to signal transduction. Faseb J *18*, 1731-1733.

Tatsuta, T., Model, K., and Langer, T. (2005). Formation of membrane-bound ring complexes by prohibitins in mitochondria. Mol Biol Cell *16*, 248-259.

Tavano, R., Contento, R. L., Baranda, S. J., Soligo, M., Tuosto, L., Manes, S., and Viola, A. (2006). CD28 interaction with filamin-A controls lipid raft accumulation at the T-cell immunological synapse. Nat Cell Biol *8*, 1270-1276.

Tavernarakis, N., Driscoll, M., and Kyrpides, N. C. (1999). The SPFH domain: implicated in regulating targeted protein turnover in stomatins and other membrane-associated proteins. Trends Biochem Sci *24*, 425-427.

Terashima, M., Kim, K. M., Adachi, T., Nielsen, P. J., Reth, M., Kohler, G., and Lamers, M. C. (1994). The IgM antigen receptor of B lymphocytes is associated with prohibitin and a prohibitin-related protein. Embo J *13*, 3782-3792.

Turner, M. S., Sens, P., and Socci, N. D. (2005). Nonequilibrium raftlike membrane domains under continuous recycling. Phys Rev Lett *95*, 168301.

Umeda, A., Fujita, H., Kuronita, T., Hirosako, K., Himeno, M., and Tanaka, Y. (2003). Distribution and trafficking of MPR300 is normal in cells with cholesterol accumulated in late endocytic compartments: evidence for early endosome-to-TGN trafficking of MPR300. J Lipid Res *44*, 1821-1832.

Umlauf, E., Csaszar, E., Moertelmaier, M., Schuetz, G. J., Parton, R. G., and Prohaska, R. (2004). Association of stomatin with lipid bodies. J Biol Chem *279*, 23699-23709.

Umlauf, E., Mairhofer, M., and Prohaska, R. (2006). Characterization of the stomatin domain involved in homo-oligomerization and lipid raft association. J Biol Chem *281*, 23349-23356.

Unfried, I., Entler, B., and Prohaska, R. (1995). The organization of the gene (EPB72) encoding the human erythrocyte band 7 integral membrane protein (protein 7.2b). Genomics *30*, 521-528.

van der Goot, F. G., and Harder, T. (2001). Raft membrane domains: from a liquid-ordered membrane phase to a site of pathogen attack. Semin Immunol *13*, 89-97.

van Meer, G., and Simons, K. (1982). Viruses budding from either the apical or the basolateral plasma membrane domain of MDCK cells have unique phospholipid compositions. Embo J *1*, 847-852.

van Meer, G., Stelzer, E. H., Wijnaendts-van-Resandt, R. W., and Simons, K. (1987). Sorting of sphingolipids in epithelial (Madin-Darby canine kidney) cells. J Cell Biol *105*, 1623-1635.

Viola, A., Schroeder, S., Sakakibara, Y., and Lanzavecchia, A. (1999). T lymphocyte costimulation mediated by reorganization of membrane microdomains. Science *283*, 680-682.

Wang, D., Mentzer, W. C., Cameron, T., and Johnson, R. M. (1991). Purification of band 7.2b, a 31-kDa integral phosphoprotein absent in hereditary stomatocytosis. J Biol Chem *266*, 17826-17831.

Wang, S., Fusaro, G., Padmanabhan, J., and Chellappan, S. P. (2002). Prohibitin co-localizes with Rb in the nucleus and recruits N-CoR and HDAC1 for transcriptional repression. Oncogene *21*, 8388-8396.

Wang, S., Nath, N., Adlam, M., and Chellappan, S. (1999a). Prohibitin, a potential tumor suppressor, interacts with RB and regulates E2F function. Oncogene *18*, 3501-3510.

Wang, S., Nath, N., Fusaro, G., and Chellappan, S. (1999b). Rb and prohibitin target distinct regions of E2F1 for repression and respond to different upstream signals. Mol Cell Biol *19*, 7447-7460.

Wang, Y., and Morrow, J. S. (2000). Identification and characterization of human SLP-2, a novel homologue of stomatin (band 7.2b) present in erythrocytes and other tissues. J Biol Chem *275*, 8062-8071.

Watari, H., Blanchette-Mackie, E. J., Dwyer, N. K., Sun, G., Glick, J. M., Patel, S., Neufeld, E. B., Pentchev, P. G., and Strauss, J. F., 3rd (2000). NPC1-containing compartment of human granulosa-lutein cells: a role in the intracellular trafficking of cholesterol supporting steroidogenesis. Exp Cell Res *255*, 56-66.

Way, J. C., and Chalfie, M. (1988). mec-3, a homeobox-containing gene that specifies differentiation of the touch receptor neurons in C. elegans. Cell *54*, 5-16.

Wetzel, C., Hu, J., Riethmacher, D., Benckendorff, A., Harder, L., Eilers, A., Moshourab, R.,

Kozlenkov, A., Labuz, D., Caspani, O.*, et al.* (2007). A stomatin-domain protein essential for touch sensation in the mouse. Nature *445*, 206-209.

Wirtz, K. W. (2006). Phospholipid transfer proteins in perspective. FEBS Lett *580*, 5436-5441.

Zacharias, D. A., Violin, J. D., Newton, A. C., and Tsien, R. Y. (2002). Partitioning of lipid-modified monomeric GFPs into membrane microdomains of live cells. Science *296*, 913-916.

Zhang, J. Z., Abbud, W., Prohaska, R., and Ismail-Beigi, F. (2001). Overexpression of stomatin depresses GLUT-1 glucose transporter activity. Am J Physiol Cell Physiol *280*, C1277-1283.

Zhang, J. Z., Hayashi, H., Ebina, Y., Prohaska, R., and Ismail-Beigi, F. (1999). Association of stomatin (band 7.2b) with Glut1 glucose transporter. Arch Biochem Biophys *372*, 173-178.

Zhang, L., Ding, F., Cao, W., Liu, Z., Liu, W., Yu, Z., Wu, Y., Li, W., and Li, Y. (2006). Stomatin-like protein 2 is overexpressed in cancer and involved in regulating cell growth and cell adhesion in human esophageal squamous cell carcinoma. Clin Cancer Res *12*, 1639-1646.

Zhang, S., Arnadottir, J., Keller, C., Caldwell, G. A., Yao, C. A., and Chalfie, M. (2004a). MEC-2 is recruited to the putative mechanosensory complex in C. elegans touch receptor neurons through its stomatin-like domain. Curr Biol *14*, 1888-1896.

Zhang, S., Ma, C., and Chalfie, M. (2004b). Combinatorial marking of cells and organelles with reconstituted fluorescent proteins. Cell *119*, 137-144.

Zhu, Y., Paszty, C., Turetsky, T., Tsai, S., Kuypers, F. A., Lee, G., Cooper, P., Gallagher, P. G., Stevens, M. E., Rubin, E.*, et al.* (1999). Stomatocytosis is absent in "stomatin"-deficient murine red blood cells. Blood *93*, 2404-2410.
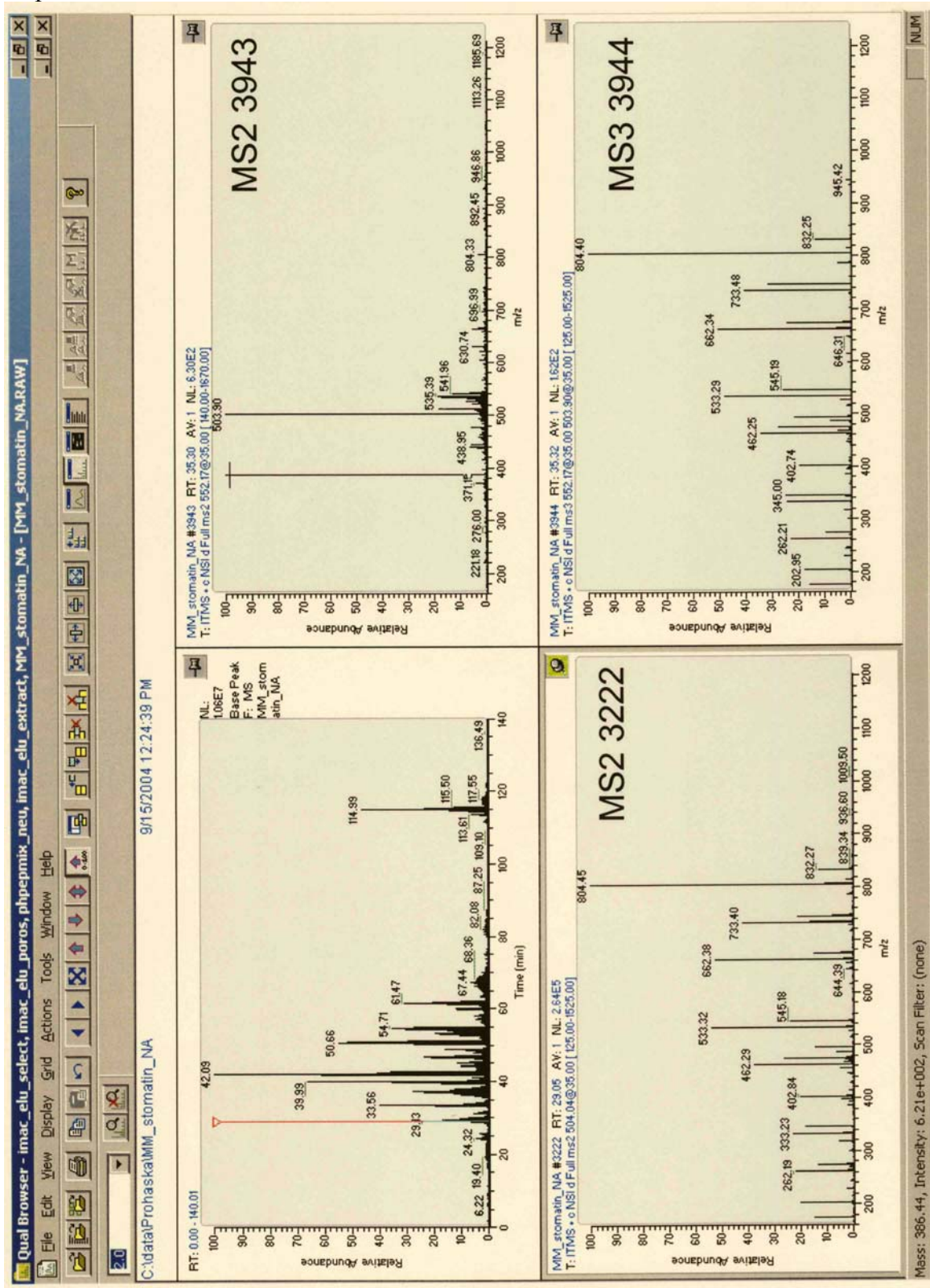
7 ABBREVIATIONS

AAA	ATPase associated with various cellular activities
AFM	atomic force microscopy
AP	alkaline phosphatase
APCs	antigen presenting cells
APS	ammoniumperoxodisulfate
ASIC	acid sensing ion channel
BAP37	B cell receptor associated protein of 37 kDa
BHK	baby hamster kidney cells
BSA	bovine serum albumine
BSE	Bovine spongiform encephalopathy, mad cow disease
C. briggsae	nematode closely related to C. elegans
C. elegans	nematode caenorhabditis elegans
C. remanei	nematode, more distantly related to C. elegans
cAMP	cyclic adenosine monophosphate, stress signal
CD	cluster of differentiation, surface antigens recognized by monoclonal antibodies
CI-M6PR	cation-independent mannose-6-phosphate receptor
CJD	Creutzfeldt-Jakob disease
CNS	central nervous system
COX	cyclooxygenase
CTB	cholera toxin B
DEG/ENaC	degenerin/epithelial sodium channel family
DMSO	dimethylsulfoxide
DNA	deoxyribonucleic acid
DRMs	detergent resistant membranes
DTT	dithiothreitol
E. coli	full name Escherichia coli, bacterium
ECS	epidermal cell surface
EDTA	ethylenediamine tetraacetic acid
EEs	early endosomes
ELMI	electron microscopy
EMBL	european molecular biology laboratories
ER	endoplasmic reticulum
ESA	epidermal surface antigen
EST	expressed sequence tag
FCS	fetal calf serum
FRAP	Fluorescence Recovery After Photobleaching
FRET	Fluorescence Resonance Energy Transfer
GABA	gamma-aminobutyric acid, neurotransmitter
GFP	green fluorescent protein
GLUT	glucose transporter
GM130	golgi membrane protein of 130 kDa
GPI	glycosylphosphatidylinositol anchor
GUVs	giant unilamellar vesicles
HA	influenza haemagglutinin
HDAC	histone deacetylase
HepG2 cells	hepatic cancer cell line
Hfl	high frequency of lysogenization
HRP	horseradish peroxidase
IEF	iso-electric focusing
IP	immunoprecipitation
LAMP	lysosome associated membrane protein

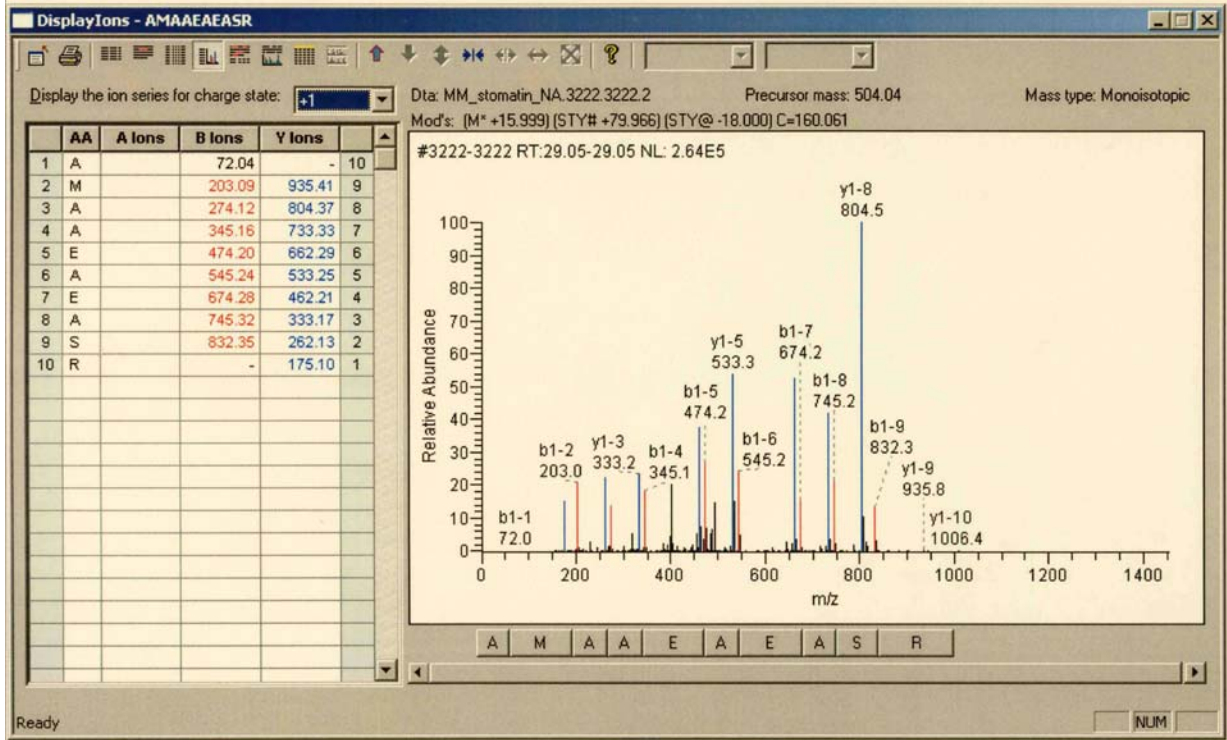|	
LAT	linker of activated T cells
LDs	lipid droplets/bodies
LEs	late endosomes
MALDI-TOF	matrix-assisted laser desorption ionization-time of flight, mass spectroscopy method
MDCK cells	Madine-Darby canine kidney cells
MEC	nematode with mechanosensory defect
MS	mass spectroscopy
MTOC	microtubule-organizing center
MW	molecular weight
NBD	Nitro-benzoxadiazole, fluorophore
NMR	nuclear magnetic resonance
nsLTP	non-specific lipid transfer protein, synonymous with SCP-2, competing designation
OHSt	overhydrated hereditary stomatocytosis, rare anemia
PAGE	polyacrylamide gel electrophoresis
PC12	rat cancer cell line derived from pheochromocytoma (adrenal gland), model for neuronal differentiation
PCR	polymerase chain reaction
PDB	protein data bank
PHB	prohibitin
PIP	phosphatidylinositol phosphate
PLAP	placental alkaline phosphatase
PM	plasma membrane
PMP70	peroxisomal membrane protein of 70 kDa
PTMs	post-translational modifications
PVP	poly-vinylpyrrolidone
RIPA	radioimmunioprecipitation assay
RNA	ribonucleic acid
ROI	region of interest
RT	room temperature
S. cerevisiae	saccharomyces cerevisiae, brewer´s little helper & budding yeast
SAGE	serial analysis of gene expression
SCP-2 domain	sterol carrier protein 2 domain
SDS	sodium dodecyl sulfate
siRNA	short interfering RNA
SL	sphingolipid
SLP	stomatin like protein
SPFH	stomatin/prohibitin/flotillin/HflK/C protein superfamily
SRO	stomatin related olfactory
SSU	suppressor of stomatin uncoordination
STL	C. elegans stomatin-like
STO	C. elegans stomatin
STOML	stomatin-like
STORP	stomatin-related protein
TCR	T cell receptor
TEMED	tetramethylethylendiamine
TfR	transferrin receptor, CD71
TIM	translocase inner mitochondrial membrane
TRITC	tetramethyl-rhodamine isothiocyanate, fluorophore
TRP	transient receptor potential
UAC cells	umbilical amniotic cells, epithelial cell line
UNC	uncoordinated nematode
UTR	untranslated region (of mRNA)
VA	volatile anesthetic

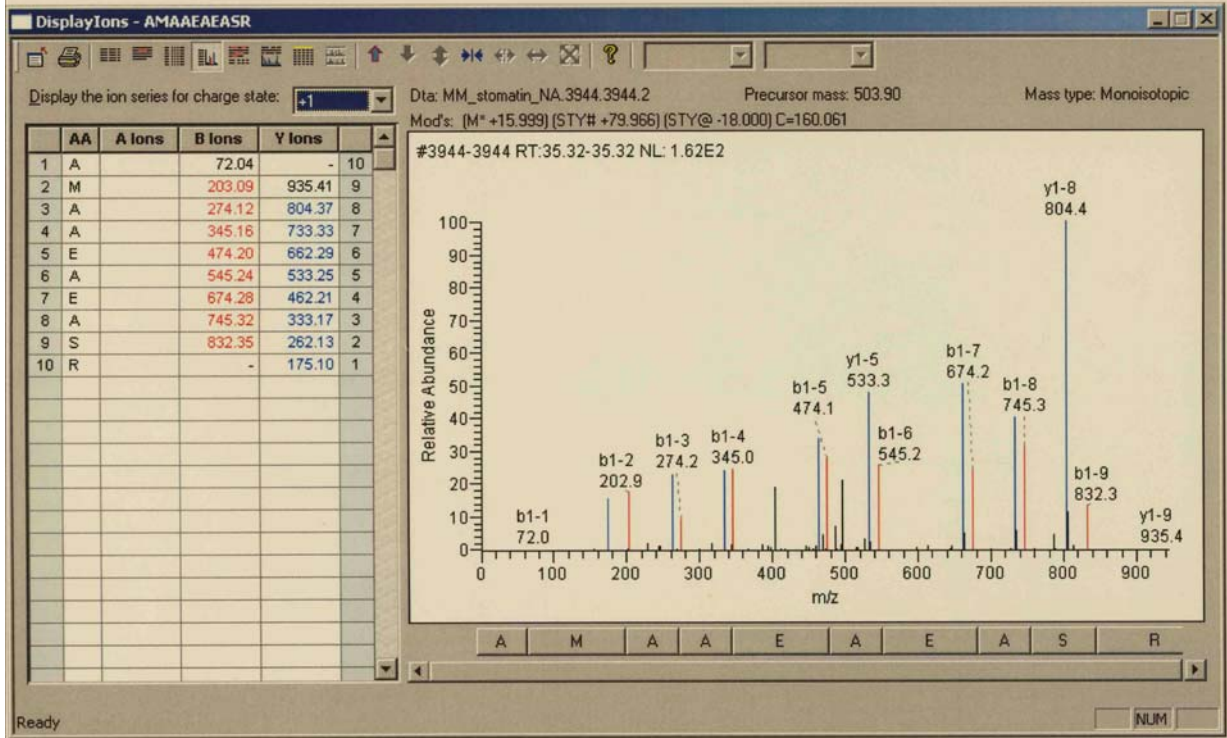Mass spectrometry data for three stomatin peptides with a kryptic modification:
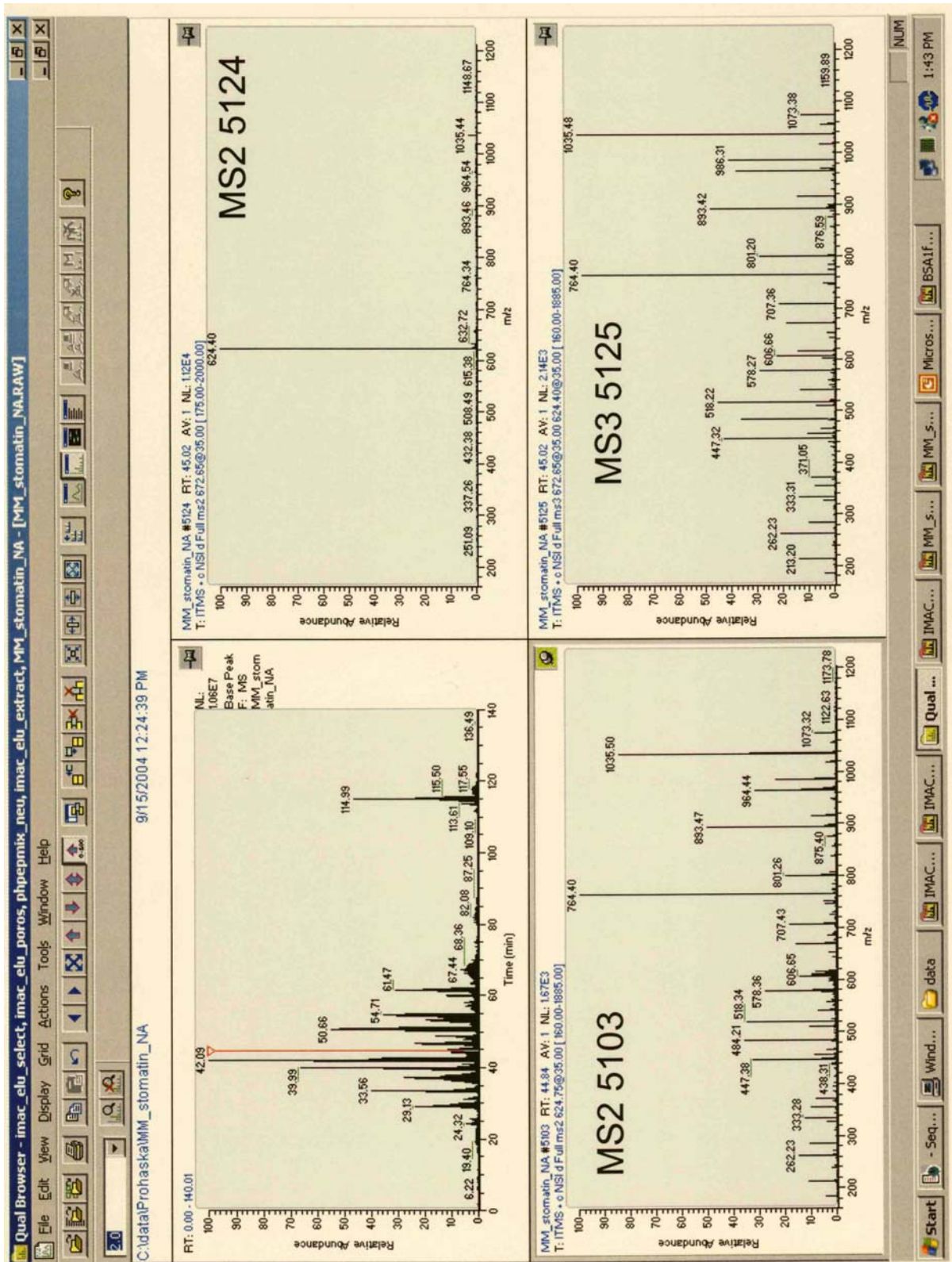
1: Peptide AMAEAEASR

MS2 3222

DisplayIons - AMAAEAEASR

Display the ion series for charge state: `+1`

Dta: MM_stomatin_NA.3222.3222.2   Precursor mass: 504.04   Mass type: Monoisotopic
Mod's: (M* +15.999) (STY# +79.966) (STY@ -18.000) C=160.061

#3222-3222 RT:29.05-29.05 NL: 2.64E5

	AA	A Ions	B Ions	Y Ions	
1	A		72.04	-	10
2	M		203.09	935.41	9
3	A		274.12	804.37	8
4	A		345.16	733.33	7
5	E		474.20	662.29	6
6	A		545.24	533.25	5
7	E		674.28	462.21	4
8	A		745.32	333.17	3
9	S		832.35	262.13	2
10	R		-	175.10	1

A M A A E A E A S R

Ready   NUM

MS3 3944

DisplayIons - AMAAEAEASR

Display the ion series for charge state: `+1`

Dta: MM_stomatin_NA.3944.3944.2   Precursor mass: 503.90   Mass type: Monoisotopic
Mod's: (M* +15.999) (STY# +79.966) (STY@ -18.000) C=160.061

#3944-3944 RT:35.32-35.32 NL: 1.62E2

	AA	A Ions	B Ions	Y Ions	
1	A		72.04	-	10
2	M		203.09	935.41	9
3	A		274.12	804.37	8
4	A		345.16	733.33	7
5	E		474.20	662.29	6
6	A		545.24	533.25	5
7	E		674.28	462.21	4
8	A		745.32	333.17	3
9	S		832.35	262.13	2
10	R		-	175.10	1

A M A A E A E A S R

Ready   NUM

PhD thesis   *Mario Mairhofer*
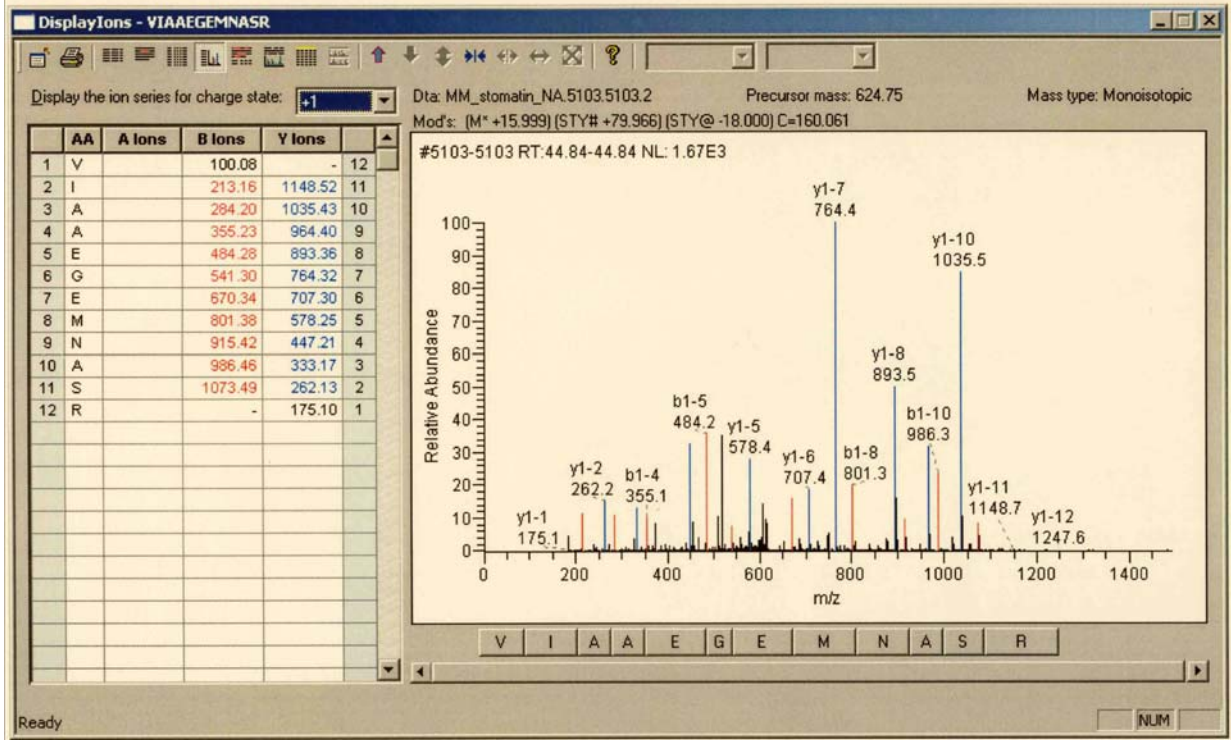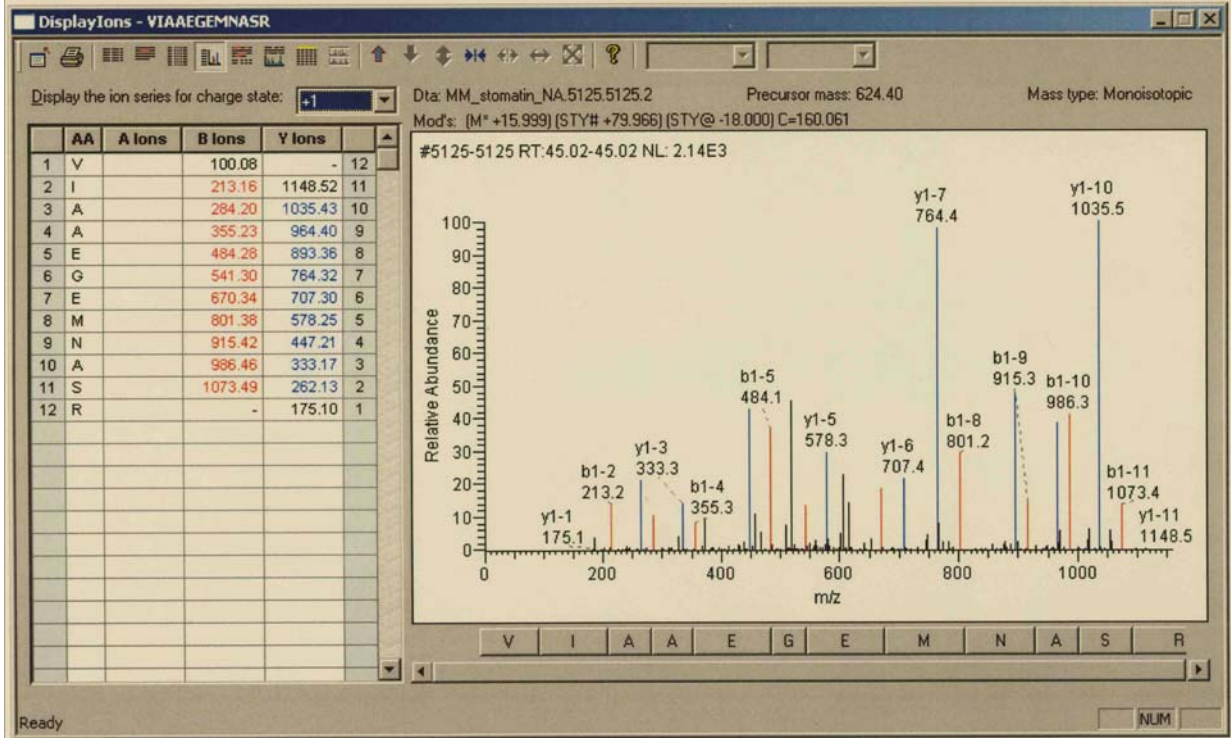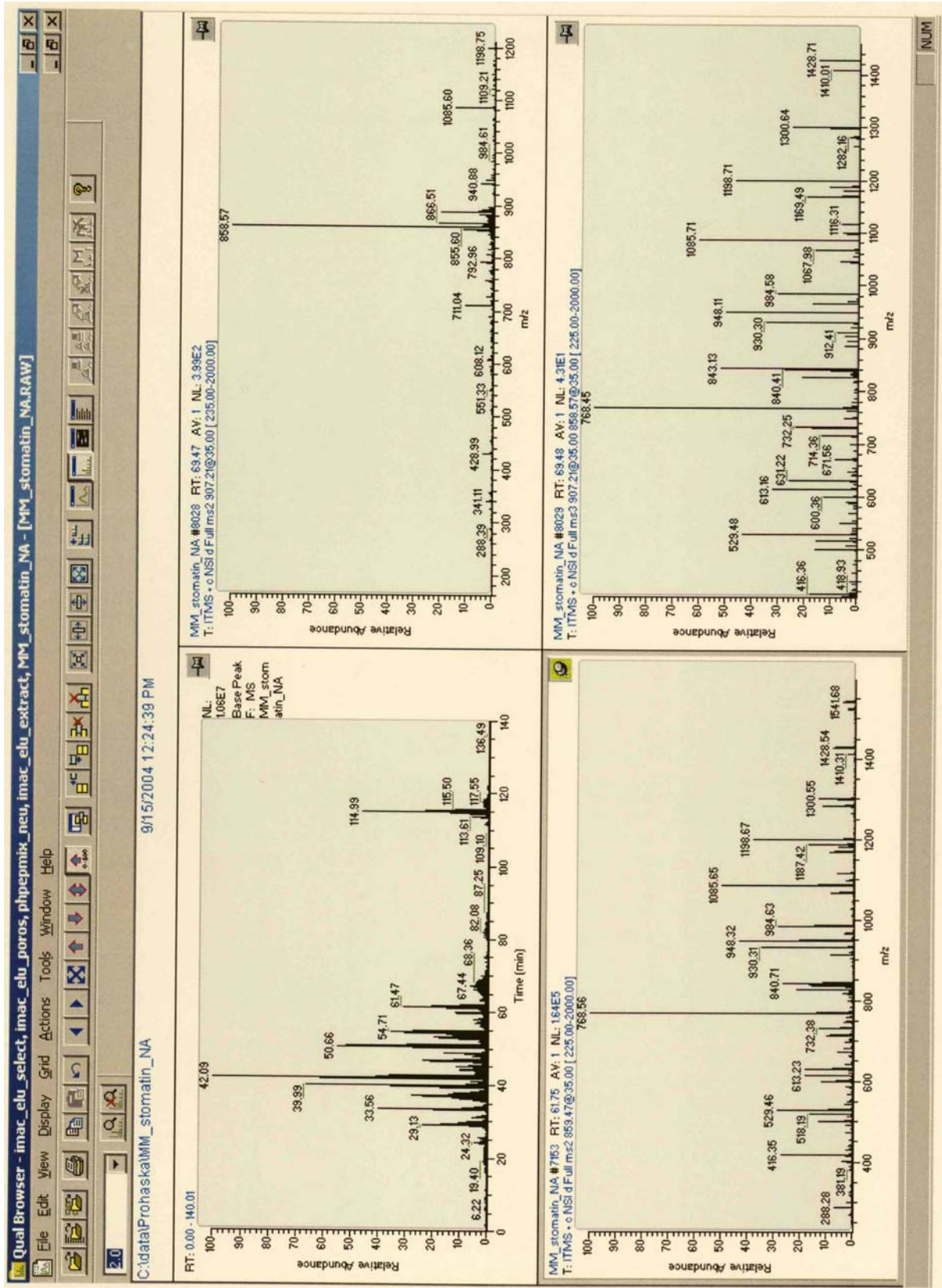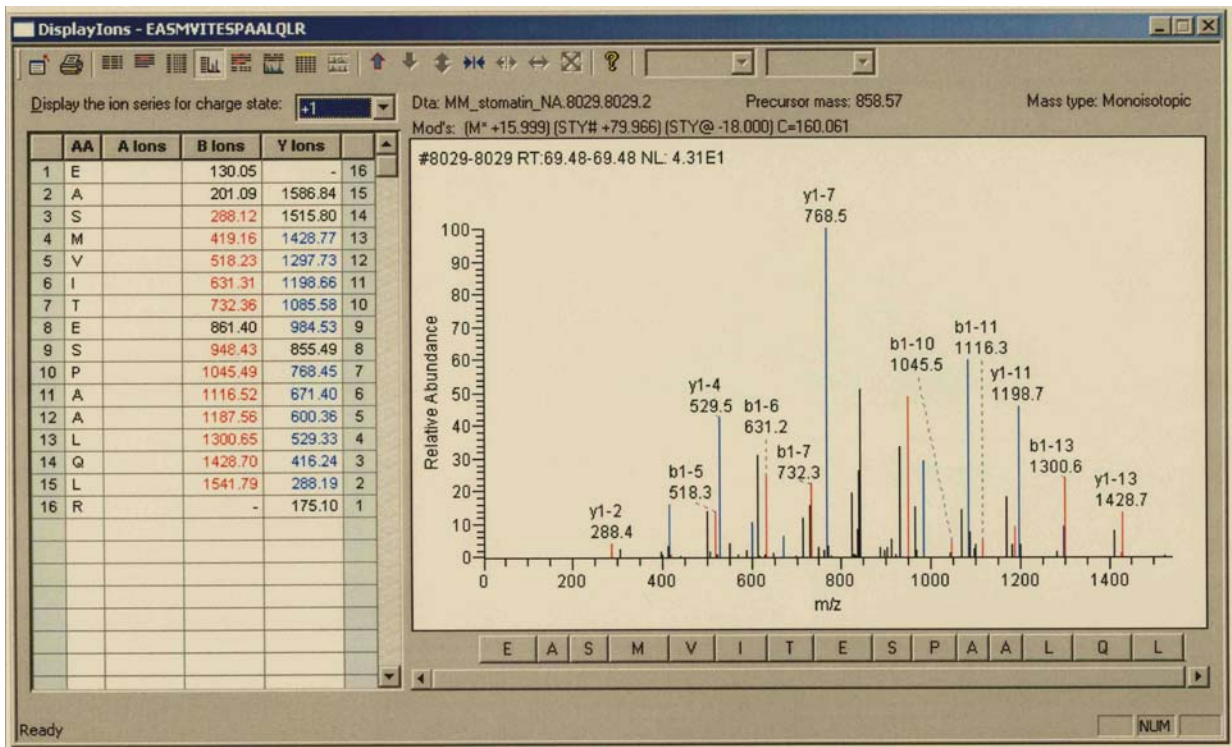
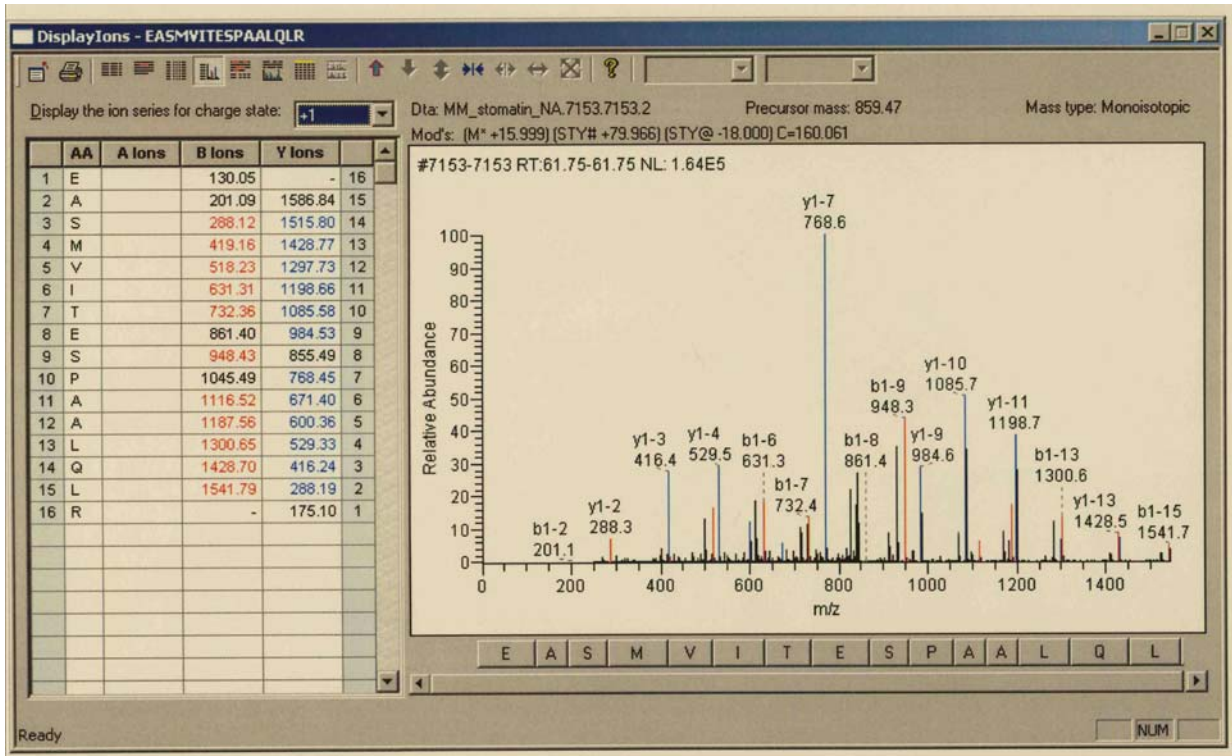2: Peptide VIAAGEMNASR

MS2 5103

MS3 5125

3: Peptide EASMVITESPAAL

9 CURRICULUM VITAE

Mag. Mario Mairhofer

Schwarzspanierstraße 18/7, 1090 Wien, TEL 0 699 / 11967121

E-MAIL mario.mairhofer@gmx.at

Personal Details:		
	Date of Birth	23.12.1974
	Place of Birth	Linz, Austria
	Nationality	Austria
	daughter Emma	born 07.08.2006

Education:		
	03/2007 - current	Work in EU-project CRYSTAL on cryopreservation of hematopoietic stem cells
	01/2003 – 12/2006	Continuation of PhD thesis with the topic: ´Cell biological characterization of stomatin and stomatin-like proteins´, completion of experiments in December 2006
	05/2002 -12/2002	Military service in Linz, OÖ
	12/2001- 04/2002	start of practical work for PhD thesis under supervision of Ao. Prof. Dr. Rainer Prohaska (rainer.prohaska@univie.ac.at)
	01/2000 - 11/2001	Diploma thesis in the Laboratory of Ao. Prof. Dr. Rainer Prohaska under the supervision of Dr. Ulrich Salzer (ulrich.salzer@univie.ac.at), graduation on 27 November 2001.
	1993 - 1999	Studies of chemistry, special topic biochemistry, at the University of Vienna, completion of first section (equivalent to newly established bachelor´s degree) on 8 February 1997.
	1985 - 1993	Grammar school in Rohrbach
	1981 - 1985	Primary school in Altenfelden

Scientific achievements:

Publications:

Salzer U, Mairhofer M, Prohaska R.
Stomatin: A New Paradigm of Membrane Organization Emerges.
Dynamic Cell Biology 2007 Jun; 1 (1): 20-33.

Umlauf E, Mairhofer M, Prohaska R.
Characterization of the Stomatin Domain Involved in Homo-oligomerization and Lipid Raft Association.
J Biol Chem. 2006 Aug 18;281(33):23349-56. Epub 2006 Jun 9.

Mairhofer M, Steiner M, Mosgoeller W, Prohaska R, Salzer U.
Stomatin is a major lipid-raft component of platelet alpha granules.
Blood. 2002 Aug 1;100(3):897-904.

Poster presentations:

Stomatin – a granular, oligomeric lipid raft protein in platelets and neutrophils.
Mairhofer M, Salzer U, Prohaska R
Annual Meeting of the Austrian Society of Biochemistry and Molecular Biology (ÖGBM), September 2003
Analysis of Platelet Lipid Rafts by 2D-PAGE: Influence of Platelet Activation on Lipid Raft Composition.
Mairhofer M, Salzer U, and Prohaska R
Annual Meeting ÖGBM, September 2004

Oral presentations:

Stomatin-Like Protein-1: An endosomal, stomatin-interacting lipid raft protein
Mario Mairhofer, Seminar Department of Medical Biochemistry 18.11.2005